

**Investigation of the Role of Freeze Bonds on the Development of
Ice Rubble Strength**

By

© Marjan Taghi Boroojerdi

A thesis submitted to the

School of Graduate Studies

in partial fulfilment of the requirements for the degree of

Doctor of Philosophy

Faculty of Engineering and Applied Science

Memorial University of Newfoundland

October 2020

St. John's, Newfoundland and Labrador

ABSTRACT

Freeze bonds are one of the controlling factors in ice ridge and rubble failure. Strength and failure properties of freeze bonds are therefore important to study, to better understand the overall strength development of ice ridges/rubble. This research aims to understand the strength development and failure of freshwater freeze bonds through a series of experiments, conducted under different conditions of contact time, deformation rate, and confinement pressure. Freeze bonds were formed between two cylindrical ice samples, confined under a normal pressure at the two ends, which were submerged in a freshwater bath for a specific period of time. Freeze-bonded samples were then sheared using the Asymmetric Four-Point Bending (AFPB) apparatus installed on the Materials Testing System (MTS) servo-hydraulic testing machine at Memorial University's coldroom.

Increasing the submersion time from 1 minute to 14 days, freeze bond strength was observed to be initially controlled by heat transfer processes, increasing with submersion time and reaching a peak after 5 minutes. Strength then decreased as ice reached equilibrium temperature with surrounding water, after which it remained constant. Sintering and creep processes were believed to be the dominating mechanism in long submersion times, resulting in an increase in strength after 1 day, until reaching the strength of solid ice after 14 days.

Confinement pressure effects were investigated for four different submersion times that were chosen based on the stages of bond development observed in the submersion time tests. Strength values increased linearly as confinement increased from 10 to 100 kPa for

all submersion times tested. The rate of this increase followed the trends observed in submersion time tests, with the highest amount of increase occurring after one week of submersion. Sintering-creep and crushing of asperities in contact were introduced as the responsible processes, which are known to be intensified with increase in confinement and contact time.

Increasing the deformation rate during shear from 0.01 to 100 mm/s, freeze bond failure strength was observed to decrease. This decrease was associated with higher amounts of strain before failure of freeze bonds at lower deformation rates, which is a result of the higher capacity of energy dissipation and creep at lower rates. Ice rubble and ice ridge experiments studied to date follow similar trendlines of strength-confinement and strength-deformation rate observed in present study, which highlights the important role of block to block freeze bond strength development and failure on the overall strength properties of ice rubble/ridges.

*I dedicate this thesis to my loving parents, Mohammad and
Nooshin, my dear sister, Mehrnoosh, and my beloved
husband, Saeed, for their unconditional love and unfailing
support, and because they always understood.*

I love you all dearly.

ACKNOWLEDGMENTS

I express my sincere appreciation to those who helped me throughout my PhD journey, without whom this research would have not been possible.

First and foremost, I would like to thank my supervisors Dr. Eleanor Bailey and Dr. Rocky Taylor for introducing me to this exciting field of research and for their continuous support and guidance throughout my program. I was fortunate to have Dr. Bailey as my supervisor, not only for her technical insights and advice, but because her office door was always open for me to talk about challenges, ups and downs, and frustrations. I am sincerely thankful to Dr. Taylor for his helpful suggestions and constructive criticism throughout my program, and for helping me grow as an independent scholar. Many thanks go to my committee member, Dr. Robert Sarracino, for his instructions and feedbacks during my PhD program.

I would like to express my gratitude to C-CORE, for all the support I received during my PhD, and for providing me with the expertise and experimental equipment needed for my research. Special thanks to Mr. Robert Pritchett, for all the technical help and discussions, without whom not a single test would be possible. And to the laboratory technicians of the Thermal Lab of the Memorial University's Engineering department, Mr. Craig Mitchell, Mr. Matt Curtis, and Mr. Trevor Clark, for all those days of staying late so that I could finish testing. None of these would of course be possible without the help of our dear workterm students, Mr. John Stamp, Mr. Harrison Lake, Mr. Tim Purdy, Mr. Seamus MacDonald, Mr. Zachary Burt, Mr. Igor Tchouiko and Mr. Daniel Thorsen, who did not mind the long hours of work at subzero temperatures. I would also like to thank my

colleagues, Mr. Soroosh Afzali, and Mr. Ridwan Hossain for their help during the tests. I am grateful to my mentor, Mr. Darrell Cole, for all the weekly meetings, uncountable emails, and encouragement in the past year.

I would like to acknowledge the financial support from the School of Graduate Studies at Memorial University, InnovateNL, Natural Sciences and Engineering Research Council (NSERC), and Hibernia Management and Development Company Ltd. (HMDC) that made this research possible. I am truly grateful to the selection committees of the Emera Graduate Scholarship and SNAME's John W. Davies Memorial Award for supporting my research. And to the Canada Foundation for Innovation, for recognizing me in their promotional campaign.

Finally, I would also like to express my heartfelt thanks to my Mom and Dad, and my sister for always believing in me and for encouraging me to explore new directions in life. Thank you for helping me keep on going when times were tough, although you were miles away. And my dear friends in St. John's, who are like a second family to me, for always lending an ear and listening to my rants! And finally, to my husband and my best friend, Saeed, who was by my side during this PhD, living every single minute of it. Thank you for being patient with me and cheering me up when I was frustrated.

TABLE OF CONTENTS

ABSTRACT	i
ACKNOWLEDGMENTS	iv
LIST OF TABLES	xi
LIST OF FIGURES	xii
NOMENCLATURE	xx
1. INTRODUCTION AND OVERVIEW	1
1.1. General Introduction	1
1.2. Objectives and Scope of Research	5
1.3. Organization of the Thesis	9
1.4. References	12
2. LITERATURE REVIEW.....	16
2.1. Preface	16
2.2. Chapter Abstract.....	17
2.3. Freeze Bonds at Ridge and Rubble Scale.....	18
2.4. Freeze Bonds at Block Scale	30
2.5. Freeze Bonds at Particle Scale	42
2.6. References	50

3. SUBMERSION TIME EFFECTS	55
3.1. Preface	55
3.2. Chapter Abstract.....	56
3.3. Introduction	57
3.4. Background	60
3.5. Experimental Method.....	65
3.5.1. Sample preparation	65
3.5.2. Freeze bond tests.....	66
3.5.3. Thermal equilibrium test.....	70
3.6. Results	72
3.6.1. Freeze bond tests.....	72
3.6.2. Solid ice tests	80
3.6.3. Thermal behavior of samples.....	81
3.6.4. Change in freeze bond diameter.....	83
3.7. Analysis and Discussion.....	84
3.7.1. Empirical relationships	84
3.7.2. Physical processes influencing bond strength development.....	89
3.7.2.1. Thermal bonding mechanism.....	90
3.7.2.2. Sintering-creep bonding mechanism.....	92

3.7.3.	Comparison with other data	96
3.8.	Conclusions	99
3.9.	References	101
4.	CONFINEMENT PRESSURE EFFECTS.....	108
4.1.	Preface	108
4.2.	Chapter Abstract.....	109
4.3.	Introduction	110
4.4.	Experimental Methodology	114
4.5.	Results	116
4.5.1.	Tests with 30 minutes of submersion time	119
4.5.2.	Tests with 3 hours of submersion time	120
4.5.3.	Tests with 3 days of submersion time	122
4.5.4.	Tests with 7 days of submersion time	123
4.6.	Discussion	124
4.6.1.	Analysis and discussion of results	124
4.6.2.	Discussion of physical mechanisms.....	126
4.6.3.	Comparison of freeze bond shear strengths with other data	130
4.6.4.	Discussion of implications for ice rubble shear strength	133
4.7.	Conclusions	140

4.8.	References	141
5.	RATE DEPENDENCY OF FREEZE BOND STRENGTH.....	145
5.1.	Preface	145
5.2.	Chapter Abstract.....	146
5.3.	Introduction	147
5.4.	Experimental Setup and Methodology.....	149
5.5.	Results	155
5.5.1.	Observed Failure Mode.....	155
5.5.2.	Shear strength.....	165
5.6.	Discussion	167
5.6.1.	Comparison with previous freeze bond experiments.....	167
5.6.2.	Comparison with rate effects in solid ice.....	170
5.6.3.	Comparison with ice rubble tests	172
5.7.	Conclusions	178
5.8.	References	180
6.	CONCLUSIONS AND RECOMMENDATIONS FOR FUTURE WORK	186
6.1.	Conclusions	186
6.1.1.	Submersion time effects.....	187
6.1.2.	Confinement effects	188

6.1.3.	Deformation rate effects.....	190
6.1.4.	Comparison of the effects of parameters tested	191
6.1.5.	Implications of freeze bond strength on strength of ice rubble/ridges.....	193
6.2.	Recommendations for Future Work.....	195
6.3.	References	198
Appendix A: Preliminary freeze bond experiments, presented at the 2016 Arctic Technology conference, St. John’s, NL.....		
		200
Appendix B: Freeze bond field experiments, presented at the 2018 Arctic Technology Conference, Huston, Texas		
		211

LIST OF TABLES

Table 1.1. Organization of the thesis	9
Table 2.1. Sintering constant values for each dominant mechanism [31].	44
Table 3.1. Freeze bonds test matrix. Parameters in the table are: submersion time (t), initial ice temperature (T_i), Actuator rate (V), confinement (σ), number of tests (n), normal pressure drop ($\Delta\sigma$), average normal pressure ($\bar{\sigma}$), average shear strength (S).....	74
Table 3.2. Coefficient values	88
Table 4.1. Confinement pressure test matrix. Parameters in the table are: submersion time (t), initial ice temperature (T_i), actuator rate (V), confinement (σ), number of tests (n), mean shear strength (τ_{mean}), shear strength values for each test (τ), minimum and maximum strength (τ_{min} , τ_{max}), standard deviation (STD), failure load (F_{max}).	118
Table 5.1. Test matrix. Parameters in the table are: submersion time (t), initial ice temperature (T_i), confinement (σ), Actuator rate (V), number of tests (n), mean shear strength (τ_{mean}), shear strength values for each test (τ), minimum and maximum strength (τ_{min} , τ_{max}), standard deviation (STD), failure load (F_{max}), and displacement at failure (δ).	154

LIST OF FIGURES

Figure 1.1. Schematic illustration of compressive ice ridge formation (a), and shear ice ridge formation (b).....	2
Figure 1.2. Schematic illustration of the multi-scale properties of ice rubble where factors influencing ridge loads are governed by: a) freeze bond properties, b) contact conditions at the block interface and c) sintering and junction growth at the asperity level.....	4
Figure 2.1. Mohr-Coulomb failure hypothesis.	19
Figure 2.2. Results of shear strength values as a function of deformation rate of previous ice rubble strength tests, where H_{rubble} is the ice rubble thickness. $H_{ice\ sheet}$ is the ice block thickness, η is the rubble porosity, V is the displacement rate, and t is the consolidation time.	28
Figure 2.3. Results of shear strength values as a function of confinement of previous ice rubble strength tests, where H_{rubble} is the ice rubble thickness. $H_{ice\ sheet}$ is the ice block thickness, η is the rubble porosity, V is the displacement rate, and t is the consolidation time.	29
Figure 2.4. Results of shear strength values as a function of consolidation time of previous ice rubble strength tests, where H_{rubble} is the ice rubble thickness, η is the rubble porosity, V is the displacement rate.....	30

Figure 2.5. Schematic illustration of test set-ups used in previous freeze bond studies showing the 45° method (a), direct shear method (b), and Asymmetric Four-Point Bending (AFPB) method (c). 31

Figure 2.6. Plot showing the measured shear strength values versus submersion time in previous freeze bond experiments for a) saline ice, and b) freshwater ice, where T_i is the initial temperature of ice and σ is confinement pressure. 39

Figure 2.7. Plot showing the measured shear strength values versus confinement in previous freeze bond experiments. In this plot T_i is the initial temperature of ice and t is the submersion time. 40

Figure 2.8. Plot showing the measured shear strength values versus deformation rate in previous freeze bond experiments. In this plot σ is confinement pressure, T_i is the initial temperature of ice and t is the submersion time..... 40

Figure 2.9. The geometry of sintered ice particles and sintering mechanisms (after [22]). 44

Figure 2.10. Interaction of asperities loaded under a shear and normal stress (after [32]). 48

Figure 2.11. Schematic illustration of crushing of asperities and recrystallization at contact interface..... 49

Figure 3.1. Schematic illustration of the multi-scale properties of ice rubble where factors influencing ridge loads are governed by: a) freeze bond properties, b) contact conditions at the block interface and c) sintering and junction growth at the asperity level.....60

Figure 3.2. Plot showing the measured shear strength values versus submersion time in previous freeze bond experiments for a) saline ice, and b) freshwater ice. In this figure σ refers to confinement pressure and T_i to initial ice temperature.65

Figure 3.3. Figures showing design drawing and photographs of a) the confinement frame and b) the confinement frame loaded in the AFPB rig.67

Figure 3.4. AFPB rig, showing diagrams of a) the experimental set-up, b) the shear forces, and c) the bending moments (after Bailey et al. [58]).69

Figure 3.5. Wireless temperature sensors (MicroTs) frozen in the ice sample after submersion.71

Figure 3.6. Normal pressure measured for samples that were submerged for 5 min and had an initial ice temperature of -18°C . In this figure σ is the normal pressure and $\bar{\sigma}$ is the average normal pressure.....73

Figure 3.7. Typical load curves showing a) brittle and b) ductile behaviour observed during the freeze bond tests. Both tests were conducted for 4 minutes of submersion time and initial ice temperature of -18°C76

Figure 3.8. Freeze bond shear strength vs. submersion time for ice with an initial temperature of -18°C that was confined under a confinement of 23 kPa and deformed at a constant rate of 5 mm/s.	77
Figure 3.9. Freeze bond shear strength vs. submersion time for ice with an initial temperature of -10°C that was confined under a nominal confinement pressure of 23 kPa and deformed at a constant rate of 5 mm/s.	78
Figure 3.10. Comparison of freeze bond shear strength vs. submersion time for ice with an initial temperature of -10°C and -18°C	80
Figure 3.11. Solid ice and freeze bond shear strengths as a function of submersion time.	81
Figure 3.12. Temperature data recorded by the MicroTs placed at locations $z = 5, 10$ and 15 cm and numerical results for a solid ice block with an initial temperature of -18°C , along with zoomed in plot of the temperature from 20 to 50 min after submersion for $z = 10$ cm and numerical results.	82
Figure 3.13. Measured values for amount of increase in diameter a) and rate of increase in freeze bond diameter b) during submersion period of freeze bonds.	84
Figure 3.14. Thermal bonding mechanism curves for the two initial ice temperatures of -18°C and -10°C	86
Figure 3.15. Sintering-creep bonding mechanism curves for the two initial ice temperatures of -18°C and -10°C	87

Figure 3.16. Combined freeze bond strength curves for initial ice temperatures of -18°C and -10°C.	89
Figure 3.17. The five stages of freeze bond development as submersion time increases..	90
Figure 3.18. Photos showing a) shape of ice cylinders before submersion, b) shape of cylinder after 14 days of submersion, showing a curved profile with increased area near the freeze bonded region, and c) a schematic illustration of the growth behavior as a result of sintering-creep.....	95
Figure 3.19. a) Comparison of the shear strength values of present work with Ettema and Schaefer (1986) and Shafrova and Hoyland (2008), Bueide and Høyland (2015), and C-CORE (2012), b) zoomed in plot of Ettema and Schaefer (1986). In this figure σ is the confinement pressure and T_i is the initial ice temperature.	99
Figure 4.1. Plot showing the measured shear strength values versus confinement in previous freeze bond experiments. In this plot, S_w is the salinity of submergence liquid, t is the submersion time and T_i is the initial ice temperature.....	112
Figure 4.2. Figures showing the design of (a) confinement frame and (b) the asymmetric four-point bending apparatus.	116
Figure 4.3. Comparison of shear strength over confinement for 30 minutes submersion time, with linear fit to the data.	120

Figure 4.4. Comparison of shear strength over confinement for 3 hours submersion time.	121
Figure 4.5. Comparison of shear strength over confinement for 3 d submersion time....	122
Figure 4.6. Comparison of shear strength over confinement for 7 d submersion time....	124
Figure 4.7. Linear fit of confinements over confinement for the submersion times tested.	125
Figure 4.8. Schematic illustration of processes affecting freeze bond strength development.	126
Figure 4.9. Comparison of the results of present study with previous freeze bond experiments.	132
Figure 4.10. Results of shear strength values as a function of confinement of previous ice rubble strength tests, where H_{rubble} is the ice rubble thickness. $H_{ice\ sheet}$ is the ice block thickness, η is the rubble porosity, and V is the displacement rate.	139
Figure 5.1. a) Confinement frame, b) AFPB rig, and c) ice samples loaded in confinement frame and submerged in water.	151
Figure 5.2. Positioning of loading pins on the asymmetric four-point bending (AFPB) apparatus.	152

Figure 5.3. Shear force-time curves for ice that was submerged for 30 min, for deformation rates of 0.01 to 100 mm/s.....155

Figure 5.4. Comparison of the shear force-displacement curves for different deformation rates.157

Figure 5.5. Time to failure as a function of the deformation rate.158

Figure 5.6. Schematic illustration of shear strain, where δ is the displacement, $t_{total}=2\alpha L$ is the length between the indenters, γ is the shear strain, γ_{ice} is the shear strain of ice, γ_{FB} is the shear strain of freeze bond, $t_{ice_{1,2}}$ are the thickness of ice between the indenters, and t_{FB} is the thickness of freeze bond layer (Dimensions are not to scale and are expanded for illustration purposes only).....159

Figure 5.7. Critical strain as a function of nominal strain rate.....161

Figure 5.8. Comparison of shear strength as a function of deformation rate for submersion times of 30 min and 24 h.....166

Figure 5.9. Shear strength as a function of critical strain.167

Figure 5.10. Plot showing the comparison of measured shear strength values versus deformation rate in previous freeze bond experiments and present study (a), and zoomed-in plot of Ettema and Schaefer [3] (b). In this plot σ is confinement pressure, T_i is the initial temperature of ice and t is the submersion time.....169

Figure 5.11. Compressive strength as a function of strain rate. Blue rectangle shows the range of strain rates used in present study (after [34] and [26]).172

Figure 5.12. Rubble shear strength measurements of Yasunaga et al. [17], Urroz and Ettema [16], Hellmann [13], and Weiss et al. [12] as a function of deformation rate. In this figure where H_{rubble} is the ice rubble thickness. $H_{ice\ sheet}$ is the ice block thickness, η is the rubble porosity, V is the displacement rate, and t is the consolidation time.175

Figure 5.13. Berm pressure data for DIRKS and PIRAM projects.....177

NOMENCLATURE

Abbreviations

RTD	Resistance Temperature Detectors
AFPB	Asymmetric Four-Point Bending
MTS	Materials Testing System
DAQ	Data Acquisition
PIRAM	Pipeline Ice Risk and Mitigation
DIRKS	Development of the Ice Ridge Keel Strength
STD	Standard Deviation

Symbols and Units

h	Hour(s)
min	Minutes(s)
s	Second(s)
kPa	Kilopascal
N	Newtons
m	Meters

cm	Centimeters
mm	Millimeters
°C	Degree Celsius
S_w	Salinity of submergence liquid
T_i	Initial ice temperature
T_w	Water temperature
t	Submersion time
g	Gravity
e	Bulk porosity of ice rubble/ridge
c	Cohesion
R	Radius of ice block
L	Length of ice block
H_{rubble}	Ice rubble thickness
$H_{ice\ sheet}$	Ice sheet thickness
V	Displacement rate
P_{max}	Maximum shear force
F_{max}	Failure load

T	Temperature (as a variable)
C_p	Specific heat capacity of ice
k	Conductivity of ice/ Boltzmann's constant (in creep equation)
S	Average shear strength
n	Number of tests
D	Diameter of ice samples
G_{eff}	Effective shear elastic modulus of the freeze bonds
E	Elastic modulus
z	Longitudinal distance from one end of the ice sample
z_k	Position from the bottom of the keel
r	Radius (as a variable)
x	Radius of the neck during sintering
R_{tip}	Initial radius of the tip of the ice cones in contact
a_0	Instantaneous radius of contact
$a(t)$	Time-dependant radius
L	Sintering factor
$F_{sintering}$	Sintering force

C	Temperature-dependent constant in sintering factor
A_{Th}	Function representing thermal effects
B_{sint}	Function representing sintering effects
ρ_w	Water density
ρ_i	Ice density
σ_z	Vertical component of the bulk pressures of a ridge keel
τ	Shear stress/strength
σ	Normal confinement pressure
$\bar{\sigma}$	Average normal confinement pressure
$\Delta\sigma$	Normal pressure drop
φ	Friction angle
τ_{max}	Maximum shear stress/shear strength
τ_{ice}	Shear strength of solid ice
$\tau_{FB,Th}$	Freeze bond strength as a result of thermal mechanisms
$\tau_{FB,sint}$	Freeze bond strength as a result of sintering-creep mechanisms
τ_{FB}	Freeze bond strength
τ_R	Ice rubble strength

τ_{mean}	Mean shear strength
τ_{min}	Minimum shear strength
τ_{max}	Maximum shear strength
$\dot{\epsilon}$	Strain rate
η	Ice rubble porosity
δ	Displacement at failure
γ	Shear strain/surface free energy
α	A function of the distance of loading pins
αL	Length between the inner indenter and the freeze bond
ν	Poisson's ratio
ϵ	Activation energy during creep
$\sigma_{tensile}$	Tensile strength
σ_c	Normal confinement pressure

1. INTRODUCTION AND OVERVIEW

1.1. General Introduction

Increasing demand for natural resources in recent years, in combination with decreasing ice cover has resulted in increased interest from companies seeking to develop resources in Arctic and sub-Arctic regions. The Arctic holds one-quarter of the world's oil and gas reserves [1]. The environmental conditions of the Arctic, such as cold temperatures, rough waves, and most importantly ice features such as icebergs and ice ridges require the design of structures and infrastructure that can withstand the loads from these features. Moreover, with the increasing rate of Arctic ice decline in the past recent years, shipping in the northern shipping routes (the Northeast Passage, the Northwest Passage, and the Transpolar Sea Route) seems to be more feasible than before [2]. Arctic transportation, however, requires the design of ships that can resist the loads of ice features in shipping routes. Furthermore, brash ice accumulations in northern shipping channels can be a hazard for ships navigating through Arctic regions.

Ice ridges and rubble fields are common ice features that often govern the design loads for structures and ships operations. These are also the dominant ice features in freshwater lakes such as Lake Erie.

Ice rubble is formed as a result of compression or shear of the ice cover (Figure 1.1), and consists of a pile of randomly oriented blocks of ice that are in contact with different angles and contact areas. Rubble fields can form in rivers resulting in jamming of the river, which

can cause operational problems for ocean vessels, and high ice loads due to ice rubble pile-ups that can exert extra load on structures [3, 4].

Ice ridges, large accumulations of ice rubble, are ice features several meters high and several meters deep, which are composed of three main components as shown in Figure 1.2. The sail, is the above water section, while the keel is the submerged section with water filling the pores. The consolidated layer, a layer of refrozen ice blocks at the waterline, is formed through the lifetime of the ridge. The rate of growth and properties of the consolidated layer are however a function of environmental conditions such as air and water temperature, as well as currents [5].

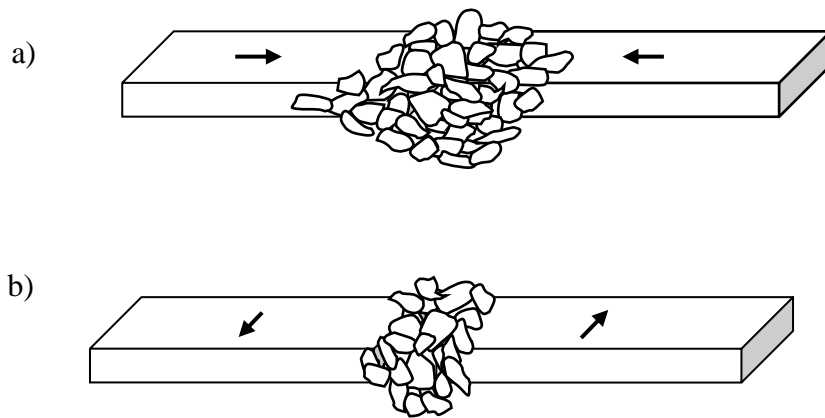


Figure 1.1. Schematic illustration of compressive ice rubble formation (a), and shear ice rubble formation (b)

The size and magnitude of an ice ridge is a function of the thickness of level ice, as well as the amount of ice broken during the ridging process. Due to their depth and size, these features are considered a hazard to both surface and subsea structure/infrastructure [6].

While the sail of an ice ridge is 1 to 4 m high, the keel can be up to 30 m deep, thus imparting

greater loads during interactions than the sail [7]. Freezing processes between the submerged ice blocks in the keel also contribute to higher loads applied by this portion of the ridge [8]. For instance, first-year ice ridges have been identified as the dominant ice feature in regions such as the Baltic Sea, Baydarata Bay, and Lake Erie, where subsea pipelines (e.g., the Millennium Pipeline Project and the Baltic Pipeline System) are subject to impacts from scouring ice ridge keels [9]. Ice ridge and rubble interactions with bridge piers and lighthouses are another issue in regions such as Eastern Canada. For example, more than 6000 ice ridge and rubble interactions are recorded per year on the piers of the Confederation Bridge [10].

The failure of the ridge as a whole depends on the interlocking forces and friction between ice blocks, the strength of each ice block, and the degree of consolidation between adjacent blocks in the keel [11]. Understanding the properties of each of these parameters is therefore the key to understanding first-year ice ridge properties.

Immediately after the formation of an ice ridge/rubble, ice blocks start to bond together in what are called freeze bonds (Figure 1.2a). Formation of the freeze bonds will eliminate the interlocking forces that exist between the ice blocks prior to bond formation [12]. Freeze bonds initially form as a result of heat transfer from water to ice blocks that are at temperatures colder than surrounding water, which causes freezing at the boundaries between the ice blocks. Once the ice blocks reach thermal equilibrium with the surrounding water, sintering and pressure bonding of asperities are believed to control further bond growth (Figure 1.2b). Sintering is defined as the process of mass transfer between particles, which forms a neck between them (Figure 1.2c). Sintering has been used to explain the

increase in friction at low sliding velocities, where contacting asperities adhere, causing increased friction [13].

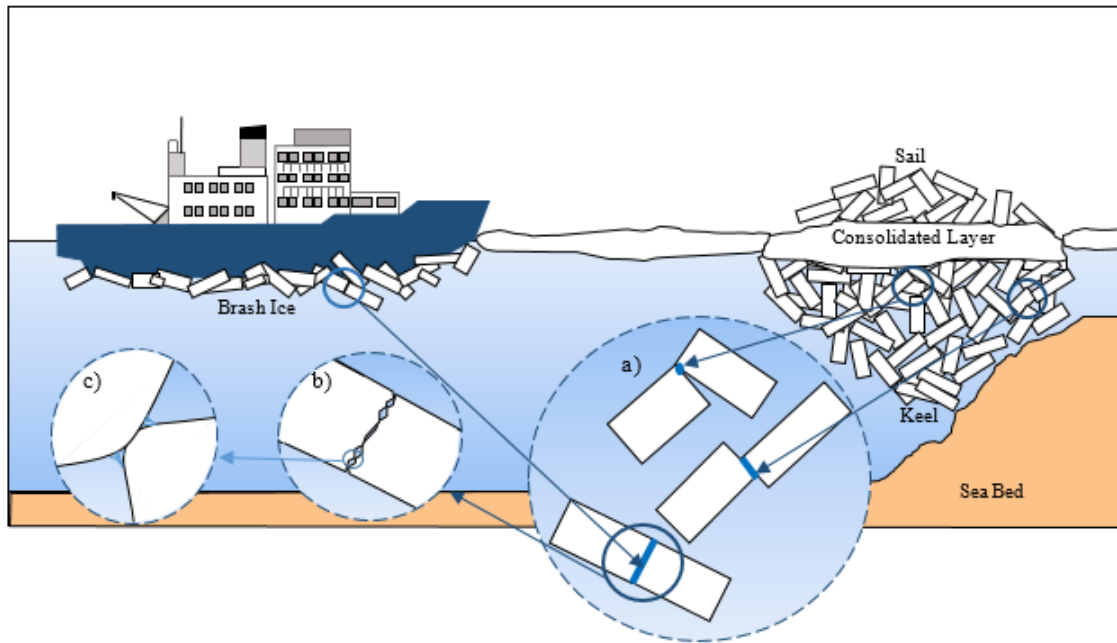


Figure 1.2. Schematic illustration of the multi-scale properties of ice rubble where factors influencing ridge loads are governed by a) freeze bond properties, b) contact conditions at the block interface, and c) sintering and junction growth at the asperity level.

Although an appreciable amount of literature exists on the strength properties of level ice, the processes affecting the strength development and failure of ice ridges and rubble have not been fully understood. Several experimental programs have been conducted in recent years to investigate the strength properties of ice rubble, as well as the strength and failure properties of ice ridges during interactions with structures or gouging events [14-19]. Parameters such as confinement pressure, deformation rate, porosity, and initial ice

temperature have been identified as factors influencing the failure strength of unconsolidated rubble.

To investigate this matter, several studies have been conducted to understand freeze bond strength development and failure between two blocks of ice and the processes affecting them [20–26]. Submersion/contact time, confinement pressure, initial ice temperature and deformation rate are among the parameters studied. A detailed review of these studies has been presented in Chapter 2 of this thesis.

1.2. Objectives and Scope of Research

The main intent of this thesis is to enhance understanding of freeze bond strength development and failure, which directly influences the strength and failure mechanics of ice ridges and rubble. This has been achieved through a series of freeze bond experiments that investigate the strength development and failure of freeze bonds, with focus on the effects of submersion period, and confinement pressure on strength development, as well as deformation rate dependency of freeze bond strength. Having evaluated the existing freeze bond strength studies, the following knowledge gaps were identified:

1. Submersion time or contact period of the bonds is one of the main factors determining freeze bond strength properties that should be studied for a wide range of submersion times. Previous freeze bond research has focused on submersion times ranging from 5 minutes to 60 hours. The strength development of freeze

bonds in prolonged submersion times, as well as the processes involved such as pressure sintering has yet to be studied. Freeze bonds in ice ridges and rubble may be subject to submersion times of the order of days or weeks before an interaction occurs, signifying the importance of understanding strength properties in extended submersion times. Conversely, during ship-ice interactions, freeze bonds will be formed and broken more frequently between brash ice pieces based on the frequency of ship traffic in the area, thus highlighting the importance of understanding bond formation processes for shorter submersion times. Shorter submersion times are also of interest in rubble pile-up events, where newly formed bonds may be constantly broken.

2. Confinements used in previous freeze bond studies are mainly within the range of the confining pressures that are expected to occur through the thickness of an ice ridge as a result of the vertical component of the buoyancy forces (0-4 kPa). The vertical component of the buoyancy force in a ridge keel is a function of the porosity of the ridge, as well as the depth, and is defined as:

$$\sigma_z = (\rho_w - \rho_i)(1 - e)gz_k \quad (1.1)$$

where ρ_w and ρ_i are water and ice density respectively, e is the bulk porosity of the ridge keel, g is the gravitational acceleration, and z_k is the position from the bottom of the keel [4, 20]. Considering a 10 m deep keel, with a porosity of 30%, the maximum global pressures resulting from buoyancy forces can be estimated to be around 7 kPa [27]. Bruneau [4] discusses that confinements between individual blocks of ice in contact can be much higher than the global confinement of the ridge,

depending on the porosity of the ridge and contact area of the ice blocks [4, 28]. As discussed by Bailey [27] for the same keel, considering that only 10% of the ice blocks are in contact, the pressure between each ice block can reach to 70 kPa. It should also be noted that, while the net buoyant forces acting on the keel are in the vertical direction, buoyancy force distributions surrounding the keel assert confinements to the ice blocks in all directions. Considering the buoyancy force only (discarding the porosity and weight of the ridge) as a function of depth, z , ($\rho_w g z$), confining pressures from water acting on the ridge keel can be as high as 100 kPa at a depth of 10 m.

Furthermore, these confinements can be highly intensified during ice ridge-structure interactions and gouging events. Serré [29] for instance has presented cases of highly confined ice ridge during full-scale interaction events between the Norstromsgrund lighthouse, where the ice blocks of the ridge were fused together due to the high pressures applied to them. Buoyant forces also add extra confinement to the incoming ice, which further increase the applied pressure. Understanding the role of higher confining pressures in freeze bond development in different stages of ice ridge formation is therefore an important factor in ridge keel models.

3. The effects of deformation rate on failure of freeze bonds have only been investigated for a limited range of rates, while ice rubble and ridges are subject to a wide range of deformation rates during interactions with structures or ships. Interaction rates of ice ridges with structures are a function of mean drift speed of the floating ridge, which itself is a function of wind, current, and wave speeds.

First-year ice ridge loading events on the Molikpaq for instance recorded drift speeds ranging from 0.1 to 0.75 m/s, with 0.1 m/s as the dominant drift speed [30]. The velocity of ice during ice rubble pile-up events and ice-structure interactions can be within the range of 0.1 to 1.5 m/s as discussed by Schulson [31] and as recorded during rubble pile-up events in the confederation bridge [32]. This highlights the need for a detailed investigation of rate effects of freeze bond failure, as freeze bond failure has been identified as one of the controlling mechanisms of ice ridge and rubble strength and failure [33]. Previous freeze bond studies [8], however, have only studied rate effects for a narrow range of 0.44 mm/s to 0.84 mm/s, which was not wide enough to show any rate dependency of freeze bond strength on deformation rate.

In this context, the main objectives of this thesis can be summarized as the following:

- Address data and knowledge gaps in freeze bond strength development in short submersion times that correspond to rubble formation in brash ice channels.
- Improve understanding and modelling of strength development of freeze bonds in prolonged submersion times and the effects of sintering in bond strength development to simulate freeze bond development in ice ridges.
- Enhance understanding the role of high confinements, which are likely to occur between individual blocks in an ice ridge, and in ice ridge-structure interactions, on freeze bond strength development.

- Rate-dependency of freeze bond failure, which plays an important role in ice rubble structure interactions as well as ice ridge keel gouging, which has been neglected to date.
- Investigate the implications of freeze bond strength on the overall strength and development of ice rubble/ridges.

1.3. Organization of the Thesis

This thesis is written in the manuscript format (paper-based). The organization of the thesis and the papers reporting the results of this research are presented in Table 1.1.

Table 1.1. Organization of the thesis

Chapter	Supporting paper and chapter title
Chapter 1: Introduction	Not applicable
Chapter 2: Literature review	Not applicable
Chapter 3: Submersion time effects	Experimental study of the effect of submersion time on the strength development of freeze bonds, <i>Cold Regions Science and Technology</i> , 2020.

Chapter 4: Confinement pressure effects	Experimental Study of the Effect of Confining Pressure on the Shear Strength of Freeze Bonds in Freshwater Ice, <i>to be submitted</i> .
Chapter 5: Rate-dependency of freeze bond strength	Experimental Investigation of Rate Dependency of Freeze Bond Strength, <i>accepted for publication in the journal of Cold Regions Science and Technology</i> .
Chapter 6: Conclusions and recommendations for future work	Not applicable
Appendix A: Preliminary freeze bond experiments	Experimental study on shear strength of freeze-bonds in freshwater ice, <i>presented at the Arctic Technology Conference, St. John's, Canada, 2016</i> .
Appendix B: Freeze bond field experiments	Field Experiments on Shear Strength of Solid and Freeze-bonded Sea ice, <i>presented at the Arctic Technology Conference, Texas, USA, 2018</i> .

Chapter 2 reviews previous research on the strength properties of ice rubble and ridges, freeze bond formation processes, as well as the strength development between individual ice blocks, and ice at the particle scale.

Chapter 3 discusses the effect of submersion time on the strength development of freeze bonds, describing a series of experiments conducted varying submersion period of freeze bonds from 1 minute to 14 days. Physical mechanisms contributing to strength development with regards to submersion time have been discussed, and an analytical equation has been

presented to estimate freeze bond strength based on the results. Special focus has been paid to the strength development after prolonged submersion times.

Chapter 4 presents the results of a series of tests focusing on the effects of confinement pressure, ranging from 10 to 100 kPa, on the strength of freeze bonds. Tests were performed for four different submersion times, representative of the stages of bond development observed in submersion time tests. The simultaneous effect of submersion time and confinement pressure on freeze bond strength especially at higher confinements and prolong submersion times has been investigated, and similarities with submersion time results have been studied.

Chapter 5 investigates the influence of deformation rate on freeze bond failure and strength, varying the deformation rate from 0.01 to 100 mm/s, in particular highlighting the role of rate-dependency of freeze bond failure on ice ridges/rubble deformation processes.

Chapter 6 provides a summary of the thesis and the main conclusions from this work, as well as recommendations for future work.

Preliminary results of the freeze bond tests presented at the 2016 Arctic Technology Conference have been presented in Appendix A. Appendix B presents the results of solid and freeze bond field experiments conducted in St. Anthony, NL, which aimed to investigate the feasibility of using the freeze bond testing method used in this thesis in field conditions.

1.4. References

- [1] Ø. Harsem, A. Eide, and K. Heen, “Factors influencing future oil and gas prospects in the Arctic,” *Energy policy*, vol. 39, no. 12, pp. 8037–8045, 2011.
- [2] A. Bu uixadé Farré, S.R. Stephenson, L. Chen, M. Czub, Y. Dai, D. Demchev, Y. Efimov, P. Graczyk, H. Grythe, K. Keil and Kivekäs, N., “Commercial Arctic shipping through the Northeast Passage: routes, resources, governance, technology, and infrastructure,” *Polar Geography*, vol. 37, no. 4, pp. 298–324, 2014.
- [3] S. Shafrova and K. V. Høyland, “The freeze-bond strength in first-year ice ridges. Small-scale field and laboratory experiments,” *Cold Regions Science and Technology*, vol. 54, no. 1, pp. 54–71, 2008.
- [4] S. E. Bruneau, “Development of a first-year ridge keel load model,” Memorial University of Newfoundland, 1996.
- [5] L. Zhou, J. Gao, and D. Li, “An engineering method for simulating dynamic interaction of moored ship with first-year ice ridge,” *Ocean Engineering*, vol. 171, pp. 417–428, 2019.
- [6] R. R. Parmerter and M. D. Coon, “Model of pressure ridge formation in sea ice,” *Journal of Geophysical Research*, vol. 77, no. 33, pp. 6565–6575, Nov. 1972.
- [7] T. J. O. Sanderson, *Ice mechanics : risks to offshore structures*. London: Graham & Trotman, 1988.
- [8] R. Ettema and J. A. Schaefer, “Experiments on freeze-bonding between ice blocks in floating ice rubble,” *Journal of Glaciology*, vol. 32, no. 112, pp. 397–403, 1986.
- [9] P. Liferov, “First-year ice ridge scour and some aspects of ice rubble behaviour,” 2005.
- [10] E. Lemee and T. Brown, “Review of ridge failure against the confederation bridge,” *Cold Regions Science and Technology*, vol. 42, no. 1, pp. 1–15, 2005.

- [11] M. A. Hopkins, W. D. Hibler, and G. M. Flato, “On the numerical simulation of the sea ice ridging process,” *Journal of Geophysical Research*, vol. 96, no. C3, p. 4809, 1991.
- [12] E. Kim, “Freeze-bond strength: Analysis of experiments and FE modeling of a shear test on freeze bonds,” PhD thesis, NTNU, Norway, 2009..
- [13] N. Maeno and M. Arakawa, “Adhesion shear theory of ice friction at low sliding velocities, combined with ice sintering,” *Journal of Applied Physics*, vol. 95, no. 1, pp. 134–139, 2004.
- [14] R. Weiss, A. Prodanovic, and K. Wood, “Determination of ice rubble shear properties,” in *Proceedings of the 6th IAHR International Symposium on Ice*, Quebec, Canada, 1981.
- [15] J. Hellmann, “Basic investigations on mush ice,” in *Proceedings of the 7th IAHR International Symposium on Ice*, Hamburg, Germany, 1984.
- [16] E. Bailey, J. Bruce, and R. Taylor, “The Development of Ice Ridge Keel Strengths: The influence of speed on the strength and deformation behaviour of gouging ridge keel,” in *Proceedings of the 22nd IAHR International Symposium on Ice*, Singapore, 2014.
- [17] M. Sayed, “Mechanical properties of model ice rubble,” presented at the Materials and Member Behavior, 1987, pp. 647–659.
- [18] G. E. Urroz and R. Ettema, “Simple-shear box experiments with floating ice rubble,” *Cold Regions Science and Technology*, vol. 14, no. 2, pp. 185–199, 1987.
- [19] Y. Yasunaga, S. Kioka, Y. Matsuo, A. Furuya, and H. Saeki, “The strength of the unconsolidated layer model of ice ridge,” in *Proceedings of the 16th IAHR International Symposium on Ice*, New Zealand, 2002.
- [20] R. Ettema and J. A. Schaefer, “Experiments on freeze-bonding between ice blocks in floating ice rubble,” *Journal of Glaciology*, vol. 32, no. 112, pp. 397–403, 1986.
- [21] H. Helgøy, O. S. Astrup, and K. V. Høyland, “Laboratory work on freeze-bonds in ice rubble, Part II: Results from individual freeze-bond experiments,” in *Proceedings of the 22nd*

- International Conference on Port and Ocean Engineering under Arctic Conditions*, Espoo, Finland, 2013.
- [22] A. H. V. Repetto-Llamazares, “Experimental studies of shear failure on freeze-bonds in saline ice part I: set-up, failure mode and freeze-bond strength.,” *Cold Regions Science and Technology*, vol. 65, no. 3, pp. 286–297, 2011.
- [23] A. H. Repetto-Llamazares, K. V. Høyland, and E. Kim, “Experimental studies on shear failure of freeze-bonds in saline ice:: Part II: Ice–ice friction after failure and failure energy,” *Cold Regions Science and Technology*, vol. 65, no. 3, pp. 298–307, 2011.
- [24] S. Shafrova and K. V. Høyland, “The freeze-bond strength in first-year ice ridges. Small-scale field and laboratory experiments,” *Cold Regions Science and Technology*, vol. 54, no. 1, pp. 54–71, 2008.
- [25] I. M. Bueide and K. V. Høyland, “Confined Compression Tests on Saline and Fresh Freeze-Bonds,” in *Proceedings of the International Conference on Port and Ocean Engineering Under Arctic Conditions*, Trondheim, Norway, 2015.
- [26] K. V. Høyland and A. Møllegaard, “Mechanical behavior of laboratory made freeze-bonds as a function of submersion time, initial ice temperature and sample size,” in *Proceedings of the 22nd IAHR International Symposium on Ice*, Singapore, 2014.
- [27] E. Bailey, R. Taylor, and K. R. Croasdale, “Mechanics of Ice Rubble over Multiple Scales,” in *Proceedings of the 34th International Conference on Ocean, Offshore and Arctic Engineering*, St. John’s, NL, Canada, 2015.
- [28] H. Shayanfar, “An experimental investigation on the strength and failure behavior of freshwater ice rubble,” MSc thesis, Memorial University of Newfoundland, Canada, 2018..
- [29] N. Serré, “Mechanical Properties of Model Ice Ridge Keels,” *Cold Regions Science and Technology*, vol. 67, pp. 89–106, 2011.

- [30] G. W. Timco and R. P. Burden, “An analysis of the shapes of sea ice ridges,” *Cold Regions Science and Technology*, vol. 25, no. 1, pp. 65–77, 1997.
- [31] E. M. Schulson, “The structure and mechanical behavior of ice,” *Jom*, vol. 51, no. 2, pp. 21–27, 1999.
- [32] D. C. Mayne and T. G. Brown, “Rubble pile observations,” in *Proceedings of the 10th International Offshore and Polar Engineering Conference*, Seattle, Washington, USA, 2000.
- [33] P. Liferov and B. Bonnemaire, “Ice rubble behaviour and strength: Part I. Review of testing and interpretation of results,” *Cold Regions Science and Technology*, vol. 41, no. 2, pp. 135–151, Feb. 2005.

2. LITERATURE REVIEW

2.1. Preface

This chapter provides an overview of the previous research conducted on bond strength development and failure of freeze bonds, focusing on bond development in different scales of ice rubble and ridge, block to block contact, and between the asperities and properties affecting it. Data obtained in previous studies have been presented and analyzed, and the knowledge gaps in this area have been identified.

2.2. Chapter Abstract

Ice ridge/rubble strength development and failure, and the mechanisms contributing to strength properties of these features have been of interest in the past few decades for the design of offshore structures and infrastructure in Arctic and sub-Arctic seas, as well as the safety of ships operating in these regions. The strength and failure properties of an ice ridge as a whole depends on the strength of the freeze bonds between the ice blocks, as well as the strength of individual ice blocks [1], each of which are a function of the ridge history, and the failure mode upon deformations. These conditions include the formation period, confinement, initial ice temperature, void ratio, ice blocks size, as well as drift rate and rate of deformation during interactions.

While the mechanical properties of level ice have been widely studied, bond formation processes and how they influence the overall strength of ice ridges/rubble, thus the load they apply to structures during interactions has yet to be fully understood. Research conducted on bond formation processes in different scales of ridges, ice blocks, and ice particles have been reviewed in this chapter. Sections are broken down by ridge scale, starting at full scale, then ice block level and eventually at the particle scale. Based on a thorough review of available literature, gaps in this area of research have been identified.

2.3. Freeze Bonds at Ridge and Rubble Scale

Ice ridges consist of three parts: sail, consolidated layer, and keel (Figure 1.1a). When calculating ice ridge loads, the loads from each part of the ridge (sail, consolidated layer, and keel) are calculated separately and added together to define the overall loads from the ice ridge. The consolidated layer is usually treated as thick level ice with its thickness and flexural and compressive strength defining the amount of load it can apply to a structure. Several ridge keel-structure load analytical models have been developed over the years to estimate the external load applied by first-year ice ridges to structures, considering that ridge keels behave as a cohesive-frictional material (e.g., Mohr-Coulomb and Drucker-Prager models) [2]. Majority of these analytical models such as the work of Dolgoplov et al. [3] are based on the local failure of the ridge [3, 4], while some others consider global failure [5, 6]. In a more comprehensive study, Bruneau [7] developed a new ice ridge load model by conducting a regression analysis of previous ice rubble indentation and shear experiments.

Cohesive-Frictional models have been primarily used in soil mechanics and granular materials, for which it is assumed that the material will fail in shear. Among the cohesive-frictional models, the Mohr-Coulomb model has been widely used in soil mechanics as the failure criterion of rocks and soils. These materials have limited or no tensile strength; as it is the case for ice that has a relatively low tensile strength. Based on the Mohr-Coulomb model, the material will fail when the shear stress, τ , reaches a critical value proportional to the applied normal pressure, σ . This critical shear stress is obtained by the following equation:

$$\tau = c + \sigma \tan \varphi \quad (2.1)$$

where c is the material cohesion and φ is the friction angle. The $\tau - \sigma$ diagram is therefore a line, which is developed based on the Mohr's circles. The material will fail when the largest circle touches the envelope (Figure 2.1).

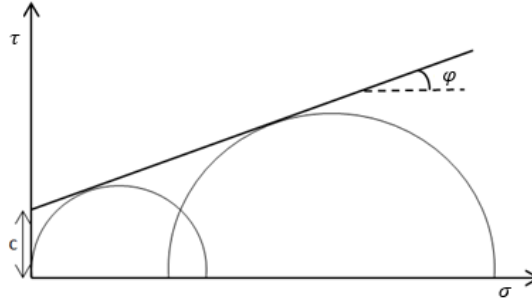


Figure 2.1. Mohr-Coulomb failure hypothesis.

Ice rubble failure, however, is different from rock failure in several respects as discussed by Bailey et al. [8]. Firstly, cohesion in soil and gravel is due to electrostatic attraction, while cohesion in ice rubble is a result of freeze bonds and sintering between the blocks. Secondly, cohesion-frictional models consider that the material fails due to shear while ice rubble can also fail by crushing, tension or a combination of failure modes. Thirdly, these models fail to simulate the volumetric changes of rubble. The volumetric changes (dilation) in rubble occur as the material is expanding continuously due to plastic deformation and increase in higher friction angles during shear [2]. Finally, the cohesion-frictional models do not consider the compaction of material in keels due to hydrostatic pressure. However, the simplicity of Mohr-Coulomb model has made it the material model of choice in many laboratory experiments (small and medium scale tests), in-situ tests, and theoretical models

(numerical simulations). While the Mohr-Coulomb model estimates the shear strength as a function of normal pressure, from an ice mechanics point of view, several parameters affect the overall strength of ice ridges, which are not accounted for in the Mohr-Coulomb model. Parameters that influence strength development of ice rubble and ice ridges include properties such as confinement pressure (stress state), initial ice temperature, consolidation time, ice block properties, porosity, and void ratio, as well as external factors such as water and air temperature, currents, and flow of water between the voids [9]. The failure strength is influenced by the interaction conditions such as the rate of interaction/deformation rate and type of structure (sloped/vertical). Several experimental programs have therefore been undertaken to understand the strength properties of ice rubble for different conditions of formation and deformation. Experimental methods to date include direct shear tests, punch tests, compression, vertical shear, and simple shear. A detailed discussion on the experimental methods used and the results obtained from these studies has been presented in Bruneau [7], and topics that are in relevance to the scope of this thesis are discussed in the next paragraphs.

Direct shear box tests were among the first methods used for the strength measurement of ice rubble [10]. Weiss et al. conducted a series of direct shear box tests on saline ice rubble, investigating the effects of confinement pressure, ice rubble thickness, and deformation rate on the shear strength of unconsolidated ice rubble submerged in saline water [11]. Varying the confinement from 0 to 28 kPa, and the deformation rate from 3 mm/s (defined as slow tests) to 25 mm/s (defined as fast tests), they found the strength to increase with increase in confinement for all deformation rates tested, and slow tests showed a higher

strength in comparison to fast tests. While not studied, the authors note that other parameters which may have influenced the variations in the test data include void ratio, ice rubble thickness, and water and ice salinity. It should also be noted that the ice used to create the rubble for these experiments was used in several tests (stirred well before each test to break any bond that may have formed) before being replaced, which might have influenced the results.

Hellmann [12] investigated ice rubble strength for different types of freshwater ice (fishery, milled ice, and ice chips), sheared under deformation rates of around 1, 10, and 100 mm/s and confined under a normal pressure ranging from 0 to 3 kPa. The failure process of the ice rubble was recognized to follow three phases. Phase 1 is associated with the packing of ice blocks before shear, where the confinement remains constant while the shear force increases. Phase 2, where the peak shear stress is observed, is associated with an increase in both shear and normal pressures as a result of dilation. Results of shear strength-normal stress during this phase, for two deformation rates of 1.6 and 10.9 mm/sec show that in general, strength increases with decrease in deformation rate. For a constant normal stress, strength was found to be about 2 times higher in slower deformation rate compared to higher rates. Further shearing after this phase resulted in friction between the ice blocks, which was described as phase 3. Milled ice showed higher shear forces in general compared to ice chips, and fishery ice had the lowest shear force measurement.

Urroz and Ettema [13] used the simple-shear box method to measure the strength of unconsolidated ice rubble, for three different sizes of freshwater ice blocks. These tests were conducted with shear rates ranging from 0.004 to 0.045 s⁻¹ (1.4 to 15.75 mm/s),

confined under a confinement of 69 kPa. Shear strength showed a general decreasing trend with increase in shear rate and increased with increase in confinement pressure. The shear rate-dependency of strength was believed to be a result of dynamic freeze-bonding of shearing ice blocks, which is expected to be intensified at slower rates. As also observed in a series of slid-hold-slide tests by Schulson and Fortt [14], during slow deformations, ice blocks have more time to fuse together and form new freeze bonds that have to be failed in order to resume sliding. Comparison of the strength values for each ice rubble thickness tested with regards to block size show that while medium ice blocks show higher strength values in comparison to small and large blocks, strain rate has a more pronounced effect on strength in ice rubble with a higher thickness.

Sayed [15] conducted biaxial plane strain tests on dry ice rubble, confined under confinements ranging from 2.45 to 35 kPa, and strain rates ranging from 6.5×10^{-5} to $1.7 \times 10^{-3} \text{ s}^{-1}$. Stress-displacement curves during the failure of ice rubble showed two distinct mechanisms to take place with regards to strain rate. At higher strain rates, the stress curve is accompanied by frequent sharp drops, resulting from local fractures, before reaching the peak stress. Decreasing the strain rate, the number of stress drops decreased, and stress continuously increased as displacement continued. Following the Mohr-Coulomb failure criteria, values were reported with an increasing stress-confinement linear relationship. Comparison of these trendlines for each strain rate tested showed the shear stress to decrease with increase in strain rate.

Yasunaga et al. [16] conducted a series of direct shear tests targeting the effects of deformation rate and confinement on the strength of saline ice rubble subject to a confining

pressure of 1.8 to 11.29 kPa, sheared under a deformation rate of 0.1 to 24 mm/s. Similar to previous studies, shear strength of ice rubble followed a Mohr-Coulomb type of failure, linearly increasing with increase in confinement for all block sizes, and rubble porosities tested. The shear strength of rubble was found to increase with increase in deformation rate up to a deformation rate of 0.1 mm/s, after which the strength gradually decreased. They attribute this deformation rate dependency of shear strength, to the rate dependency of expansion in ice rubble. Investigation of the state of the ice blocks after each test showed that the probability of failure of the ice blocks increased with increase in deformation rate and then became constant. Prodanovic [17] also used the direct shear box method for a 0.3 m deep floating ice rubble confined under confinements ranging from 0 to 3 kPa for two ice sheet thicknesses of 19 and 38 mm. Similar to previous experiments, strength measurement showed the shear strength of the rubble to increase with confinement.

To investigate the effects of consolidation time, Azarnejad and brown [18] conducted a series of punch tests on freshwater ice rubble, for consolidation times varying from 0 to 3 hours, and deformation rates of 9 to 120 mm/s. In contrast to the generally decreasing trend of rate-dependency of strength observed in previous studies, shear strength of ice rubble increased with increase in deformation rate for all consolidation times used in these tests. It should be noted however that the results of longer consolidation times (i.e. 2 and 3 hours) have not been included in the analysis of the results due to adfreeze between the test tank and ice, which may have influenced the results. While consolidation time effects were not implicitly investigated, comparison of the results of shear strength as a function of ice

rubble thickness and speed showed that after 1 hour of consolidation, higher strengths were attained compared to 0 hour for all cases.

In a more extended test program, Shayanfar et al. [10] conducted a series of medium-scale punch tests to investigate the role of consolidation time, as well as confinement pressure on strength development of ice rubble. Ice rubble beams with a thickness of 50 cm were used in all tests, which were deformed at a rate of 5 mm/s. Varying the confinement from 0 to 40 kPa for a submersion period of 4 hours, a general increasing trend of shear strength was observed with increasing confinement. Values of strength were analyzed in terms of both shear and flexural strength of the ice rubble due to the failure modes observed in the experiments. Shear strength was defined as the peak shear force divided by the failure area, which was defined by the failure plane extended over the width of the punch box at the time of failure, and flexural failure was defined using the four-point beam bending equation. Varying the consolidation time from 0 to 70 hours for unconfined ice rubble, the strength of ice rubble was observed to remain almost constant up to 4 hours, where a sudden jump in strength was observed before decreasing again up to reaching 70 hours of consolidation time. Failure of the rubble was seen to switch from shear to a combination of shear and bending after this submersion time. The change in the failure behavior of the rubble the authors believe is a function of freeze-bonding between the ice blocks, which is intensified at longer consolidation times, leading the beam to fail in a solid material nature. While consolidation time highly influenced the strength and specifically failure of the ice rubble beam, confinement was found to have a higher influence on the strength

development of ice rubble in general. This has significant importance in gouging ridges, where higher confinements are expected to occur.

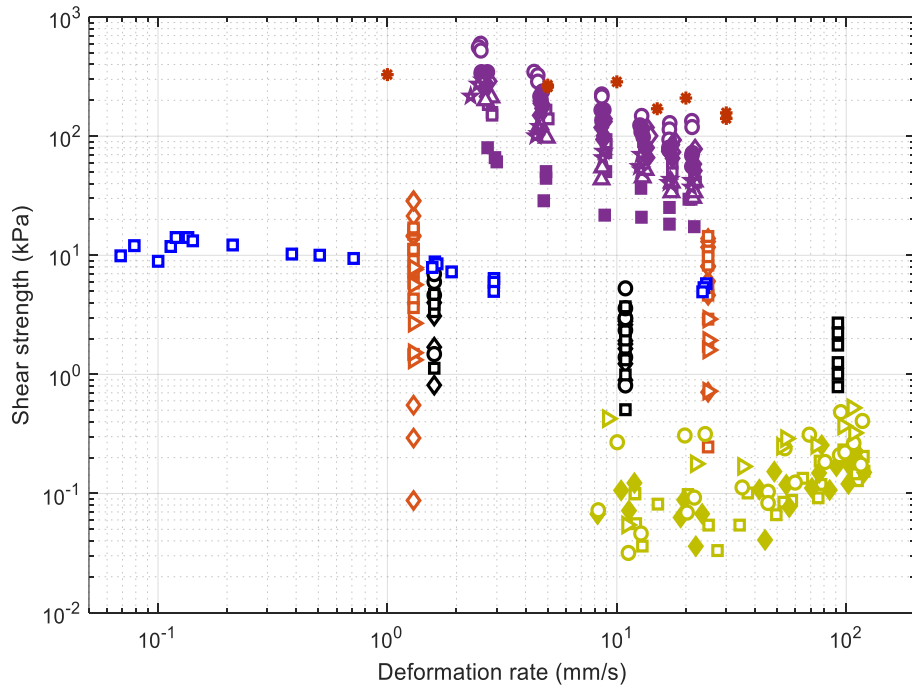
A series of near full-scale keel-gouge tests were conducted during the Development of Ice Ridge Keel Strength (DIRKS) and Pipeline Ice Risk Assessment and Mitigation (PIRAM) programs at C-CORE, studying the effects of initial confining pressure (surcharge load), ice temperature, consolidation time, and shear rate [19–22]. Tests were conducted on ice ridge keels 4 m in length, 3.5 m in width, and 1.7 m in depth, formed in a custom-built frame, where a vertical confinement load was applied to the ridge keel, as a soil tray was sheared horizontally past it. During shear, the surcharge load and velocity as well as the velocity of soil tray were measured. While the majority of the DIRKS tests were conducted for ice with initial temperature of -18°C , one test was conducted for ice with initial temperature of -3°C , where lower peak pressures were measured as expected. Increasing the consolidation time from 20 to 48 hours in these tests, peak pressures increased. This is likely a result of freeze-bonding processes being more pronounced at higher consolidation times. Peak pressures were observed to increase from 123 to 320 kPa as confining pressure increased from 5 to 62 kPa. This the authors attribute to the keel being more compacted into the soil at higher confinements, which in turn increased the contact area between the ice blocks. The increasing contact area results in higher friction angles and promotes freeze bond formation, which in turn increases the load required to shear the keel. Increasing the velocity from 1 to 30 mm/s peak pressures were observed to decrease from 329 to 150 kPa. During the slow deformation of the keel, ice blocks were believed to have more time to reorient and compact, which would increase the strength. Dynamic-freeze bonding was also

considered as one of the processes contributing to the increase in peak pressures at slow rates.

More detailed discussions on laboratory and in-situ ice rubble tests can be found in [2, 14, 15]. Figure 2.2-Figure 2.4 present the results of discussed papers, presenting the shear strength values measured in these experiments as a function of deformation rate, confinement pressure and consolidation time, respectively. Direct comparison of these results is impossible, as tests were performed under different test conditions, geometrical scales, as well as reported in inconsistent formats. Despite these differences, it is evident that most literature has focused on processes affecting the failure of ice rubble (i.e. deformation rate and confinement during failure). The influence of processes involved in the formation and lifetime of ice rubble/ridges, such as consolidation time, and confinement during the formation process are also important to study and should not be neglected.

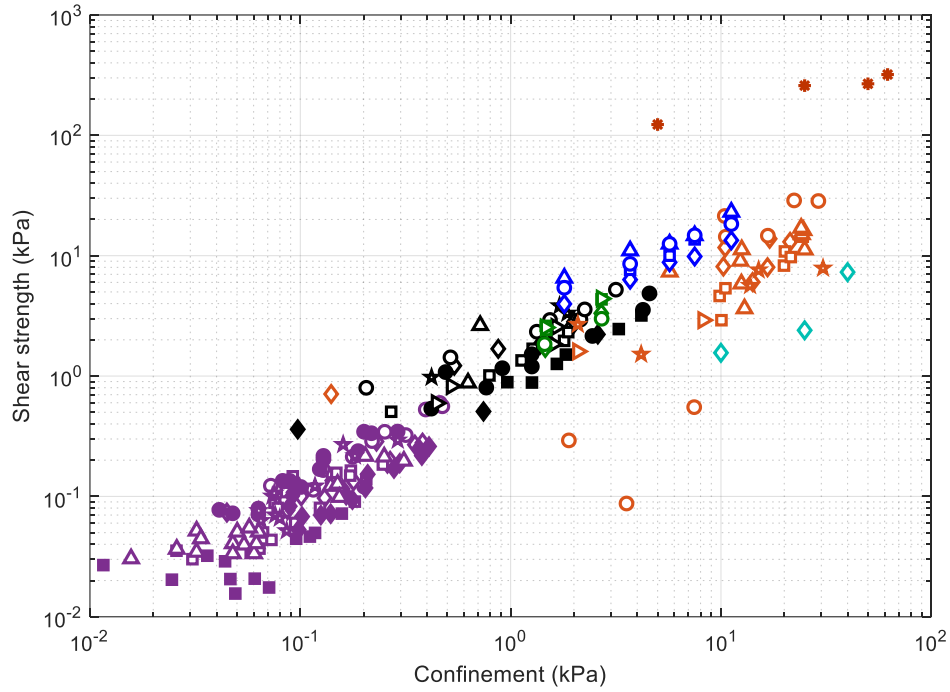
The strength of unconsolidated ice rubble is controlled by a combination of interlocking forces between ice blocks, dimension and size of ice blocks, friction at contact points of the blocks and freeze-bonding between them. Interlocking forces, however, disappear after bond formation, and strength development is primarily controlled by freeze bond formation and strength [1]. Moreover, when ice is subject to high compressive stresses, plastic deformation and crushing of asperities may lead to sintering or junction growth, which is expected to result in stronger bonds due to increase in contact area and therefore stronger rubble and ridges. This signifies the importance of understanding bond formation mechanisms between individual blocks of ice in ice rubble and parameters affecting bond strength, which ultimately contribute to the overall strength of ice rubble/ridge and their

failure behavior. In light of the importance of block to block strength development between ice pieces, which is the main scope of this thesis, section 2.2 reviews the work that has been done to date to understand freeze bond formation and strength development mechanics, as well as failure strength of these features.



◇	Urroz and Ettema (1987), $H_{\text{rubble}}=228$ mm, $\sigma=0-5$ kPa, $\eta=0.23$, Small size blocks	□	Hellman (1984), $H_{\text{rubble}}=70$ cm, Ice chips, tertiary shear mode, $\sigma=0-3$ kPa
○	Urroz and Ettema (1987), $H_{\text{rubble}}=228$ mm, $\sigma=0-5$ kPa, $\eta=0.39$, Medium size blocks	◇	Weiss et al. (1981), $H_{\text{rubble}}=46-91$ cm, $H_{\text{ice sheet}}=200$ mm, $\sigma=0-28$ kPa
□	Urroz and Ettema (1987), $H_{\text{rubble}}=200$ mm, $\sigma=0-5$ kPa, $\eta=0.36$, Large size blocks	◇	Weiss et al. (1981), $H_{\text{rubble}}=91$ cm, $H_{\text{ice sheet}}=150$ mm, $\sigma=0-28$ kPa
◆	Urroz and Ettema (1987), $H_{\text{rubble}}=152$ mm, $\sigma=0-5$ kPa, $\eta=0.31$, Small size blocks	◇	Weiss et al. (1981), $H_{\text{rubble}}=76-86$ cm, $H_{\text{ice sheet}}=80$ mm, $\sigma=0-28$ kPa
●	Urroz and Ettema (1987), $H_{\text{rubble}}=152$ mm, $\sigma=0-5$ kPa, $\eta=0.4$, Medium size blocks	□	Yasunaga et al. (2002), $H_{\text{ice sheet}}=42.5$ mm, $\sigma=6$ kPa, $\eta=0.3$
■	Urroz and Ettema (1987), $H_{\text{rubble}}=133$ mm, $\sigma=0-5$ kPa, $\eta=0.41$, Large size blocks	◇	Azarnejad and Brown (2001), $H_{\text{rubble}}=200$ mm, $t=0,1$ h
△	Urroz and Ettema (1987), $H_{\text{rubble}}=76$ mm, $\sigma=0-5$ kPa, $\eta=0.36$, Small size blocks	◇	Azarnejad and Brown (2001), $H_{\text{rubble}}=300$ mm, $t=0,1$ h
★	Urroz and Ettema (1987), $H_{\text{rubble}}=76$ mm, $\sigma=0-5$ kPa, $\eta=0.4$, Medium size blocks	○	Azarnejad and Brown (2001), $H_{\text{rubble}}=400$ mm, $t=0,1$ h
◇	Hellman (1984), $H_{\text{rubble}}=70$ cm, Ice chips, primary shear mode, $\sigma=0-3$ kPa	◇	Azarnejad and Brown (2001), $H_{\text{rubble}}=500$ mm, $t=0,1$ h
○	Hellman (1984), $H_{\text{rubble}}=70$ cm, Ice chips, secondary shear mode, $\sigma=0-3$ kPa	●	Bailey et al. (2014), $\sigma=25$ kPa, $\eta=0.3$

Figure 2.2. Shear strength of ice rubble as a function of deformation rate, where H_{rubble} is the ice rubble thickness. $H_{\text{ice sheet}}$ is the ice block thickness, η is the rubble porosity, V is the displacement rate, and t is the consolidation time.



◇	Urroz and Ettema (1987), $H_{\text{rubble}}=228$ mm, $V=1.4-15.75$ mm/s, $\eta=0.23$, Small size blocks	◇	Weiss et al. (1981), $H_{\text{rubble}}=46-91$ cm, $H_{\text{ice sheet}}=200$ mm, $V=25$ mm/sec, $\eta=0.39-0.5$
○	Urroz and Ettema (1987), $H_{\text{rubble}}=228$ mm, $V=1.4-15.75$ mm/s, $\eta=0.39$, Medium size blocks	○	Weiss et al. (1981), $H_{\text{rubble}}=46-91$ cm, $H_{\text{ice sheet}}=200$ mm, $V=1$ mm/sec, $\eta=0.39-0.5$
□	Urroz and Ettema (1987), $H_{\text{rubble}}=200$ mm, $V=1.4-15.75$ mm/s, $\eta=0.36$, Large size blocks	□	Weiss et al. (1981), $H_{\text{rubble}}=91$ cm, $H_{\text{ice sheet}}=150$ mm, $V=25$ mm/sec, $\eta=0.28-0.36$
◇	Urroz and Ettema (1987), $H_{\text{rubble}}=152$ mm, $V=1.4-15.75$ mm/s, $\eta=0.31$, Small size blocks	◇	Weiss et al. (1981), $H_{\text{rubble}}=91$ cm, $H_{\text{ice sheet}}=150$ mm, $V=1$ mm/sec, $\eta=0.28-0.36$
●	Urroz and Ettema (1987), $H_{\text{rubble}}=152$ mm, $V=1.4-15.75$ mm/s, $\eta=0.4$, Medium size blocks	◇	Weiss et al. (1981), $H_{\text{rubble}}=76-86$ cm, $H_{\text{ice sheet}}=80$ mm, $V=25$ mm/sec, $\eta=0.19-0.36$
■	Urroz and Ettema (1987), $H_{\text{rubble}}=133$ mm, $V=1.4-15.75$ mm/s, $\eta=0.41$, Large size blocks	★	Weiss et al. (1981), $H_{\text{rubble}}=76-86$ cm, $H_{\text{ice sheet}}=80$ mm, $V=1$ mm/s, $\eta=0.19-0.36$
△	Urroz and Ettema (1987), $H_{\text{rubble}}=76$ mm, $V=1.4-15.75$ mm/s, $\eta=0.36$, Small size blocks	◇	Prodanovic (1979), $H_{\text{rubble}}=30$ cm, $H_{\text{ice sheet}}=19$ mm, coarse rubble
★	Urroz and Ettema (1987), $H_{\text{rubble}}=76$ mm, $V=1.4-15.75$ mm/s, $\eta=0.4$, Medium size blocks	◇	Prodanovic (1979), $H_{\text{rubble}}=30$ cm, $H_{\text{ice sheet}}=19$ mm, repacked rubble
◇	Hellman (1984), $H_{\text{rubble}}=70$ cm, Ice chips, primary shear mode	□	Prodanovic (1979), $H_{\text{rubble}}=30$ cm, $H_{\text{ice sheet}}=38$ mm, coarse rubble
○	Hellman (1984), $H_{\text{rubble}}=70$ cm, Ice chips, secondary shear mode	◇	Prodanovic (1979), $H_{\text{rubble}}=30$ cm, $H_{\text{ice sheet}}=38$ mm, repacked rubble
□	Hellman (1984), $H_{\text{rubble}}=70$ cm, Ice chips, tertiary shear mode	◇	Shayanfar et al. (2019), $H_{\text{rubble}}=50$ cm, $\eta=0.3-0.4$, $V=5$ mm/s, $t=4$ hrs
◆	Hellman (1984), $H_{\text{rubble}}=70$ cm, Fishery ice, primary shear mode	◇	Yasunaga et al. (2002), $H_{\text{ice sheet}}=22.5$ mm, $\eta=0.31$, $V=1.6$ mm/s
●	Hellman (1984), $H_{\text{rubble}}=70$ cm, Fishery ice, secondary shear mode	□	Yasunaga et al. (2002), $H_{\text{ice sheet}}=42.5$ mm, $\eta=0.34$, $V=1.6$ mm/s
■	Hellman (1984), $H_{\text{rubble}}=70$ cm, Fishery ice, tertiary shear mode	◇	Yasunaga et al. (2002), $H_{\text{ice sheet}}=65$ mm, $\eta=0.37$, $V=1.6$ mm/s
△	Hellman (1984), $H_{\text{rubble}}=70$ cm, Milled ice, primary shear mode	◇	Yasunaga et al. (2002), $H_{\text{ice sheet}}=42.5$ mm, $\eta=0.29$, $V=1.6$ mm/s
★	Hellman (1984), $H_{\text{rubble}}=70$ cm, Milled ice, secondary shear mode	★	Bailey et al. (2014), $\eta=0.3$, $V=5$ mm/s
▽	Hellman (1984), $H_{\text{rubble}}=70$ cm, Milled ice, tertiary shear mode		

Figure 2.3. Shear strength of ice rubble as a function of confinement, where H_{rubble} is the ice rubble thickness, $H_{\text{ice sheet}}$ is the ice block thickness, η is the rubble porosity, V is the displacement rate, and t is the consolidation time.

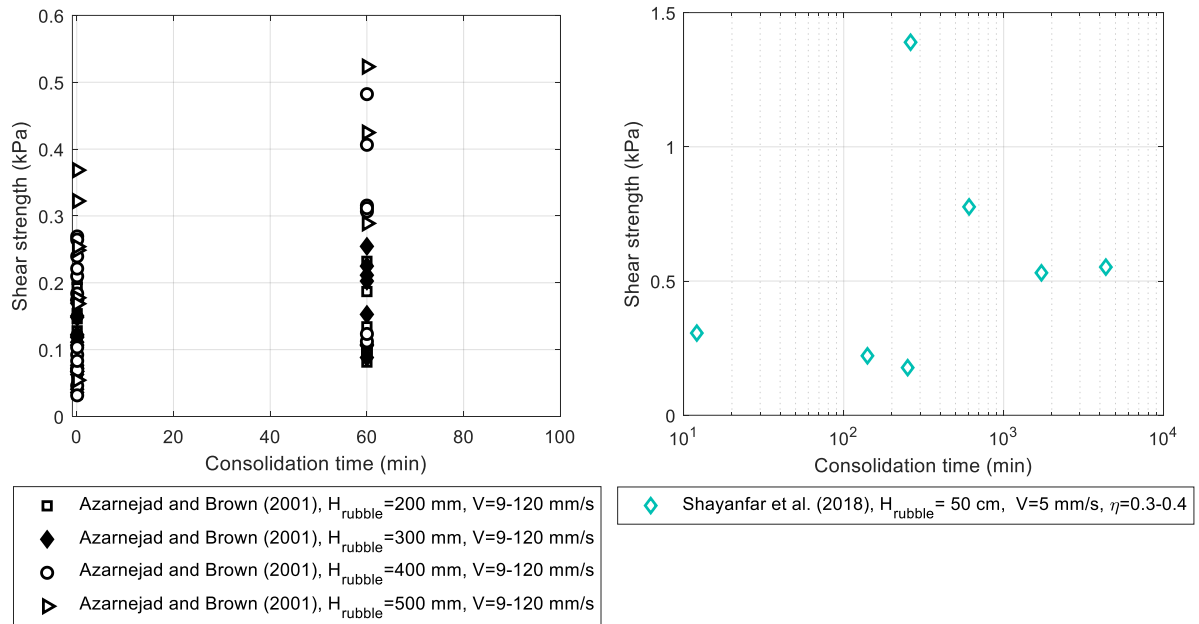


Figure 2.4. Shear strength of ice rubble as a function of consolidation time, where H_{rubble} is the ice rubble thickness, η is the rubble porosity, V is the displacement rate.

2.4. Freeze Bonds at Block Scale

Experiments have been carried out in recent years to measure the strength development and failure of the freeze bonds formed between ice blocks [1, 16-21]. In general, for these experiments, the freeze bond is formed at the interface of two contacting ice blocks, subject to a specific confining pressure or force, which are submerged/in contact for a specified period of time. The bond is subsequently sheared, and the failure stress is used to calculate the shear strength. Figure 2.5 shows a schematic illustration of the methods and set-ups used in these experiments, which include the 45° cut method (Figure 2.5a), the direct shear method (both horizontally and vertically oriented) (Figure 2.5b), and the Asymmetric Four-

Point Bending method (Figure 2.5c). While Section 3.4 provides a detailed discussion on previous freeze bond experiments, specifically effects of submersion time, a review of each of these methods and results obtained are given in the subsequent paragraphs.

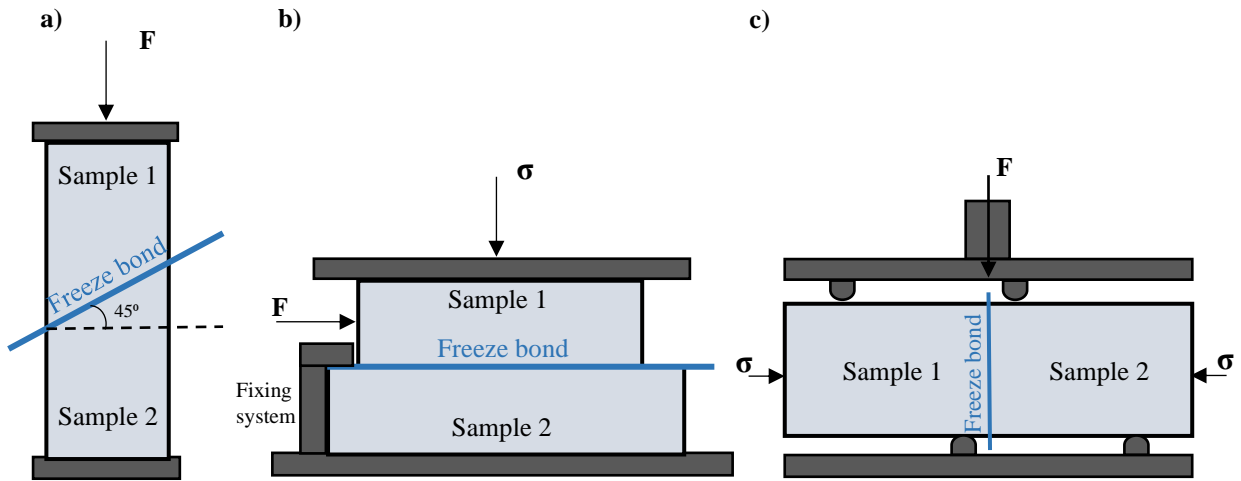


Figure 2.5. Schematic illustration of test set-ups used in previous freeze bond studies showing the 45° method (a), direct shear method (b), and Asymmetric Four-Point Bending (AFPB) method (c).

Direct shear methodology was used by Ettema and Schaefer [25], Repetto-Llamazares et al. [27], and Helgøy et al. [28]. In a series of freeze bond tests, submerged in different submersion liquids (for periods of 0 to 4 minutes), Ettema and Schaefer [25] showed the freeze bond strength to increase linearly with increasing contact period. Three nominal contact areas of 4.52×10^{-3} , 9.03×10^{-3} , $19.35 \times 10^{-3} \text{ m}^2$ were used. Samples that were submerged in water showed higher strength values compared to samples that were in contact in air. They observed a linear increase in strength when the normal pressure was increased from 0.2 to 2 kPa. The increase of strength with increase in normal pressure was found to be more pronounced for larger ice blocks compared to smaller blocks. This

may be because under increasing pressure more water is squeezed out from the void spaces at the contact interface. Also, larger blocks have higher contact area and cold reserves, allowing a stronger bond to be formed. These authors found the rate of deformation to have no effect on strength. However, this might be because the range of deformation rates used were not sufficient to show any effect (0.44 mm/s and 0.84 mm/s).

Repetto-Llamazares et al. [27] conducted a series of freeze bond tests on rectangular saline ice with dimensions of 160 by 160 mm and a thickness of 31 to 34 mm, investigating the effects of confinement, varying from 0.125 to 2 kPa, and submersion time varying from 1 to 1200 minutes for ice with initial temperature of -1 to -14°C. The displacement rate used for shearing the freeze bond was kept constant at 0.7 mm/s throughout the test program. Results from these tests showed that freeze bond strength, calculated by dividing the peak loads by nominal contact area, increased linearly with confinement, ranging from 0.2 to 195 kPa. Similar to the hypothesis of Shafrova and Høyland [1], shear strength-submersion time data followed a bell-shaped curve, where the strength initially increased with submersion time, reaching a maximum of about 20 kPa after five minutes and then gradually decreased to a constant value of 5 kPa after about 5 hours. The observed strength-submersion curve was believed to be dominated by three separate mechanisms, which have been fully discussed in Section 3.4.

Helgøy et al. [28] also used the direct shear method to study the influence of properties such as contact surface, crystal orientation, and salinity on the strength development of freeze bonds. Samples, with freeze bond contact area of 2.4×10^{-3} , 19.6×10^{-3} m², were

submerged for 10 minutes, confined under a normal pressure of 1.9 kPa and were sheared at a displacement rate of 2 mm/s. The freeze bond strengths measured varied from 1.9 to 118.3 kPa with the strongest bonds formed between two natural surfaces and the weakest between two sawn surfaces. Studying the crystal orientation of the blocks, they observed that higher freeze bond strengths were measured when the crystal columns were perpendicular to the freeze bond surface (i.e. horizontal blocks), and the lowest when the crystal columns were parallel to the freeze-bonded surface (i.e. vertical blocks). They believed this was because when brine channels were aligned normal to the freeze bond surface, brine drainage increased, which in turn caused the freeze bond strength to increase. High salinity ice samples, which contained many brine channels and voids (making them visually opaque), were found to have stronger freeze bond strengths than the visually transparent, lower salinity ice blocks. They attributed this to the permeability of the ice blocks. More saline ice is more permeable, allowing high salinity brine to drain away from the freeze bond interface. Their observations, however, were in contrast with Shafrova and Høyland [1] and Bueide and Høyland [30] where lower salinity ice resulted in higher strength in freeze bonds. This they believed was a result of differences in the physical properties of ice blocks (opaque vs. transparent ice) used in these experiments. The time-temperature history of blocks prior to being set to the testing temperature was found to have no effect on the freeze bond strength, meaning that storing the samples in a colder temperature and reheating them to the desired temperature (in this case storing them at -20°C and then at -7°C for testing) before testing at the desired temperature does not have any effect on freeze bond strength. Assembling the samples in water resulted in higher freeze bond strengths compared to the ones assembled in air. Analysis of the bonded area

showed that for samples assembled in air, the bonded area was limited to the edges of the sample (~37% of the total freeze bond contact area). Conversely, for samples that were assembled in water, the total freeze-bond contact area was bonded. Similar to the observations of Ettema and Schaefer [25], they found no notable change in strength as the deformation rate was varied from 1 mm/s to 10 mm/s.

Marchenko and Chenot [26] conducted field experiments in the Barents Sea to study the formation and strength of freeze bonds in air using the direct shear method on vertically oriented ice samples. To conduct the tests, 10-15 cm diameter ice cores were sectioned into 3-4 cm thick disks. These disks were then positioned on a large plate of ice and were left for a few days to bond together. The bonded ice blocks were then cut out from the large plate and the bond was sheared vertically in direct shear using a portable uniaxial compression rig. Results showed that the shear strength of the freeze bonds increased from 2 to 70 kPa as the air temperature decreased from -2 to -15°C. For the submerged tests, pairs of ice disks with similar dimensions to the freeze bond tests in air were submerged and held in contact by a string. It was found that after 2 days, none of the ice disks had bonded. They suggested that this was due to high oceanic heat fluxes measured during the tests. Similar to these tests, in a series of laboratory experiments, pairs of ice cores were submerged in cold water with a 1 mm gap between them in order to monitor the freeze bond formation process. To investigate the influence of water turbulence on the rate of bond growth, water was constantly mixed during the submersion period of the ice blocks using a drill in some experiments. It was observed that the increased water turbulence sped up the freeze bond formation process. This was attributed to the increase in the rate of the

transfer of cold reserves from ice to water as water was mixed. This was confirmed by the temperature profile of the samples, where samples in experiments with mixing reached water temperature faster.

Shafrova and Høyland [1], Høyland and Møllegaard [29] and Bueide and Høyland [30] used the 45° cut methodology, where ice samples were cut in half at a 45° angle (Figure 2.5a). The cut samples were then paired together and submerged to form the freeze bond, which was then broken using the uniaxial compression rig. Using this method, the freeze bond is located at a 45° angle to the direction of loading (i.e. the maximum shear plane). Shafrova and Høyland [1] conducted field and laboratory experiments on level ice and freeze-bonded ice samples. To conduct the field experiments, an opening was cut in the ice cover and six cubical ice specimens, 24 cm in length, were cut out. Half the cubes were used for the freeze bond tests, for which the samples were cut in half at a 45° angle to form the freeze bond interface, and the rest were kept for level ice tests. These samples were then submerged underwater for a period of 48 hours before shearing the bond using a uniaxial compression rig that was set to a nominal strain rate of 10^{-3} s^{-1} . Strength of the freeze bonds in these field tests varied from 14-73 kPa, and submerged level ice was on average 33 times stronger than the freeze-bonded ice. Laboratory tests in this test program included freeze bond tests on sea ice samples that were brought back from the field, laboratory-made saline ice and freshwater ice using a similar setup as the field. For these tests, however, a normal confinement of 0.25 to 0.6 kPa was applied to the samples during freeze bond formation. Higher freeze bond strengths were measured in the laboratory tests in comparison to the field tests (15-197 kPa compared to 14-73 kPa), which they attributed to the effects of

confinement. They, however, reported that differences in confinement did not affect the strength and therefore no distinction on the amount of applied confinement was made in reported values. Their results also showed that initially colder, less saline ice resulted in higher freeze bond strength.

Høyland and Møllegaard [29] performed two sets of freeze bond experiments on laboratory-grown saline ice. In the first set of experiments, the effect of submersion time on the strength of freeze bonds was investigated with no normal pressure applied to the samples, where shear strength decreased from 1583 to 42 kPa as submersion time increased from 0.5 minutes to 20 hours. Freeze bond strength was also higher for ice blocks with colder initial temperature. Samples submerged at the lower submersion times failed in the ice rather than freeze bond, and the strength values measured correspond to the failure of ice rather than freeze bond. In the second set of experiments, two large blocks of ice with dimensions of 0.4×0.4 m were put together and were submerged for 23 hours. These samples were then cut into 16 smaller freeze-bonded samples and were tested using the direct shear method with a deformation rate of 0.01 mm/s. They observed that the freeze bond was stronger for the samples that were removed from the edges of the big block, which were more exposed to the surrounding water.

Bueide and Høyland [30] used the methodology of Høyland and Møllegaard [29] to measure the strength of the bond between freshwater and saline ice. Two initial ice temperatures of -2.5 and -8.5°C were used for samples that were submerged for 0.5 to 1200 minutes, and were sheared at a deformation rate of 0.8 mm/s. A radial confinement of 7 to 99 kPa was applied during shear and no confinement was applied during submersion of the

samples. Shear strength-submersion time results followed a bell-shaped curve similar to the observations of Repetto-Llamazares et al. [27]. Freshwater samples were observed to reach the peak strength at a lower submersion time compared to saline samples, which was attributed to the lower porosity of freshwater samples. Similar to previous studies, they observed that colder samples had higher peak strength values. Using the Mohr-Coulomb criteria they measured the cohesion and friction angles and observed that saline samples had a lower cohesion but higher friction angle compared to freshwater samples. Lower initial ice temperatures also resulted in higher cohesion values compared to higher initial temperatures.

The asymmetric four-point bending (AFPB) method was used at C-CORE [31] to measure the strength of freshwater freeze bonds between two rectangular ice samples (with dimensions 175×100×50 mm) with an initial temperature of -11°C under different submersion times and confinements, sheared under a constant deformation rate of 0.44 mm/s. Samples were held in place using a wooden support stand and dead weights that were used to apply the confinement. Varying the confinement from 20 to 79 kPa for 60 minutes of submersion, they observed a linear increase in freeze bond strength from 50 to 120 kPa. Increasing the submersion time from 10 to 3945 minutes, under a constant confinement of 40 kPa, bond strength increased from 30 kPa, reaching a maximum of 170 kPa after 3 hours of submersion before decreasing to 34 kPa after 3945 minutes of submersion. A series of solid shear tests were also conducted in this test program, where solid samples with an initial temperature of -11°C were submerged for 0 to 265 minutes and then sheared. Strength measurements of solid samples showed a decreasing trend of

strength as submersion time increased, where the strength rapidly decreased from 1107 kPa to 350 kPa in the first 40 minutes of submersion, and then remained constant.

All data that is readily available in the literature has been plotted as a function of submersion time, confinement pressure and deformation rate in Figure 2.6, Figure 2.7, and Figure 2.8, respectively. The general trend of the overall strength data points with regards to submersion time presented in Figure 2.6 follows the bell-shaped curve suggested by Shafrova and Hoyland [1], which was observed for saline ice tests of Repetto-Llamazares et al. [27], and both freshwater and saline tests of Bueide and Høyland [30]. In both figures, strength initially increases as a result of heat transfer from water to ice and then decreases as ice equilibrates with the temperature of the submersion liquid. Confinement pressure (Figure 2.7) has a continuous increasing trend for all test cases, which has been linked to the Mohr-Coulomb failure criteria [27]. And finally, while deformation rate effects and rate dependency of freeze bond failure have been introduced as one of the controlling mechanisms of ice rubble failure [32], the only data available investigating this matter does not show any rate dependency in freeze bond strength (Figure 2.8) [25]. This, however, may be a result of the low range of deformation rates used in these tests. Further testing is therefore needed to investigate rate effects in freeze bond strength.

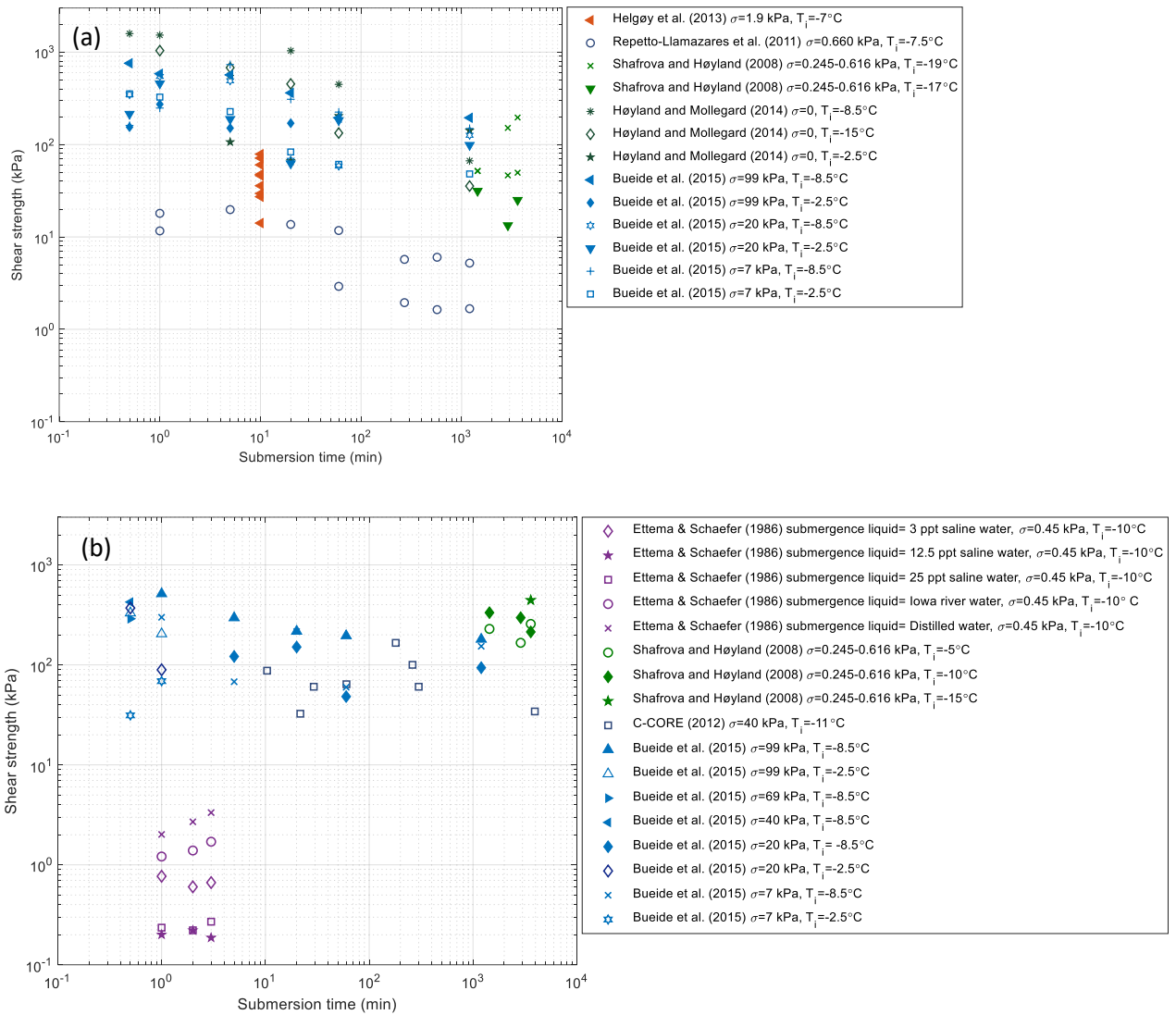


Figure 2.6. Plot showing the measured shear strength values versus submersion time in previous freeze bond experiments for a) saline ice, and b) freshwater ice, where T_i is the initial temperature of ice and σ is confinement pressure.

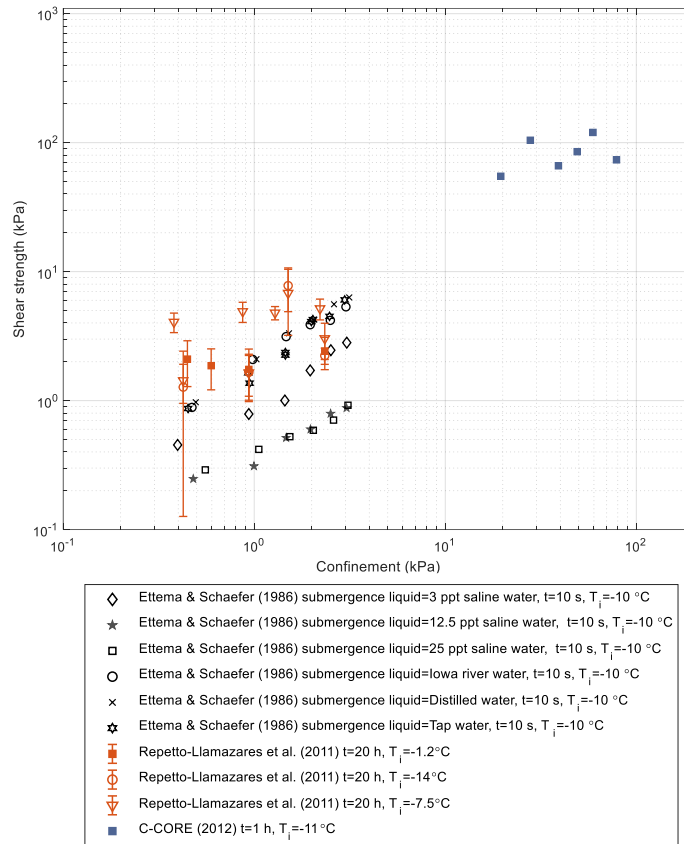


Figure 2.7. Plot showing the measured shear strength values versus confinement in previous freeze bond experiments. In this plot T_i is the initial temperature of ice and t is the submersion time.

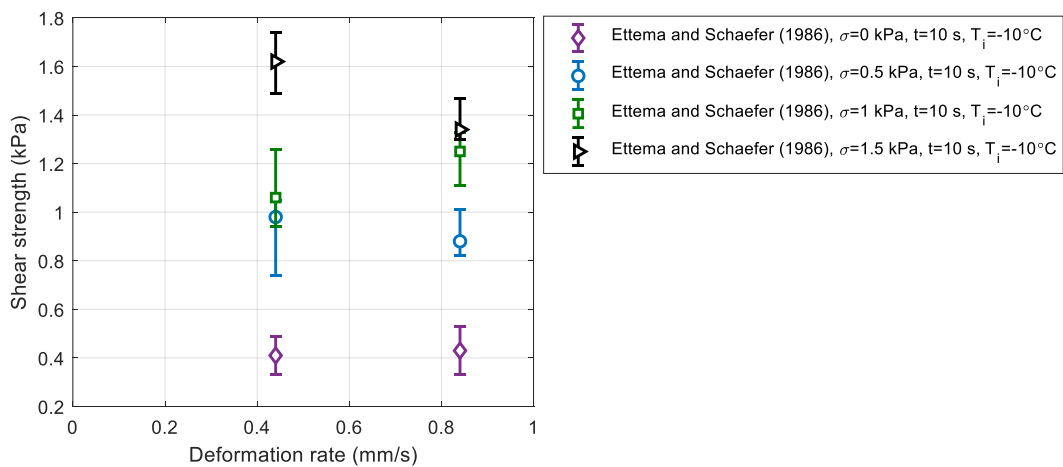


Figure 2.8. Plot showing the measured shear strength values versus deformation rate in previous freeze bond experiments. In this plot σ is confinement pressure, T_i is the initial temperature of ice and t is the submersion time.

While excellent progress has been made in these experiments to advance the knowledge of freeze bond strength development and failure, there are still areas that require further investigation. Firstly, up to present very little work has been done focusing on freshwater ice. This is principally due to the application to Arctic shipping and offshore oil and gas interests. Nonetheless, also important are applications in freshwater and low salinity environments, where rubble is a direct hazards, such as determining rubble loads on wind farms in Lake Erie, ice-jam flooding in rivers, brash ice buildup in shipping lanes (Gulf of Ob), and seabed scouring in the North Caspian Sea. Secondly, more work is needed to understand the role that pressure has on the strength of freeze bonds. Confinement pressures presented in literature are mostly limited to less than 4 kPa, which is within the range of global buoyancy forces in a keel. However, as discussed in Chapter 1, local contact pressures between contacting ice blocks could be much higher, especially in grounded or gouging ridges [8]. Thirdly, freeze bond strength development processes over extended submersion times need investigation, as ice ridges/rubble are usually formed for weeks or months before an interaction occurs. And finally, while rate dependency of freeze bond strength has been identified as one of the controlling processes in ice rubble/ridge failure, little data exists on freeze bond strength properties with regards to deformation rate. More tests are therefore required to fully investigate the effects of deformation rate on freeze bond failure and common links to the overall failure of ice rubble/ridges.

2.5. Freeze Bonds at Particle Scale

Freeze-bonding initially starts as a result of heat transfer from water to colder ice blocks. However, ice blocks ultimately reach near melting point temperatures at greater submersion times. Near melting point temperature of the ice throughout the keel in prolonged submersion times, as well as increased pressures applied to individual freeze bonds, give rise to slow bond formation processes such as pressure sintering, creep and recrystallization between asperities and ice particles at the contact interface [7]. (Figure 1.2b,c). Sintering and creep processes have been introduced in the literature as the responsible mechanisms for bonding of ice particles and asperities in contact [33].

One of the very first theories on the adhesion of ice particles was presented by Faraday [34], who suggested the existence of a liquid-like layer on the surface of the ice. Based on his theory, when two pieces of ice are brought into contact, this layer (that is in equilibrium with the surrounding environment) solidifies and forms a solid bond. Thomson [35] introduced the idea of pressure melting on the contact surface. He suggested that when any two pieces of ice are in contact, a certain amount of pressure would be applied at the contact interface, whether an external pressure is applied or not, causing a reduction in the melting temperature. This lower melting temperature induces melting at the contact interface, which would re-freeze when the pressure is relieved. Hobbs and Mason [36] discounted this theory on the basis that pressure melting fails to explain the possibility of skiing at a temperature of -20°C , since the pressure generated during skiing would not be sufficient to cause melting. More recently, sintering and creep processes were introduced as the responsible mechanism of bond formation between ice particles near melting point

especially in air, which was first addressed by Kingery [37] and Kuroiwa [30, 28]. In metallurgy, sintering is defined as the process by which powder particles adhere to each other via mass transfer. Based on Kingery's theory, when two ice spheres are pushed together, a neck is formed between the two contacting particles, and the area of contact will grow with time, even if the initial pressure is removed.

Kingery [37] introduced four mechanisms by which the material will move along the neck:

- 1- Viscous and plastic flow of material due to surface tension forces.
- 2- Evaporation of material from convex surfaces and its transfer through the environment, and condensation into the concave neck.
- 3- Volume diffusion, which is a result of local lattice vacancies that arise from loss of pressure produced by the surface tension forces at the neck.
- 4- Surface diffusion, resulting from the difference in concentration of adsorbed molecules existing at the neck and rest of the system, which is again produced by surface tension forces.

The dominant mechanism of sintering depends on several conditions, for instance, whether liquid is present or whether an external pressure is applied. The general sintering equation without the presence of liquid is defined as:

$$\left(\frac{x}{R}\right)^q = \frac{C(T)}{R^p} t \quad (2.2)$$

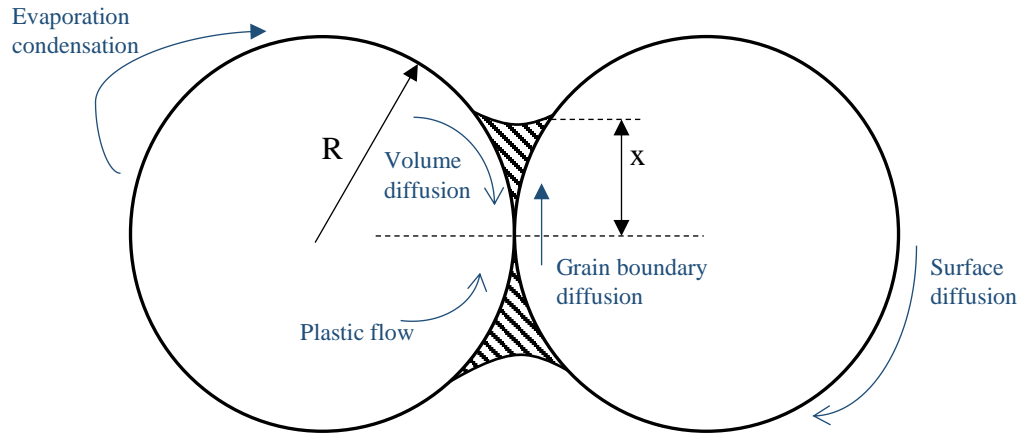


Figure 2.9. The geometry of sintered ice particles and sintering mechanisms (after [33]).

where $C(T)$ is a temperature-dependent parameter, x is the radius of the neck, R is the radius of spheres as shown in Figure 2.9, and q and p are defined based on the dominant sintering mechanism. Kuczynski [39] defined the values of q and p for each mechanism as the amounts presented below.

Table 2.1. Sintering constant values for each dominant mechanism [39].

Mechanism	q	P
volume diffusion	5	3
viscous or plastic flow of solid	2	1
surface diffusion	7	4
evaporation-condensation	3	2

Maeno and Ebinuma [40] indicate that sintering in ice is not driven by a single mechanism, and at least six parameters affect sintering simultaneously. These mechanisms include vapor diffusion, surface diffusion, surface flow, volume diffusion, plastic flow, and grain

boundary diffusion. Sintering mechanism diagrams were therefore introduced by Swinkels and Ashby [41] for pressureless sintering of two ice spheres in order to recognize the dominant sintering mechanism for different conditions. With the application of an external pressure, which is the case for asperities on contacting ice blocks in an ice rubble structure, more complicated processes come into effect, as processes such as diffusional creep, dislocation creep, and grain boundary sliding are introduced. While sintering has been mostly studied for spherical particles of ice in contact, pressure sintering and its effects coupled with creep and plastic flow, have been used in terms of the power-law creep equation (Equation 2.3) to explain adhesion and friction of ice [34–36].

Szabo and Schneebeli [44] used the power-law creep equation to measure the sub-second (10- 1000 ms) sintering between two ice cones with a 3 mm tip radius that were pushed together under a normal load ranging from 0 to 8 N. Based on their experiments, when applied normal stresses are relatively high, ice undergoes a plastic deformation, which would increase the contact area. The rate of this deformation was shown to be highly affected by the amount of applied confinement, contact time, as well as temperature, increasing with increase in pressure and contact time, as well as higher temperatures.

Using the power-law creep equation, the amount of strain rate as the ice cones are pushed together can be calculated by:

$$\dot{\epsilon}_{creep} = A\sigma^n = B\sigma^n \exp\left(-\frac{\epsilon}{kT}\right) \quad (2.3)$$

where B and n are constants, σ is the applied normal stress, ϵ is the activation energy, k is Boltzmann's constant and T is the absolute temperature. Assuming the amount of decrease

in the length of the samples due to creep (calculated from $\dot{\epsilon}_{creep}$) will be equal to the increase in the radius of the contact interface, the time-dependent radius increase has been calculated by Equation 2.4.

$$a(t) = \sqrt{R_{tip}^2 - (\sqrt{R_{tip}^2 - a_0^2} - \dot{\epsilon}_{creep} l_0 t)^2} \quad (2.4)$$

where R_{tip} is the initial radius of the tip of the ice cones, a_0 is the instantaneous radius of contact and l_0 is assumed 3 mm. The sintering force is then calculated using this radius and assuming a constant tensile strength for all conditions using Equation 2.5.

$$F_{sintering}(t) = \sigma_{tensile} \pi a(t)^2 \quad (2.5)$$

Maeno and Arakawa [42] formulated the static ice-ice friction coefficient taking into account the effects of sintering and junction growth at the contact interface. According to their theory, the friction coefficient is expressed as:

$$\mu = L \frac{\tau}{\sigma} \quad (2.6)$$

where τ is the shear stress, σ is the normal stress and L is a constant called sintering factor (L), which itself depends on the dominant sintering mechanism (q, p), radius of contact area of asperity (r), asperity radius (R), and sliding velocity (v) and is expressed as:

$$L = [1 + 2C \left(\frac{r}{R}\right)^{1-q} \frac{R^{1-p}}{v}]^{2/q} \quad (2.7)$$

Due to this effect, higher forces would be required to initiate sliding between ice pieces in contact especially at higher temperatures and lower sliding velocities. Lower sliding

velocities will provide a greater period of time for new bonds to form during sliding, as a result increasing the required force to initiate sliding.

In a series of friction tests, Schulson [43] and Schulson and Fortt [14] measured the static and kinetic friction of ice in a series of double-shear experiments. Stress curves showed that ice surface stress to reach a maximum, τ_{max} , followed by a sudden drop when sliding initiated. The static friction angle, μ_s , was described as the ratio of this maximum stress to the applied normal stress. Their results showed that up to a threshold contact time, there was no change in μ_s with increase in contact time. After this threshold, μ_s increased logarithmically as a function of contact time. This they attributed to static strengthening, which takes place as a result of sintering and creep of asperities, forming stronger bonds between the particles. Assuming a fixed number of asperities in contact, the shear resistance to sliding increases as the contact area of asperities increases, and the height of them decreases due to creep (Figure 2.10). To conserve the volume of asperities, the rate of increase in area should be equal to decrease in height (which is equal to the creep rate, $\dot{\epsilon}$). The power-law creep equation described earlier was used to define this height shortening. This area can was later used to define the friction coefficient. However, the authors note that cohesion should also be taken into account in static friction as a part of bond properties. In a series of double shear laboratory scale and ice tank scale friction tests, Lishman et al. [45] observed similar increasing trend of static friction as hold time increased from 1 to 1000 s. While detailed consideration of friction is beyond the scope of present work, increasing trends of static friction observed in these tests, highlight the effects of bonding processes on the mechanical properties of ice-ice contact interface.

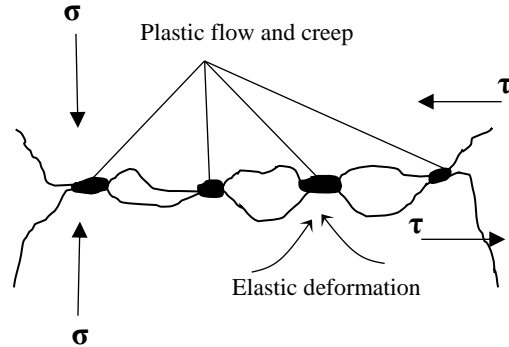


Figure 2.10. Interaction of asperities loaded under shear and normal stress (after [43]).

In addition to creep and sintering, bond formation between ice asperities has been attributed to crushing and refreezing of asperities as they are pushed together during confinement, or during shear [9, 37]. With application of normal pressure, it is possible for asperities at freeze bond interface to crush and sinter together, forming a layer of recrystallized ice, thus increasing the strength of the bonds (Figure 2.11). Singh and Jordaan [47] captured the sintering of crushed ice particles, in a series of triaxial tests on crushed ice under hydrostatic loading. Samples that were left under confinement for a short period of time (20 minutes) before testing, exhibited higher strengths in comparison to samples that were tested immediately. This is because samples that were left confined for a longer time allowed more sintering to take place between the grains during the confinement period. The sintered bonds were also observed in thin sections of the crushed samples under confinement.

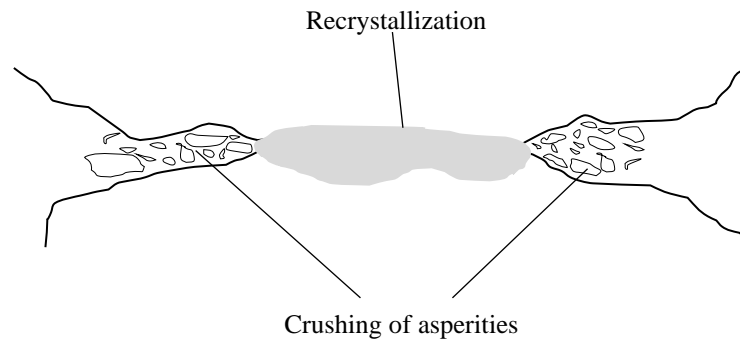


Figure 2.11. Schematic illustration of crushing of asperities and recrystallization at contact interface.

Sintering and creep studies discussed above focus on the influence of these processes on the strength and adhesion properties of contacting ice pieces under dry conditions. Sintering mechanisms between contacting ice asperities under submerged conditions need further investigation. Wet sintering processes are specifically important in ice ridge keel load models, where submerged ice blocks bonded together define the overall strength of the keel. Furthermore, understanding ice bonding processes in micro scale can help advance numerical simulations of ice rubble/ridges, where strength properties between ice asperities and ice blocks can be used to define freeze bond properties between ice blocks in the simulated rubble/ridge [39, 40].

2.6. References

- [1] S. Shafrova and K. V. Høyland, “The freeze-bond strength in first-year ice ridges. Small-scale field and laboratory experiments,” *Cold Regions Science and Technology*, vol. 54, no. 1, pp. 54–71, 2008.
- [2] M. O. ElSeify and T. G. Brown, “Formation, Behaviour and Characteristics of Ice Rubble Pile-Up and Ride-Up on a Cone,” in *Proceedings of the 18th IAHR International Symposium on Ice*, Sapporo, Japan, 2006.
- [3] Y. Dolgoplov, V. P. Afanasiev, V. A. Koren’Kov, and D. F. Panfilov, “Effect of hummocked ice on the piers of marine hydraulic structures,” in *Proceedings of the 3rd International Symposium on Ice Problems*, Hanover, the Netherlands, 1975.
- [4] M. Mellor, “Ship resistance in thick brash ice,” *Cold Regions Science and Technology*, vol. 3, no. 4, pp. 305–321, 1980.
- [5] A. Prodanovic, “Upper bounds of ridge pressure on structures,” in *proceedings of the 6th Port and Ocean Engineering Under Arctic Conditions conference*, Quebec City, Canada, 1981.
- [6] K. R. Croasdale and A. B. Cammaert, “An Improved Method for the Calculation of Ice Loads on Sloping Structure in First-Year Ice,” *Hydrotechnical Construction*, vol. 28, no. 3, pp. 174–179, 1994.
- [7] S. E. Bruneau, “Development of a first-year ridge keel load model,” PhD Thesis, Memorial University of Newfoundland, 1996.
- [8] E. Bailey, R. Taylor, and K. R. Croasdale, “Mechanics of Ice Rubble over Multiple Scales,” in *proceedings of the 34th International Conference on Ocean, Offshore and Arctic Engineering*, St. John’s, NL, Canada, 2015.

- [9] A. S. Shestov and A. Marchenko, "Thermodynamic consolidation of ice ridge keels in water at varying freezing point," *Cold Regions Science and Technology*, vol. 121, pp. 1–10, 2016.
- [10] H. Shayanfar, E. Bailey, R. Pritchett, and R. Taylor, "The effects of consolidation time on the strength and failure behavior of freshwater ice rubble," *International Journal of Naval Architecture and Ocean Engineering*, vol. 10, no. 3, pp. 403–412, 2018.
- [11] R. T. Weiss, A. Prodanovic, and K. N. Wood, "Determination of ice rubble shear properties," in *Proceedings of the 6th IAHR International Symposium on Ice*, Quebec, Canada, 1981.
- [12] J. H. Hellmann, "Basic investigations on mush ice," in *Proceedings of the 7th IAHR International Symposium on Ice*, Hamburg, Germany, 1984.
- [13] G. E. Urroz and R. Ettema, "Simple-shear box experiments with floating ice rubble," *Cold Regions Science and Technology*, vol. 14, no. 2, pp. 185–199, 1987.
- [14] E. M. Schulson and A. L. Fortt, "Static strengthening of frictional surfaces of ice," *Acta Materialia*, vol. 61, no. 5, pp. 1616–1623, 2013.
- [15] M. Sayed, "Mechanical properties of model ice rubble," in *Materials and Member Behavior*, 1987, pp. 647–659.
- [16] Y. Yasunaga, S. Kioka, Y. Matsuo, A. Furuya, and H. Saeki, "The strength of the unconsolidated layer model of ice ridge," in *Proceedings of the 16th IAHR International Symposium on Ice, Dunedin, New Zealand*, 2002.
- [17] A. Prodanovic, "Model tests of ice rubble strength," in *proceedings of the 5th Port and Ocean Engineering Under Arctic Conditions conference*, Trondheim, Norway, 1979.
- [18] A. Azarnejad and T. G. Brown, "Ice Rubble Behavior in Punch Tests," *Journal of Cold Regions Engineering*, vol. 15, no. 3, pp. 135–153, 2001.
- [19] E. Bailey, J. Bruce, A. Derradji, and M. Lau, "An overview of the development of ice ridge keels strength testing program," in *Proceedings of the 3rd Arctic Technology Conference*, Houston, Texas, 2014.

- [20] J. Bruce, G. Piercey, A. Macneill, R. Phillips, and A. Derradji, “Physical Testing Method to Study Ice Keel Strength Limits during a Gouging Process,” in *Proceedings of the 2nd Arctic Technology Conference*, Houston, Texas, 2012.
- [21] E. Bailey, J. Bruce, and R. Taylor, “The Development of Ice Ridge Keel Strengths: The influence of speed on the strength and deformation behaviour of gouging ridge keel,” in *Proceedings of the 22nd IAHR International Symposium on Ice*, Singapore, 2014.
- [22] R. Phillips, T. King, and J. Bruce, “PIRAM: Pipeline Ice Risk Assessment & Mitigation Program Overview,” in *Proceedings of the 9th International Pipeline Conference*, Calgary, Canada, 2012.
- [23] A. Palmer and K. R. Croasdale, *Arctic Offshore Engineering*. World Scientific Publishing Co., 2013.
- [24] H. Shayanfar, “An experimental investigation on the strength and failure behavior of freshwater ice rubble,” MSc Thesis, Memorial University of Newfoundland, 2018.
- [25] R. Ettema and J. A. Schaefer, “Experiments on freeze-bonding between ice blocks in floating ice rubble,” *Journal of Glaciology*, vol. 32, no. 112, pp. 397–403, 1986.
- [26] A. Marchenko and C. Chenot, “Regelation of ice blocks in the water and the air,” in *proceedings of the 20th Port and Ocean Engineering Under Arctic Conditions conference*, Luleå, Sweden, 2009.
- [27] A. H. V. Repetto-Llamazares, “Experimental studies of shear failure on freeze-bonds in saline ice part I: set-up, failure mode and freeze-bond strength.,” *Cold Regions Science and Technology*, vol. 65, no. 3, pp. 286–297, 2011.
- [28] H. Helgøy, O. S. Astrup, and K. Høyland, “Laboratory work on freeze-bonds in ice rubble, Part II: Results from individual freeze-bond experiments,” in *Proceedings of the 22nd International Conference on Port and Ocean Engineering under Arctic Conditions*, Espoo, Finland, 2013.

- [29] K. V. Høyland and A. Møllegaard, “Mechanical behavior of laboratory made freeze-bonds as a function of submersion time, initial ice temperature and sample size,” in *Proceedings of the 22nd IAHR International Symposium on Ice*, Singapore, 2014.
- [30] I. M. Bueide and K. V. Høyland, “Confined Compression Tests on Saline and Fresh Freeze-Bonds,” in *Proceedings of the International Conference on Port and Ocean Engineering Under Arctic Conditions*, Trondheim, Norway, 2015.
- [31] C-CORE, “DIRKS: Year 1 progress report,” C-CORE, St. John’s, NL, Canada, Internal report, 2012.
- [32] P. Liferov and B. Bonnemaire, “Ice rubble behaviour and strength: Part I. Review of testing and interpretation of results,” *Cold Regions Science and Technology*, vol. 41, no. 2, pp. 135–151, 2005.
- [33] J. R. Blackford, “Sintering and microstructure of ice: a review,” *Journal of Physics D: Applied Physics*, vol. 40, no. 21, p. R355, 2007.
- [34] M. Faraday, “Note on regelation,” *Proceedings of the Royal Society of London*, 1859.
- [35] W. Thomson, “III. Note on Professor Faraday's recent experiments on'regelation.'” *Proceedings of the Royal Society of London 11*, vol. 11, p. 198, 1861.
- [36] P. V. Hobbs and B. J. Mason, “The sintering and adhesion of ice,” *Philosophical Magazine*, vol. 9, no. 98, pp. 181–197, 1964.
- [37] W. D. Kingery, “Regelation, surface diffusion, and ice sintering,” *Journal of Applied Physics*, vol. 31, no. 5, pp. 833–838, 1960.
- [38] D. Kuroiwa, “A study of ice sintering,” *Tellus*, vol. 13, no. 2, pp. 252–259, 1961.
- [39] G. C. Kuczynski, “Self-diffusion in sintering of metallic particles,” *AIME TRANS*, vol. 185, pp. 169–178, 1949.

- [40] N. Maeno and T. Ebinuma, "Pressure sintering of ice and its implication to the densification of snow at polar glaciers and ice sheets," *The Journal of Physical Chemistry*, vol. 87, no. 21, pp. 4103–4110, 1983.
- [41] F. B. Swinkels and M. F. Ashby, "A second report on sintering diagrams," *Acta Metallurgica*, vol. 29, no. 2, pp. 259–281, 1981.
- [42] N. Maeno and M. Arakawa, "Adhesion shear theory of ice friction at low sliding velocities, combined with ice sintering," *Journal of Applied Physics*, vol. 95, no. 1, pp. 134–139, 2004.
- [43] E. M. Schulson, "Low-speed friction and brittle compressive failure of ice: fundamental processes in ice mechanics," *International Materials Reviews*, vol. 60, no. 8, pp. 451–478, 2015.
- [44] D. Szabo and M. Schneebeli, "Subsecond sintering of ice," *Applied Physics Letters*, vol. 90, p. 151916, 2007.
- [45] B. Lishman, P. R. Sammonds, D. L. Feltham, and A. Wilchinski, "The rate- and state-dependence of sea ice friction," *Journal of Geophysical Research: Oceans*, Vol. 116, 2009.
- [46] D. C. Hatton, P. R. Sammonds, and D. L. Feltham, "Ice internal friction: Standard theoretical perspectives on friction codified, adapted for the unusual rheology of ice, and unified," *Philosophical Magazine*, vol. 89, no. 31, pp. 2771–2799, 2009.
- [47] S. K. Singh and I. J. Jordaan, "Triaxial tests on crushed ice," *Cold Regions Science and Technology*, vol. 24, no. 2, pp. 153–165, 1996.
- [48] A. Polojärvi, J. Tuhkuri, and A. Pustogvar, "DEM simulations of direct shear box experiments of ice rubble: Force chains and peak loads," *Cold Regions Science and Technology*, vol. 116, pp. 12–23, 2015.
- [49] S. Afzali, R. Taylor, R. Sarracino, E. Bailey, and M. T. Boroojerdi, "Investigation of the Effect of Block Size, Shape and Freeze-Bond Strength on Flexural Failure of Freshwater Ice Rubble using the Discrete Element Method," Glasgow, Scotland, 2019.

3. SUBMERSION TIME EFFECTS

3.1. Preface

A version of this manuscript, titled “Experimental study of the effect of submersion time on the strength development of freeze bonds” has been published in the journal of Cold Regions Science and Technology. I am the primary author of this paper, along with the co-authors, Dr. Eleanor Bailey and Dr. Rocky Taylor. I conducted the literature review and experiments and analyzed the data. I prepared the first draft of the manuscript and subsequently revised the manuscript based on the co-authors’ feedback and also the feedback from the journal reviewers. Co-authors helped in design of experiments, analyzing the results and contributed in preparing, reviewing and revising the manuscript.

3.2. Chapter Abstract

Freeze bonds have been found to influence the mechanical properties of ice rubble and ridges, and it is therefore important to study the fundamental physical properties affecting these features. The shear strength of freeze-bonded ice blocks has been investigated through a series of asymmetric four-point bending (AFPB) experiments for different submersion times and initial ice temperatures. Ice blocks were subject to a confinement of 25 kPa and were sheared at an actuator rate of 5 mm/s. The effects of submersion time on shear strength of freeze bonds were investigated by varying the submersion time from 1 min to 14 days, for two initial ice temperatures of -18°C and -10°C . Shear strength values measured are believed to be dominated by two concurrent mechanisms. Thermal bond growth is the first mechanism, where an initial increase in strength with submersion time is observed, reaching a peak after four (4) minutes of submersion time and gradually decreasing to a constant value. Sintering-creep bond development is the second mechanism that significantly influences the bond strength in submersion times longer than 24 h, where the strength increases and eventually asymptotes to the strength of solid ice. An empirical equation that estimates the bond strength as a function of submersion time and initial ice temperature is developed.

Keywords: Freeze bond; Freshwater ice; Ice shear strength; Ice bond strength

3.3. Introduction

Ice ridges, common features in Arctic and sub-Arctic regions, are formed by an accumulation of ice rubble due to shear or compression of ice sheets. Ice ridges and rubble play an important role in many different engineering problems such as ice interaction with offshore structures, infrastructure, river and lake engineering and ship-ice interactions. Understanding the strength and failure properties of these features is therefore necessary to help mitigate potential risk and damage that can be caused by these features. The structure of an ice ridge consists of three sections: the sail, the keel and the consolidated layer (Figure 3.1). The consolidated layer forms in the upper part of the ridge keel due to atmospheric cooling which causes the water-filled voids in the rubble to freeze over time. The draft of a first-year ridge keel is typically 4-5 times greater than the height of the sail. Due to the reduced height, the load contribution from the sail is usually neglected in ridge-structure interaction models, while the consolidated layer is treated as a thick layer of level ice, and the keel as a granular material using Mohr-Coulomb models. Several analytical models, which assume continuum behavior, have been developed to estimate the ridge keel load on structures [1–4]. Several assumptions, however, are implied in these models that limit their precision and make them applicable only to cases with special boundary conditions. A number of numerical simulations have been conducted using Finite Element Method [5–7] and Discrete Element Method [8–10] in recent years to provide a deeper understanding of ridge-structure interactions.

Several experimental studies have been performed to understand the mechanical properties of ice rubble and to find appropriate values of cohesion and friction for use in Mohr-Coulomb type models. These studies include laboratory experiments (small and medium scale tests) and in-situ field tests. The laboratory methods include direct shear box [7, 11–15], punch box [16–19], simple shear box [20], biaxial shear box [21–24] and triaxial shear [25–27]. In-situ punch tests have also been carried out by Leppäranta and Hakala [28], Croasdale and Associates [29, 30] and Heinonen and Määttänen [31].

Liferov and Bonnemaire [32] reviewed much of the work conducted to date and concluded that the initial failure of the rubble is dominated by cohesion, which must be overcome before the ice blocks can mobilize. The cohesive component of rubble is controlled by the degree of freeze bonding between the ice blocks (Figure 3.1a). Once mobilized, the frictional component dominates. The frictional component is a function of the contact friction, interlocking between ice blocks and dynamic freeze-bonding [33]. Liferov and Bonnemaire [32] also found that in many cases the initial failure mode often corresponded to the peak load, signifying the importance of understanding freeze bond formation and failure processes for ridge load models.

The origin of freeze bonds between the ice blocks is uncertain, but has been attributed to thermal refreezing processes [34] and sintering as a result of buoyancy forces which increase the contact pressures between adjacent ice blocks [35]. In metallurgy, sintering is defined as the process by which particles adhere to each other by mass transfer, forming a neck between them. Sintering has been used to explain the increase in friction at low sliding velocities, where contacting asperities adhere, causing increased friction

[36]. Schulson [37] also found an increase in the static friction coefficient with contact time, which he referred to as a static strengthening stage. He suggested that the contacting asperities would creep under a normal load, causing an increase in contact area (Figure 3.1b, c). Szabo and Schneebeli [38] measured the sintering force between two ice cones under normal pressure. Using the power-law creep equation, they calculated the time-dependent area increase at the ice-ice interface, which was used to calculate the sintering force later. With the increase in contact area, they found the sintering force to increase, especially at temperatures near melting point.

A number of small-scale laboratory tests have been carried out to investigate the parameters that influence freeze bond strength [15], [32], [39–45]. A thorough review of these works is given in Section 3.2.

The processes affecting freeze bond strength and therefore ice ridge failure mechanisms are complicated, and the research conducted to date has not been able to cover all the aspects. This paper focuses on studying the strength development of freeze bonds under different submersion times and initial ice temperatures. The experiments cover a wide range of submersion times (from 1 min to 14 days) to better understand the bond growth process from the initial moments of contact for two different ice temperatures of -18°C , and -10°C . The short submersion times investigated are particularly relevant in areas where brash ice and its accumulation causes problems in Arctic shipping lanes and ice-covered harbors. Longer submersion times are more relevant in floating ridges where they are more likely to remain undisturbed for many weeks or months. Solid ice shear tests were also conducted in order to compare the strength of the freeze bonds with the

parent ice. In addition, the thermal behavior of the ice blocks, and ice growth rates during freeze bond formation were investigated and linked to the observed freeze bond strength development with submersion time.

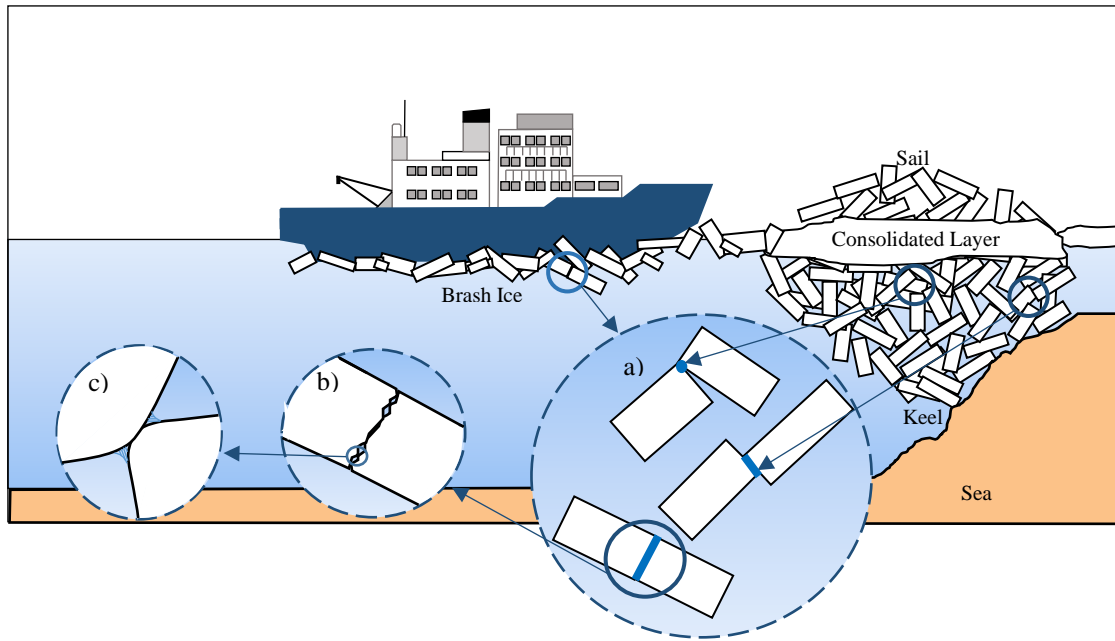


Figure 3.1. Schematic illustration of the multi-scale properties of ice rubble where factors influencing ridge loads are governed by: a) freeze bond properties, b) contact conditions at the block interface and c) sintering and junction growth at the asperity level.

3.4. Background

Freeze bond experiments have been carried out in recent years to measure the strength development between ice blocks under different conditions. The general methodology for these experiments is to form a freeze bond by placing two pieces of ice in contact, leaving them for a specified period of time and subsequently shearing the bond. Several different test setups have been considered for shearing the bond and include: the direct

shear method (where the bond is oriented both horizontally and vertically), the 45° cut method, and the asymmetric four-point bending method. Strength has been calculated by dividing the maximum force measured during shear by the contact area (freeze bond area) for both direct shear and 45° cut method and the equation used to calculate strength in the asymmetric four-point bending has been discussed in Section 3.3.2. While all tests aim to generate a pure shear failure at the bond interface, some uncertainties have been reported as a result of unwanted normal stresses generated at the failure plane during shear. While a detailed review of each of these methods and results obtained in previous experiments were provided in Section 2.4, results that are of interest in this paper are discussed below.

Ettema and Schaefer [35], Repetto-Llamazares et al. [45], Helgøy et al. [42] used the direct shear methodology where the freeze bond was oriented horizontally and a normal load was applied to the top using dead weights. Ettema and Schaefer [35] conducted the first set of freeze bond tests on freshwater ice blocks, where they showed that by increasing the contact period from 0 to 4 min, the freeze bond strength increased linearly (from 0.18 to 3.3 kPa). Tests were conducted for freeze bonds in contact in air, and submerged in distilled water, tap water, water from the Iowa River, saline solutions with a salinity of 3, 12.5 and 25 ppt. Higher strength values were measured for submerged samples in comparison to the samples that were in contact in air.

Repetto-Llamazares et al. [45] conducted freeze bond tests on saline ice, varying confinement (0.125 to 2 kPa), submersion time (1 to 1200 min), and initial ice temperature (-1 to -14°C). The strength measurements for different submersion times

showed a bell-shaped curve, where the strength initially increased with submersion time, reaching a maximum of about 20 kPa after 5 min and then gradually decreased to a constant value of 5 kPa after about 5 h. They suggested that the observed strength-submersion curve could be separated into three phases. The first phase, where the strength increased until it peaked, was dominated by heat transfer and ended when the temperature and porosity of the freeze bond reached its minimum. During the second phase, the freeze bond started to warm to the surrounding water temperature thus increasing porosity and weakening the bond strength. Repetto-Llamazares et al. [45] also suggested that brine drainage may also be taking place in the second phase, contributing to further increase in porosity. The third and final phase was when both the temperature and salinity of the freeze bond equilibrated with the water and the freeze bond strength stabilized. They also observed that the initial ice temperature had a distinct influence on freeze bond strength, where it took a longer period of time for the warmer ice blocks to form freeze bonds. This is because the warmer ice blocks had a lower temperature differential and hence rate of heat transfer. As a result they suggested that the width and height of the bell curve will be governed by the initial temperature of the ice.

Helgøy et al. [42] used the methodology of Repetto-Llamazares et al. [45], focusing on investigating the effects of physical ice properties on strength development. All samples were submerged for 10 min and were subject to a confinement of 1.9 kPa. The freeze bond strengths measured varied from 1.9 to 118.3 kPa with the strongest bonds formed between two natural surfaces and the weakest between two sawn surfaces.

Shafrova and Høyland [40], Høyland and Møllegaard [43] and Bueide and Høyland [44] used the 45° cut methodology discussed in Section 2.4. Shafrova and Høyland [40] conducted field and laboratory experiments on both freeze-bonded and level ice samples. Strength of freeze bonds in their field tests varied from 14-73 kPa, and level ice was found to be on average 33 times stronger than the freeze-bonded ice. The test set-up used for the field tests was used for a series of laboratory experiments on sea ice, laboratory-made saline ice and freshwater ice, where a normal confinement of 0.25 to 0.6 kPa was applied during freeze bond formation. Laboratory freeze bond tests showed higher strengths values in comparison to the field tests (15-197 kPa compared to 14-73 kPa), which was attributed to the effect of the confinement pressure that was applied in the laboratory tests.

Høyland and Møllegaard [43] investigated the effects of submersion time on the strength of freeze bonds formed using the 45° method without applying a normal pressure. While the initial increasing peak observed in the results of Shafrova and Høyland [40], Repetto-Llamazares et al. [45], and Bueide and Høyland [44] was not observed in these tests, consistent with the decreasing section of strength-submersion time curve of these studies, shear strength decreased from 1583 to 42 kPa as submersion time increased from 0.5 minutes to 20 hours. It should be noted that for most of the tests with submersion times of 0.5 to 5 min, they observed ice block failure instead of freeze bond failure, and the higher strength values measured corresponded to ice failure rather than freeze bond failure.

Similar to the method used by Høyland and Møllegaard [43], Bueide and Høyland [44] measured the strength of the bond between both freshwater and saline ice blocks, which were radially confined under a confinement of 7 to 99 kPa during compression (similar to biaxial compression test). Initial ice temperatures of -2.5 and -8.5°C were used and submersion time was varied from 0.5 to 1200 min. Their results for the shear strength vs. submersion time showed a bell-shaped curve similar to what was observed by Repetto-Llamazares et al. [45], with freshwater samples reaching the peak strength at a lower submersion time than saline samples. They attribute this to the lower porosity of freshwater samples resulting in a higher thermal conductivity, which increased the rate of energy transfer, causing the peak strength to occur sooner.

The Asymmetric Four-Point Bending (AFPB) method was used at C-CORE [46] in a series of freshwater freeze bond tests between two rectangular ice samples with an initial temperature of -11°C. Increasing the submersion time from 10 to 3945 min, under a constant confinement of 40 kPa, freeze bond strength increased from 30 kPa to 170 kPa after 3 hours of submersion and then decreased to 34 kPa after 3945 minutes of submersion. A constant deformation rate of 0.44 mm/s was applied for all these tests.

Since the focus of this paper is the role of submersion time on freeze bonds, all data that is readily available in literature has been plotted as a function of submersion time in Figure 3.2. This plot includes the results for both saline and freshwater ice blocks where submersion times vary from 0.5 min to 60 h, and the strength varies from 0.2 to about 1600 kPa.

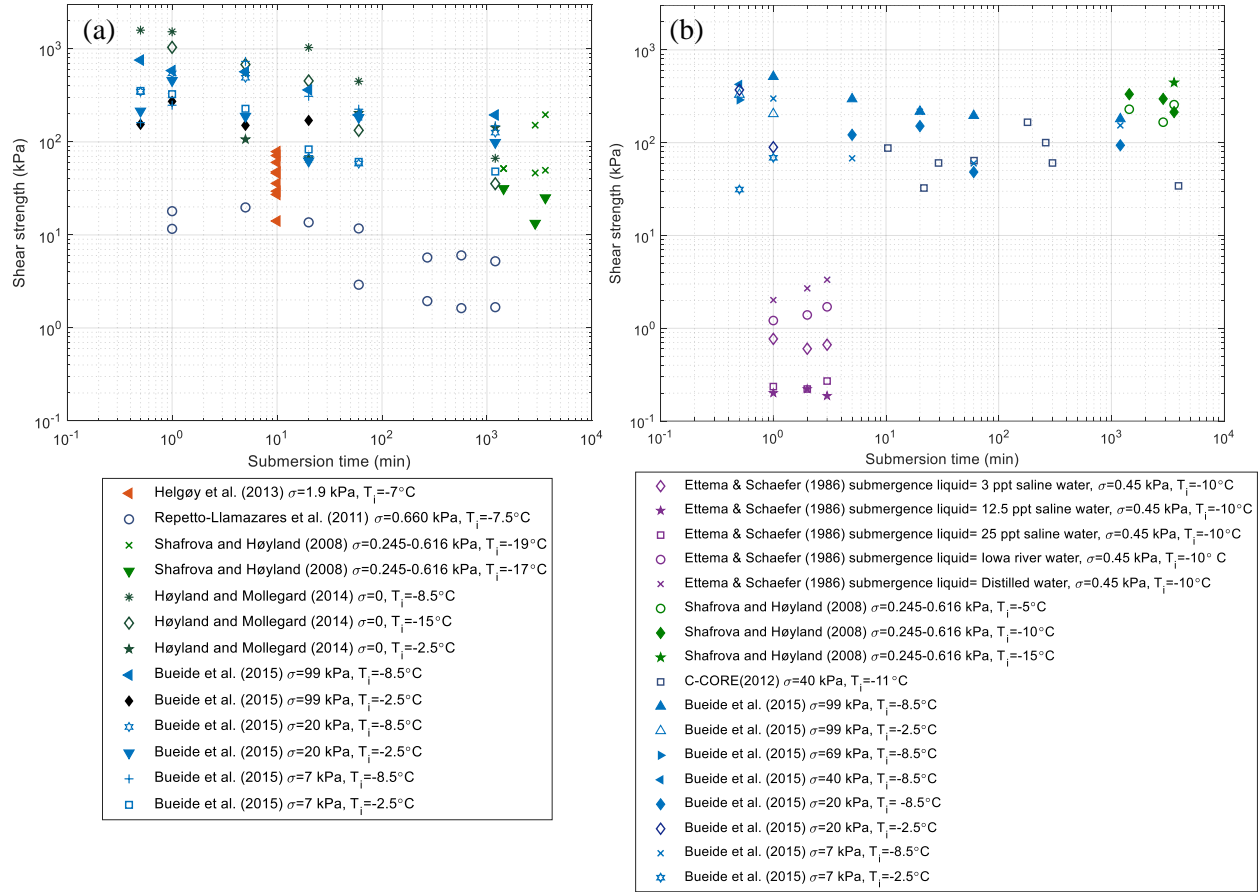


Figure 3.2. Plot showing the measured shear strength values versus submersion time in previous freeze bond experiments for a) saline ice, and b) freshwater ice. In this figure σ refers to confinement pressure and T_i to initial ice temperature.

3.5. Experimental Method

3.5.1. Sample preparation

Ice blocks were prepared using the same methodology as the DIRKS project [47, 48] previously conducted to investigate the strength and failure mechanisms of gouging ridge keels. To grow the ice, ice trays of 1 m^2 by 0.12 m were filled with freshwater and

left to freeze at -18°C in the C-CORE cold room. A divider was placed in each tray to help break the ice into large blocks when removed from the tray. Once frozen, the trays were removed from the cold room for about 20 min, allowing the ice to melt at the edges to facilitate removal. Ice blocks were first rough cut on the band saw and subsequently lathed into $9 (\pm 0.002)$ cm diameter cylinders and milled to a length of $20 (\pm 0.02)$ cm. For the freeze bond tests, the sample was then cut in half using a custom made jig which ensured they were cut perpendicular, whereas for the solid ice tests they were left intact.

3.5.2. Freeze bond tests

Freeze bonds were formed using a confinement frame (Figure 3.3a), which applies a normal load to two cylindrical specimens during submersion and shear testing. Cylindrical ice blocks were chosen to provide uniform transformation of heat transfer and sintering during bond formation, and to avoid corner or edges that would influence these processes. This is also the case in sintering studies where spherical ice particles are usually used. To ensure samples were perfectly aligned three support wedges were used; two under the ends of the samples and the third directly under the freeze bond. These were left in place during submersion and easily removed prior to shear testing with minimal effect to the bond. The normal load was applied using a hand-driven gear that moved one end forwards while the other remained fixed to a 900 N capacity load cell. Three springs were used to ensure that the load was transferred uniformly to the samples. Once the specified normal load was reached, the frame was submerged in a

freshwater bath held at 0°C which was monitored using a Resistance Temperature Detector (RTD). Cold room temperature was held at a nominal temperature of 0°C during the tests to prevent changes in temperature during testing. During submersion, the normal load and water temperature were recorded continuously using a standard data acquisition (DAQ) system and software.

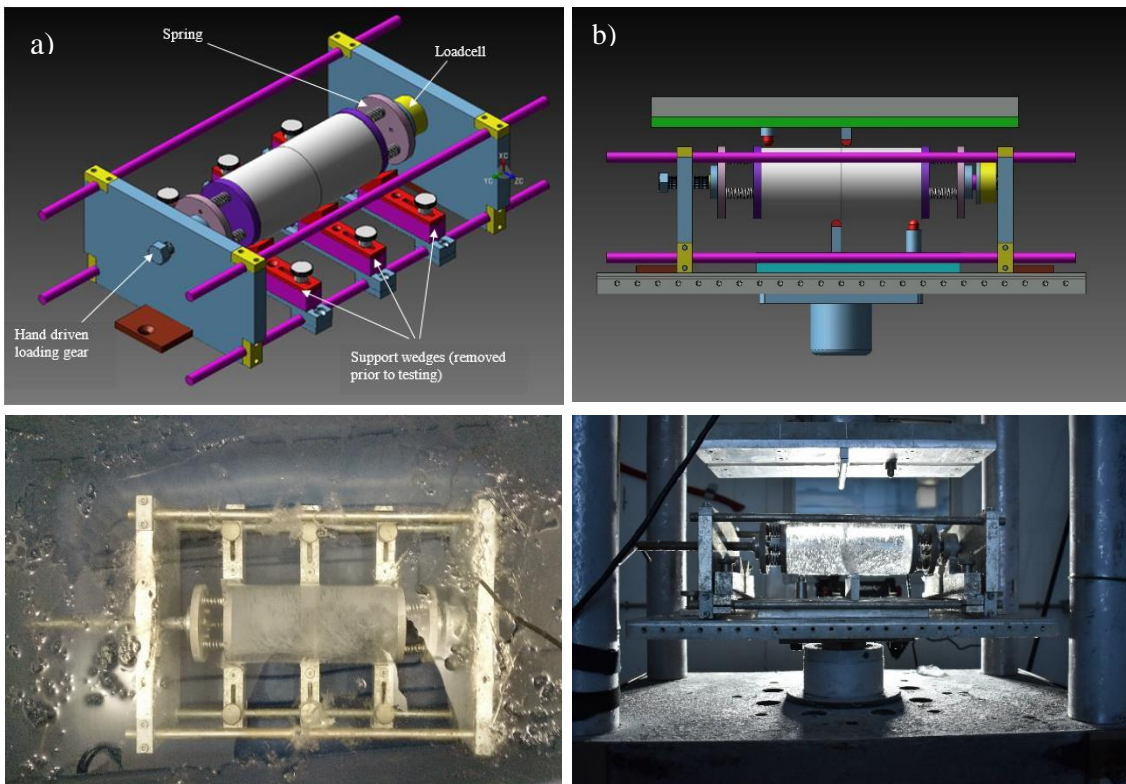


Figure 3.3. Figures showing design drawing and photographs of a) the confinement frame and b) the confinement frame loaded in the AFPB rig.

After the pre-specified submersion time, the frame was carefully removed from the water and loaded in the Asymmetric Four-Point Bending (AFPB) rig (Figure 3.3b) following

the methodology of Frederking and Timco [49, 50] and Bailey [51, 52]. The bottom plate was fixed to the pedestal of a Materials Testing System (MTS) servo-hydraulic testing machine, while the upper plate was attached to a hemispherical alignment seat so that it was free to rotate about the load-application point. The concept behind this apparatus is that the load is applied at four points on a beam, which are positioned asymmetrically about the loading axis. Under these conditions, the inner bars create a force in the clockwise direction, while the outer bars create a counter-clockwise rotation. This generates a near-pure shear cross-section across the freeze-bonded area, allowing the shear strength of the bond to be measured. Assuming that simple beam theory applies and that there are no normal forces acting on the plane of failure, the maximum shear stress, τ_{max} , at the center of the specimen (i.e. freeze bond strength), can be calculated using the equation below:

$$\tau_{max} = \frac{4}{3} \frac{(1 - \alpha)}{(1 + \alpha)} \frac{P_{max}}{\pi r^2} \quad (3.1)$$

where P_{max} is the peak load at failure, r is the nominal radius of the sample, and α relates the position of the inner and outer loading pins. Figure 3.4 shows a schematic of the AFPB apparatus, the shear forces and bending moments.

The confinement frame was positioned in the AFPB rig so that the freeze bond was at the center of the loading axis and equidistant from the loading pins. The outer (L) and inner (αL) loading bars were positioned 7.44 cm and 0.79 cm from the centerline, respectively (i.e. $\alpha=0.106$). The shear load and displacement was measured using the MTS machine load cell and internal displacement transducer, as well as an external

string potentiometer. A high-speed video camera, synchronized with the load-displacement data through an electrical trigger, was used to observe the failure behavior. During some tests, the diameter of the sample was measured before and after submersion to infer information about changes in the freeze bond diameter.

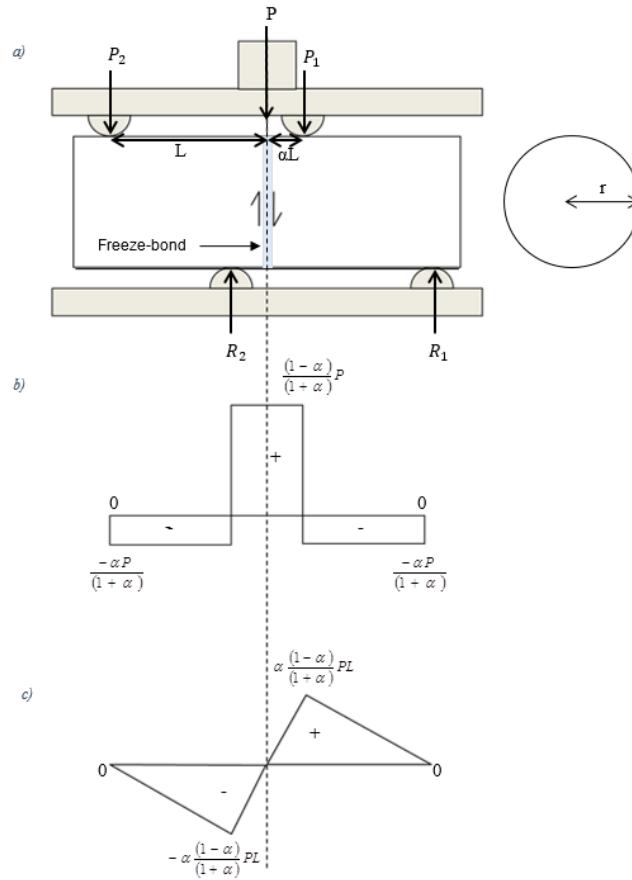


Figure 3.4. AFPB rig, showing diagrams of a) the experimental set-up, b) the shear forces, and c) the bending moments (after [52]).

3.5.3. Thermal equilibrium test

Thermal equilibrium tests were done to determine the time required for a solid ice block to equilibrate to the surrounding water temperature. This provides information about the thermal evolution inside the ice block and the amount of new ice growth around the ice sample. To set up a test, three equally distanced holes were drilled along the centerline of the sample at locations $z = 5, 10$ and 15 cm to a depth of 4.5 cm such that the temperature sensors were in the center of the sample ($r=0$ in Figure 3.5). Temperature sensors with on-board data loggers (MicroTs by Phase IV Engineering Inc.) were inserted into each hole and frozen in place (see Figure 3.5). Samples were tempered overnight in a freezer held at the required temperature before being submerged in a freshwater bath held at 0°C . The ice samples were held in place underwater using weights and string. A small diameter string was used to limit the effects of heat transfer between the rope and the water on the sample. The temperature was measured in the ice samples every 10 seconds and in the water every 2 min.

The temperature profile of the samples was also obtained by solving the transient heat conduction equation (Equation 3.2) for an ice block submerged in water using the Finite Difference Method (FDM).

$$\rho_i C_p \frac{\partial T}{\partial t} = \nabla \cdot (k \nabla T) \quad (3.2)$$

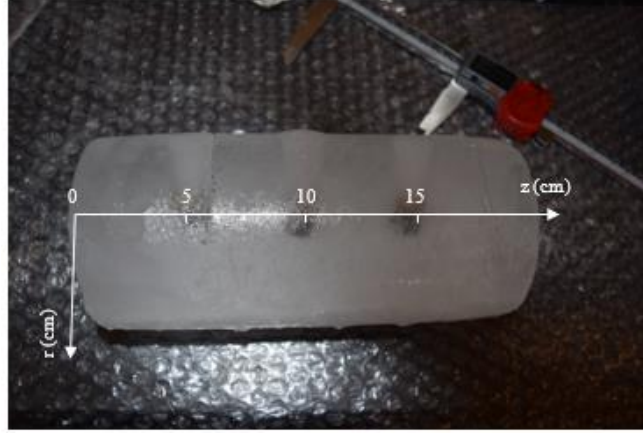


Figure 3.5. Wireless temperature sensors (MicroTs) frozen in the ice sample after submersion.

In Equation 3.2, ρ_i is the ice density, C_p is the specific heat capacity of ice, k is the conductivity of ice, and T is the temperature of ice. Considering the problem to be a 2-D axisymmetric problem, Equation 3.2 can be expanded in the form of Equation 3.3.

$$\frac{1}{\alpha} \frac{\partial T}{\partial t} = \frac{1}{r} \frac{\partial}{\partial r} \left(r \frac{\partial T}{\partial r} \right) + \frac{\partial^2 T}{\partial z^2} \quad (3.3)$$

with initial condition of $T_i = -18^\circ\text{C}$ at $t=0$, subject to the boundary conditions:

$$\left\{ \begin{array}{ll} \frac{\partial T}{\partial r} = 0, & r = 0 \\ T = T_w = 0, & r = R \\ T = T_w = 0, & z = 0, L \end{array} \right. \quad (3.4)$$

where α is the thermal diffusivity of ice defined as $\frac{k}{\rho C_p}$, t is time, R is the radius and L is the length of the cylinder, T_i and T_w are ice and water temperature respectively, and the directions of z and r are shown in Figure 3.5. Further tests and numerical simulations of heat transfer and ice growth in ice blocks using COMSOL Multiphysics can be found in [53].

3.6. Results

3.6.1. Freeze bond tests

A total of 69 tests were completed in this test program targeting the effect that submersion time has on the strength development of freeze bonds while a nominal normal pressure of 25 kPa was applied to the ice blocks. Two initial ice temperatures (T_i) of -18°C and -10°C were investigated. The submersion times for the tests with $T_i = -18^\circ\text{C}$ were varied from 1 min to 14 days, while the $T_i = -10^\circ\text{C}$ were carried out for submersion times ranging from 1 min up to 7 d. The 14 d test condition was not carried out for the -10°C case due to the limited availability of testing time in the Coldroom Laboratory. Four shear tests were also conducted on solid ice blocks for comparison with the freeze bond test results. Similar to the freeze bond tests, the samples were also placed in the confinement frame under a normal load for the duration of the submersion time and during the shear test. All samples in the test program were deformed at a rate of 5 mm/s. The parameters used in each test are given in Table 3.1, as well as the shear strength calculated using Equation 3.1, along with the average normal pressure and normal pressure drop. A radius of 4.5 cm was used in strength calculations since insufficient data was available to normalize the strength values based on the contact area after submersion.

Analysis of the confinement data showed a small drop in the normal pressure ($\Delta\sigma$ in Table 3.1) was recorded over the period of submersion, which we believe may have been caused by creep of ice blocks due to the applied pressure and/or perhaps relaxation of

the springs. An example of the typical normal pressure behavior measured during submersion is shown in Figure 3.6, where the target pressure was 25 kPa. In this example, an initial pressure of 26.26 kPa was applied to the samples and after 5 minutes of submersion, the normal pressure had dropped by 1.87 kPa. To ensure reported values reflect this relaxation effect, confinement values reported in Table 3.1 are the time-averaged values taken over the duration of the experiment. The average drop of pressure in all the experiments is 2.65 kPa, with the maximum drop happening in the test where the ice was submerged for 7 days for ice with an initial temperature of -18°C .

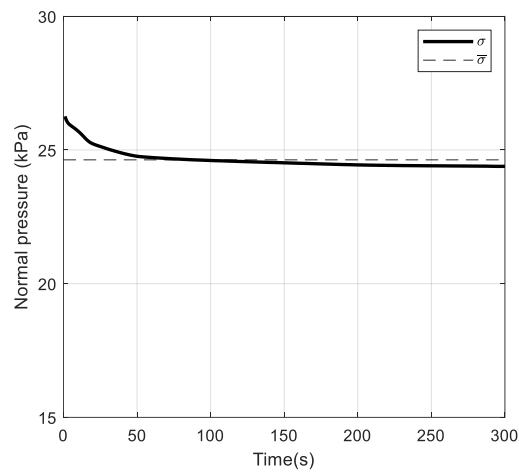


Figure 3.6. Normal pressure measured for samples that were submerged for 5 min and had an initial ice temperature of -18°C . In this figure σ is the normal pressure and $\bar{\sigma}$ is the average normal pressure.

Table 3.1. Freeze bonds test matrix. Parameters in the table are: submersion time (t), initial ice temperature (T_i), Actuator rate (V), confinement (σ), number of tests (n), normal pressure drop ($\Delta\sigma$), average normal pressure ($\bar{\sigma}$), average shear strength (S).

Freeze bond tests							
t	T_i (°C)	V (mm/s)	σ (kPa)	n	$\Delta\sigma$	$\bar{\sigma}$ (kPa)	S (kPa)
1 min				1	4.3	20.9	172.1
2 min				4	2.22	24.31	187.9
3 min				2	6.19	21.5	184.1
4 min				2	-0.6	23.09	197.0
5 min				3	2.13	23.54	170.2
10 min				1	2.61	22.64	158.8
20 min				1	1.38	23.33	130.9
30 min				2	1.02	24.58	102.6
1 h				1	1.12	25.34	107.7
3 h	-18	5	25	2	2.91	23.28	59.5
5 h				1	2.84	23.25	51.1
7 h				2	1.69	23.61	149.6
17 h				1	-	-	57.2
1 d				2	6.63	19.45	44.4
2 d				2	2.01	23.53	131.9
3 d				2	2.27	22.54	164.7
5 d				1	1.05	24.56	172.1
7 d				3	4.51	21.15	188.2
14 d				1	2.62	25.44	302.9
1 min				2	3.79	23.26	97.2
2 min				3	1.21	25.57	167.2
3 min				3	2.04	23.74	165.5
4 min				2	0.44	24.91	189.5
5 min				3	1.93	23.81	153.5
10 min				1	0.98	25.03	125.4
20 min				1	4.68	20.27	91.7
30 min				2	5.01	21.7	69.2
1 h	-10	5	25	2	1.03	25.44	73.6
3 h				2	4.02	22.83	68.3
5 h				1	7.17	19.98	38.7
7 h				1	4.06	20.72	40.3
1 d				2	2.31	23.66	153.1
2 d				2	1.02	25.51	142.1
3 d				2	2.26	23.90	152.8
7 d				2	2.36	23.37	290.5
Solid ice tests							
1 min					0.01	25.28	390.8
1 h	-10	5	25	1	2.43	22.58	328.2
1 d					0.2	24.5	381.7
7 d					1.84	23.9	440.7

3.6.1.1. Specimen response

While visual observations and videos recorded of the tests did not show any apparent difference in the nature of the bond failure (all resulted in a sudden catastrophic failure of the bond), comparing the load-time curves during shearing of the freeze-bond highlights that while many samples exhibited elastic, brittle behavior, in some cases specimens exhibited more ductile behavior prior to failure. Figure 3.7 shows representative plots of the observed failure curves for both types of behavior. The first plot shows a typical brittle event, which was characterized by an abrupt and near-instantaneous drop-off load (Figure 3.7a). The second plot shows a more ductile response where a period of strain hardening took place before failure (Figure 3.7b). After bond failure, a residual frictional force remains as the samples are pushed together and sheared further past each other. It is interesting to note that samples that behaved in a ductile manner showed a higher residual strength compared to brittle ones, resulting from a higher friction between the blocks. While it is generally expected that colder samples would exhibit more brittle behavior, no evident relationship was observed in the failure curves for the different initial ice temperatures. The occurrence of ductile/brittle response was plotted against submergence time and was found to not exhibit any trend. Consequently, this aspect of specimen behavior is not considered further.

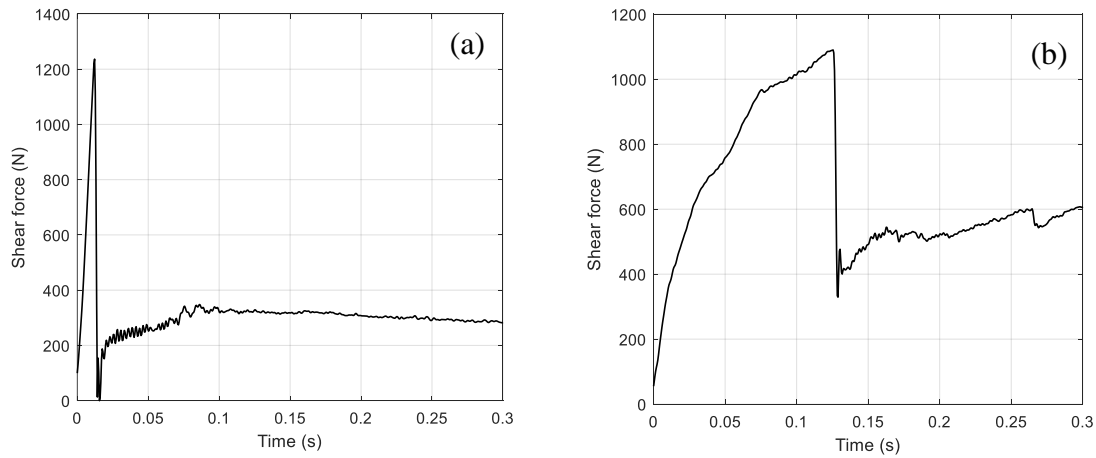


Figure 3.7. Typical load curves showing a) brittle and b) ductile behavior observed during the freeze bond tests. Both tests were conducted for 4 minutes of submersion time and an initial ice temperature of -18°C .

3.6.1.2. Freeze bond shear strength

Freeze bond shear strength values for ice with $T_i = -18^{\circ}\text{C}$ have been plotted as a function of submersion time in Figure 3.8. The values presented are averaged over the number of tests conducted for each submersion time plus/minus the standard deviation (see Table 3.1 for the number of tests for each submersion time). The strength of the bond initially increased with submersion time, reaching a maximum strength of 197 kPa after 3 to 4 minutes of submersion, before gradually decreasing to about 50 kPa after 3 hours of submersion. The shear strength then remained around 50 kPa from 3 to 24 hours of submersion, before increasing almost linearly up to 14 days submersion. In fact, the highest shear strength of 300 kPa was measured after 14 days of submersion. Note that the variability was higher in the longer submersion tests perhaps due to the changes in the physical mechanisms, which will be discussed in greater detail in Section 3.5.2. Considering the upper bound of the range of data at each submersion time, it is observed

that the same increasing trend is reflected in the maximum strength values. An outlier in the trend observed in the results is the strengths measured for 7 hours of submersion. First test conducted for this submersion time showed an unexpectedly high value (190 kPa) and was therefore repeated. The value of the test that was repeated lies within the range of other experiments (109 kPa) and we believe the higher value is due to the natural variability of the ice as no apparent problem was observed in this test.

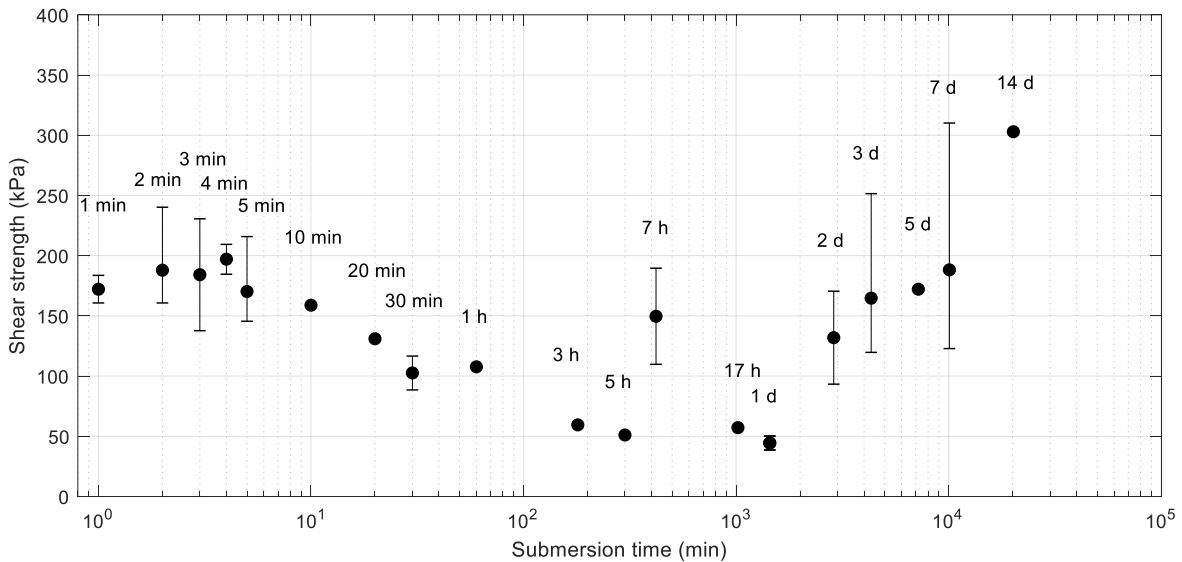


Figure 3.8. Freeze bond shear strength vs. submersion time for ice with an initial temperature of -18°C that was confined under a confinement of 23 kPa and deformed at a constant rate of 5 mm/s.

Figure 3.9 shows the shear strength of the freeze bonds for samples with $T_i = -10^{\circ}\text{C}$ where the submersion time was varied from 1 min to 7 d. In three tests, conducted after short submersion times, the samples were sufficiently bonded to cause failure in the surrounding ice rather than at the freeze bond location. These tests have been marked using a star symbol, as opposed to the circle used to represent freeze bond failure. If we

neglect the values where the sample failed in the solid ice, a similar bond strength-submersion time trend is observed in the -10°C tests, where the strength initially increased to 189.5 kPa after 2 to 4 minutes of submersion, then decreased and levelled out to a constant value just under 50 kPa after 30 minutes of submersion. The strength started to increase again after 7 hours of submersion, reaching a maximum of 300 kPa after 7 d. It is interesting to note that the freeze bond strength after 7 d was similar to those where the sample failed in the solid ice rather than at the freeze bond.

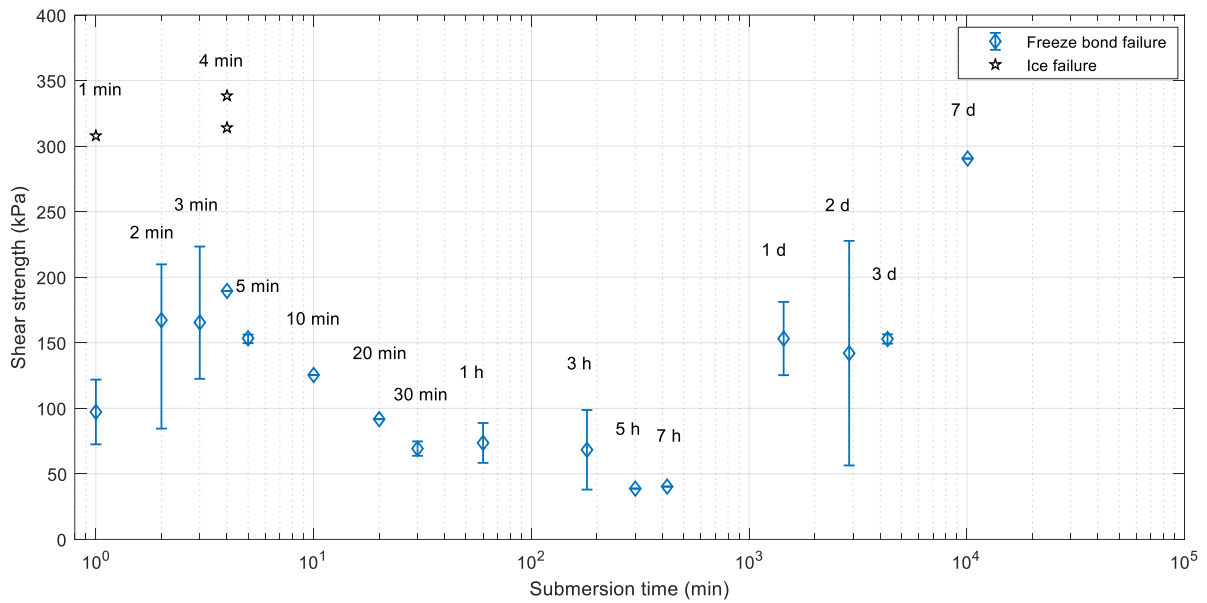


Figure 3.9. Freeze bond shear strength vs. submersion time for ice with an initial temperature of -10°C that was confined under a nominal confinement pressure of 23 kPa and deformed at a constant rate of 5 mm/s.

Figure 3.10 shows the comparison of the strength-submersion time curves for the two initial ice temperatures tested. While trends are similar for both temperatures, it is clear that samples with $T_i = -10^{\circ}\text{C}$ had lower overall strength values compared to samples with

$T_i = -18^\circ\text{C}$ during the first hour of submersion. This is firstly because the colder the ice, the greater the rate of heat transfer and the more ice growth that will take place. Secondly, colder freeze bonds will be stronger due to the well-known increase in the plastic flow stress that occurs with decreasing temperature [54]. It is difficult to determine exactly when the peak strength occurred for shorter submersion times, however, it appears to have taken place around 2 to 4 min for both temperatures. It was anticipated that peak strength would have occurred sooner for $T_i = -10^\circ\text{C}$, as the negative sensible heat would have been used up sooner. It is difficult to determine whether this occurred using the available data as there is a lot of variability in the bond strengths measured for shorter submersion times, which may potentially be due to some localized crushing effects taking place on the loading pins when the freeze bonds were strong, and also due to the more random nature of brittle fracture which tends to be more dominant for colder ice [55]. The Figure also shows that it took less time for $T_i = -10^\circ\text{C}$ to level out to a constant value when compared to $T_i = -18^\circ\text{C}$ (30 min compared with 3 h). This is expected as the colder ice would take longer to equilibrate with the surrounding water temperature. The final increase in strength took place after 24 h for $T_i = -10^\circ\text{C}$, while for $T_i = -18^\circ\text{C}$ this increase occurred after 48 hours of submersion. Both temperatures demonstrate an increasing trend after this, reaching the maximum strength observed after 7 and 14 days of submersion for $T_i = -10^\circ\text{C}$ and $T_i = -18^\circ\text{C}$, respectively.

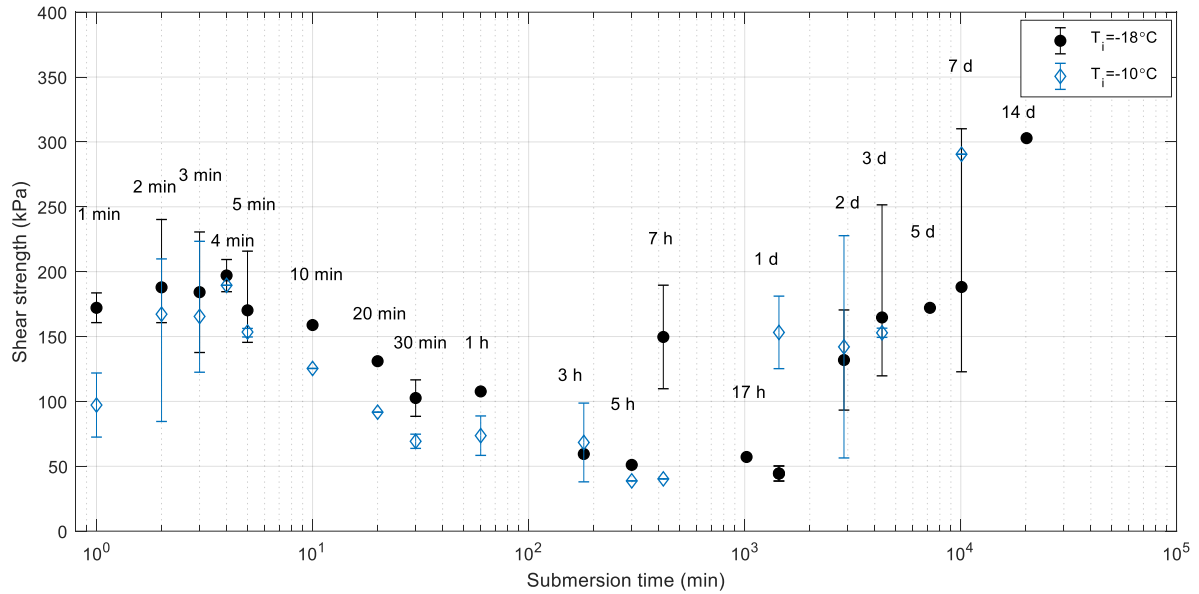


Figure 3.10. Comparison of freeze bond shear strength vs. submersion time for ice with an initial temperature of -10°C and -18°C .

3.6.2. Solid ice tests

Four solid ice shear tests were conducted on samples with $T_i = -10^\circ\text{C}$ that were submerged for 1 min, 1 h, 24 h, and 7 d while under a confinement of 25 kPa. The solid ice shear strengths are plotted in Figure 3.11 as a function of submersion time, as well as the freeze bond strengths measured under the same conditions. Included in the results are the three tests that resulted in the failure of the solid ice rather than the freeze bonds. It is noted that while the strength of solid blocks also increases somewhat for longer submergence times, the rate of increase in solid ice strength for longer submersion times is considerably less than is observed for the freeze bond specimens. The mechanisms associated with such behavior are discussed later on. Note that the highest value

measured for freeze bond strength, which occurred after 14 days of submersion for $T_i = -18^\circ\text{C}$, is almost equal to the lowest solid ice strength.

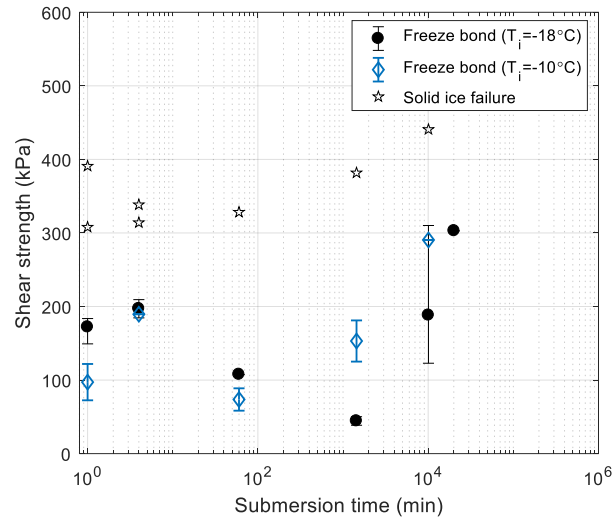


Figure 3.11. Solid ice and freeze bond shear strengths as a function of submersion time.

3.6.3. Thermal behavior of samples

Figure 3.12 shows the temperature data recorded by the MicroTs, as well as the temperature profile at the center of ice specimen ($r=0$, $z=10$ cm) obtained from the numerical model plotted as a function of submersion time. Based on the results of the numerical simulation, samples reach the equilibrium temperature with the surrounding water after 30 minutes of submersion. This is in good agreement with the observations of the values measured with the MicroTs. However, as can be seen in the zoomed-in part of the figure, it took marginally longer for the MicroTs located in the center of the sample ($z=10$ cm) to reach 0°C compared to the numerical results as well as the MicroT

measurements at $z=5, 15$ cm. This can be partly due to a lag in MicroT data. Additionally, the heat flux near the center of the sample is primarily radial with very little lateral heat transfer, whereas, near the ends, lateral heat transfer is more significant allowing the ice at the ends to equilibrate faster. Additionally, it can be observed that the rate of decrease in temperature is highest in the first 5 minutes of submersion, after which the temperature drops at a lower rate.

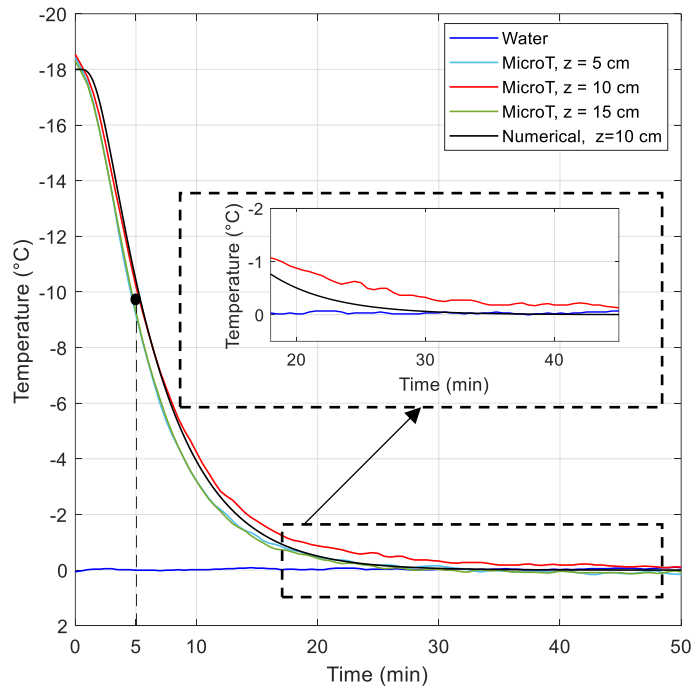


Figure 3.12. Temperature data recorded by the MicroTs placed at locations $z = 5, 10$ and 15 cm and numerical results for a solid ice block with an initial temperature of -18°C , along with zoomed-in plot of the temperature from 20 to 50 min after submersion for $z = 10$ cm and numerical results.

3.6.4. Change in freeze bond diameter

The diameters of the samples were measured using a pair of digital calipers (± 0.03 mm) for a number of tests before and after submersion (i.e. immediately prior to shear testing) to investigate the amount of ice growth during freeze bond formation. Two measurements were taken for each sample, one on each side of the freeze bond interface, and averaged. They were intentionally not done on the bond itself to ensure it would not affect the integrity of the bond. As can be seen from Figure 3.13a, the diameter of the freeze-bonded region of the ice specimens increased with submersion time, with the total change in diameter reaching 5-6 mm after extended submersion times. In Figure 3.13b, the increase in ice specimen diameter divided by the submersion time ($\Delta D/t$) is plotted as a function of the submersion time. The figure shows an increase in $\Delta D/t$ as the samples are initially submerged in water with a peak value occurring at 2 min, after which $\Delta D/t$ decreased with time, reaching almost zero after 3 hours of submersion.

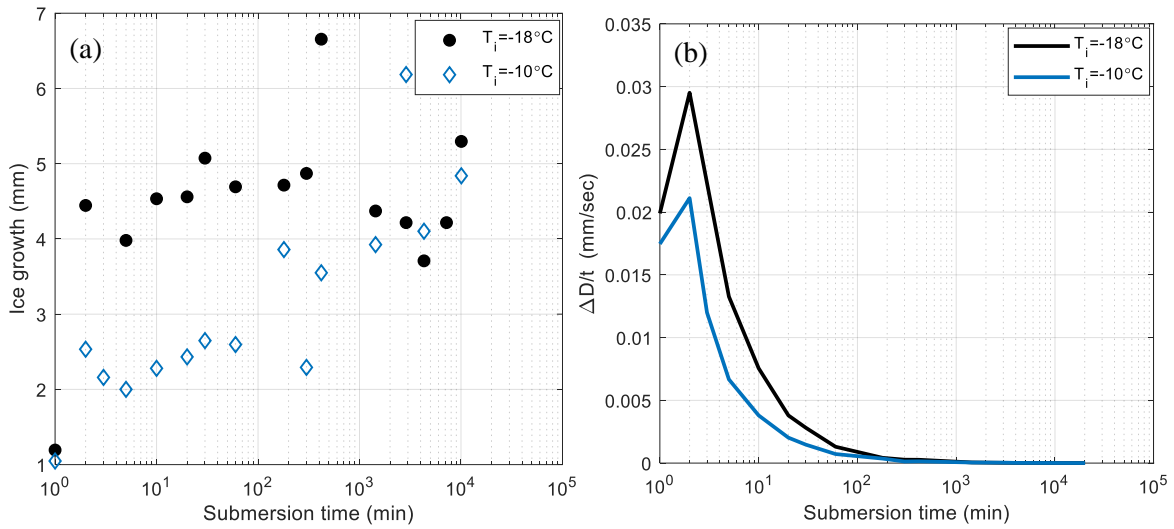


Figure 3.13. Measured values for the amount of increase in diameter a) and rate of increase in freeze bond diameter b) during submersion period of freeze bonds.

3.7. Analysis and Discussion

3.7.1. Empirical relationships

Two concurrent mechanisms are believed to contribute to the overall strength development of freeze bonds as a function of submersion time. Freeze bond formation starts due to heat transfer processes, which govern the first mechanism, referred to as the thermal bond growth mechanism in this paper. The second mechanism contributing to further bond strength development after prolonged submersion times is a result of sintering and creep. Based on the data collected in the present work, two empirical equations are suggested as the governing equations for each mechanism, relating submersion time and initial ice temperature to the strength of freeze bonds.

Figure 3.14 presents the general curves of thermal bond growth, derived from the experimental data. As observed in the figure, a bell-shaped curve as suggested by Shafrova and Høyland [56] is evident for both initial ice temperatures tested (i.e. -18 and -10°C). Although in our work we suggest that at $t=0$ (when the samples are initially put together) a frictional force will exist between ice blocks that results in a non-zero strength. Understanding frictional properties is beyond the scope of this paper, therefore curves are initiated at 1 min, which is when the first data point was collected. The curves are shown to asymptote at around 50 kPa once the freeze bond temperature has equilibrated with the surrounding water temperature. The general equation fitted to the data can be written as:

$$\tau_{FB,Th} = \tau_{ice} \cdot A_{Th}(T_i, t) \quad (3.5)$$

where $A_{Th}(T_i, t)$ is a function representing thermal effects, as given by the expression:

$$A_{Th}(T_i, t) = \frac{1}{g(T_i)} \exp[f(T_i) \cdot (\ln(t) - j(T_i))^{1.8}] \quad (3.6)$$

In the above equation, which is valid for $\ln(t) > j(T_i)$, τ_{ice} is the strength of solid ice in kPa, t is time in minutes, and $g(T_i)$, $f(T_i)$ and $j(T_i)$ are coefficients that are a function of initial ice temperature (T_i).

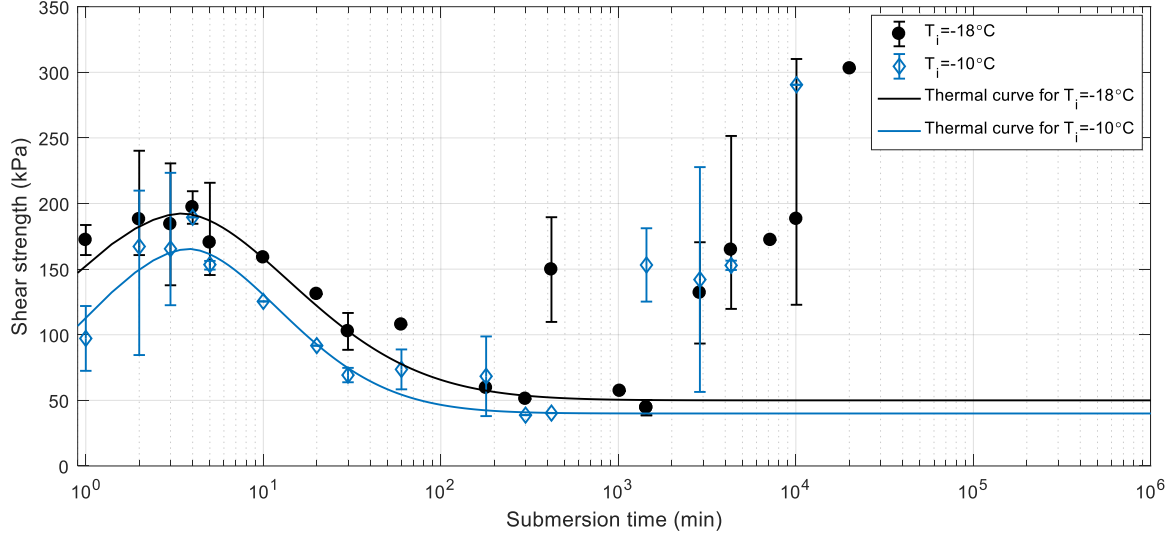


Figure 3.14. Thermal bonding mechanism curves for the two initial ice temperatures of -18°C and -10°C .

The second mechanism (Figure 3.15), sintering-creep, does not contribute to bond formation during low submersion times because it is a slow process. As such, the contribution to bond strength from this mechanism is assumed to be zero at $t=0$. The strength of the bond then increases as mass is transferred to the bond interface, which asymptotes as it reaches the strength of the parent ice (solid ice). The freeze bond strength was bounded by the strength of the parent ice based on the solid ice shear test results (Section 4.2), which showed that the strength of the bond after 14 days of submersion was very close to the solid ice shear strength (Figure 3.11). The strength development behavior due to sintering and creep can be characterized by an equation of the form:

$$\tau_{FB,sint} = \tau_{ice} \cdot B_{sint}(T_i, t) \quad (3.7)$$

where the function $B_{sint}(T, t)$ represents the effects of sintering-creep on bond strength as given by:

$$B_{sint}(T_i, t) = \tanh(h(T_i) \cdot t^{0.77}) \quad (3.8)$$

Here τ_{ice} is the strength of solid ice in kPa, t is time in seconds, and $h(T_i)$ is a coefficient that is a function of initial ice temperature (T_i).

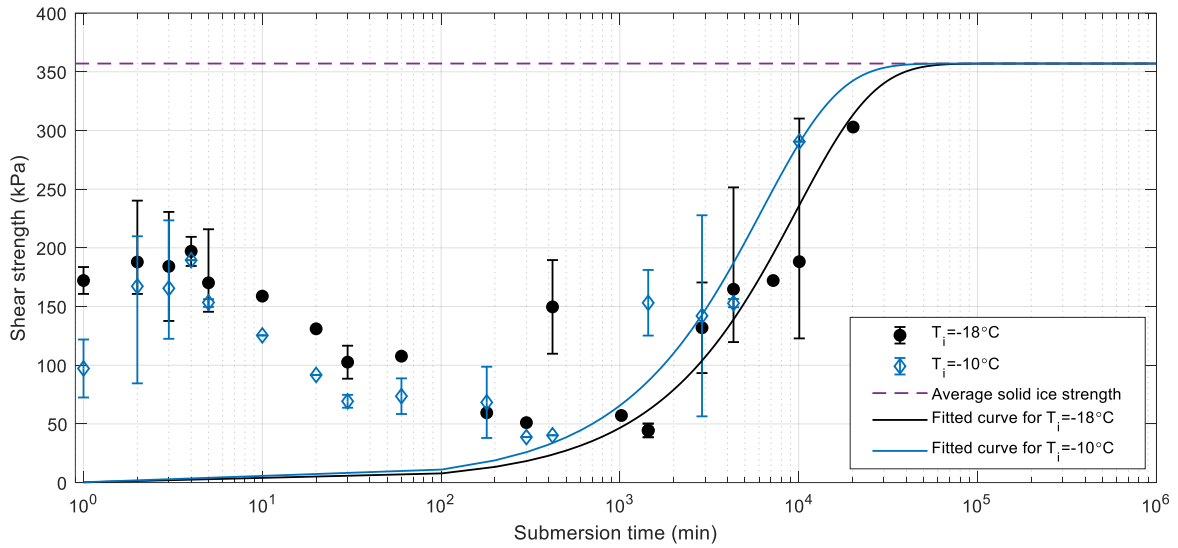


Figure 3.15. Sintering-creep bonding mechanism curves for the two initial ice temperatures of -18°C and -10°C .

As mentioned earlier, in real physical systems, these two mechanisms occur simultaneously, leading to the overall strength behavior observed in these tests. A combined curve (Figure 3.16) and associated equation is therefore suggested which takes both thermal ($\tau_{FB,Th}$) and sintering-creep ($\tau_{FB,sint}$) components into consideration. The overall freeze-bond strength development relationship therefore has been defined as:

$$\tau_{FB} = \tau_{FB,Th} + \tau_{FB,sint} \quad (3.9)$$

Substituting Equation 3.5-Equation 3.8 into Equation 3.9 and simplifying yields the expression below for the strength of freshwater freeze bonds as a function of temperature and time, including the effects of both thermal and sintering-creep processes:

$$\tau_{FB} = \tau_{ice} \left[\frac{1}{g(T)} \exp[f(T_i)(\ln(t) - j(T_i))^{1.8}] + \tanh(h(T_i) \cdot t^{0.77}) \right] \quad (3.10)$$

where $h(T_i)$, $g(T_i)$, $f(T_i)$, $j(T_i)$ are temperature-dependent coefficients. Values of these coefficients for the curves plotted in Figure 3.16 and corresponding to the temperatures considered in our test program ($T_i = -18^\circ\text{C}$ and -10°C) are given in Table 3.2.

Table 3.2. Coefficient values

	$h(T_i)$	$g(T_i)$	$f(T_i)$	$j(T_i)$
$T_i = -18^\circ\text{C}$	6.6×10^{-4}	1.85	-0.13	1.12
$T_i = -10^\circ\text{C}$	1×10^{-3}	2.34	-0.22	1.4

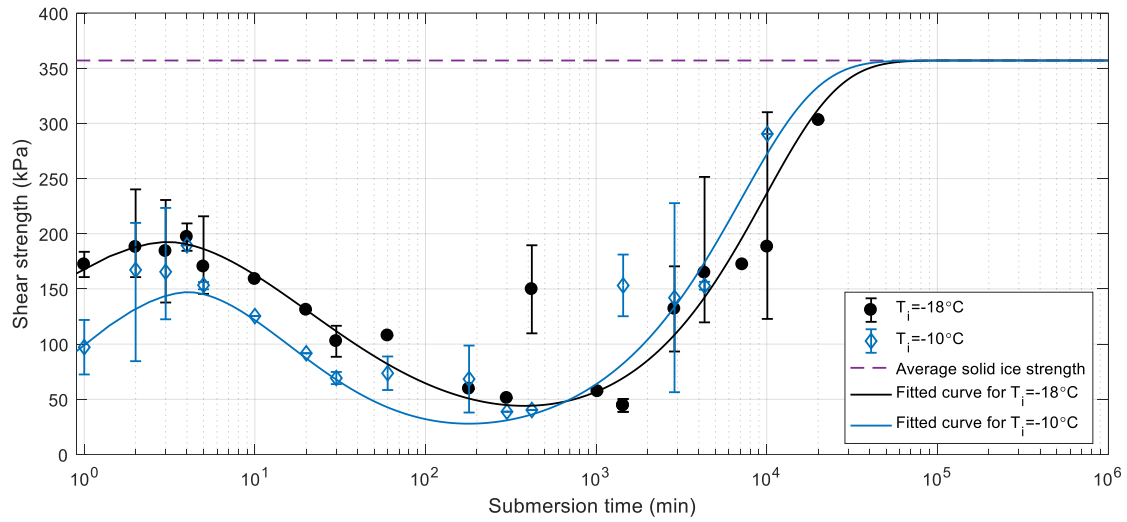


Figure 3.16. Combined freeze bond strength curves for initial ice temperatures of -18°C and -10°C .

3.7.2. Physical processes influencing bond strength development

Five stages have been identified for which distinct physical processes take place (Figure 3.17). Thermal bonding mechanisms dominate during stages 1-2, which is followed by a transition period in stage 3, while sintering-creep processes dominate in stages 4-5. Each stage is discussed in the associated subsection below.

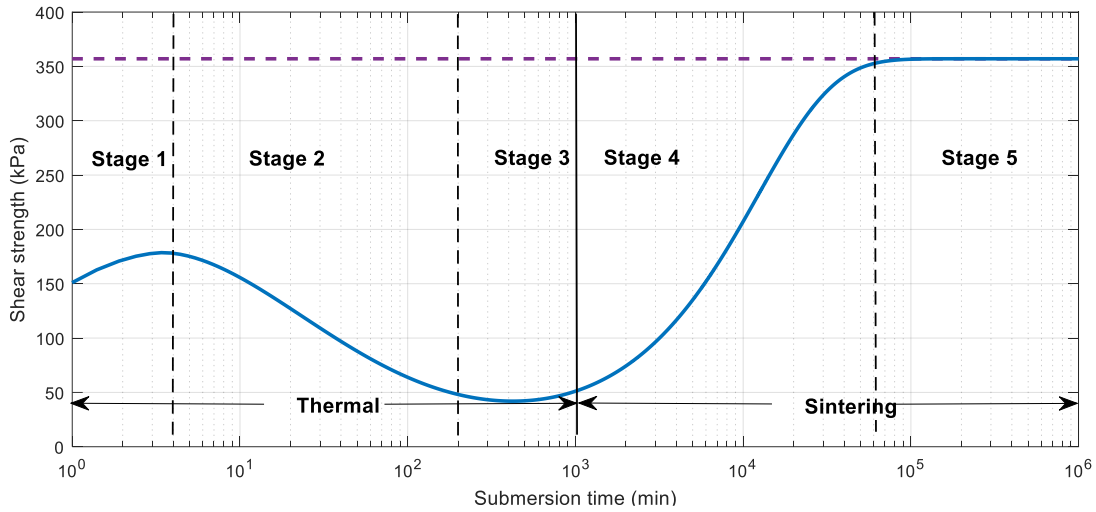


Figure 3.17. The five stages of freeze bond development as submersion time increases.

3.7.2.1. Thermal bonding mechanism

The first stage of freeze bond development, stage 1, is associated with the initial increase in strength in short submersion times, which occurred from 1 to 4 min in the present tests. This stage, termed here as the thermal strengthening stage, is driven by the temperature differential that exists between the water and the ice blocks. As the temperature profiles recorded during the thermal equilibrium test showed (Figure 3.12), the temperature gradient was highest in the first 5 minutes of submersion, after which the rate of heat transfer started to decrease. As heat is transferred from the water into the ice, new ice growth takes place both at the bond interface and around the parent ice resulting in an increase in strength. From the ice growth measurements, it was shown that peak growth rates occurred at two minutes (Figure 3.13b), leading to the peak strengths observed here. Peak strength in this stage coincides with the time that the freeze

bond temperature is at its coldest and at times the freeze bond strength was high enough to result in failure of the parent ice (Figure 3.9).

Stage 2 is associated with a thermal softening stage where the bond strength decreased from its peak value to its minimum between 4 and 200 min (3 h). This reduction in strength is driven by the increase in freeze bond temperature as it equilibrates to the surrounding water temperature. It is interesting to note that based on the temperature profiles given in Figure 3.12, the solid ice block had equilibrated with the water after 30 minutes of submersion (for the initial ice temperature of -18°C). This was not consistent with the measured strength minimum, perhaps suggesting a weakening of the internal structure of the ice.

Stage 3, is a transition period, where the freeze bond strength stays roughly constant, and mechanism dominance is believed to switch from thermal processes to sintering and creep. During this stage, no temperature gradient existed (Figure 3.12) and near-zero growth rates were observed (Figure 3.13b), signifying that the thermal bond growth mechanism no longer plays a significant role in the freeze bond strength development, leading to a change in the mechanism of strength development.

3.7.2.2. Sintering-creep bonding mechanism

After submersion times greater than 1000 min (17 h), the freeze bond strength was seen to increase again, which denotes stage 4 in Figure 3.17. As no thermal gradients existed during this stage, sintering-creep processes are believed to be the primary bond strength development mechanism in this stage. Sintering and creep induced deformations are believed to simultaneously contribute to bond development at the contact interface of ice blocks. Each of these will be discussed in the following paragraphs.

Sintering is a well-known and widely studied phenomenon in powder metallurgy that describes the formation of bonds between particles close to their melting temperature. The main driving force for sintering is the reduction of surface free energy. The Young-Laplace equation gives the stress or pressure associated with a surface $\sigma = 2\gamma/r$, where γ is the surface energy and r is the radius of curvature. This implies that for a sphere, the smaller the radius of curvature, the higher the surface stress and hence the higher the surface energy. This is why when there is a protrusion on a surface, the surface energy tends to smooth out the protrusion [57]. In the case of the freeze-bonded samples, the contact interface acts as an imperfection that induces transfer of mass from other regions of the ice specimen to the center (freeze bond area). Figure 3.18 shows a comparison of the freeze bond samples before (Fig. 18a) and after 14 days of submersion (Figure 3.18b). As seen in Figure 3.18b, ice growth is not uniform along the length of the cylinders, with maximum growth taking place in the center of the sample where the freeze bond is located. This suggests that mass was being transferred from the edges of the sample towards the center and thus increasing its strength through the increased

freeze-bonded area (Figure 3.18c). While no thin-sections of intact freeze bonds were taken after long submergence times in the present study, this would be of interest for future studies as microstructural changes to the ice in the freeze-bond region may also occur over time and influence the bond strength.

Several mechanisms (surface diffusion, grain boundary diffusion, plastic flow, etc.) have been shown to contribute to the process of sintering in the absence of external pressure. With application of an external pressure, which is the case for our tests, these mechanisms are accelerated [62, 63]. At the contact interface of the two ice specimens, strength develops as a result of the asperities being pushed together, resulting in localized creep, particle rearrangement and even crushing. This creep-induced deformation can result in bulging of the specimen for prolonged submersion times. While ice growth measurements were not collected for all specimens, observations from available data (Figure 3.13a) are consistent with this assessment, showing a continued increase in the diameter of the sample with increased submersion time. Strength development due to creep was also observed in solid ice tests, where the same trend of strength development was observed. However, observed changes over longer submersion time are much less pronounced for solid ice than for freeze-bonded samples, suggesting that sintering effects play a more dominant role than creep in the case of freeze bond strength development.

Power-law creep has been used many times in literature to describe sintering processes when an external pressure is present. For instance, Szabo and Schneebeli [38] found that when a normal stress is applied to contacting ice cones, the ice undergoes a non-

recoverable deformation which would increase the contact area. The rate of this deformation was shown to be dependent on stress, temperature and contact time, where higher pressures, temperatures and contact times gave rise to more pronounced effects of sintering. Sintering effects were, in particular, accelerated when the ice was close to the melting point, which is also likely the case in our experiments. As can be seen in Figure 3.16 the increase in bond strength in stage four occurs at an earlier submersion time for warmer ice (-10°C) compared to colder ice (-18°C). This is due to the fact that ice with initial temperature of -10°C reaches the equilibrium temperature in sooner than the -18°C ice, causing the sintering-induced bond strength increase to occur sooner. Maeno and Arakawa [59] and Schulson and Fortt [60] also used the concept of creep to explain the increase in ice-ice friction at low sliding velocities. They suggested that deformation at the asperity level resulted in increased contact areas resulting in higher rates of friction.

Comparing the range of strengths measured for each submersion time, it was observed that the variability of the measured strengths in stage 4 was higher than previous stages. This we believe is due to the fact that at long submersion times the various mechanisms discussed above are simultaneously contributing to the strength development. Sintering experiments are usually conducted at the microscopic level, under controlled conditions. Investigating their effects at macroscopic, ice-block level, therefore likely introduces variation in results that cannot be controlled at this scale.

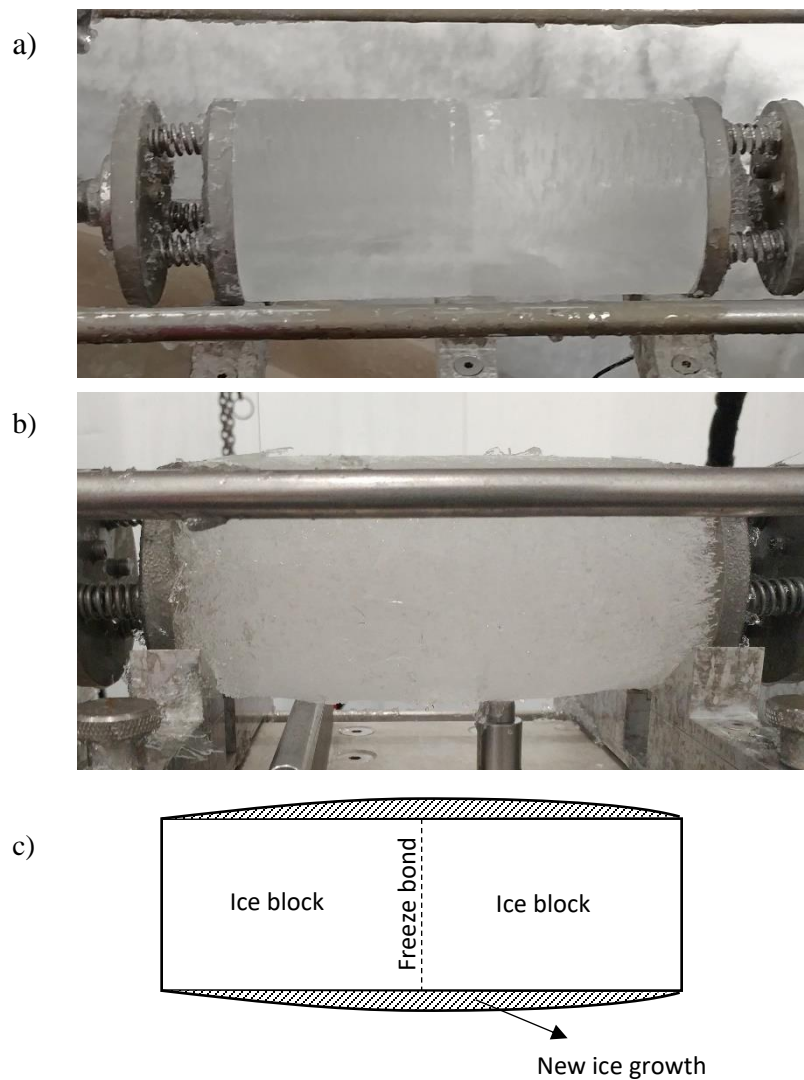


Figure 3.18. Photos showing a) shape of ice cylinders before submersion, b) shape of cylinder after 14 days of submersion, showing a curved profile with increased area near the freeze bonded region, and c) a schematic illustration of the growth behavior as a result of sintering-creep.

The sintering-creep bond development phase continued until it reached the strength of solid ice (stage 5 in Figure 3.17). It is suggested that any bond development after this stage will induce failure in the parent ice rather than the freeze bond. This is supported by the solid ice shear results (Figure 3.11), which showed that the freeze bond strength

approached that of the solid ice after extended submersion times. Ice rubble piles were observed to reach the strength of level ice in the field experiments of Scourfield et al. [61], where double-shear experiments were conducted between ice floes with presence of ice rubble between the sliding surfaces. In these experiments, samples that were left in contact for long contact times (16 hours) were observed to fail in the level ice rather than the ice rubble. The authors attributed this to the strength of the consolidated rubble exceeding the level ice strength as a result of thermodynamic and mechanical strengthening of the rubble with increasing contact time. This may have important implications for ridge-keel loading models, which currently assume the rubble behaves as a Mohr-Coulomb material. As such, under increased submersion times it may be more valid to model the rubble as a porous solid material, which would also permit failure in the parent ice as well as the freeze-bonded interfaces.

3.7.3. Comparison with other data

Comparison of the results of the current study to previous freshwater freeze bond experiments has been shown in Figure 3.19. The reported shear strength values differ due to different test parameters (confinement, initial ice temperature, contact area and loading rate) and test methodologies (direct shear, AFPB, and 45° cut method), which have previously been discussed in Section 3.2.

Despite these differences, similarities can be observed between the different data sets. For example, Ettema and Schaefer [35] observed a similar increasing trend of strength

with increase in submersion from 1 to 3 min. C-CORE [46] results for short submersion times are in the range of the results presented in the current study but are not consistent with our results for submersion time longer than 300 min (5 h). This may be due to the different confinement pressure (40 kPa), deformation rate (0.44 mm/s) used in these tests, and also the test setup. During submersion of the samples in C-CORE [46] tests, wooden angle brackets were used to hold the rectangular freeze-bonded samples in place, which were both problematic to remove for shear testing and likely prevented mass transfer mechanisms from taking place, resulting in reduced freeze bond strengths.

The freshwater results of Shafrova and Høyland [40] are higher than those measured in this program and show no evident relationship with submersion time. Repetto-Llamazares et al. [45] suggested that the constant strength values observed by Shafrova and Høyland [40] were because the samples were in the equilibrium phase (which is referred to as transition stage in this paper i.e. stage 3 in Figure 3.17). The higher strengths are likely due to differences in test methodology, as similar rates of deformation were used in both test programs and increased freeze bond strength is expected with higher confinement. Bueide and Høyland [44] reported a bell-shaped curve dependency of strength to submersion time. This is consistent with the trendline suggested by Shafrova and Høyland [40], where a bell-shaped curve is believed to dominate the strength development with regards to submersion time for both freshwater and saline ice. A similar curve was observed by Repetto-Llamazares et al. [45], where a bell-shaped curve dominated the strength development for submersion times of up to 20 h. The height and the width of the bell were suggested to be a function of initial ice

temperature, thermal properties and size of the samples. While the size of the samples remained constant in the current tests, the initial ice temperature was shown to affect the height and width of the bell, where colder ice temperatures result in a higher width and height. It should be noted however that, Repetto-Llamazares et al. [45] also attributed the time dependency of freeze bond strength to the porosity of the freeze bond, suggesting that the first stage of bond development occurs due to freezing and stops when salinity and temperature of freeze bonds reach their minimums; the second stage happens as the bond weakens due to the porosity of samples increasing as the temperature rises, and the third phase as a result of the temperature and salinity of the samples reaching that of surrounding water. Observing a similar curve in present study during the thermal bonding mechanism, which was done on freshwater ice, suggests that freeze bond strength development during the submersion period is driven principally by thermal processes. Reported strength values by Bueide and Høyland [44] for 20 kPa of radial confinement are in the range of those reported in the current study. Their data also appears to show a relationship with confinement, where increased confinement resulted in higher strength values.

Perhaps most importantly in considering this ensemble dataset is that the general stages of bond development discussed here, initial strengthening (stage 1) and weakening (stage 2) due to the thermal bonding mechanism, followed by a transition range (stage 3), which is followed by an increase in bond strength over longer times (stages 4-5) due to the sintering-creep mechanism can be observed.

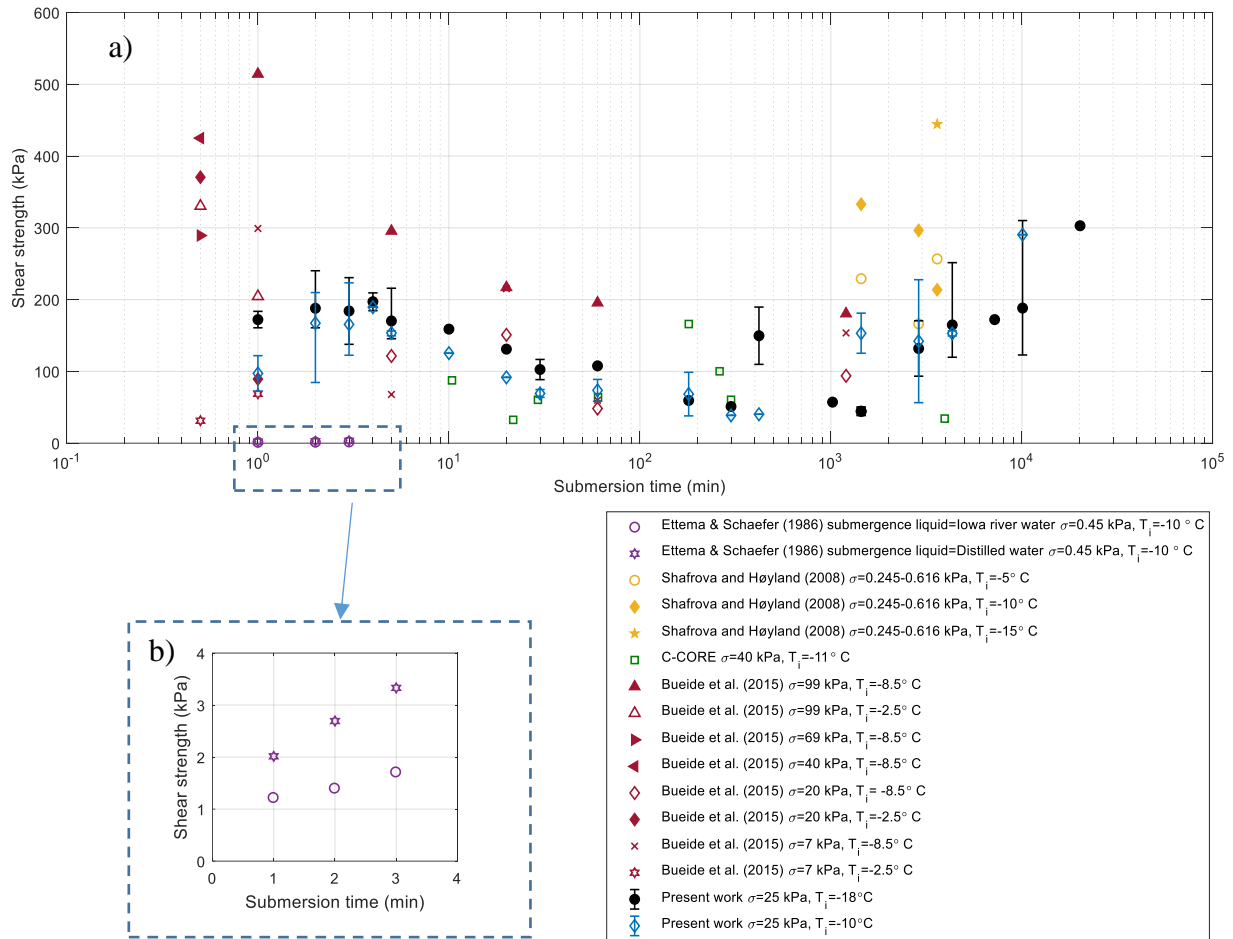


Figure 3.19. a) Comparison of the shear strength values of present work with Ettema and Schaefer [35], Shafrova and Høyland [40], Bueide and Høyland [44], and C-CORE [46], b) zoomed-in plot of Ettema and Schaefer [35]. In this figure, σ is the confinement pressure and T_i is the initial ice temperature.

3.8. Conclusions

A series of shear tests were conducted to investigate the strength development of freeze bonds as a function of submersion time and initial ice temperature. An empirical equation was introduced by fitting a curve through the collected data, allowing estimation

of strength as a function of submersion time and initial ice temperature. Two concurrent mechanisms were suggested to govern the strength-submersion time behavior of the freeze bonds: thermal and sintering-creep bond growth. The thermal bonding mechanism was dominated by heat transfer processes, which lead to the initial peak strength at short submersion times. This fast, thermal driven, bonding mechanism has implications for applications such as Arctic shipping where brash ice and its accumulation causes increased vessel resistance and impedes access to ports and harbors. After this initial peak, the bond strength was observed to decrease as the temperature of the ice and newly formed bond equilibrated with the surrounding water. The sintering-creep mechanism leads to the development of freeze bond strength after a prolonged submersion time, where the bond strength may continue to increase until it reaches the strength of solid ice. Mass transfer processes due to the sintering were observed to increase the freeze bonded contact area, which was accelerated by the applied confinement pressure through creep deformation. Further investigations of microstructural changes to the ice in the freeze-bond region over time are recommended to help provide additional insight into how the mechanical properties of these bonds evolve over time. Understanding these sintering processes is of particular importance for ridges, where freeze bonds could have been formed many weeks/months before an interaction occurs. Visual observations of first-year sea ice ridge keels show smoothed ice block surfaces and substantial neck growth between contacting ice blocks, indicative of sintering-creep mechanism [41]. Despite the numerous suggestions that sintering may contribute to further ridge/rubble consolidation, up to present it has received little

attention in the literature. This is the first study, as far as the authors are aware, where sintering processes have been explicitly considered in the context of freeze bond strength development. We hope that this paper encourages future experiments and modeling in this area. Understanding the importance of confinement on freeze bond strength development is the focus of ongoing future work by the current research group.

3.9. References

- [1] Y. Dolgoplov, V. Afanasiev, V. Koren'Kov, and D. Panfilov, "Effect of hummocked ice on the piers of marine hydraulic structures," in *Proceedings of the 3rd International Symposium on Ice Problems*, Dartmouth College, Hanover, Germany, 1975.
- [2] J. Hoikkanen, "Measurements and analysis of ice pressure against a structure in level ice and in pressure ridges," in *Proceedings of the 7th IAHR International Symposium on Ice*, Hamburg, Germany, 1984.
- [3] K. R. Croasdale and A. B. Cammaert, "An Improved Method for the Calculation of Ice Loads on Sloping Structure in First-Year Ice," *Hydrotechnical Construction*, vol. 28, no. 3, pp. 174–179, 1994.
- [4] M. O. ElSeify and T. G. Brown, "Formation, Behaviour and Characteristics of Ice Rubble Pile-Up and Ride-Up on a Cone," in *Proceedings of the 18th IAHR International Symposium on Ice*, Sapporo, Japan, 2006.
- [5] P. Liferov, A. Jensen, K. Høyland, and S. Løset, "On analysis of punch tests on ice rubble," in *Proceedings of the 16th IAHR International Symposium on Ice*, Dunedin, New Zealand, 2002.

- [6] J. Heinonen, *Constitutive modeling of ice rubble in first-year ridge keel*. PhD thesis, VTT Technical Research Centre of Finland, Finland, 2004.
- [7] N. Serré, “Numerical Modelling of Ice Ridge Keel Action on Subsea Structures,” *Cold Regions Science and Technology*, vol. 67, pp. 107–119, 2011.
- [8] A. Polojärvi and J. Tuhkuri, “Simulation of Ice Pile-Up Process with 2D Combined Finite-Discrete Element Method,” in *Proceedings of the 20th International Conference on Port and Ocean Engineering under Arctic Conditions*, Luleå, Sweden, 2009.
- [9] L. Liu, E. Bailey, R. Sarracino, R. Taylor, and C. Stanbridge, “Numerical Simulation of Ice Ridge Gouging,” in *Proceedings of the 34th International Conference on Ocean, Offshore and Arctic Engineering*, St. John’s, Canada, 2015.
- [10] E. Bailey, K. Croasdale, and R. Taylor, “Strength Tests on Grounded Rubble,” in *Proceedings of the 26th International Offshore and Polar Engineering Conference*, Rhodes, Greece, 2016.
- [11] A. Keinonen and T. Nyman, “An experimental model scale study on the compressible, frictional and cohesive behavior of broken ice mass,” in *Proceedings of Int. Symp. on Ice*. Lulea, Sweden, 1978.
- [12] A. Prodanovic, “Model tests of ice rubble strength,” in *proceedings of the 5th Port and Ocean Engineering Under Arctic Conditions conference*, Trondheim, Norway, 1979.
- [13] R. Weiss, A. Prodanovic, and K. Wood, “Determination of ice rubble shear properties,” in *Proceedings of the 6th IAHR International Symposium on Ice*, Quebec, Canada, 1981.
- [14] J. Hellmann, “Basic investigations on mush ice,” in *Proceedings of the 7th IAHR International Symposium on Ice*, Hamburg, Germany, 1984.
- [15] N. Serré, A. H. Repetto-Llamazares, and K. V. Høyland, “Experiments on the relation between freezebond and ice rubble strength, part I: shear box experiments,” in *Proceedings*

- of the 21st International Conference on Port and Ocean Engineering Under Arctic Conditions*, Montreal, Canada, 2011.
- [16] A. Azarnejad and T. G. Brown, “Observations of ice rubble behaviour in punch test,” in *Proceedings of the 14th IAHR International Symposium on Ice*, Rotterdam, The Netherlands, 1998.
- [17] A. Jensen, S. Løset, K.V. Høyland, P. Liferov, J. Heinonen, K.U. Evers and M. Määttänen, “Physical modeling of the first year ice ridges, Part II: Mechanical properties,” in *Proceedings of the 16th International Conference on Port and Ocean Engineering under Arctic conditions*, Ottawa, Canada.
- [18] E. Lemee and T. Brown, “Small-scale plane strain punch tests,” in *Proceedings of the 16th IAHR International Symposium on Ice*, Dunedin, New Zealand, 2002.
- [19] H. Shayanfar, “An experimental investigation on the strength and failure behavior of freshwater ice rubble,” MSc Thesis, Memorial University of Newfoundland, 2018.
- [20] R. Ettema and G. E. Urroz, “On internal friction and cohesion in unconsolidated ice rubble,” *Cold Regions Science and Technology*, vol. 16, pp. 237–247, 1989.
- [21] G. Timco, E. F. Funke, M. Saved, and P. Laurich, “A laboratory apparatus to measure the behavior of ice rubble,” in *Proceedings of the 11th International Conference on Offshore Mechanics and Arctic Engineering*, Calgary, Canada, 1992.
- [22] M. Sayed, G. Timco, and L. Sun, “Testing model ice rubble under proportional strains,” in *Proceedings of the 11th International Conference on Offshore Mechanics and Arctic Engineering*, Calgary, Canada, 1992.
- [23] S. Løset and M. Sayed, “Proportional strain tests of fresh-water ice rubble,” *Journal of Cold Regions Engineering.*, vol. 7, no. 2, pp. 44–61, 1993.

- [24] A. Cornett and G. Timco, "Mechanical properties of dry saline ice rubble," in *Proceedings of the 6th International Offshore and Polar Engineering Conference*, Los Angeles, USA, 1996.
- [25] A. Gale, T. Wong, D. Segó, and N. Morgenstern, "Stress-strain behaviour of cohesionless broken ice," in *Proceedings of the 9th International Conference on Port and Ocean Engineering under Arctic conditions*, Fairbanks, Alaska, 1987.
- [26] T. Wong, N. Morgenstern, and D. Segó, "A constitutive model for broken ice," *Cold Regions Science and Technology*, vol. 17, no. 3, pp. 241–252, 1990.
- [27] S. K. Singh and I. J. Jordaan, "Triaxial tests on crushed ice," *Cold Regions Science and Technology*, vol. 24, no. 2, pp. 153–165, 1996.
- [28] M. Leppäranta and R. Hakala, "The structure and strength of first-year ridges in the Baltic Sea," *Cold Regions Science and Technology*, vol. 23, pp. 279–290, 1992.
- [29] Croasdale and Associates, "In-situ ridge strength measurements - 1998," A study sponsored by NRC (PERD) and Exxon Production Research Co., 1998.
- [30] Croasdale and Associates, "In-situ ridge strength measurements - 1997," A study sponsored by NRC (PERD) and Exxon Production Research Co., 1997.
- [31] J. Heinonen and M. Määttänen, "LOLEIF Ridge-Loading Experiments - Analysis of Rubble Strength in Ridge Keel Punch Test," in *Proceedings of the 15th IAHR International Symposium on Ice*, Gdansk, Poland, 2000.
- [32] P. Liferov and B. Bonnemaire, "Ice rubble behaviour and strength: Part I. Review of testing and interpretation of results," *Cold Regions Science and Technology*, vol. 41, no. 2, pp. 135–151, Feb. 2005.
- [33] K. R. Croasdale, "Ice load models for first year pressure ridges and rubble fields," *Report to Industry and The National Energy Board*, Calgary, Canada, 1995.

- [34] G. W. Timco and L. Goodrich, "Ice rubble consolidation," in *Proceedings of the 9th IAHR International Symposium on Ice*, Supporo, Japan, 1988.
- [35] R. Ettema and J. A. Schaefer, "Experiments on freeze-bonding between ice blocks in floating ice rubble," *Journal of Glaciology*, vol. 32, no. 112, pp. 397–403, 1986.
- [36] N. Maeno and M. Arakawa, "Adhesion shear theory of ice friction at low sliding velocities, combined with ice sintering," *Journal of Applied Physics*, vol. 95, no. 1, pp. 134–139, 2004.
- [37] E. M. Schulson, "Low-speed friction and brittle compressive failure of ice: fundamental processes in ice mechanics," *International Material Reviews*, vol. 60, no. 8, pp. 451–478, 2015.
- [38] D. Szabo and M. Schneebeli, "Subsecond sintering of ice," *Applied Physics Letters*, vol. 90, p. 151916, 2007.
- [39] R. Ettema and J. A. Schaefer, "Experiments on freeze-bonding between ice blocks in floating ice rubble," *Journal of Glaciology*, vol. 32, no. 112, pp. 397–403, 1986.
- [40] S. Shafrova and K. V. Høyland, "The freeze-bond strength in first-year ice ridges. Small-scale field and laboratory experiments," *Cold Reg Sci Technol*, vol. 54, no. 1, pp. 54–71, 2008.
- [41] A. Marchenko and C. Chenot, "Regelation of ice blocks in the water and the air," in *proceedings of the 20th Port and Ocean Engineering Under Arctic Conditions conference*, Luleå, Sweden, 2009.
- [42] H. Helgøy, O. S. Astrup, and K. Høyland, "Laboratory work on freeze-bonds in ice rubble, Part II: Results from individual freeze-bond experiments," in *Proceedings of the 22nd International Conference on Port and Ocean Engineering under Arctic Conditions*, Espoo, Finland, 2013.

- [43] K. V. Høyland and A. Møllegaard, “Mechanical behavior of laboratory made freeze-bonds as a function of submersion time, initial ice temperature and sample size,” in *Proceedings of the 22nd IAHR International Symposium on Ice*, Singapore, 2014.
- [44] I. M. Bueide and K. V. Høyland, “Confined Compression Tests on Saline and Fresh Freeze-Bonds,” in *Proceedings of the 23rd International Conference on Port and Ocean Engineering Under Arctic Conditions*, Trondheim, Norway, 2015.
- [45] A. H. V. Repetto-Llamazares, “Experimental studies of shear failure on freeze-bonds in saline ice part I: set-up, failure mode and freeze-bond strength.,” *Cold Regions Science and Technology*, vol. 65, no. 3, pp. 286–297, 2011.
- [46] C-CORE, “DIRKS: Year 1 progress report,” C-CORE, St. John’s, NL, Canada, Internal report, 2012.
- [47] E. Bailey, J. Bruce, A. Derradji, and M. Lau, “An overview of the development of ice ridge keels strength testing program,” in *Proceedings of the 3rd Arctic Technology Conference*, Houston, Texas, 2014.
- [48] E. Bailey, J. Bruce, and R. Taylor, “The Development of Ice Ridge Keel Strengths: The influence of speed on the strength and deformation behaviour of gouging ridge keel,” in *Proceedings of the 22nd IAHR International Symposium on Ice*, Singapore, 2014.
- [49] R. M. W. Frederking and G. W. Timco, “Field measurements of the shear strength of columnar-grained sea ice,” presented at the IAHR Ice Symposium 18-22 August 1986, 1986, vol. 1, pp. 279–292.
- [50] R. M. W. Frederking and G. W. Timco, “Measurement of shear strength of granular/discontinuous-columnar sea ice,” *Cold Regions Science and Technology*, vol. 9, pp. 215–220, 1984.
- [51] E. Bailey, “The consolidation and strength of rafted sea ice,” PhD thesis, University College London, 2011.

- [52] E. Bailey, P. Sammonds, and D. Feltham, “The consolidation and bond strength of rafted sea ice,” *Cold Regions Science and Technology*, vol. 83, pp. 37–48, 2012.
- [53] M. Ghobadi, E. Bailey, and R. Taylor, “Thermal behaviour and growth of submerged ice blocks: Experimental and Numerical Results,” in *Proceedings of the 34th International Conference on Ocean, Offshore and Arctic Engineering*, St. John’s, Canada, 2015.
- [54] J. W. Glen, “The creep of polycrystalline ice,” *Proc. R. Soc. Lond. A*, vol. 228, no. 1175, pp. 519–538, 1955.
- [55] T. J. O. Sanderson, *Ice mechanics : risks to offshore structures*. London: Graham & Trotman, 1988.
- [56] S. Shafrova and K. V. Høyland, “The freeze-bond strength in first-year ice ridges. Small-scale field and laboratory experiments,” *Cold Reg. Sci. Technol.*, vol. 54, no. 1, pp. 54–71, 2008, doi: 10.1016/j.coldregions.2007.11.005.
- [57] J. R. Blackford, “Sintering and microstructure of ice: a review,” *Journal of Physics D: Applied Physics*, vol. 40, no. 21, p. R355, 2007.
- [58] D. Wilkinson, “A pressure-sintering model for the densification of polar firn and glacier ice,” *Journal of Glaciology*, vol. 34, no. 116, pp. 40–45, 1988.
- [59] N. Maeno and M. Arakawa, “Adhesion shear theory of ice friction at low sliding velocities, combined with ice sintering,” *Journal of Applied Physics*, vol. 95, no. 1, pp. 134–139, 2004.
- [60] E. M. Schulson and A. L. Fortt, “Static strengthening of frictional surfaces of ice,” *Acta Materialia*, vol. 61, no. 5, pp. 1616–1623, 2013.
- [61] S. Scourfield, P. Sammonds, B. Lishman, and A. Marchenko, “The effect of ice rubble on ice-ice sliding,” in *Proceedings of the 23rd International Conference on Port and Ocean Engineering under Arctic Conditions*, Trondheim, Norway, 2015.

4. CONFINEMENT PRESSURE EFFECTS

4.1. Preface

The contents of this chapter are based on a manuscript that has been prepared for publication in a peer-reviewed journal and will be submitted in the near future. I am the primary author of this paper, along with the co-authors, Dr. Rocky Taylor and Dr. Eleanor Bailey. I conducted the literature review and experiments, analyzed the data, and prepared the first draft of the manuscript. The co-authors helped with the design of experiments, and provided feedback on the test plan, analysis of data, and revised the manuscript.

4.2. Chapter Abstract

The effects of confining pressure on the development and strength of freshwater freeze bonds were investigated in a series of Asymmetric Four-Point Bending (AFPB) experiments. Ice blocks with an initial temperature of -18°C were submerged for four different submersion times of 30 minutes, 3 hours, 3 days and 7 days. A normal confinement pressure varying from 10 to 100 kPa was applied during the formation and shear of the freeze bond, which was sheared with an actuator rate of 5 mm/s. The shear strength of freeze bonds were observed to be highly influenced by confinement pressure, increasing with an increase in confinement. The rate of increase in strength was found to be strongly dependent on submersion time, following the trends of strength-submersion time curve of freeze bond observed in previous studies. Sintering-creep and crushing of asperities are believed to be dominant mechanisms of strength development with regards to confinement. Trends of strength-confinement observed in freeze bond studies follow similar trends observed in ice rubble strength tests, signifying the importance of freeze bond strength on ice rubble/ridge strength development.

Keywords: Freeze bond strength; Confinement pressure; Freshwater ice; Ice rubble strength

4.3. Introduction

Ice ridges and ice rubble are common sea ice features that are formed due to compression or shear of two ice sheets. These features must be considered in the design of offshore structures, infrastructure and marine vehicles operating in Arctic and sub-Arctic waters, as they can assert a considerable load during events such as ice rubble pile-up against structures, ice-ridge structure interactions, ice ridge keel scouring of subsea infrastructure, and refrozen brash ice channels in river and oceans.

Ice rubble strength has been attributed to the consolidation of ice blocks (i.e. freeze bonds) as well as the strength of ice blocks themselves [1]. Freeze bonds formation starts as a result of heat transfer from water to the ice blocks, causing freezing at the contact points. Bond strength continues to develop after this initial formation as a result of pressure-related sintering created by buoyancy forces in floating rubble and ridges, and the weight of sail in an ice ridge [2]. This value can be significantly higher in grounded keels, where an external confinement pressure is applied as the keel is pushed in to the ground [3].

Ettema and Schaefer [4], Shafrova and Høyland [1], Repetto-Llamazares et al. [5], Bueide and Høyland [6], and C-CORE [7] studied the effects of confinement pressure on freeze bond strength development and failure. Using the direct shear methodology, Ettema and Schaefer [4] investigated the effects of confinement on shear strength of freshwater freeze bonds formed in different submersion liquids (saline and freshwater). Samples with an initial temperature of -10°C were submerged for 10 s and were sheared at a rate of 0.84 mm/s. Increasing the confinement from 0.2 to 2 kPa, they observed the shear strength

to increase from 1 to 7 kPa. Repetto-Llamazares et al. [5] also used the direct shear method to measure the shear strength of the freeze bond between saline ice specimens with three initial ice temperatures of -1.2, -7 and -14°C, which were submerged for 20 h, and were sheared with a shear rate of 0.7 mm/s. A general increase in strength was observed in these tests as confinement increased from 0.125 to 2 kPa. Bueide and Høyland [6] used tri-axial compression tests to measure the strength of freeze bonds formed between cylindrical saline and freshwater ice samples that were cut in half at a 45° angle. Tests were conducted for submersion times ranging from 0.5 min to 20 h, for two initial ice temperatures of -2.5 and -8.5°C and a compression rate of 0.8 mm/s. No confinement was applied during the submersion period of the bonds, and a radial confinement ranging from 7 to 99 kPa was applied during compression. Strength values were found to increase with increase in confinement in general. Using the Mohr-Coulomb model, they measured the cohesion and friction angles for freeze bond strength. The freeze bond cohesion and friction coefficients were found to vary from 3 to 99 kPa and from 0.28 to 0.78, respectively. Shafrova and Høyland [1] also used the 45° angle method in a series of field and laboratory experiments, where they measured the shear strength of freshwater and saline freeze bonds. While the field experiments were conducted with no confinement, two confinements of 20 and 50 N were used in their laboratory experiments. No difference in the amount of strength was observed with change in confinement, and results have thus been reported without distinguishing between the amounts of confinement applied, and no comparison can be made between the different confinements used. A series of Asymmetric Four-Point Bending tests were also conducted at C-CORE [7] for freshwater samples with an initial temperature of -11°C that were sheared with an actuator rate of 0.44 mm/s. Varying the

confinement from 10 to 80 kPa, they observed the shear strength to increase from 50 to 120 kPa. The results of the reviewed studies have been plotted in Figure 4.1. Excluded from the plotted results are the results of Bueide and Høyland [6], as no confinement has been applied during the formation period of the freeze bonds, which is of interest in the present paper.

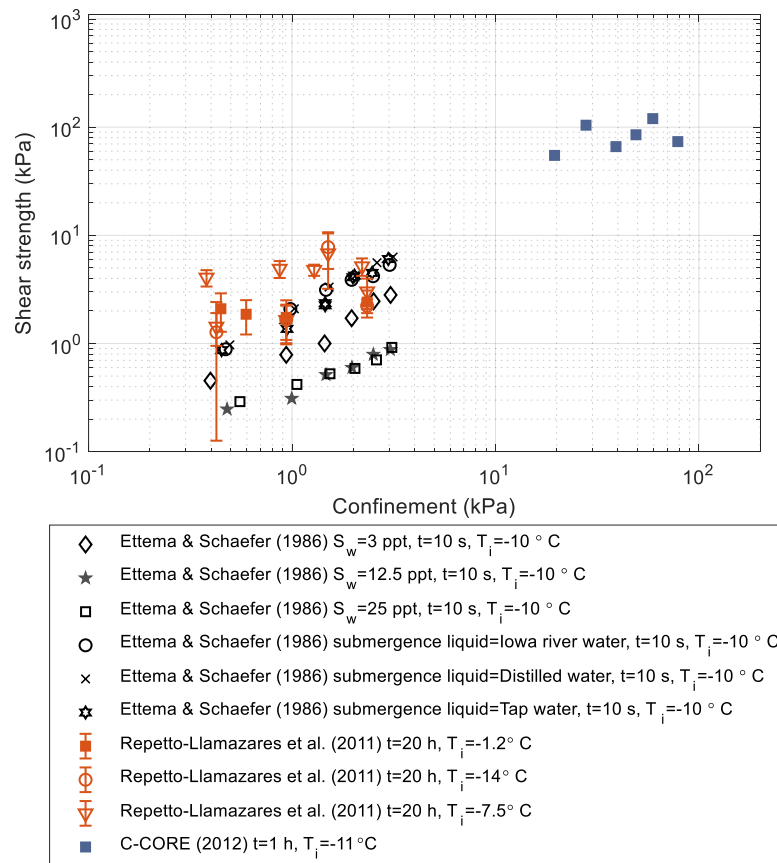


Figure 4.1. Plot showing the measured shear strength values versus confinement from previous freeze bond experiments. In this plot, S_w is the salinity of submergence liquid, t is the submersion time and T_i is the initial ice temperature.

As seen in Figure 4.1 confinement pressures applied during formation of freeze bonds to date have mostly been limited to less than 4 kPa, which is within the range of buoyancy

forces in a ridge keel, assuming that the buoyancy forces are evenly distributed across the keel. In reality however, local contact pressures between contacting ice blocks could be much higher, especially in grounded or gouging ridges. The vertical component of the bulk pressures of a ridge keel, σ_z , is determined using the equation below:

$$\sigma_z = (\rho_w - \rho_i)(1 - e)gz_k \quad (4.1)$$

where ρ_w and ρ_i are water and ice density, respectively. e is the bulk porosity of the ridge keel, g is the gravitational acceleration and z_k is the position from the bottom of the keel [8]. Considering a bulk porosity of 40%, σ_z can reach a value of 15 kPa for a 20 m deep keel. This value, however, is much higher at the contact interface of individual ice blocks as discussed by Bruneau [8]. Using this notion, Bailey et al. [3] discuss that for a 10 m deep keel, where the bulk pressures would be around 7 kPa, considering that only 10% of the area of the ice blocks are in contact with the surrounding ice, the local pressures can be as high as 70 kPa. Equation 4.1 describes the net vertical component of buoyant forces as well as the gravitational component of the ice ridge/rubble structure. It does not, however, account for confinement forces in other directions. Considering the buoyancy portion of Equation 4.1 as a function of depth of the keel ($\rho_w gz_k$), for the same ice ridge keel discussed above confining pressures from water applied in all directions, can be as high as 100 kPa. This signifies the importance of understanding bond formation properties at higher confinements.

Similar to ice rubble failure mechanics, the Mohr-coulomb criteria has been used in the literature to describe the shear strength of freeze bonds in relation to confinement, defining shear strength, τ , as:

$$\tau = c + \sigma \tan \varphi \quad (4.2)$$

where σ is the normal confinement, c is cohesion, and φ is the friction angle [9]. While the Mohr-Coulomb model identifies cohesion and friction angle as a function of shear and normal stress, these two parameters are also a function of properties such as contact time, temperature of ice blocks, salinity, and deformation rate [10]. More work is therefore needed to understand how these parameters influence freeze bond strength development as a function of confinement.

This paper is one of a series of three papers that investigate freeze bond development between two freshwater ice blocks under different conditions of time, temperature, deformation rate, and confinement, with current paper focusing on the effects of confinement on the strength development of the bond [2, 11]. Tests have been conducted for confinements ranging from 10 to 100 kPa for freshwater ice samples that had an initial temperature of -18°C , and were sheared with a deformation rate of 5 mm/s. As submersion time was found to highly influence the freeze bond strength during the first series of experiments focusing on effects of submersion time (Section 3, [2]), current tests were conducted for four different submersion times of 30 minutes, 3 hours, 3 days, and 7 days.

4.4. Experimental Methodology

To form the freeze bonds, cylindrical ice samples, 10 cm in length and 9 cm in diameter, were put together using a frame that was capable of applying a confinement ranging from 10 to 100 kPa (Figure 4.2a). Confinement was applied using a hand-driven gear at one end

of the frame and its magnitude was monitored using an inline 900 N loadcell. The load was transferred to the ice samples via three springs that ensured the load was uniformly distributed to the ice specimens. Three support wedges were put underneath the ice specimens to ensure they are perfectly aligned, which were removed prior to shearing. Once in the correct position, the samples were submerged in a water bath held at 0°C for a pre-specified period of time. Coldroom temperature was held at 0°C for all tests, and coldroom and water bath temperatures were recorded using Resistance Temperature Detectors (RTD).

Samples were sheared using the Asymmetric Four-Point Bending (AFPB) apparatus, shown in Figure 4.2b, immediately after being removed from the water. The AFPB method applies a load to the specimen via four loading pins that are positioned asymmetrically about the loading axis, where the inner pins generate a clockwise moment and outer pins generate a counterclockwise moment resulting in a region of pure shear between the inner pins (e.g. the freeze bond region). The bottom plate of the AFPB apparatus was fixed to the pedestal of a Materials Testing System (MTS) servo-hydraulic testing machine, and the top plate was attached to a hemispherical alignment seat that allowed rotation around the loading point to ensure the loading pins were perfectly touching the samples. The maximum shear stress at the center of the samples, τ_{max} , i.e. the freeze-bonded area, was calculated by:

$$\tau_{max} = \frac{4}{3} \frac{(1 - \alpha)}{(1 + \alpha)} \frac{P_{max}}{\pi r^2} \quad (4.3)$$

In this equation, P_{max} is the maximum shear load observed at failure, r is the radius of ice block, and α is a function of the distance of the loading pins. α , which is the product of the fraction of the distance between the center of inner pins and the loading axis divided by the distance of the center of the outer pins, was set to 0.106 in these experiments. More details on the set-up and test procedure of the experiments have been provided in Section 3 and [2].

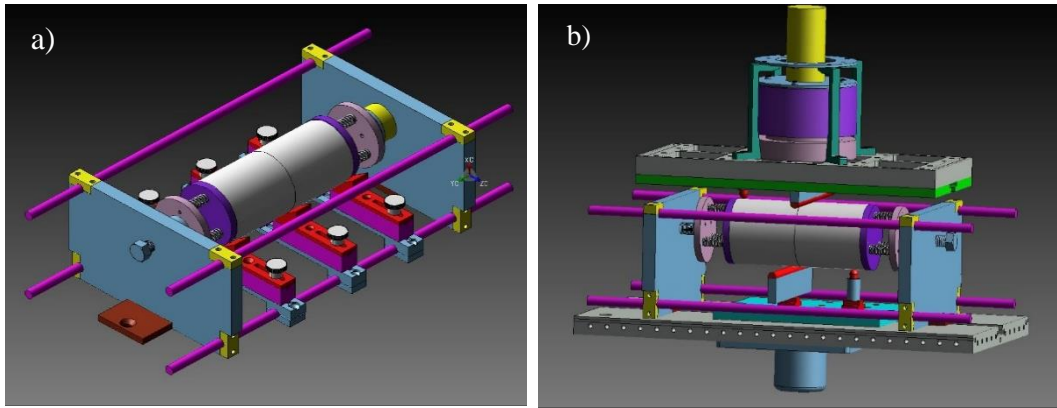


Figure 4.2. Figures showing the design of (a) confinement frame and (b) the Asymmetric Four-Point Bending apparatus.

4.5. Results

A total of 46 tests were conducted for four different submersion times of 30 minute, 3 hours, 3 days, and 7 days. Submersion times used for these experiments were chosen based on the results of the first series of experiments conducted in this test program, focusing on the effects of submersion time on bond strength development (Section 3, [2]). In these tests, five stages were identified for freeze bond strength development, each dominated by distinct physical mechanisms. The 30-minute submersion time is within the thermal

strengthening stage of bond development, where strength development is driven by heat transfer from water to the ice specimens, resulting in new ice growth at the bond interface. The 3-hour submersion time is within the transition period, where the dominant mechanism is believed to switch from thermal to sintering-creep processes with lower freeze bond strengths developed. The 3-day and 7-day submersion times are dominated by sintering-creep processes, where sintering and creep contribute to an increase in strength. For all tests in this study, ice specimens had an initial temperature of -18°C and were sheared at a constant rate of 5 mm/s.

Freeze bond shear strength values obtained at each submersion time, have been discussed in the next subsequent sections, and the results obtained have been summarized in Table 4.1. Values of strength for each confinement are averaged over the number of repeats for each test, along with the deviation from the average.

Table 4.1. Confinement pressure test matrix. Parameters in the table are: submersion time (t), initial ice temperature (T_i), actuator rate (V), confinement (σ), number of tests (n), mean shear strength (τ_{mean}), shear strength values for each test (τ), minimum and maximum strength (τ_{min} , τ_{max}), standard deviation (STD), failure load (F_{max}).

t	T_i (°C)	V (mm/s)	σ (kPa)	n	τ_{mean} (kPa)	τ (kPa)	τ_{min} (kPa)	τ_{max} (kPa)	STD (kPa)	F_{max} (N)
30 min	-18	5	10	2	110.1	157.9 62.32	62.32	157.9	67.5	932.0 367.8
			15	2	173.7	237.9 109.5	109.5	237.9	90.7	1404.2 646.3
			25	3	102.6	116.7 88.56	88.56	116.7	19.8	688.8 522.7
			40	2	179.29	112.7 245.88	112.7	245.88	94.1	665.2 1451.3
			50	2	143.7	134.2 153.2	134.2	153.2	13.4	792.1 904.2
			75	2	192.5	158.8 226.2	158.8	226.2	47.6	937.3 1335.1
			100	2	158.6	215.3 102	102	215.3	80.1	1270.8 602
			3 hr	-18	5	10	2	91.3	119.3 63.3	63.32
15	3	183.4				217.4 261.8 71.1	71.1	261.18	99.7	1283.2 1545.3 419.6
25	2	90.9				59.4 122.4	59.4	122.4	44.5	350.6 722.4
40	4	110.7				150.6 143.4 105.7 43.2	43.2	150.6	49.1	888.9 846.4 623.9 254.9
50	2	97.7				121.9 73.6	73.6	121.9	34.1	719.5 434.4
75	2	122.7				134 111.5	111.5	134	15.9	790.9 658.1
100	3	216.7				144 388.5 117.7	117.7	388.5	149.3	849.9 2293.1 694.7
3 d	-18	5				10	2	127.7	186.1 64.4	65.4
			25	3	164.7	119.7 251.5 122.9	119.7	251.5	75.1	706.5 1484.5 725.4
			50	1	130	130	-	-	-	767.3
			100	1	213.4	213.4	-	-	-	1259.6
7 d	-18	5	10	1	190.8	190.8	-	-	-	1126.2
			25	3	188.2	122.9 131.5 310.2	119.7	251.5	105.7	725.4 776.2 1831
			50	1	330.8	330.8	-	-	-	1952.6
			75	1	269.1	269.1	-	-	-	1588.4
			100	1	387.8	387.8	-	-	-	2289

4.5.1. Tests with 30 minutes of submersion time

A total of 15 tests were conducted for a submersion time of 30 minutes, varying the confinement from 10 to 100 kPa. Results of these tests presented in Figure 4.3 show a general increasing trend of shear strength as confinement increases, with the average strength ranging from 100 to 160 kPa. Using a linear curve fit through the average strength values, the shear strength-confinement relationship for the 30-minute submersion time tests can be presented as Equation 4.4. Since the failure of freeze bonds is governed by brittle fracture across the bond interface, the authors suggest that modelling freeze-bonded ice rubble as a porous brittle solid is more physically representative than treating it as a Mohr-Coulomb material. Nonetheless, since the relationships between the freeze bond shear strength (τ_{FB}) and the applied normal stress (σ_c) over the range of conditions considered in these tests may be approximated using a linear relationship, this expression will take on a similar form to a Mohr-Coulomb type model. It is important to note that despite the similarities in the form of these expressions, the physical interpretation of the freeze bond strength relationship as a function of confinement given in Equation 4.4 is not the same as for a classical Mohr-Coulomb type relationship. Equation 4.4 reflects how the brittle fracture of solid ice in the freeze bond between two masses of ice changes with confining pressure, whereas Mohr-Coulomb theory is a continuum approximation that relates the shear strength of granular materials to cohesion and friction within large volumes of small granular particles (which two freeze-bonded cylindrical ice specimens clearly are not). This is an important distinction, since future directions should focus on better understanding of the physics and modelling of processes. Linking processes across

different scales will require a different approach than simply extracting parameter values based on small-scale tests and extrapolating them to larger scales. Extending this work to full-scale rubble requires careful consideration of assumptions and approximations to ensure research results from small-scales are connected to full-scale ridges and rubble in a physically representative way, as is presently being considered in the work of Afzali et al. [12].

$$\tau_{FB} = 129 + 0.49\sigma_c \quad (4.4)$$

where τ_{FB} is the shear strength, and σ_c is the normal confinement pressure.

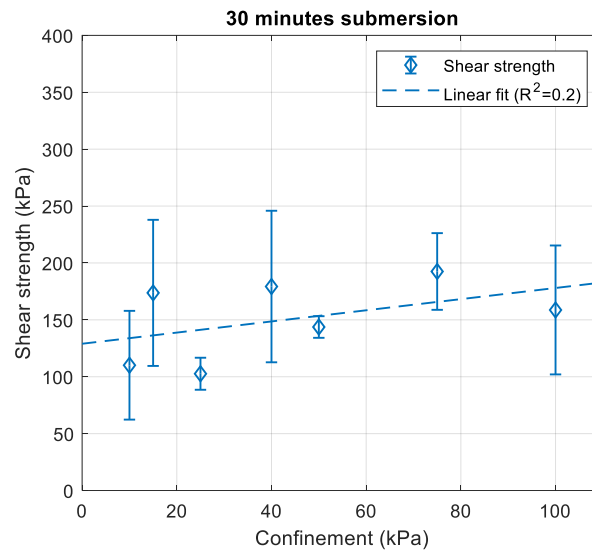


Figure 4.3. Comparison of shear strength over confinement for 30 minutes submersion time, with linear fit to the data.

4.5.2. Tests with 3 hours of submersion time

A total of 17 tests were conducted for 3-hour submersion and results showed a similar increasing trend as confinement increased (Figure 4.4). Comparing the strength values of

3-hour tests to the results of 30 min submersion time tests, it is observed that while the strength values for the 30-minute strength values are generally higher than the 3-hour tests, the rate of increase in average strength is higher for the 3-hour tests, varying from 90 to 260 kPa (compared to 100 to 160 kPa in 30-min tests). Similar to the 30 min submersion time tests, a linear curve has been fit through the average strength values, and the strength-confinement relationship for this submersion time can be expressed as Equation 4.5.

$$\tau_{FB} = 96 + 0.77\sigma_c \quad (4.5)$$

where τ_{FB} is the freeze bon shear strength, and σ_c is the normal confinement pressure.

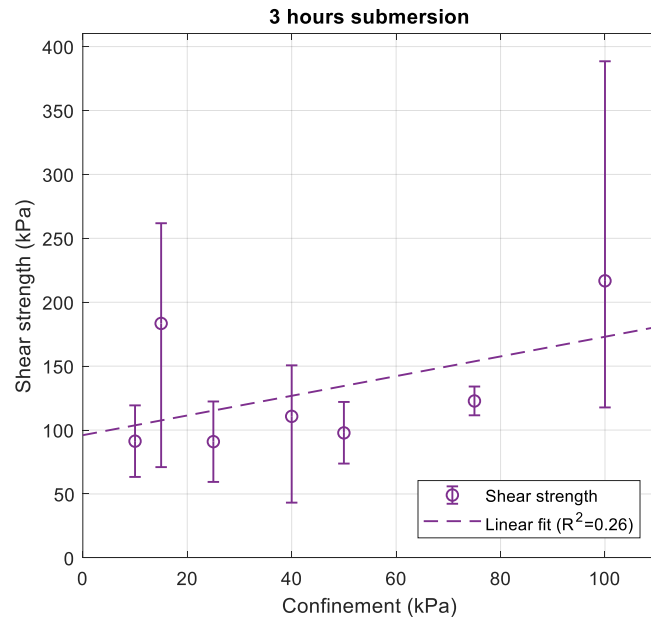


Figure 4.4. Comparison of shear strength over confinement for 3 hours submersion time.

4.5.3. Tests with 3 days of submersion time

Figure 4.5 presents the results of the seven tests conducted for three days of submersion, where confinements of 15, 25, 50, and 100 kPa were used. Consistent with the results of 30-minute and 3-hour submersion time tests, a clear increasing trend is observed with increase in confinement. The average strength of freeze bond for this submersion time is within the range of 120 to 213 kPa, and the strength-confinement relationship can be expressed by:

$$\tau_{FB} = 120 + 0.84\sigma_c \quad (4.6)$$

where τ_{FB} is the freeze bond shear strength, and σ_c is the normal confinement pressure.

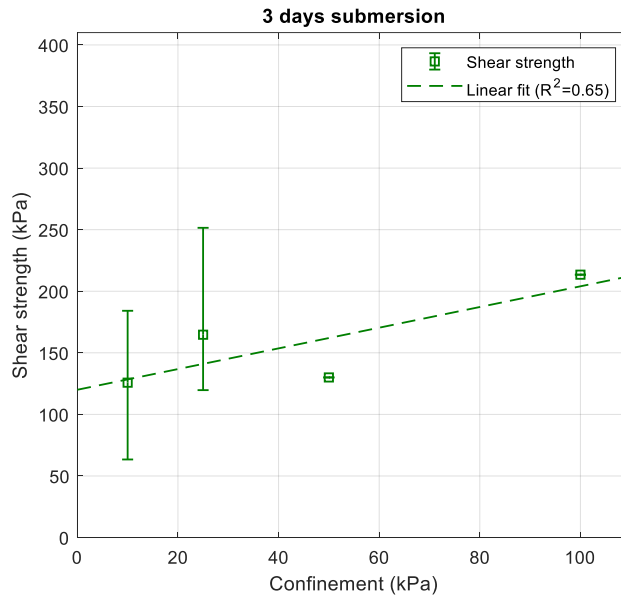


Figure 4.5. Comparison of shear strength over confinement for 3 days submersion time.

4.5.4. Tests with 7 days of submersion time

Tests with seven days submersion time were conducted with the aim of investigating the concurrent influence of prolonged submersion times and confinement pressure on strength of freeze bonds. Due to the testing time limitations for this submersion time, limited number of tests were conducted for confinements ranging from 10 to 100 kPa. Shear strength values obtained in these tests have been plotted against confinement pressure in Figure 4.6. As seen in this figure, freeze bond strength values are clearly higher than the strength values measured for shorter submersion times. The rate of increase in strength is also higher, ranging from 188 to 387 kPa. The linear fit to the average strength values can be expressed by Equation 4.7.

$$\tau_{FB} = 165 + 2.1\sigma_c \quad (4.7)$$

where τ_{FB} is the freeze bond shear strength, and σ_c is the normal confinement pressure.

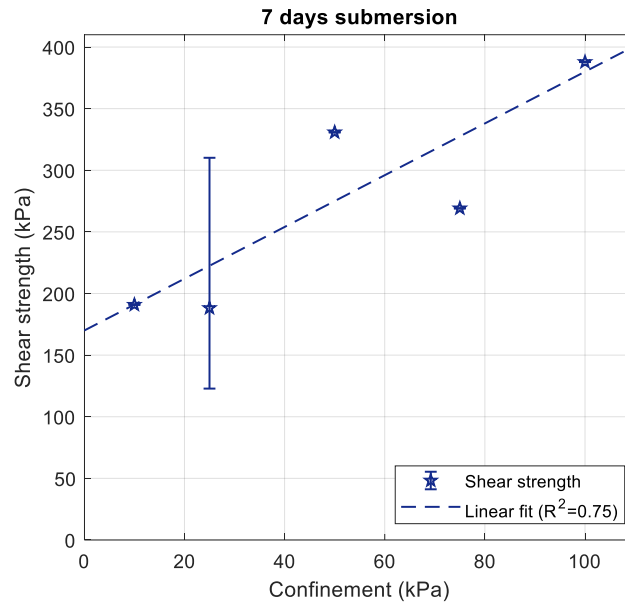


Figure 4.6. Comparison of shear strength over confinement for 7 d submersion time.

4.6. Discussion

4.6.1. Analysis and discussion of results

It is clear from the results presented in Section 4.3 that increase in confinement results in an increase in the shear strength of freeze bonds. Trendlines of shear strength with regards to confinement pressure for each submersion time discussed in the previous section (Equation 4.4- Equation 4.7) have been presented together in Figure 4.7. Comparing the rate of increase in strength for each submersion time, it is observed that increasing confinement has a positive influence on freeze bond strength for shorter submersion times (less than three days), which is more pronounced for longer submersion times (more than three days).

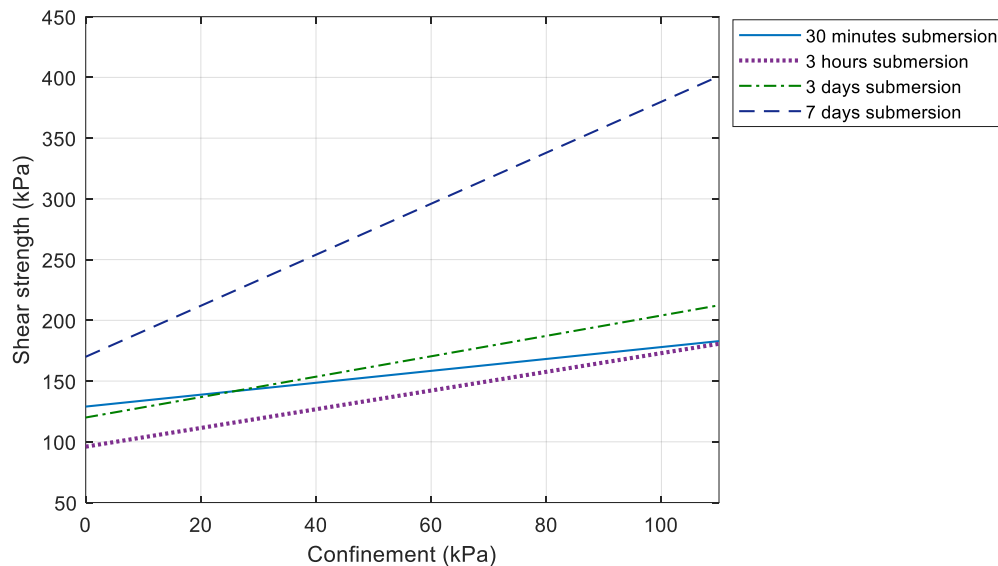


Figure 4.7. Linear fit of confinements over confinement for the submersion times tested.

Trends observed in Figure 4.7 are consistent with the observations from the submersion time tests (Section 3.5.2, [2]). Similar to those tests, the 30-minute submersion, which is within the thermal strengthening stage of bond development has higher values in comparison to 3-hour tests for lower confinements, after which the dominant mechanism is believed to switch from thermal to sintering-creep processes with lower freeze bond strengths developed. The switch to sintering dominant bonding at higher pressures however appears to result in a more pronounced confinement pressure dependency in 3-hour tests, where the rate of increase in strength is higher. For the 3-day and 7-day submersion times, the dominance of sintering-creep processes contribute to an increase in strength. These processes are accelerated with increase in confinement and submersion time. Similar behavior has been reported in sintering studies [13], as well as ice-ice friction tests [14],

although for lower range of confining pressure, which will be discussed in Section 4.4.2. This is highly important for ice features in nature, as they are likely to be subject to confinements for weeks/months before an interaction occurs.

4.6.2. Discussion of physical mechanisms

During the submersion period of the bonds, several processes simultaneously influence bond development on the asperity level, each influenced by the degree of confinement pressure applied. Figure 4.8 presents a schematic illustration of the processes taking place between the asperities of the contacting ice blocks.

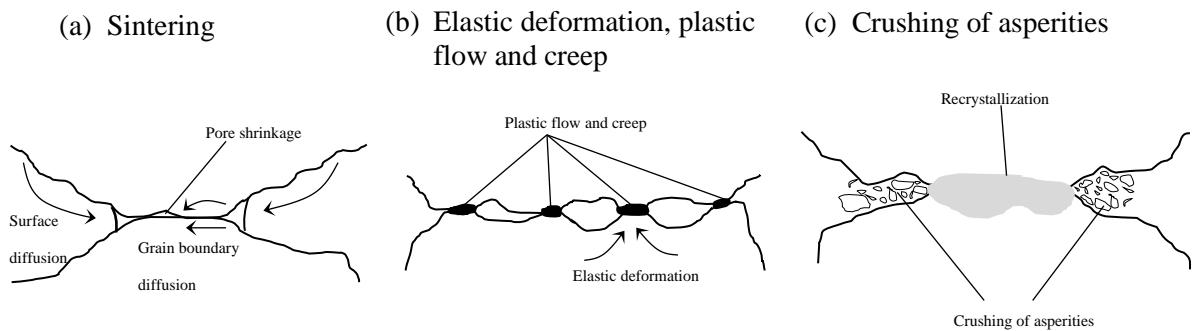


Figure 4.8. Schematic illustration of processes affecting freeze bond strength development.

In the presence of an external pressure, sintering and creep processes (Figure 4.8a, b) have been explained as the mechanisms causing bond development between two contacting ice pieces [15]. Sintering is known as the process of mass transfer between two contacting materials close to their melting point, forming a bond between them. When two asperities

are brought into contact, the tendency to minimize surface free energy drives mass from surrounding parts to the contact interface. In the absence of external pressures, several mechanisms are known to be responsible for sintering: vapor diffusion, surface diffusion, surface flow, volume diffusion, plastic flow, and grain boundary diffusion [13]. With application of an external pressure, more complicated processes such as diffusional creep, dislocation creep, and grain boundary sliding govern bond formation [16]. Several ice sintering studies have been conducted on spherical ice particles in contact [15–18]. In a broader context, sintering as well as creep and plastic flow (Figure 4.8b) have been used to explain adhesion and friction of ice using the power-law creep equation [12-13, 19-20]. Maeno and Arakawa [14] used the concept of sintering to study the static friction coefficient of ice-ice interface. According to their theory, ice-ice friction is higher at slower sliding velocities as a result of junction growth and sintering of asperities. This process, also known as dynamic freeze-bonding, allows for new bonds to be formed during the slow movement of ice blocks past each other, which in turn increases the required force to initiate/resume sliding. The effects of sintering were found to be more pronounced at higher temperatures and lower sliding velocities. In a series of slide-hold-slide shear tests, Schulson and Fortt [21] found the static friction of ice-ice interface confined under a normal load to increase with increase in hold time. They attribute this behavior to the creep of asperities in contact. Considering that the contact interface includes a number of asperities being pushed together (Figure 4.8b), with continuous application of a normal pressure, the height of these asperities start to decrease as a result of creep. According to Schulson and Fortt [21], as the height of asperities decrease due to creep, contact area of these asperities increases, which results in an increase in the shear resistance, or shear strength of the bonds formed, as well

as the number of asperities in contact [4]. The power-law creep equation, shown in Equation 4.8, has been used to formulate the amount of decrease in height (i.e. strain) which directly translates to the area increase. In this equation, $\dot{\epsilon}$ is the strain rate, B is a constant that is a function of temperature, σ is the normal pressure, n is a constant that is a function of the dominant creep or sintering process.

$$\dot{\epsilon} = B\sigma^n \quad (4.8)$$

Szabo and Schneebeli [13] investigated the sub-second sintering of ice for contacting ice cones under a normal pressure. According to their theory, the contact area of contacting ice cones increases with application of pressure as a result of creep and plastic deformation. The rate of creep was found to be highly influenced by the amount of normal pressure, and contact time, increasing with increase in both parameters. Creep and sintering rates were also accelerated in near melting temperatures. This has specific importance in our experiments, as samples reach thermal equilibrium with surrounding water after 30 minutes and tests conducted longer than this period are at near zero temperatures.

Ice block diameter measurements before and after the tests in our experiments did not show any dependency of contact area on the amount of confinement applied. However, we believe that, although not visually observable in macro-scale, sintering and creep processes are likely to result in an increase in the area of asperities in contact at the freeze bond interface as discussed by Schulson and Fortt [21], although there are likely localized ice crushing processes that also are at play. As discussed earlier, these processes are accelerated at higher pressures, which is consistent with the increasing trends of strengths observed in

our experiments. Similar to the observations of Szabo and Schneebeli [13], sintering-creep effects in our experiments appear to be more pronounced in higher submersion times, as 3-day and 7-day submersion time results showed higher strengths compared to shorter submersion times. Furthermore, with continuous application of pressure, the number of asperities in contact increase, which further increases the contact area [22].

It is possible for the opposing asperities in contact, confined under a high normal load, to crush and form a layer of crushed ice at the freeze bond interface (Figure 4.8c) [20, 21]. Crushed particles of ice at the freeze bond interface would significantly increase the total contact area that can sinter together as a result of the confinement pressures applied, thus increasing the shear strength of the bonds. This was captured by Singh and Jordaan [23] in a series of triaxial tests on crushed ice under hydrostatic loading. Confining the samples for short periods of time (20 minutes) before testing resulted in higher strengths compared to tests that were conducted immediately. This is a result of sintering between the crushed particles of ice, which is accelerated with increase in contact period and confinement. Thin sections of the samples in their tests also confirmed this theory, where sintered grains of ice were observed. Microscopic analysis of the bond interface in present study is required to confirm whether a similar sintered crushed ice layer exists at the bond interface. Thin section analysis was attempted but was however not successful as the sample broke. We hypothesize that the freeze bond interface would contain smaller grains and more crushed ice at higher confinements and longer periods of submersion. This is an important area for continued research.

Strength development mechanisms discussed above are expected to be influenced by the contact surface conditions (e.g. surface roughness). Samples in this test program were milled to minimize randomness in contact surface properties. It is however of interest to study how different surface conditions would influence the sintering, creep and crushing processes discussed above. While the surface roughness was not measured, freeze bond experiments of Helgøy et al. [24] showed natural ice surfaces to create stronger bonds in comparison to artificially prepared surfaces. Higher surface roughness has also been observed to increase friction forces between ice, which is attributed to increase in contact area and interlocking between asperities during sliding [25]. The effects of surface roughness on confinement pressure dependency of freeze bond strength are therefore an important topic for consideration in future tests.

4.6.3. Comparison of freeze bond shear strengths with other data

Values from C-CORE [7], Ettema and Schaefer [4], and Repetto-Llamazares et al. [5] have been compared to the results of present paper and are presented in Figure 4.9. This plot has been presented in log-scale due to the scatter in the data. Excluded from these results are the experiments of Bueide et al. [6], as the radial confinement used in those experiments was applied only during the shear of freeze bonds and not formation. Although direct comparison of the results of these experiments is not possible due to the differences in test conditions, for the range of confinements used in the literature, the shear strength of the freeze bonds was observed to increase with increase in confinement. The best fit to the

data of previous freeze bond experiments as well as the results of present study follow a power-law equation as:

$$\tau_{FB} = 1.52\sigma_c^{1.17} \quad (4.9)$$

where τ_{FB} is the freeze bond shear strength and σ_c is the normal confinement. The overall increasing trend of freeze bond strength with confinement will increase until it reaches the strength of solid ice.

A series of tests were conducted in this test program, measuring the shear strength of solid ice samples of the same dimensions used in freeze bond tests (Section 3.4.2). Varying the submersion time from 1 minute to 7 days, under a confinement of 25 kPa, the average strength of solid ice was found to be 357 kPa, which has been shown with a dashed line in Figure 4.9 [2]. The strength values of the 7-day submersion time tests show that the strength values for high confinements (>50 kPa) are within a close range of the average shear strength of solid ice, supporting this notion.

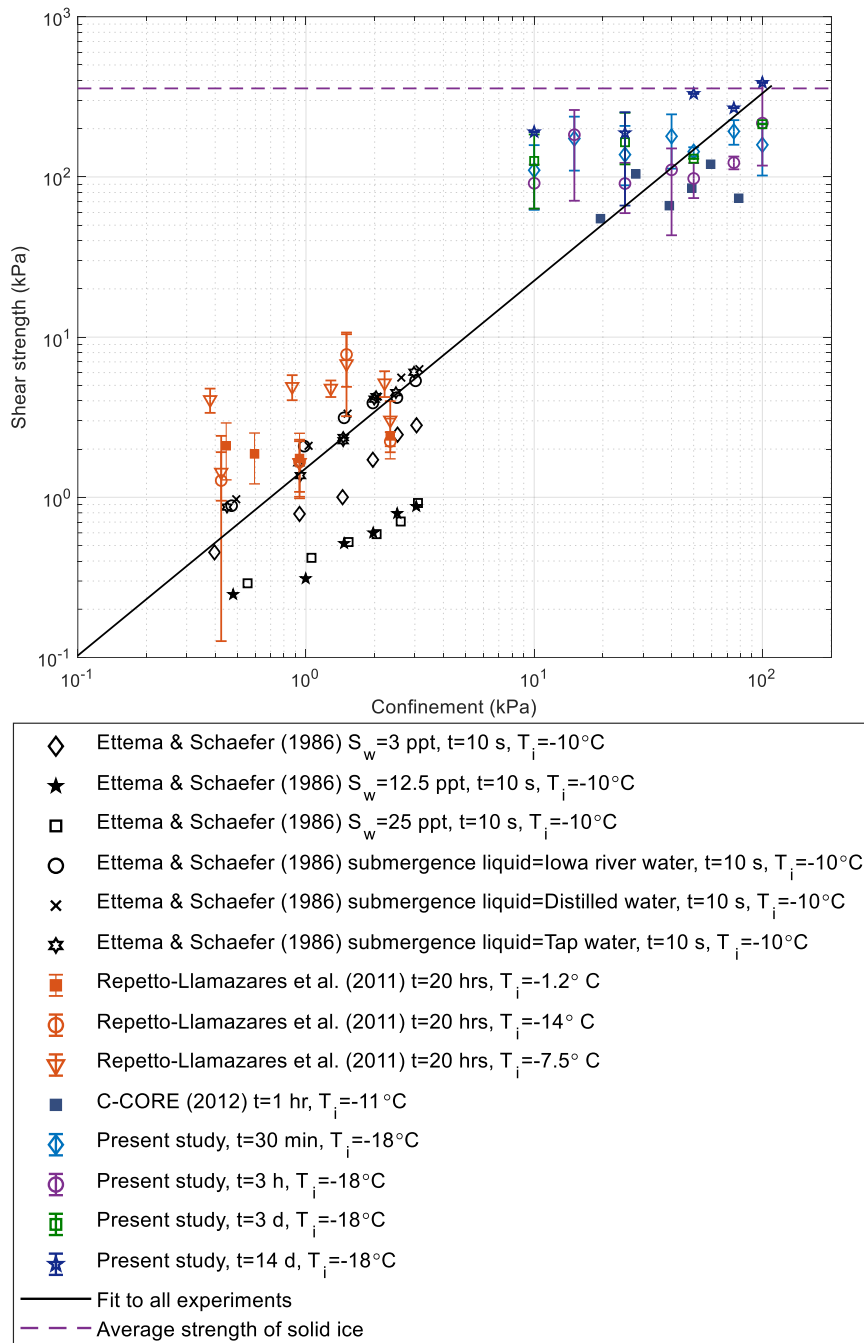


Figure 4.9. Comparison of the results of the present study with previous freeze bond experiments.

4.6.4. Discussion of implications for ice rubble shear strength

Several studies have focused on understanding the strength development and failure properties of ice rubble as a function of confinement [23–29]. Urroz and Ettema, [29] conducted a series of simple shear box experiments to measure the shear strength of unconsolidated ice rubble, for three different cubic block sizes with representative lengths of 18 mm (small), 26 mm (medium) and 70 mm (large). The strength of the ice rubble showed a general increasing trend with increase in confinement, with smaller blocks showing a higher strength value compared to larger blocks. They attributed this to the freeze bond forces being more significant in smaller blocks. Smaller ice blocks allow for more pronounced formation of freeze bonds between asperities, which in turn increases the strength. Medium size blocks however were an outlier, showing higher strength values compared to small and large blocks. This the authors believed was a result of the shape of the samples, as medium blocks had sharp edges in contrast to the rounded edges of small and large blocks, possibly increasing the interlocking forces during shear. This however, may also be a result of sintering between the blocks, as sharper edges in contact induce more, and are more likely to experience localized crushing between asperities. In a series of shear box tests, Weiss et al. [30] investigated the role of confining pressure, ranging from 0 to 28 kPa, on the strength of ice rubble with three different ice block thicknesses of 8, 16, and 20 cm, and ice rubble layer thicknesses ranging from 46 to 91 cm, which were deformed under two rates of 3-5 mm/s (slow) and 25 mm/s (fast). Using the Mohr-Coulomb model, they observed that the rubble strength increases with increase in the amount of confinement. Ice blocks used to create the rubble for one test in these tests were used for a

number of following tests before being replaced by new ice blocks. This can highly influence the size and shape of the samples, as samples that have been used a few times are likely to have more rounded edges, influencing bonding and sintering processes, and thus the results. Hellmann [26] also used the shear box method for three different types of ice (Milled, fishery, and ice chips) sheared at deformation rates ranging from 1 to 100 mm/s, confined under a confinement of 0 to 6 kPa. Three shear phases were identified during the shear of the ice rubble. Phase one was associated with a steep increase in shear force while the normal force is constant, which is a result of the packing of ice blocks before the real shearing event. The second phase was associated with the simultaneous increase of shear and normal forces. The increase in normal force in this phase was attributed to the dilatation of the ice blocks into the side walls. Maximum shear strength was also observed at this stage. Shear force dropped in the third phase as shearing continued. For all shear phases identified, shear strength increases linearly with an increase in confinement. Primary and secondary shear modes exhibited a considerable amount of cohesion, whereas tertiary shear mode was cohesionless. Using the direct shear box method for a 0.3 deep floating ice rubble and two ice block thicknesses of 19 and 38 mm, Prodanovic [27] found the strength of ice rubble to linearly increase when confinement was increased from 0 to 3 kPa. Yasunaga et al. [31] conducted a series of direct shear tests on saline ice rubble, confined under confinement pressures ranging from 1.8 to 11.29 kPa, which were sheared at rates ranging from 0.1 to 24 mm/s. The Mohr-Coulomb model was used in these tests as well, and strength was found to linearly increase from 5 to 30 kPa with increasing confinement

It is noted that in all of these tests, authors measure the shear strength of unconsolidated ice rubble and have thus not taken into account the influence of consolidation time, i.e. freeze bond formation between the ice blocks, on strength development. The increasing trend observed in those studies is therefore mostly due to compaction of ice rubble and is of a more frictional nature, with low cohesion between the ice blocks, since the formation of freeze bonds in these experiments is limited to the short amount of time before each and in some cases bonds are intentionally broken before the tests [29].

More recently, to address the effects of consolidation time, Shayanfar [25, 29] conducted a series of medium-scale ice rubble punch tests, for ice rubble with a thickness of 50 cm, deformed at a rate of 5 mm/s. Both shear and flexural strength analysis were used to analyze the results, where shear strength was defined as the peak shear force divided by the apparent failure area, and flexural strength was calculated by the four-point beam bending equation. Increasing the confinement from 0 to 40 kPa for a submersion period of 4 hours, shear strength was observed to linearly increase. Strength values also slightly increased as consolidation time increased from 0 to 70 h. Similar to the observations of present study, sintering processes were identified as the responsible mechanism contributing to further strength development of the ice rubble for cases where the ice blocks were in thermal equilibrium with the surrounding water. Ice blocks in these tests reached equilibrium temperature with surrounding water after two hours of submersion, meaning that no new ice growth would take place after this submersion time. Strength values however were observed to slightly increase after this submersion time, which was attributed to sintering effects.

The influence of confinement on strength development of ice rubble was found to be much higher in comparison to consolidation time in ice rubble tests of Shayanfar [25, 29]. This is while freeze bond strength development in block-block scale has been proved to be highly affected by submersion time. Confinement effects in present study were observed to be significantly intensified in prolonged submersion times, which allow for more sintering to take place between the asperities, thus increasing the strength. The results of Shayanfar [25, 29] however suggest the confining pressure to have a more pronounced influence on strength development, and compaction appears to be a highly important mechanism promoting bond development. It is believed that the consolidation times used in ice rubble tests may not have been long enough to capture submersion time effects on the overall strength development of ice rubble. Due to the complexities of observing internal block block contacts in ice rubble, further ice rubble tests to study these effects for prolonged submersion times are recommended to help better understand these effects. Since larger masses of ice also have more thermal mass, this could delay the onset of sintering-creep processes. Ice blocks in experiments of present work reached equilibrium temperature with the surrounding water after 30 minutes of submersion, while it took 2 hours for the ice rubble to reach equilibrium temperature in the ice rubble tests of Shayanfar [25]. This suggests that the time scales of strength development processes may be longer in large masses of ice rubble, and longer consolidation times may be required to observe similar submersion time effects in ice rubble as were observed in block-block freeze bond tests.

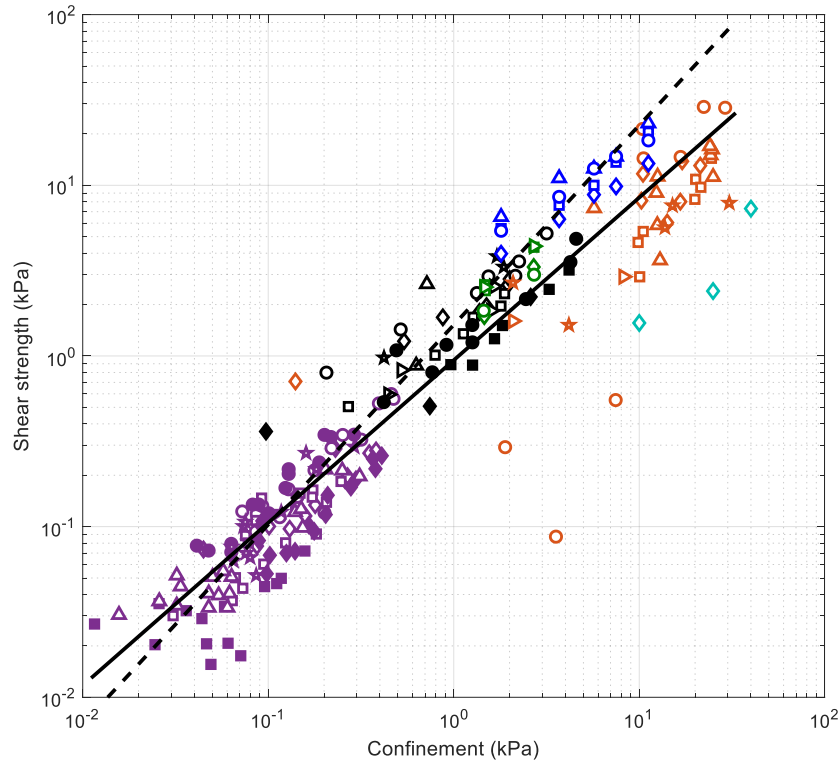
Despite these differences, results of ice rubble experiments mentioned above show similar increasing trends with block-block freeze bond strength tests. Figure 4.10 presents the

strength values obtained in ice rubble experiments as a function of confinement pressure, which was presented earlier in Figure. 2.3. Fitting a power-law curve through the data points, the increasing strength-confinement relationship for all ice rubble tests can be expressed as:

$$\tau_R = 0.94\sigma_c^{0.95} \quad (4.10)$$

where τ_R is the shear strength of the ice rubble and σ_c is the normal confinement. Comparing Equation 4.10 to the equation obtained from freeze bond experiments (Equation 4.9) in Figure 4.10, it is observed that the rate of increase in strength as a result of confinement is higher in freeze bond tests. During the failure of ice rubble, processes such as compaction, local fracture, and crushing are likely to take place, which influence the impact of the role of confining pressure on strength. Freeze bond experiments however have investigated the sole effects of confining pressures by isolating the effects of these other parameters. Furthermore, submersion time proved to highly affect the rate of strength development with increasing confinement in freeze bonds. This is while ice rubble studies to date have not properly addressed consolidation time effects and compaction has been identified as a major contributing mechanism to strength of ice rubble for conditions considered to date. In ice rubble structure, there would be considerable variability in size, shape, orientation, hydrostatic pressure, block temperature, and other conditions which would contribute to variability in local freeze bond strength throughout a keel, or rubble. More work is therefore needed to investigate common links in these two scales, specifically the role of prolonged consolidation times in strength development of ice rubble. Also of interest are the contact pressures between individual blocks of ice in the ice rubble structure.

Contact areas and pressures between blocks are highly influenced by compaction and are thus not solely dependent on the average confinement applied, since factors such as block size, shape, orientation and packing will also have an effect. An investigation of these effects is recommended in future studies, since this work would provide valuable insights to allow for better comparison of results between ice rubble and freeze bond tests.



◇	Urroz and Ettema (1987), $H_{rubble}=228$ mm, $V=1.4-15.75$ mm/s, $\eta=0.23$, Small size blocks	◇	Weiss et al. (1981), $H_{rubble}=46-91$ cm, $H_{ice\ sheet}=200$ mm, $V=25$ mm/sec, $\eta=0.39-0.5$
□	Urroz and Ettema (1987), $H_{rubble}=228$ mm, $V=1.4-15.75$ mm/s, $\eta=0.39$, Medium size blocks	○	Weiss et al. (1981), $H_{rubble}=46-91$ cm, $H_{ice\ sheet}=200$ mm, $V=1$ mm/sec, $\eta=0.39-0.5$
□	Urroz and Ettema (1987), $H_{rubble}=200$ mm, $V=1.4-15.75$ mm/s, $\eta=0.36$, Large size blocks	□	Weiss et al. (1981), $H_{rubble}=91$ cm, $H_{ice\ sheet}=150$ mm, $V=25$ mm/sec, $\eta=0.28-0.36$
◆	Urroz and Ettema (1987), $H_{rubble}=152$ mm, $V=1.4-15.75$ mm/s, $\eta=0.31$, Small size blocks	△	Weiss et al. (1981), $H_{rubble}=91$ cm, $H_{ice\ sheet}=150$ mm, $V=1$ mm/sec, $\eta=0.28-0.36$
●	Urroz and Ettema (1987), $H_{rubble}=152$ mm, $V=1.4-15.75$ mm/s, $\eta=0.4$, Medium size blocks	★	Weiss et al. (1981), $H_{rubble}=76-86$ cm, $H_{ice\ sheet}=80$ mm, $V=25$ mm/sec, $\eta=0.19-0.36$
■	Urroz and Ettema (1987), $H_{rubble}=133$ mm, $V=1.4-15.75$ mm/s, $\eta=0.41$, Large size blocks	○	Weiss et al. (1981), $H_{rubble}=76-86$ cm, $H_{ice\ sheet}=80$ mm, $V=1$ mm/s, $\eta=0.19-0.36$
△	Urroz and Ettema (1987), $H_{rubble}=76$ mm, $V=1.4-15.75$ mm/s, $\eta=0.36$, Small size blocks	◇	Prodanovic (1979), $H_{rubble}=30$ cm, $H_{ice\ sheet}=19$ mm, coarse rubble
★	Urroz and Ettema (1987), $H_{rubble}=76$ mm, $V=1.4-15.75$ mm/s, $\eta=0.4$, Medium size blocks	○	Prodanovic (1979), $H_{rubble}=30$ cm, $H_{ice\ sheet}=19$ mm, repacked rubble
◇	Hellman (1984), $H_{rubble}=70$ cm, Ice chips, primary shear mode	□	Prodanovic (1979), $H_{rubble}=30$ cm, $H_{ice\ sheet}=38$ mm, coarse rubble
○	Hellman (1984), $H_{rubble}=70$ cm, Ice chips, secondary shear mode	△	Prodanovic (1979), $H_{rubble}=30$ cm, $H_{ice\ sheet}=38$ mm, repacked rubble
□	Hellman (1984), $H_{rubble}=70$ cm, Ice chips, tertiary shear mode	◇	Shayanfar et al. (2019), $H_{rubble}=50$ cm, $\eta=0.3-0.4$, $V=5$ mm/s, $t=4$ hrs
◆	Hellman (1984), $H_{rubble}=70$ cm, Fishery ice, primary shear mode	◇	Yasunaga et al. (2002), $H_{ice\ sheet}=22.5$ mm, $\eta=0.31$ $V=1.6$ mm/s
●	Hellman (1984), $H_{rubble}=70$ cm, Fishery ice, secondary shear mode	□	Yasunaga et al. (2002), $H_{ice\ sheet}=42.5$ mm, $\eta=0.34$ $V=1.6$ mm/s
■	Hellman (1984), $H_{rubble}=70$ cm, Fishery ice, tertiary shear mode	△	Yasunaga et al. (2002), $H_{ice\ sheet}=65$ mm, $\eta=0.37$ rate= 1.6 mm/s
△	Hellman (1984), $H_{rubble}=70$ cm, Milled ice, primary shear mode	○	Yasunaga et al. (2002), $H_{ice\ sheet}=42.5$ mm, $\eta=0.29$ rate= 1.6 mm/s
★	Hellman (1984), $H_{rubble}=70$ cm, Milled ice, secondary shear mode	—	Fit to ice rubble data (Eq. 4.10)
▽	Hellman (1984), $H_{rubble}=70$ cm, Milled ice, tertiary shear mode	- - -	Fit to freeze bond data (Eq. 4.9)

Figure 4.10. Results of shear strength values as a function of confinement of previous ice rubble strength tests, where H_{rubble} is the ice rubble thickness, $H_{ice\ sheet}$ is the ice block thickness, η is the rubble porosity, and V is the displacement rate.

4.7. Conclusions

Results presented in this paper discuss the effects of confinement on the strength development of freeze bonds. Of the data available in the literature that has studied the effects of confinement on freeze bond strength, confinements used in earlier studies were not high enough to simulate the range of confinements expected between individual blocks of ice in a ridge keel. It is believed that contact pressures between individual blocks of ice in an ice ridge keel can reach as high as 70 kPa. High confinements are also likely to occur during ice ridge keel gouging and ship-ice interactions, where high pressure between adjacent ice blocks are expected. The work presented in this chapter has attempted to better understand bond strength development in a wide range of confinements, taking into account the simultaneous effect of submersion time.

The shear strength of freeze bonds was found to be significantly influenced by the amount of confinement applied to the samples, increasing with an increase in confinement. The rate of increase in strength was found to be a function of submersion time, following the trends observed in Section 3.4.1.2 and [2], where the highest increase in strength was observed after 7 days of submersion. The increasing trend of shear strength with increase in confinement was attributed to sintering and creep, plastic flow, as well as crushing-enhanced sintering of asperities of ice in contact at higher pressures. While similar increasing trends of strength with confinement have been observed in ice rubble strength tests, further tests are required to better understand the role of consolidation time on the overall strength properties of ice rubble and ridges. Submersion time proved to highly

influence the impact of confining pressure in strength development on block-block scale, and further ice rubble tests can help investigate common links between these two scales.

Mechanisms of strength development in freeze bonds should be further analyzed through detailed investigations of freeze bond interfaces at the microscale to better understand the physics associated with the results observed. The interactions between multiple factors, such as confining pressure and submersion time are complex, but highly important and this topic is an important area recommended for future research.

4.8. References

- [1] S. Shafrova and K. V. Høyland, “The freeze-bond strength in first-year ice ridges. Small-scale field and laboratory experiments,” *Cold Regions Science and Technology*, vol. 54, no. 1, pp. 54–71, 2008.
- [2] M. T. Boroojerdi, E. Bailey, and R. Taylor, “Experimental study of the effect of submersion time on the strength development of freeze bonds,” *Cold Regions Science and Technology*, p. 102986, 2020.
- [3] E. Bailey, R. Taylor, and K. R. Croasdale, “Mechanics of Ice Rubble over Multiple Scales,” in *Proceedings of the 34th International Conference on Ocean, Offshore and Arctic Engineering*, St. John’s, Canada 2015.
- [4] R. Ettema and J. A. Schaefer, “Experiments on freeze-bonding between ice blocks in floating ice rubble,” *Journal of Glaciology*, vol. 32, no. 112, pp. 397–403, 1986.

- [5] A. H. V. Repetto-Llamazares, “Experimental studies of shear failure on freeze-bonds in saline ice part I: set-up, failure mode and freeze-bond strength.,” *Cold Regions Science and Technology*, vol. 65, no. 3, pp. 286–297, 2011.
- [6] I. M. Bueide and K. V. Høyland, “Confined Compression Tests on Saline and Fresh Freeze-Bonds,” in *Proceedings of the 23rd International Conference on Port and Ocean Engineering Under Arctic Conditions*, Trondheim, Norway, 2015.
- [7] C-CORE, “DIRKS: Year 1 progress report,” C-CORE, St. John’s, NL, Canada, Internal report, 2012.
- [8] S. E. Bruneau, “Development of a first-year ridge keel load model,” PhD Thesis, Memorial University of Newfoundland, 1996.
- [9] A. H. Repetto-Llamazares, K. V. Høyland, and E. Kim, “Experimental studies on shear failure of freeze-bonds in saline ice:: Part II: Ice–ice friction after failure and failure energy,” *Cold Regions Science and Technology*, vol. 65, no. 3, pp. 298–307, 2011.
- [10] R. Ettema and G. E. Urroz, “On internal friction and cohesion in unconsolidated ice rubble,” *Cold Regions Science and Technology*, vol. 16, pp. 237–247, 1989.
- [11] M. T. Boroojerdi, E. Bailey, and R. Taylor, “Experimental Investigation of Rate Dependency of Freeze Bond Strength,” *Cold Regions Science and Technology*, Under Revision.
- [12] S. Afzali, R. Taylor, R. Sarracino, E. Bailey, and M. T. Boroojerdi, “Investigation of the Effect of Block Size, Shape and Freeze-Bond Strength on Flexural Failure of Freshwater Ice Rubble using the Discrete Element Method,” Glasgow, Scotland, 2019.
- [13] D. Szabo and M. Schneebeli, “Subsecond sintering of ice,” *Applied Physics Letters*, vol. 90, p. 151916, 2007.
- [14] N. Maeno and M. Arakawa, “Adhesion shear theory of ice friction at low sliding velocities, combined with ice sintering,” *Journal of Applied Physics*, vol. 95, no. 1, pp. 134–139, 2004.

- [15] J. R. Blackford, "Sintering and microstructure of ice: a review," *Journal of Physics D: Applied Physics*, vol. 40, no. 21, p. R355, 2007.
- [16] N. Maeno and T. Ebinuma, "Pressure sintering of ice and its implication to the densification of snow at polar glaciers and ice sheets," *The Journal of Physical Chemistry*, vol. 87, no. 21, pp. 4103–4110, 1983.
- [17] S. C. Colbeck, "Pressure melting and ice skating," *American Journal Physics*, vol. 63, no. 10, pp. 888–890, 1995.
- [18] P. V. Hobbs and B. J. Mason, "The sintering and adhesion of ice," *Philosophical Magazine*, vol. 9, no. 98, pp. 181–197, 1964.
- [19] W. D. Kingery, "Regelation, surface diffusion, and ice sintering," *Journal of Applied Physics*, vol. 31, no. 5, pp. 833–838, 1960.
- [20] E. M. Schulson, "Low-speed friction and brittle compressive failure of ice: fundamental processes in ice mechanics," *International Materials Reviews*, vol. 60, no. 8, pp. 451–478, 2015.
- [21] E. M. Schulson and A. L. Fortt, "Static strengthening of frictional surfaces of ice," *Acta Materialia*, vol. 61, no. 5, pp. 1616–1623, 2013.
- [22] D. C. Hatton, P. R. Sammonds, and D. L. Feltham, "Ice internal friction: Standard theoretical perspectives on friction codified, adapted for the unusual rheology of ice, and unified," *Philosophical Magazine*, vol. 89, no. 31, pp. 2771–2799, 2009.
- [23] S. K. Singh and I. J. Jordaan, "Triaxial tests on crushed ice," *Cold Regions Science and Technology*, vol. 24, no. 2, pp. 153–165, 1996.
- [24] H. Helgøy, O. S. Astrup, and K. Høyland, "Laboratory work on freeze-bonds in ice rubble, Part II: Results from individual freeze-bond experiments," in *Proceedings of the 22nd International Conference on Port and Ocean Engineering under Arctic Conditions, Espoo, Finland*, 2013.

- [25] A.-M. Kietzig, S. G. Hatzikiriakos, and P. Englezos, “Ice friction: the effects of surface roughness, structure, and hydrophobicity,” *Journal of Applied Physics*, vol. 106, no. 2, p. 024303, 2009.
- [26] J. H. Hellmann, “Basic investigations on mush ice,” in *Proceedings of the 7th IAHR International Symposium on Ice*, Hamburg, Germany, 1984.
- [27] A. Prodanovic, “Model tests of ice rubble strength,” in *proceedings of the 5th Port and Ocean Engineering Under Arctic Conditions conference*, Trondheim, Norway, 1979.
- [28] H. Shayanfar, “An experimental investigation on the strength and failure behavior of freshwater ice rubble,” MSc Thesis, Memorial University of Newfoundland, 2018.
- [29] G. E. Urroz and R. Ettema, “Simple-shear box experiments with floating ice rubble,” *Cold Regions Science and Technology*, vol. 14, no. 2, pp. 185–199, 1987.
- [30] R. T. Weiss, A. Prodanovic, and K. N. Wood, “Determination of ice rubble shear properties,” in *Proceedings of the 6th IAHR International Symposium on Ice*, Quebec, Canada, 1981.
- [31] Y. Yasunaga, S. Kioka, Y. Matsuo, A. Furuya, and H. Saeki, “The strength of the unconsolidated layer model of ice ridge,” in *Proceedings of the 16th IAHR International Symposium on Ice, Dunedin, New Zealand*, 2002.
- [32] H. Shayanfar, E. Bailey, and R. Taylor, “Medium-scale laboratory investigation of the effects of confining pressure on ice rubble strength and failure behavior.,” *Cold Regions Science and Technology*, Under Review.

5. RATE DEPENDENCY OF FREEZE BOND STRENGTH

5.1. Preface

This chapter is based on a manuscript, titled “Experimental Investigation of Rate Dependency of Freeze Bond Strength” has been accepted for publication in the journal of Cold Regions Science and Technology. I am the primary author of this paper, along with the co-authors, Dr. Eleanor Bailey and Dr. Rocky Taylor. I conducted the literature review and experiments and analyzed the data. I prepared the first draft of the manuscript and subsequently revised the manuscript based on the co-authors’ feedbacks and the feedback from the journal reviewers. Co-authors helped in the design of experiments, analyzing the results and contributed in preparing, reviewing and revising the manuscript.

5.2. Chapter Abstract

The effects of deformation rate on the shear strength of freeze bonds have been investigated through a series of Asymmetric Four-Point Bending (AFPB) experiments. Two submersion times of 30 min and 24 h have been considered, while the deformation rate has been varied from 0.01 to 100 mm/s. Ice specimens with an initial temperature of -18°C have been subjected to a constant confinement of 25 kPa during the formation and shearing of the freeze bonds. Failure of the bonds proved to be highly dependent on deformation rate, where more strain was observed prior to the failure of the bond for slower deformation rates. Shear strength of the bond for both submersion times showed a general decreasing trend with increased deformation rate, which is of significant importance in characterizing the properties of ice ridge/rubble strength. Previous ice rubble strength experiments, as well as ice ridge keel gouging tests, have reported the same failure rate-dependency, highlighting the role of freeze bond failure on rate effects. Compressive strength measurements of solid ice presented in the literature have been observed to follow similar trends within the range of strain rates used in the present study, where the failure mode appears to transition from ductile to brittle with increasing deformation rate. While more work is needed to understand the mechanisms associated with the rate dependency of freeze bond failure, this general observation suggests the rate dependency of ice ridges/rubble may indeed be related to the behavior of ice as a material, rather than being associated primarily with factors such as inertial and pore pressure effects, which have been previously proposed as the principal controlling mechanism.

Keywords: Freeze bond; Freshwater ice; Ice shear strength; Deformation rate; Ice Rubble

5.3. Introduction

Ice ridges, an aggregate of bonded ice blocks, are considered to be one of the key design ice features of interest for ships, bridges, offshore platforms or other coastal structures in Arctic and sub-Arctic regions. Understanding the strength and failure properties of ice ridges is therefore important for better estimation of the loads applied to marine structures. While several failure modes can occur during ice ridge/rubble-structure interactions, shear and compression have been recognized as the dominant failure mode [1]. The failure and strength of an ice ridge or rubble pile is governed by the degree of consolidation of the freeze bonds between the ice blocks, as well as the strength of the individual submerged ice blocks [2, 3].

Freeze bond strength and its influencing properties have been the focus of several studies in the past decade. While excellent work has been carried out to understand the role parameters such as initial ice temperature, submersion time and confinement have on the strength development of freeze bonds [2- 9], the effects of deformation rate on the failure of freeze bonds have yet to be systematically studied. This is important during ice ridge and rubble interaction events, where speed has been shown to influence the failure load of these features and can vary considerably over the time scales of interest in many engineering applications.

Load-rate dependency of ice rubble has been attributed to four distinct processes introduced by Azarnejad and Brown [10] and later discussed by Liferov and Bonnemaire [11]. These include:

- Inertia component due to acceleration of ice rubble,
- Effect of high pore pressures that do not have time to dissipate at high loading rates,
- Loading rate dependency of freeze bond failure, and
- Change of failure mode.

The authors of this paper agree with the observations of Liferov and Bonnemaire [11], who highlight that a change of failure mode cannot be defined as a distinct process, but is rather a result of inertial component, pore pressures, and loading rate effects. A full discussion on each process can be found in Liferov and Bonnemaire [11] and will not be discussed further here since the aim of this paper is to study the loading-rate dependency of freeze bonds.

The influence of deformation rate on ice ridge and rubble loading has been studied by several researchers [12–17], where a general increase in strength was observed as the deformation rate decreased. Two explanations have been proposed as the mechanisms responsible for this behavior: (1) the suppression of dilatancy at very low strain rates [11]; and (2) dynamic freeze-bonding at slower deformation rates, where new freeze bonds are constantly formed as the blocks of ice are slowly moved past each other [16]. We propose another contributing mechanism to the increase in strength is an associated rate dependence affecting the failure strength of individual freeze bonds, similar to that observed in solid ice compression tests [18–21].

Very little data exists on rate effects in freeze bond failure strength. The only tests reported in the literature are those of Ettema and Schaefer [3], where the strengths of the bonds were measured over a narrow range of rates from 0.44 mm/s to 0.84 mm/s. In these tests, the deformation rate was found to have no significant effect on the shear strength of the freeze bond. This is likely due to the narrow range of the deformation rates tested, which may have not been large enough to show any variation in strength or failure behavior. Further tests are therefore needed to study the strength development of freeze bonds under different deformation rates, which is the focus of the current paper.

In the present study, the effects of deformation rate on the strength of freeze bonds have been investigated by conducting shear tests using the asymmetric four-point bending (AFPB) method. The actuator rate was varied from 0.01 to 100 mm/s, while the initial ice temperature and confinement applied to the samples were held constant. Rate effects were investigated for two submergence times: 30 min and 24 h. Details of the experimental setup and methodology are provided in section 5.2. The results of these experiments have been presented in section 5.3, and have been analyzed and discussed in section 5.4. Concluding remarks are presented in section 5.5.

5.4. Experimental Setup and Methodology

To conduct these tests, a pair of freshwater ice cylinders 9 cm in diameter and 10 cm in length were installed in the confinement frame shown in Figure 5.1a, which was adjusted

to apply a 25 kPa normal pressure to the samples during submersion and shear. The load was applied with a hand-driven gear and recorded by an inline 900 N load cell. Three springs were used at each side of the ice blocks to ensure the load was uniformly transferred to the sample, and three support wedges were placed underneath the specimens during setup and submersion to ensure that they were aligned. Once the ice specimens were in place, the frame was submerged in a water bath held at 0°C for the specified period of time.

Once the samples were ready to test, the confinement frame was placed in the asymmetric four-point bending (AFPB) rig shown in Figure 5.1b. The AFPB method is used to measure the shear strength of materials, in which a load is applied via four loading pins, which are positioned asymmetrically about the loading axis. Under these conditions, the inner pins generate a force in the clockwise direction, while the outer pins generate a counterclockwise force about the loading axis. This results in a near-pure shear region between the inner pins, allowing the shear strength of the freeze bonds to be measured (Figure 5.2). The bottom plate of the AFPB apparatus was fixed to the pedestal of a Materials Testing System (MTS) servo-hydraulic testing machine, while the top plate was attached to a hemispherical alignment seat. Using simple beam theory, the shear stress at the center of the samples, which correspond to the freeze-bonded area, can be calculated by:

$$\tau_{max} = \frac{4}{3} \frac{(1 - \alpha)}{(1 + \alpha)} \frac{P_{max}}{\pi r^2} \quad (5.1)$$

where P_{max} is the peak load at failure, r is the radius of the sample, and α is related to the positioning of the loading pins from the loading axis (shown in Figure 5.2), which was set

to 0.106 in these experiments. During all tests, the shear load and displacements were measured using the MTS machine, as well as an external string potentiometer that was connected to the AFPB apparatus. Additional details of this test set-up and procedure can be found in Boroojerdi et al. [9].

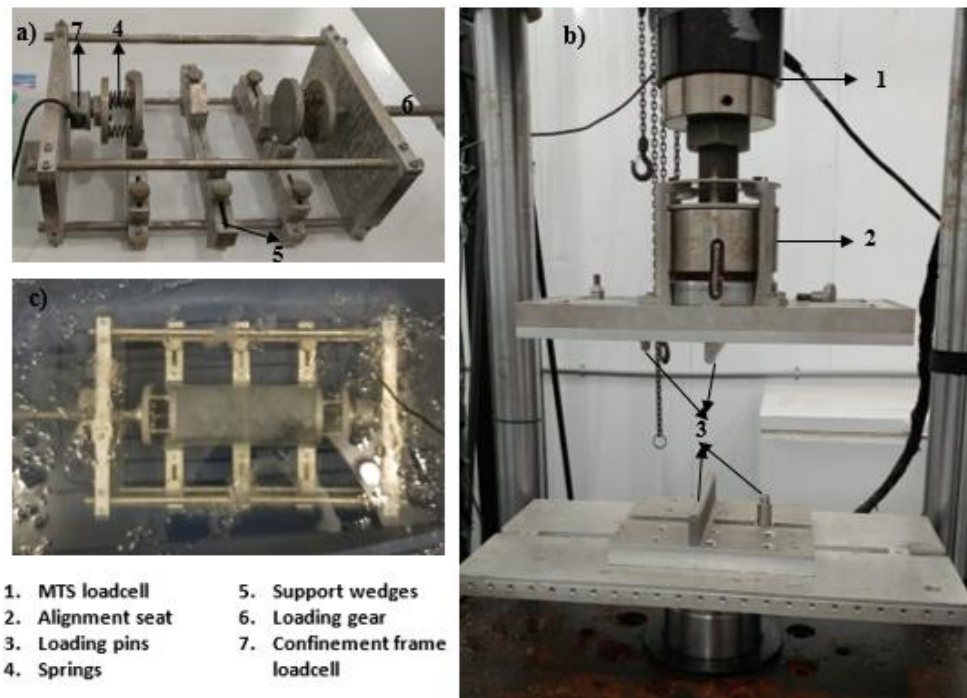


Figure 5.1. a) Confinement frame, b) AFPB rig, and c) ice samples loaded in confinement frame and submerged in water.

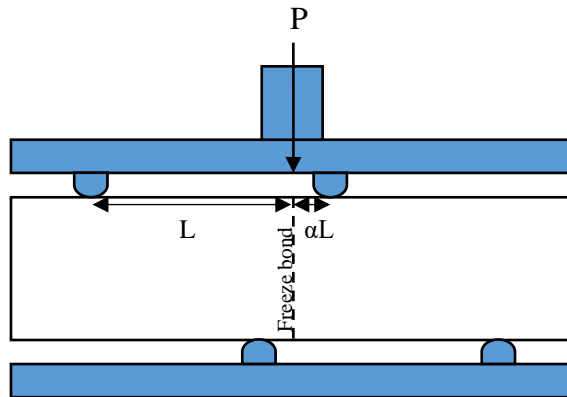


Figure 5.2. Positioning of loading pins on the asymmetric four-point bending (AFPB) apparatus.

A total of 48 tests were conducted for two submersion times of 30 min and 24 h, while the confinement pressure and initial temperature of the ice blocks was held constant at 25 kPa and $-18\text{ }^{\circ}\text{C}$, respectively, and the deformation rate was varied from 0.01 to 100 mm/s. The parameters used in each test are given in Table 5.1. The 30-minute submersion time corresponds to the time required for a $-18\text{ }^{\circ}\text{C}$ ice block of these dimensions to achieve thermal equilibrium with the surrounding water temperature, as found experimentally and numerically by [9, 22], which was discussed in Section 3. The 24-hour submersion time corresponds to the end of the transition period, where the freeze bond strength is at its minimum and mechanism dominance is believed to switch from thermal processes to sintering and creep. During this stage, no temperature gradient exists and near-zero growth rates were observed, signifying that thermal processes no longer play a significant role in the freeze bond strength development. The 24 h submersion time also corresponds to the submersion time used in the Pipeline Ice Risk and Mitigation (PIRAM) and Development of the Ice Ridge Keel Strength (DIRKS) programs [14, 23–25] during which the strength

and failure behavior of gouging freshwater ice rubble keels was investigated through ice tank experiments. Ice block dimensions and ice growth mechanisms during this freeze bond testing program were based on those used in the DIRKS testing program so as to provide an enhanced understanding of the rate-dependency of freeze bond strength and its effects on the overall ridge-keel strength.

Table 5.1. Deformation rate test matrix. Parameters in the table are: submersion time (t), initial ice temperature (T_i), confinement (σ), Actuator rate (V), number of tests (n), mean shear strength (τ_{mean}), shear strength values for each test (τ), minimum and maximum strength (τ_{min} , τ_{max}), standard deviation (STD), failure load (F_{max}), and displacement at failure (δ).

t	T_i ($^{\circ}\text{C}$)	σ (kPa)	V (mm/s)	n	τ_{mean} (kPa)	τ (kPa)	τ_{min} (kPa)	τ_{max} (kPa)	STD (kPa)	F_{max} (N)	δ (mm)
30 min	-18	25	0.01	3	245	212.6	212.6	277.5	26.49	1255	1.72
						277.5				1638	1.75
						245.1				1446	0.6
			0.05	4	290.6	404.4	161.8	404.4	86.9	2387	1.69
						281.2				1659	1.09
						315.3				1861	1.83
			0.1	4	228.9	304	147.5	304	57.26	1794	3.63
						252.5				1490	2.1
						147.5				870	0.88
			0.5	3	155	146.7	146.7	167.8	9.32	865	0.4
						149.7				883	0.16
						167.8				990	0.1
			1	4	211.6	229.5	168.6	245.6	29.18	1354	0.70
						168.6				995	0.52
245.6	1449	0.30									
5	2	102.6	116.6	88.5	116.6	14.05	688	0.82			
			88.5				522	0.59			
			10				3	178.1	190.8	124.1	219.4
219.4	1295	0.15									
124.1	732	0.17									
100	3	54.5	32.2	32.2	79.3	19.3	190	0.05			
			52.1				307	0.04			
			79.3				468	0.09			
24 h	-18	25	0.01	2	279.8	285.7	274	285.7	5.85	1686	1.79
						274				1617	2.69
			0.05	2	193.8	186.4	186.4	201.3	7.45	1100	0.83
						201.3				1188	1.61
			0.1	2	205.5	218.7	192.4	218.7	13.15	1291	1.34
						192.4				1135	1.78
			0.5	2	150.9	170.1	131.7	170.1	19.2	1004	0.46
						131.7				777	0.56
			1	3	208.5	277	155	277	50.9	1635	0.97
						193.5				1142	0.35
155.0	914	0.23									
5	3	100.5	50.2	38.6	212.7	79.4	296	0.13			
			38.6				227	0.73			
			212.7				1255	0.31			
10	2	78.3	72.9	72.9	83.7	5.4	430	0.07			
			83.7				494	0.05			
100	2	60.4	57.1	57.1	63.7	3.3	337	0.15			
			63.7				376	0.09			

5.5. Results

5.5.1. Observed Failure Mode

During testing, it was observed that failure generally occurred very rapidly and was characterized by a sudden catastrophic failure, typical of brittle failure. Load-time curves for each test reflect this brittle failure as the dominant failure type in these tests. Figure 5.3 shows the shear force-time curves for each deformation rate for 30 min submersion time. As seen in the figure, for slow deformation rates (≤ 0.05 mm/s) a stage of strain hardening takes place, where the shear load slowly increases with time up to failure. For tests with higher deformation rates, the shear load-time curve becomes more linear and drops off suddenly upon failure. Similar trends were observed for freeze bonds submerged for 24 h, where deformation rates less than 0.05 mm/s resulted in a more non-linear behavior.

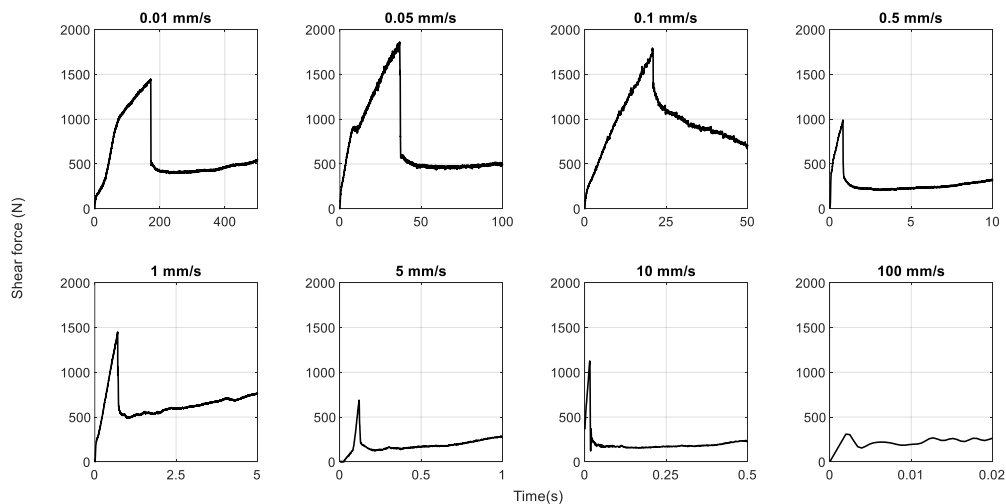


Figure 5.3. Shear force-time curves for ice that was submerged for 30 min, for deformation rates of 0.01 to 100 mm/s.

Shear force-displacement curves for each deformation rate for samples that were submerged for 30 min are given in Figure 5.4. From this figure, it may be observed that freeze bond strengths tend to be higher at the lower range of deformation rates, and correspondingly larger peak forces and higher displacements are observed for lower deformation rates. It is noted that while no evidence of localized permanent deformation due to creep or crushing of ice under the pins was observed, it is possible that these aspects contributed in part to the total measured displacements. It is therefore recommended in future test programs that additional displacement measurements be taken which will allow for better isolation of the potential contributions of the components of local deformation due to ice-pin contact, ice sample deformation and freeze bond deformation. A more detailed post-failure examination of the failed freeze bond is also recommended to determine if fracture surface observations provide any further information that may be correlated with observed strain rate effects.

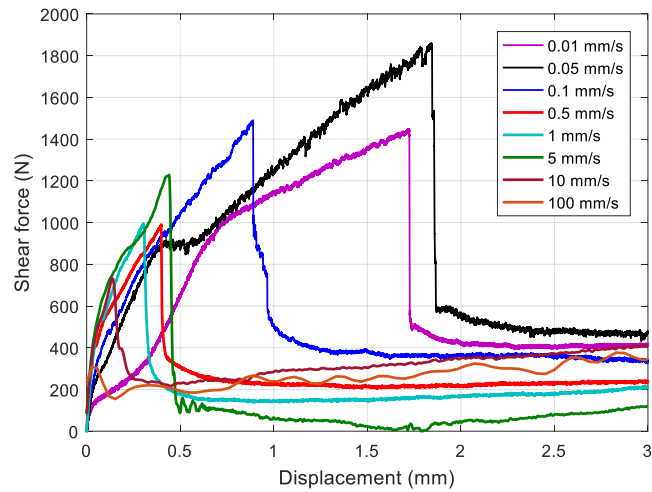


Figure 5.4. Comparison of the shear force-displacement curves for different deformation rates.

A comparison of time to failure with regards to deformation rate for the two submersion times tested is shown in Figure 5.5, where data points correspond to the average time to failure for each deformation rate and the error bars show the maximum and minimum values observed. It may be observed from this figure that for the submersion times considered (30 minutes and 24 hours), submergence time does not have a significant effect on the time to failure as a function of deformation rate. It is also observed that while the time to failure increases with decreasing deformation rate, as expected, the best fit lines plotted in Figure 5.5 do not follow the 1:1 line plotted, suggesting that this relationship is non-linear in nature. This observation reflects the higher capacity of ice for energy dissipation at lower deformation rates, which in turn means that the ice can undergo larger deformations before failure occurs resulting in longer interaction times and displacements (e.g. [26]). As the deformation rate increases, slower mechanisms such as dislocation glide

and climb cannot dissipate as much energy, resulting in a more rapid accumulation of stresses, ultimately triggering crack initiation and propagation events that lead to a more rapid brittle failure [27].

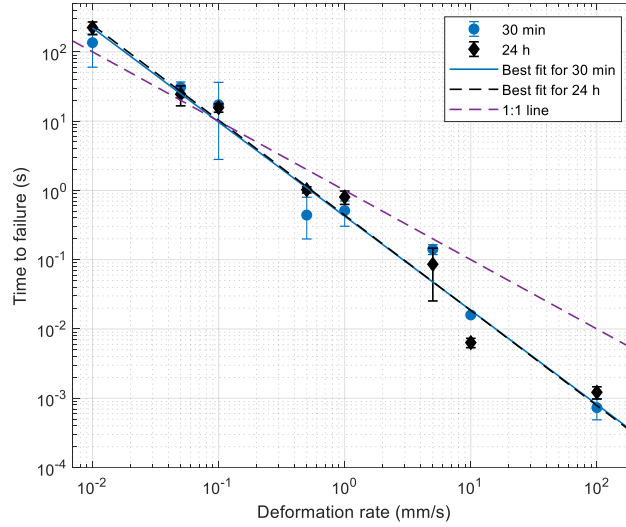


Figure 5.5. Time to failure as a function of the deformation rate.

Total shear strain during shear of the freeze bond is the sum of the shear strain of the freeze bond layer, and shear strain of the ice between the inner indenters, as shown in Figure 5.6.

Defining $\gamma = \frac{\delta}{t_{total}}$, shear strain can be defined as:

$$\gamma = \frac{\delta}{t_{total}} = \frac{\delta_{ice} + \delta_{FB}}{t_{ice} + t_{FB}} \quad (5.2)$$

where γ is the total shear strain, t_{total} is the total thickness of the layer between the inner indenters, t_{FB} is the thickness of the freeze-bonded layer, and $t_{ice} = t_{total} - t_{FB}$ is the thickness of the ice between the inner indenters. Since for these tests the freeze bonds occur between

two planar ice surfaces that are in full contact under confinement, the bond thickness, t_{FB} , may be assumed to be within the range of the surface roughness of the contacting ice blocks. While surface roughness was not directly measured in this program, based on [28], the roughness may be estimated to be on the order of 0.5×10^{-6} m. Approximating the freeze bond width as twice the surface roughness, t_{FB} can be estimated as $t_{FB} \sim 1.0 \times 10^{-6}$ m. On this basis, it is reasonable to assume that the thickness of ice is much greater than that of the freeze bond ($t_{ice} \gg t_{FB}$) and t_{total} can be approximated as being equal to t_{ice} .

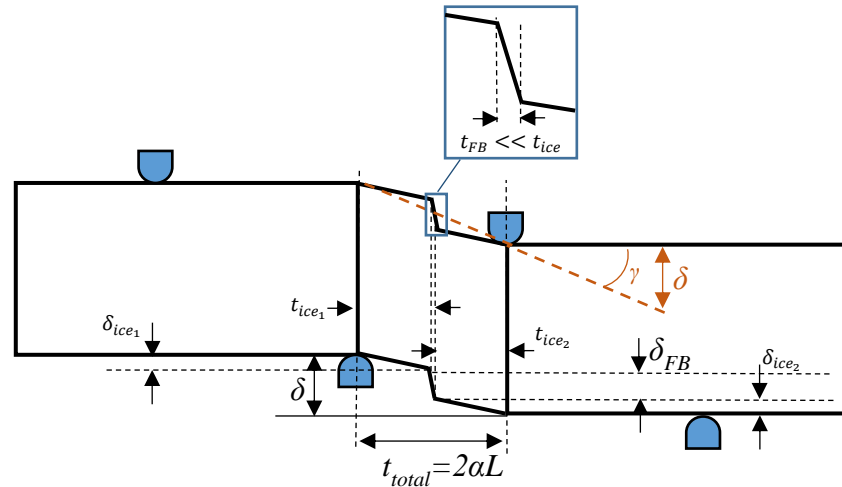


Figure 5.6. Schematic illustration of shear strain, where δ is the displacement, $t_{total}=2\alpha L$ is the length between the indenters, γ is the shear strain, γ_{ice} is the shear strain of ice, γ_{FB} is the shear strain of freeze bond, $t_{ice1,2}$ are the thickness of ice between the indenters, and t_{FB} is the thickness of freeze bond layer (Dimensions are not to scale and are expanded for illustration purposes only).

In these tests, deformations during shear of the bond were measured from the MTS machine and not directly on adjacent sides of the ice bond, and it is thus not possible to differentiate directly from the measurements the deformation of the bond versus that of the surrounding ice. Consequently, it is noted that shear strain in this study refers to the nominal total shear

strain between the indenters that can be estimated according to Equation 5.3, and Figure 5.6.

$$\gamma = \frac{\delta}{t_{total}} = \frac{\delta}{2\alpha L} \quad (5.3)$$

where γ is the shear strain, δ is the measured displacement from the MTS and external string potentiometer, and $2\alpha L$ is the length between the inner indenters. As is illustrated in Figure 5.6, the estimated deformation of the ice between the pins occurs over a much thicker region, t_{ice} , and yet is believed to contribute significantly less to the total deformation. By comparison, the deformation across the freeze bond, is believed to be much larger and yet occurs across a much thinner portion of the test section, of thickness t_{FB} .

Plotting the nominal total strain values at failure (e.g. critical strains) in Figure 5.7, it may be observed that similar values are found for both submersion times. In general, critical strain, γ_{crit} , is observed to decrease with increase in strain rate. If γ_{crit} was constant with changes in deformation rate, the time to failure would be directly proportional to strain rate, and would follow the constant critical strain (1:1 line) case plotted in Figure 5.5. The decreasing trend observed in Figure 5.7 highlights the non-linear nature of these parameters and provides useful information that may be used in guiding the development of bond failure for numerical models used for ice rubble simulations, such as the discrete element method model of Paavilainen and Tuhkuri [29], Polojärvi and Tuhkuri [30], Liu et al. [31], Molyneux et al. [32], Yulmetov et al. [33], and Afzali et al. [34].

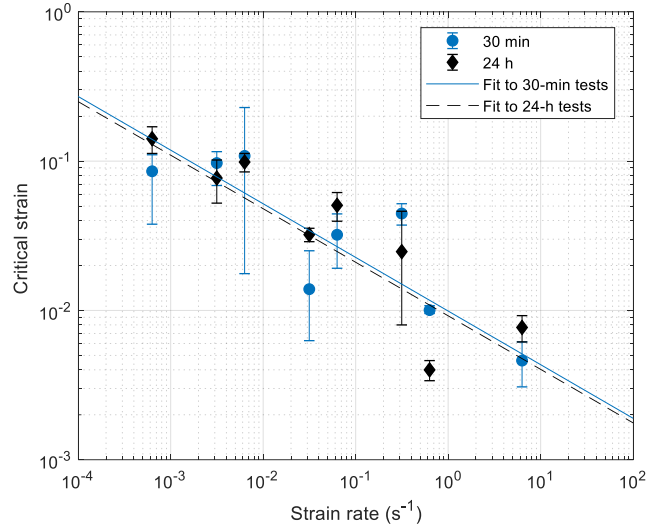


Figure 5.7. Critical strain as a function of nominal strain rate.

To aid with the interpretation of results based on nominal total strain, some additional discussion is warranted. For an elastic material, the shear modulus G may be estimated based on the modulus of elasticity E and the Poisson's ratio ν , according to:

$$G = \frac{E}{2(1 + \nu)} \quad (5.4)$$

For polycrystalline ice, the Poisson's ratio is $\nu = 0.33$ and the elastic modulus, E , is around 9 GPa [35]. This yields a shear modulus of ice, G_i , of around 3.3 GPa using Equation 5.4.

To provide values for comparison, nominal total shear strain values from this test program given in Equation 5.3, can be used to estimate the effective shear elastic modulus [36] of the freeze bonds, G_{eff} , as:

$$G_{eff} = \frac{\tau}{\gamma} = \frac{\tau}{\left(\frac{\delta}{2\alpha L}\right)} = 2\alpha L \frac{\tau}{\delta} \quad (5.5)$$

Using the slope of the stress-displacement curves to provide a first-order estimate of $\frac{\tau}{\delta}$ and Equation 5.5 with the value of $\alpha L = 7.9$ mm, estimated values of effective shear moduli G_{eff} were found to be in the range of 2 to 20 MPa. These effective moduli values are much less than the shear modulus of ice, highlighting the extent to which the freeze bond behavior dominates the response of the tested specimens. To quantify the relative contribution of the elastic ice response, if one assumes the ice between the pins behaves elastically, from elasticity theory we may write:

$$\tau = G_i \gamma_i = G_i (\delta_{ice} / t_{ice}) \quad (5.6)$$

Since $t_{FB} \ll t_{ice}$, it may be approximated that $t_{ice} \sim t_{total}$, and this expression can be written as:

$$\tau = G_i (\delta_{ice} / t_{tot}) \quad (5.7)$$

Since the stress at failure τ for any given specimen may be calculated from the measured force and known geometry, the component of deformation associated with the elastic response of the ice δ_{ice} at the point of failure may be calculated using

$$\delta_{ice} = t_{tot} (\tau / G_i) \quad (5.8)$$

Subtracting the deformation of the ice, δ_{ice} , from the total deformation, δ , gives the estimated freeze bond deformation, δ_{FB} , as:

$$\delta_{FB} = \delta - \delta_{ice} \quad (5.9)$$

Correspondingly, the strain in the freeze bond may be then calculated using Equation 5.10 as:

$$\gamma_{FB} = \delta_{FB}/t_{FB} \quad (5.10)$$

Using sample data from Test 1 presented in Table 5.1, where $\tau = 245 \times 10^3$ Pa, $\delta = 1.75 \times 10^{-3}$ m, $G_i = 3.3 \times 10^9$ Pa, $t_{tot} = 2\alpha L = 2 \times 7.9 \times 10^{-3}$ m = 15.8×10^{-3} m, the elastic ice deformation δ_{ice} may be estimated as:

$$\begin{aligned} \delta_{ice} &= t_{tot} (\tau/G_i) = 15.8 \times 10^{-3} m \times (245 \times 10^3 Pa / 3.3 \times 10^9 Pa) \\ &= 1.17 \times 10^{-6} m \end{aligned} \quad (5.11)$$

Correspondingly, the freeze bond deformation may be calculated as:

$$\delta_{FB} = \delta - \delta_{ice} = (1.75 \times 10^{-3} m) - (1.17 \times 10^{-6} m) \sim 1.75 \times 10^{-3} m \quad (5.12)$$

Based on the above results, it may be concluded that the elastic deformation of the parent ice between the pins is very small in comparison to that of the freeze bond. Approximating the freeze bond thickness as about two times the surface roughness yields an approximate value $t_{FB} \sim 1.0 \times 10^{-6}$ m. If one were to calculate elastic strain in the freeze bond based on this estimate of t_{FB} , it becomes apparent that the assumption of elasticity for the freeze bond is not appropriate, at least not based on the measurements taken to date. However, there are several sources of uncertainty in this analysis. For example, it is possible that the effective width of the bond may be larger than this estimate since microstructural changes in the ice

surrounding the bond may occur, which would make the effective thickness of the bond greater than the value assumed above. The treatment of ice as elastic is an approximation which contributes to the uncertainty. In addition, while no evidence of permanent deformation under the pins was observed, the potential contribution of these localized deformations are also a source of uncertainty in assessing the components of strain. However, despite these uncertainties, it is believed based on observations from the test program that permanent inelastic deformation across the freeze bonds are the most significant contributor to the measured deformation. In the present program, while standard practice for AFPB test have been followed, the noted uncertainties about details of the local response in the ice between the pins and difficulties in enumerating the relative contributions of these strain components, highlights the need to collect direct measurements across the bond and at the pins in future tests. In the absence of such data, it is not possible to differentiate with confidence what the relative contributions of these components to the total strain are, and therefore this is noted as a limitation of current data and standard AFPB tests, which should be addressed in future programs. Such measurements will help further improve understanding of these details of freeze bond behavior, although the addition of such measurements would not affect the freeze bond strength results, which are the focus of this paper.

5.5.2. Shear strength

Shear strength values for both submersion times tested are plotted as a function of deformation rate in Figure 5.8. The values presented are averages for each deformation rate, where error bars denote the maximum and minimum strength at each deformation rate. As seen in Figure 5.8, for samples that were submerged for 30 min, the strength of the bond initially increased with strain rate, reaching a maximum strength of 300 kPa for a deformation rate of 0.05 mm/s. The strength then decreased with increase in strain rate, reaching a minimum of 50 kPa for deformation rate of 100 mm/s.

Strength measurements of freeze bonds for 24 hours of submersion showed that the shear strength has a general decreasing trend, where it decreased from 280 to 60 kPa, as the strain rate increased. Comparison of the results of the two submersion times tested shows that both submersion times show an overall decreasing trend of shear strength as strain rate increases. The strength values of the tests conducted for the 30 minutes of submersion are, on average, slightly higher than the 24 hours submersion tests. This difference in strength with submergence time is not large, consistent with earlier work conducted by the group, which focused on the role submersion time had on the strength and failure behavior of freeze bonds [9]. Boroojerdi et al. [9] found that for shorter submersion times (i.e. 30 minutes), thermal processes dominated the strength behavior of freeze bonds. This resulted in higher strength values for 30 minutes of submersion compared to 24 hours of submersion, where the bond strength is at its minimum and is believed to be in a transition

period where bond strength development mechanism change from thermal to sintering-creep processes.

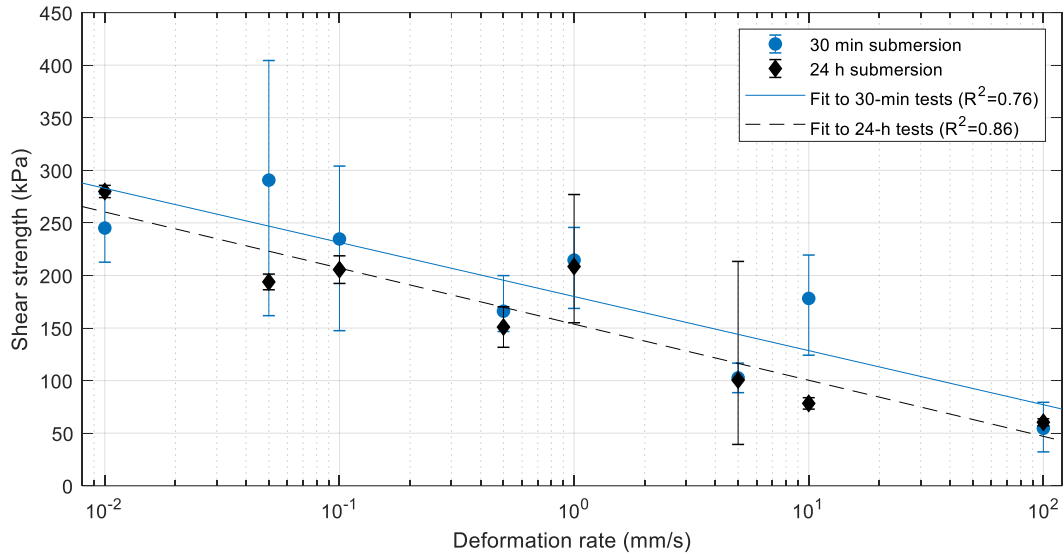


Figure 5.8. Comparison of shear strength as a function of deformation rate for submersion times of 30 min and 24 h.

The relationship between shear strength and critical strain is presented in Figure 5.9. As seen in the figure, the magnitude of shear strength corresponds closely with critical strain, where higher critical strain is associated with higher shear strength. This is due to the higher energy dissipation during deformation and creep at slower deformation rates, which results in a higher overall failure strength. Such processes allow for dissipation of local internal stresses to prevent crack initiation and growth, which allows the specimen to sustain higher forces prior to brittle failure.

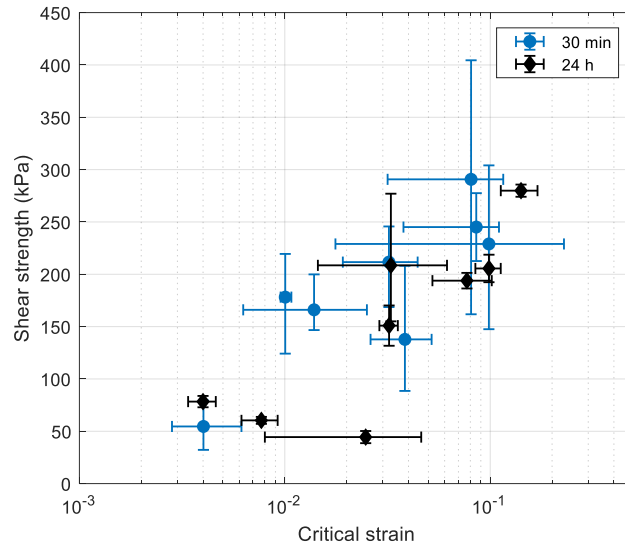


Figure 5.9. Shear strength as a function of critical strain.

5.6. Discussion

5.6.1. Comparison with previous freeze bond experiments

While previous freeze bond studies have made excellent progress in terms of understanding processes affecting strength development during the formation of freeze bonds, processes affecting the failure of these features, such as deformation rate have received little attention. Ettema and Schaefer [3] were the first to address the rate-dependency of freeze bonds in a series of direct shear tests conducted on freshwater ice samples in air and submerged in water. To conduct the tests, one rectangular block of ice was put on top of a larger base layer. A normal pressure was then applied to the samples by putting dead weights on the top ice sample. Samples were either left in air for dry freeze bond tests or were submerged

for a short period of time (0-4 minutes) for submerged tests. Freeze bonds were eventually sheared by pulling a cable attached to the top sample, which was attached to a traveling cross-head. A load cell was attached to the cross-head, measuring the shear load. Preliminary tests investigating rate-dependency of freeze bond strength were conducted on ice with initial temperature of -10°C , under four confinements ranging from 0 to 1.5 kPa, where freeze bonds were deformed at two rates of 0.44 and 0.84 mm/s. Shear strength values for these tests have been plotted against deformation rate in Figure 5.10. As seen in this figure, strength values obtained in these tests are much lower than the range of strength values observed in this study, ranging from 0.2 to 1.8 kPa, primarily due to the shorter submersion time and confinements used in these tests. Deformation rate is observed to have minimal effect on shear strength of freeze bonds, and no direct conclusions can be made on the influence of deformation rate on freeze bond failure strength in these tests. This, however, is likely due to the narrow range of rates tested in these experiments.

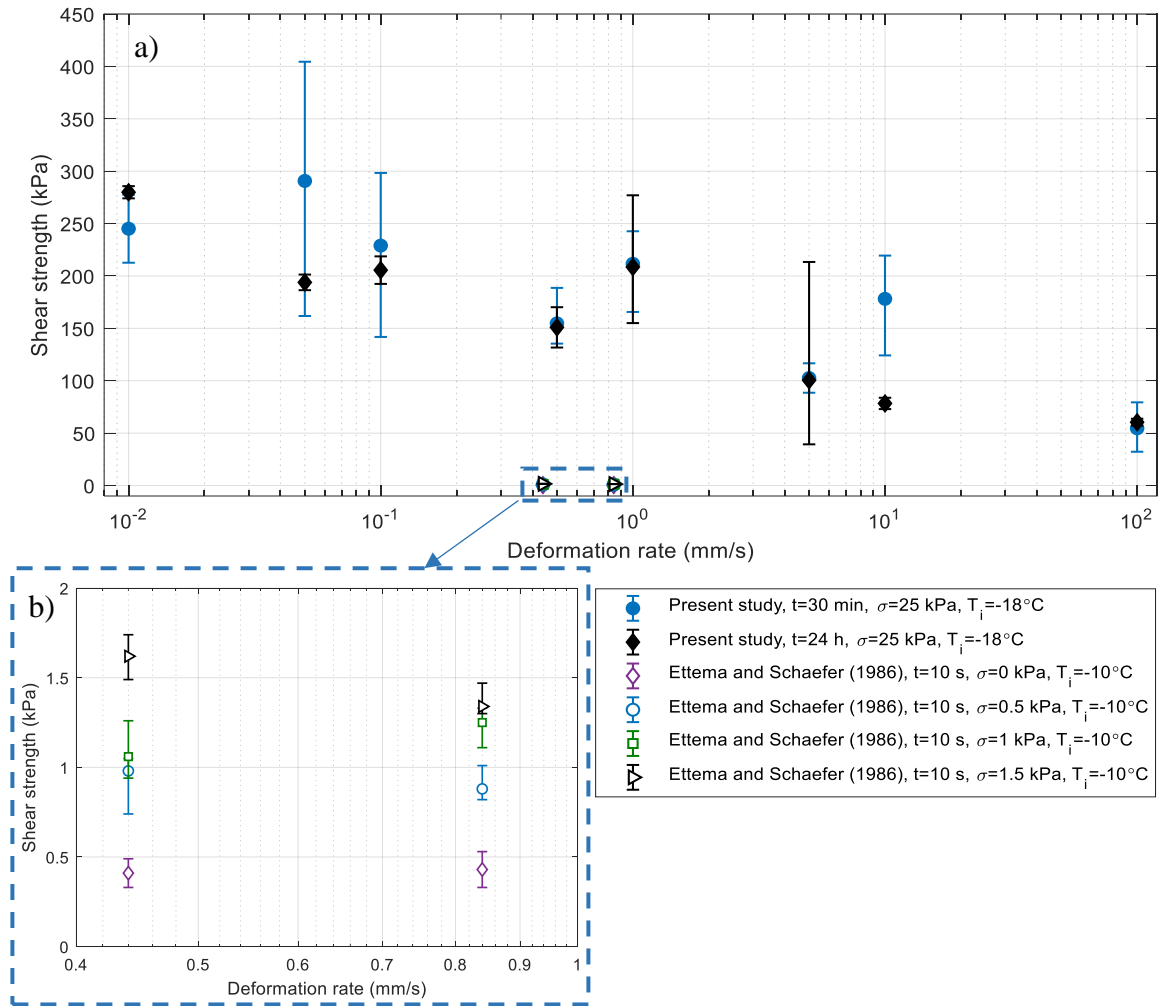


Figure 5.10. Plot showing the comparison of measured shear strength values versus deformation rate in previous freeze bond experiments and present study (a), and zoomed-in plot of Ettema and Schaefer [3] (b). In this plot σ is confinement pressure, T_i is the initial temperature of ice and t is the submersion time.

5.6.2. Comparison with rate effects in solid ice

While the tensile strength of ice has been found to be independent of strain rate for the range of interest in engineering applications, the compressive strength of ice has been found to be highly rate-dependent [37].

The effects of deformation rate on compressive strength of solid ice have been studied by several researchers using the uniaxial compression method [18–21, 37–39]. Figure 5.11 presents the results of reported compressive strength values, for strain rates ranging from 10^{-8} to 10^{-2} s^{-1} . Schulson [35] distinguished two failure modes, ductile and brittle, for these results (shown in Figure 5.11), where the ductile failure is believed to occur at strain rates smaller than 10^{-3} s^{-1} , and brittle failure taking place at strain rates higher than 10^{-3} s^{-1} . As also noted by Schulson [37], a clear trend of increase in strength can be observed in this figure upon reaching a maximum at the point where the transition from ductile to brittle failure occurs. The ductile regime is controlled by flow, recrystallization and dislocation processes, where basal glide is the major strain-producing mechanism and dislocation climb is responsible for strain-rate hardening [37]. The strength then decreases upon entering the brittle failure region as strain rate increases. During compression, failure occurs as a result of the shear of grain boundaries. After the nucleation of the first crack between the grain boundaries, the two opposing faces of the crack start to slide across each other, creating a shear force along the grains. This explains the observation of coulombic shear faults during triaxial compression tests, where failure has been seen to occur at a $45 \pm 5^\circ$ angle, which corresponds to the plane of maximum shear stress, highlighting the

dependency of shear strength on deformation rate [26]. The formation of such shear cracks are important in the spalling of ice during ice-structure interactions and have been linked to scale effects in compressive ice failure pressures, which are an important consideration in engineering design [41].

The freeze bond strength of the 30 min tests (shown in Figure 5.8) appear to initially increase slightly with increase in deformation, followed by a decreasing trend beyond 0.05 mm/s, which corresponds to a strain rate of $3 \times 10^{-3} \text{ s}^{-1}$. Shear strength values for 24 h submersion time exhibit a general decreasing trend with increasing deformation rate. Comparison of these results with rate dependency of compressive strength of ice suggests the freeze bonds to be in a transition zone between ductile to brittle failure, before switching to brittle failure at strain rates higher than $3 \times 10^{-3} \text{ s}^{-1}$. A lower range of strain rates should be considered to investigate this matter further.

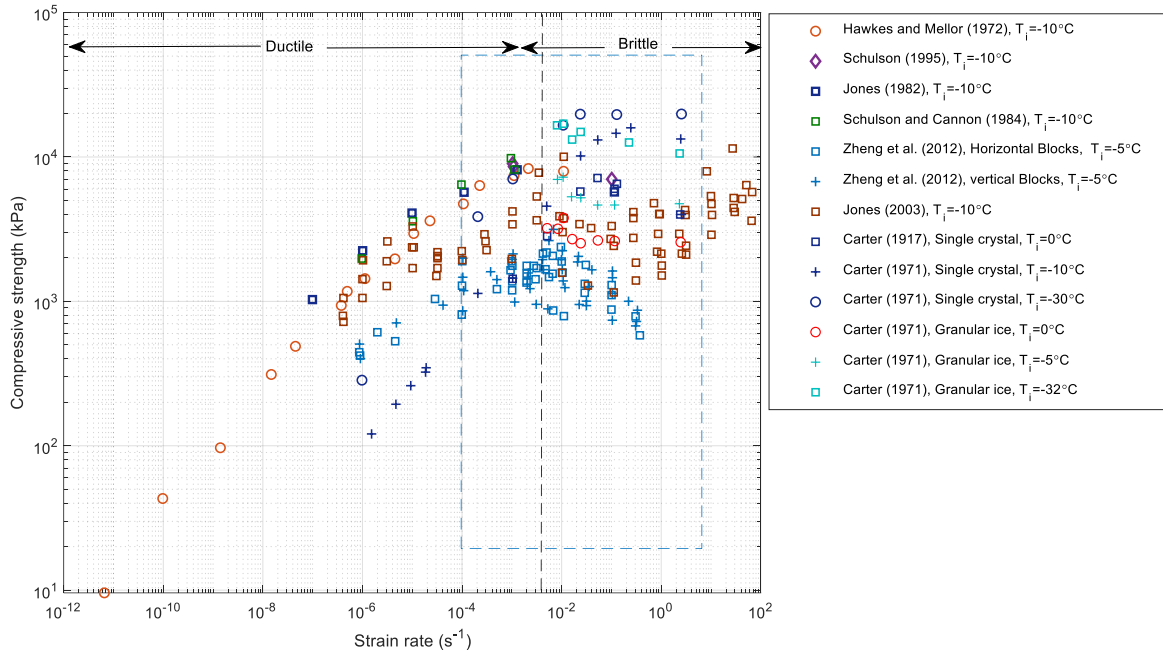


Figure 5.11. Compressive strength as a function of strain rate. Blue rectangle shows the range of strain rates used in present study (after [35] and [26]).

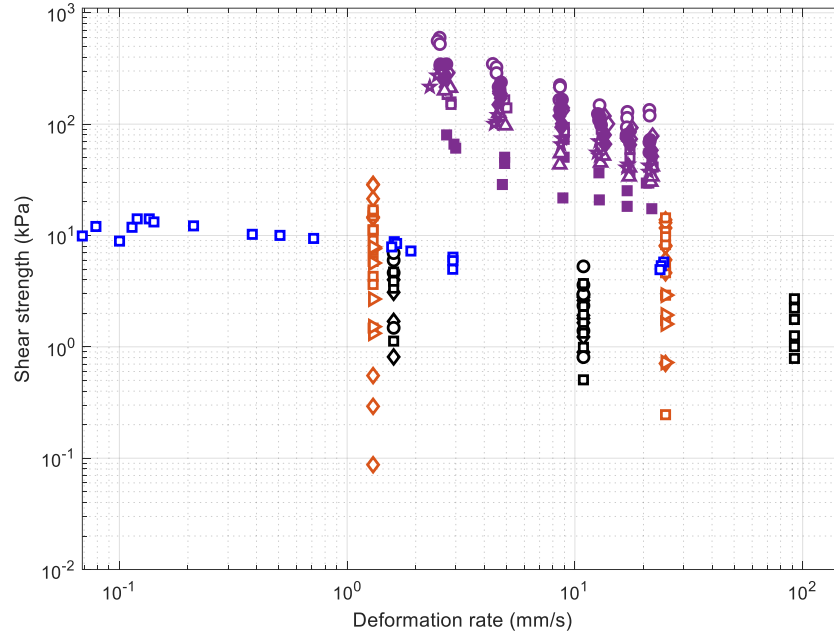
5.6.3. Comparison with ice rubble tests

Deformation rate effects have been the focus of several ice rubble experiments. For instance, Yasunaga et al. [17] conducted a series of direct shear tests to study the effects of deformation rate on the strength of saline ice rubble, which was subject to a confining pressure of 6 kPa and had an initial ice temperature of -3°C . While deformation rate, varying from a nominal amount of 0.1 to 24 mm/s, was adjusted in each test to a constant value, some variation in the rates was observed. The authors found that the shear strength of the rubble peaked at a deformation rate a little higher than 0.1 mm/s, after which the

strength gradually decreased with increase in deformation rate. They attribute this deformation rate dependency of shear strength, to the rate dependency of expansion in ice rubble. Comparing the amount of vertical and horizontal deformation at each deformation rate, they observed a decrease in the amount of expansion as deformation rate increased. The increase in shear strength at slower deformation rates was therefore proposed to be a result of energy used for expansion at these rates. Investigation of the state of the ice blocks after each test showed that the probability of failure of the ice blocks was higher for higher deformation rates. Weiss et al. [12] also found, in a series of direct shear box tests on saline ice, similar decrease in strength with increasing deformation rate. These tests were conducted for a range of confinements ($\sigma = 0$ to 28 kPa) and ice rubble thicknesses ($t_{rubble} = 8$ to 20 cm), where two deformation rates of 3 mm/s (defined as slow tests) and 25 mm/s (defined as fast tests) were used. Using the Mohr-Coulomb material criterion they fitted a linear function to the strength vs. confinement data. Strength values obtained were observed to decrease with increasing deformation rate by a maximum amount of about 15 kPa. Hellmann [13] also investigated rate effects in ice rubble through a series of shear box tests on freshwater ice confined under normal pressures ranging from 0 to 3 kPa. The maximum shear stress was observed to increase with decreasing deformation rate for deformation rates of 1.6 and 10.9 mm/s. It was also observed that for a constant normal stress, the strength of the rubble was about twice as high for slower deformation rates compared with higher rates. Urroz and Ettema [16] conducted simple-shear box experiments for three different sizes of freshwater ice blocks, varying the shear rates from 0.004 to 0.045 s⁻¹ (1.4 to 15.75 mm/s) with a confinement of 69 kPa. For all block sizes and

rubble thicknesses tested in these experiments, shear strength was reported to decrease as the deformation rate increased. The authors attributed this behavior to the dynamic freeze-bonding of adjacent ice blocks, which is more pronounced during slow deformations. A comparison of the strength values for each ice rubble thickness tested with regards to block size showed that while the medium ice blocks showed higher strength values in general compared to small and large blocks, strain rate has a more pronounced effect on strength in ice rubble with a higher thickness. Similarly, Sayed [15] conducted plain strain compression tests on ice rubble for strain rates of 6.5×10^{-5} and $1.7 \times 10^{-1} \text{ s}^{-1}$, varying the confining stress from 2.45 to 35 kPa. Similar to previous experiments, comparing the shear stress-confinement relationship derived from the Mohr-Coulomb criterion, they observed that shear strength was higher for slower deformation rates.

Direct comparison of all rubble test data was not possible, as tests were performed under different test conditions, geometrical scales, as well as reported in inconsistent formats. Despite these differences, it is evident that a clear rate effect exists in the aggregate ice rubble data. Figure 5.12 presents the results of the above-noted papers, presenting measured strength values in these experiments as a function of deformation rate. The trend of decreasing strength with increasing deformation rate has been attributed to dynamic freeze-bonding of ice blocks during deformation and suppression of dilatancy [11]. Comparison of the results of the present study with these ice rubble experimental results suggests that freeze bond failure is likely an important contributor to observed rate effects in ice rubble and ridge failure.



◇ Urroz and Ettema (1987), $H_{\text{rubble}}=228$ mm, $\sigma=0-5$ kPa, $\eta=0.23$, Small size blocks	◇ Hellman (1984), $H_{\text{rubble}}=70$ cm, Ice chips, primary shear mode, $\sigma=0-3$ kPa
○ Urroz and Ettema (1987), $H_{\text{rubble}}=228$ mm, $\sigma=0-5$ kPa, $\eta=0.39$, Medium size blocks	○ Hellman (1984), $H_{\text{rubble}}=70$ cm, Ice chips, secondary shear mode, $\sigma=0-3$ kPa
□ Urroz and Ettema (1987), $H_{\text{rubble}}=200$ mm, $\sigma=0-5$ kPa, $\eta=0.36$, Large size blocks	□ Hellman (1984), $H_{\text{rubble}}=70$ cm, Ice chips, tertiary shear mode, $\sigma=0-3$ kPa
◆ Urroz and Ettema (1987), $H_{\text{rubble}}=152$ mm, $\sigma=0-5$ kPa, $\eta=0.31$, Small size blocks	◇ Weiss et al. (1981), $H_{\text{rubble}}=46-91$ cm, $H_{\text{ice sheet}}=200$ mm, $\sigma=0-28$ kPa
● Urroz and Ettema (1987), $H_{\text{rubble}}=152$ mm, $\sigma=0-5$ kPa, $\eta=0.4$, Medium size blocks	□ Weiss et al. (1981), $H_{\text{rubble}}=91$ cm, $H_{\text{ice sheet}}=150$ mm, $\sigma=0-28$ kPa
■ Urroz and Ettema (1987), $H_{\text{rubble}}=133$ mm, $\sigma=0-5$ kPa, $\eta=0.41$, Large size blocks	▷ Weiss et al. (1981), $H_{\text{rubble}}=76-86$ cm, $H_{\text{ice sheet}}=80$ mm, $\sigma=0-28$ kPa
△ Urroz and Ettema (1987), $H_{\text{rubble}}=76$ mm, $\sigma=0-5$ kPa, $\eta=0.36$, Small size blocks	□ Yasunaga et al. (2002), $H_{\text{ice sheet}}=42.5$ mm, $\sigma=6$ kPa, $\eta=0.3$
★ Urroz and Ettema (1987), $H_{\text{rubble}}=76$ mm, $\sigma=0-5$ kPa, $\eta=0.4$, Medium size blocks	

Figure 5.12. Rubble shear strength measurements of Yasunaga et al. [17], Urroz and Ettema [16], Hellmann [13], and Weiss et al. [12] as a function of deformation rate. In this figure where H_{rubble} is the ice rubble thickness, $H_{\text{ice sheet}}$ is the ice block thickness, η is the rubble porosity, V is the displacement rate, and t is the consolidation time.

In addition to the above ice rubble tests, the influence of deformation rate on the failure mechanics of gouging ridge keels was investigated in a joint project between C-CORE and the National Research Council of Canada during PIRAM and DIRKS programs [14, 23-25]. Tests consisted of mounting a manufactured freshwater ice keel (dimensions 1.7 m depth,

4 m length and 3.5 m width) in the test frame and applying a vertical surcharge pressure while pushing a soil tray horizontally into the keel at a range of velocities. Results from these tests showed a clear change in behavior of the keel as the speed was reduced from 30 mm/s to 1 mm/s. In particular, it was observed that for the slower moving keels, peak pressures on the berm were higher (Figure 5.13), and a greater amount of uplift, as well as higher friction angles were observed. Bailey et al. [25] attributed this behavior to the degree of compaction of the ice rubble, whereby ice blocks in slower-moving keels had more time to reorient and compact during the initial application of the surcharge pressure. They suggested this influenced the magnitude of dilation, whereby more compacted ice rubble keels expanded more rapidly, as has been observed in soil mechanics [42], which resulted in the observed increase in peak pressures and uplift for slower-moving keels. The degree of compaction also influenced the friction angle of the rubble, whereby the more compact, slower-moving keels had higher friction angles than the less compact faster-moving keels [25]. In light of the findings of this paper, we may further interpret from DIRKS/PIRAM results that the compaction of the ice rubble during slow deformation tests may have resulted in an increase in the number and strength of freeze bonds formed, which contributed to the overall strength of the keel. Furthermore, the confining pressure of the bonded ice blocks is expected to increase during the compaction of the keels, resulting in further increase in the strength of freeze bonds as has been observed in Section 4.3 and Ettema and Schaefer [3], Boroojerdi et al. [43] and Repetto-Llamazares [5].

In Figure 5.13, the peak pressures measured on the berm during the DIRKS and PIRAM tests are plotted against deformation rates. It is important to highlight that while a direct

comparison cannot be made between pressures shown in Figure 5.13, which are for the aggregate rubble, similar trends are observed in both the DIRKS/PIRAM results and in the new freeze bond data presented here. This evidence supports the notion that freeze bond strength and failure behavior are important contributors to the macroscopic strength of ridges. It may also be observed from Figure 5.13 that total drop of pressure with increase of deformation rate from 0.5 to 15 mm/s in the DIRKS tests is 187 kPa, which is close in magnitude to the decrease observed in this study (130 kPa) over a similar range of rates (Figure 5.8).

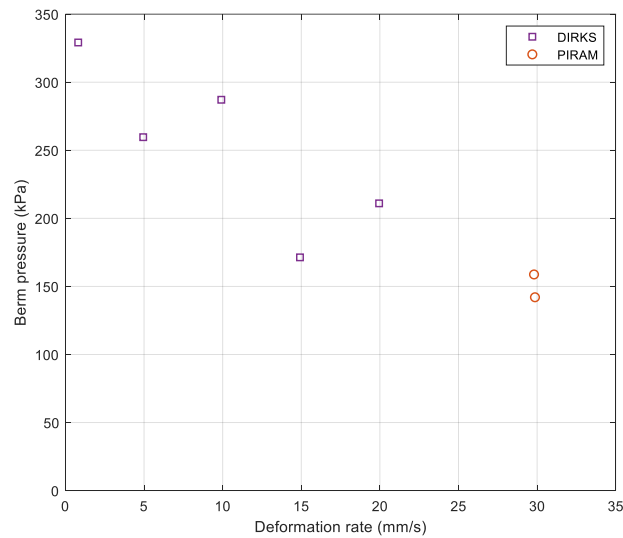


Figure 5.13. Berm pressure data for DIRKS and PIRAM projects.

While failure processes in full-scale rubble and ridges are considerably more complicated than the failure of individual freeze bonds, the similarities discussed above highlight the need for further work to investigate the linkages between freeze bond properties and the

overall strength of ridges. Further research to study the effects of rubble compaction on the degree of freeze-bonding between blocks within a rubble aggregate is also needed to better understand the nature of the relationship between individual freeze bonds and overall ice rubble strength rate dependence.

5.7. Conclusions

A series of shear strength tests was conducted to investigate the effects of deformation rate on the strength of freeze bonds between freshwater ice blocks. These tests were conducted for two submersion times: 30 min, and 24 h. The 30-minute submergence time was chosen to correspond to the time it takes the ice block temperatures to equilibrate with the surrounding water. The 24-hour time was chosen as the period during which the freeze bond strength is estimated to be at a minimum, which corresponds to the transition from thermal to sintering-creep dominated bond formation processes [9]. For both submersion times considered it was observed that the freeze bond strength is highly dependent on deformation rate. This has direct application for ice rubble and ridge strength development since strength of such features has been described as being governed by three main mechanisms: inertia effects, pore pressure effects and freeze bond strengths. By isolating the freeze bonds from inertial and pore pressure effects in current program, the freeze bond strength was observed to decrease with increase in deformation rate. This is consistent with rate-dependency observed in ridge/rubble strengths measurements, as well as rate dependency of ice under compression, suggesting that rate effects in ice ridges and rubble

may be closely tied to the properties and behavior of ice as a material, rather than simply inertial or pore pressure effects.

Comparison of the shear strengths measured in the present work with previous compressive strength measurements conducted on solid ice showed that in general, both properties decrease with increases in deformation rate for the range of strain rates used in this study. Rate dependency of solid ice under compression is controlled by dislocation motions such as basal glide/climb, internal cracking, and dynamic-recrystallization. Further work is needed to examine if the same mechanisms may dominate freeze bond failure, or if other processes relating to dynamic freeze-bonding and local microstructural changes in the ice may be occurring. Detailed examination of the ice around the bond interface is of interest since changes to the ice microstructure may also result in the effective bond thickness exceeding the theoretical estimate based on surface roughness discussed here. Strain values reported in this paper were nominal total strains, which is consistent with past AFPB testing in the literature. Given the noted uncertainties in assessing the relative contributions of ice deformation, freeze bond deformations and potential local deformations under the pins (although no permanent deformations under the pins were observed for data used in this analysis), it is recommended that future tests include direct measurement of deformation across the bond, so as to provide greater confidence in the interpretation and modelling of strain components. Such measurements would improve understanding and modelling of the strain response, but would not affect measured strength values, which were the focus of this paper.

In assessing the links between this work and full-scale observations, it was concluded that trends observed for shear strength from ridge and rubble tests reported in the literature are in good general agreement with these tests, and the observed trend of decreasing strength with increased deformation rate is consistent between lab and field scales. Comparisons of the berm pressure values measured for a series of near full-scale keel-gouge tests in the DIRKS and PIRAM programs show the drop in pressure with increase in deformation rate to be within the range of the drop in strength in present study. This highlights the importance of the role of freeze bonds on the overall strength of ridges for different deformation rates, which has received little attention to date. This is the first study, as far as the authors are aware, where effects of deformation rate on the strength development of freeze bonds have been explicitly studied for deformation rates ranging from 0.01 to 100 mm/s. We hope that this study encourages additional experimentation to further study these effects, and to directly aid in the development of improved rubble and ridge models, linked to the underpinning mechanics of ice rubble strength.

5.8. References

- [1] A. Patil, B. Sand, L. Fransson, and H. Daiyan, "Constitutive Models for Sea Ice Rubble in First Year Ridges: A Literature Review," in *Proceedings of the 26th IAHR International Symposium on Ice*, Beijing, China, 2012.

- [2] S. Shafrova and K. V. Høyland, “The freeze-bond strength in first-year ice ridges. Small-scale field and laboratory experiments,” *Cold Regions Science and Technology*, vol. 54, no. 1, pp. 54–71, 2008.
- [3] R. Ettema and J. A. Schaefer, “Experiments on freeze-bonding between ice blocks in floating ice rubble,” *Journal of Glaciology*, vol. 32, no. 112, pp. 397–403, 1986.
- [4] A. Marchenko and C. Chenot, “Regelation of ice blocks in the water and the air,” in *proceedings of the 20th Port and Ocean Engineering Under Arctic Conditions conference*, Luleå, Sweden, 2009.
- [5] A. H. V. Repetto-Llamazares, “Experimental studies of shear failure on freeze-bonds in saline ice part I: set-up, failure mode and freeze-bond strength.,” *Cold Regions Science and Technology*, vol. 65, no. 3, pp. 286–297, 2011.
- [6] H. Helgøy, O. S. Astrup, and K. Høyland, “Laboratory work on freeze-bonds in ice rubble, Part II: Results from individual freeze-bond experiments,” in *Proceedings of the 22nd International Conference on Port and Ocean Engineering under Arctic Conditions*, Espoo, Finland, 2013.
- [7] K. V. Høyland and A. Møllegaard, “Mechanical behavior of laboratory made freeze-bonds as a function of submersion time, initial ice temperature and sample size,” in *Proceedings of the 22nd IAHR International Symposium on Ice*, Singapore, 2014.
- [8] I. M. Bueide and K. V. Høyland, “Confined Compression Tests on Saline and Fresh Freeze-Bonds,” in *Proceedings of the 23rd International Conference on Port and Ocean Engineering Under Arctic Conditions*, Trondheim, Norway, 2015.
- [9] M. T. Boroojerdi, E. Bailey, and R. Taylor, “Experimental study of the effect of submersion time on the strength development of freeze bonds,” *Cold Regions Science and Technology*, p. 102986, 2020.

- [10] A. Azarnejad and T. G. Brown, "Ice Rubble Behavior in Punch Tests," *Journal of Cold Regions Engineering*, vol. 15, no. 3, pp. 135–153, 2001.
- [11] P. Liferov and B. Bonnemaire, "Ice rubble behaviour and strength: Part I. Review of testing and interpretation of results," *Cold Regions Science and Technology*, vol. 41, no. 2, pp. 135–151, 2005.
- [12] R. Weiss, A. Prodanovic, and K. Wood, "Determination of ice rubble shear properties," in *Proceedings of the 6th IAHR International Symposium on Ice*, Quebec, Canada, 1981.
- [13] J. Hellmann, "Basic investigations on mush ice," in *Proceedings of the 7th IAHR International Symposium on Ice*, Hamburg, Germany, 1984.
- [14] E. Bailey, J. Bruce, and R. Taylor, "The Development of Ice Ridge Keel Strengths: The influence of speed on the strength and deformation behaviour of gouging ridge keel," in *Proceedings of the 22nd IAHR International Symposium on Ice*, Singapore, 2014.
- [15] M. Sayed, "Mechanical properties of model ice rubble," presented at the Materials and Member Behavior, 1987, pp. 647–659.
- [16] G. E. Urroz and R. Ettema, "Simple-shear box experiments with floating ice rubble," *Cold Regions Science and Technology*, vol. 14, no. 2, pp. 185–199, 1987.
- [17] Y. Yasunaga, S. Kioka, Y. Matsuo, A. Furuya, and H. Saeki, "The strength of the unconsolidated layer model of ice ridge," in *Proceedings of the 16th IAHR International Symposium on Ice, Dunedin, New Zealand*, 2002.
- [18] I. Hawkes and M. Mellor, "Deformation and fracture of ice under uniaxial stress," *Journal of Glaciology*, vol. 11, no. 61, pp. 103–131, 1972.
- [19] S. J. Jones, "The confined compressive strength of polycrystalline ice," *Journal of Glaciology*, vol. 28, no. 98, pp. 171–178, 1982.

- [20] E. M. Schulson and N. P. Cannon, “The effect of grain size on the compressive strength of ice,” in *Proceedings of the 7th IAHR International Symposium on Ice*, Hamburg, Germany, 1984.
- [21] E. M. Schulson, “The brittle compressive fracture of ice,” *Acta Materialia*, vol. 38, no. 10, pp. 1963–1976, 1990.
- [22] M. Ghobadi, E. Bailey, and R. Taylor, “Thermal behaviour and growth of submerged ice blocks: Experimental and Numerical Results,” in *Proceedings of the 34th International Conference on Ocean, Offshore and Arctic Engineering*, St. John’s, Canada, 2015.
- [23] J. Bruce, G. Piercey, A. Macneill, R. Phillips, and A. Derradji, “Physical Testing Method to Study Ice Keel Strength Limits during a Gouging Process,” in *Proceedings of the 3rd Arctic Technology Conference*, Houston, Texas, 2012.
- [24] R. Phillips, T. King, and J. Bruce, “PIRAM: Pipeline Ice Risk Assessment & Mitigation Program Overview,” in *Proceedings of the 9th International Pipeline Conference*, Calgary, Canada, 2012.
- [25] E. Bailey, J. Bruce, A. Derradji, and M. Lau, “An overview of the development of ice ridge keels strength testing program,” in *Proceedings of the 3rd Arctic Technology Conference*, Houston, Texas, 2014.
- [26] E. M. Schulson and P. Duval, *Creep and Fracture of Ice*. ISBN 978-0-521-80620-6: Cambridge University Press, 2009.
- [27] M. A. Maleque and M. S. Salit, “Mechanical failure of materials,” in *Materials Selection and Design*, Springer, 2013, pp. 17–38.
- [28] E. M. Schulson and A. L. Fortt, “Friction of ice on ice,” *Journal of Geophysical Research: Solid Earth*, vol. 117, no. B12, 2012.

- [29] J. Paavilainen and J. Tuhkuri, "Parameter effects on simulated ice rubbing forces on a wide sloping structure," *Cold Regions Science and Technology*, vol. 81, pp. 1–10, Sep. 2012.
- [30] A. Polojärvi and J. Tuhkuri, "On modeling cohesive ridge keel punch through tests with a combined finite-discrete element method," *Cold Regions Science and Technology*, vol. 85, pp. 191–205, Jan. 2013.
- [31] L. Liu, E. Bailey, R. Sarracino, R. Taylor, and C. Stanbridge, "Numerical Simulation of Ice Ridge Gouging," in *Proceedings of the 34th International Conference on Ocean, Offshore and Arctic Engineering*, St. John's, Canada, 2015.
- [32] D. Molyneux, D. Spencer, and L. Liu, "Loads due to first year ice ridges on a vertical cylinder," in *Proceedings of the 32nd International Conference on Ocean, Offshore and Arctic Engineering*, St. John's, Canada, 2013.
- [33] R. Yulmetov, E. Bailey, and F. Ralph, "A discrete element model of ice ridge interaction with a conical structure," in *Proceedings of the 24th International Conference on Port and Ocean Engineering under Arctic Conditions*, Busan, Korea, 2017.
- [34] S. Afzali, R. Taylor, R. Sarracino, E. Bailey, and M. T. Boroojerdi, "Investigation of the Effect of Block Size, Shape and Freeze-Bond Strength on Flexural Failure of Freshwater Ice Rubble using the Discrete Element Method," in *Proceedings of the 38th International Conference on Ocean, Offshore and Arctic Engineering*, Glasgow, Scotland, 2019.
- [35] E. M. Schulson, "The structure and mechanical behavior of ice," *Jom*, vol. 51, no. 2, pp. 21–27, 1999.
- [36] M. Mellor, "Mechanical behavior of sea ice," in *The geophysics of sea ice*, Springer, 1986, pp. 165–281.
- [37] E. M. Schulson, "Brittle failure of ice," *Reviews in mineralogy and geochemistry*, vol. 51, no. 1, pp. 201–252, 2002.

- [38] D. Carter and B. Michel, “Lois et Mechanismes de Lapparente Fracture Fragile de la Glace de Riviere et de Lac, Univ,” *Laval, Faculte des Sciences, Department de Genie Civil, Rep. S-22*, 1971.
- [39] S. J. Jones, R. E. Gagnon, A. Derradji, and A. Bugden, “Compressive strength of iceberg ice,” *Canadian Journal of Physics*, vol. 81, no. 1–2, pp. 191–200, 2003.
- [40] L. Zhang, Z. Li, Y. Wang, G. Li, and M. Han, “Model Tests of Ice Forces on Conical Structures for a Harbor Design in Bohai,” in *Proceedings of the 18th International Conference on Port and Ocean Engineering under Arctic Conditions*, Potsdam, 2005.
- [41] R. S. Taylor and I. J. Jordaan, “Probabilistic fracture mechanics analysis of spalling during edge indentation in ice,” *Engineering Fracture Mechanics*, vol. 134, pp. 242–266, 2015.
- [42] G. T. Houlsby, “How the dilatancy of soils affects their behaviour,” in *Proceedings of the 10th European Conference on Soil Mechanics and Foundation Engineering (ECSMFE)*, Florence, Italy, 1991.
- [43] M. T. Boroojerdi, E. Bailey, M. Ghobadi, and R. Taylor, “Experimental Study on Shear Strength of Freeze Bonds in Freshwater Ice,” in *Proceedings of the Arctic Technology Conference*, St. John’s, NL, Canada, 2016.

6. CONCLUSIONS AND RECOMMENDATIONS FOR FUTURE WORK

6.1. Conclusions

Strength development and failure properties of freeze bonds and their influence on the overall strength development of ice rubble/ridges were investigated in this thesis. Freeze bonds were formed by placing two cylindrical freshwater ice samples in contact in a confinement frame. Samples, confined under a constant normal pressure, were then submerged for a specific period of time. Once taken out of the water, the Asymmetric Four-Point Bending (AFPB) apparatus was used to shear the freeze bond. The shear strength of the freeze bonds were then calculated based on the load required to fail the bond. Three series of tests were conducted to investigate the effects of submersion time, confinement pressure and deformation rate on strength development and failure of freeze bonds.

6.1.1. Submersion time effects

Over the submersion times tests, shear strength was observed to vary from a minimum of around 50 kPa to a maximum of around 300 kPa, i.e. showing that submersion time can cause strength to vary by a factor of around 6. The strength development of freeze bonds with regards to submersion time was observed to follow 5 distinct phases:

- In phase 1, the shear strength of the freeze bond was observed to initially increase as a result of thermal processes as heat was transferred from the water to the ice blocks, reaching a peak of 197 kPa after 4 minutes of submersion.
- The bond strength decreased in phase 2 (after the initial increase) to a low constant value of around 50 kPa after 3 hours of submersion as ice blocks equilibrated with surrounding water temperature.
- In phase 3, which occurred between 3 to 24 hours of submersion, the shear strength remained constant at around 50 kPa. Samples in this stage were in thermal equilibrium with surrounding water, and no new freezing could take place at the freeze bond interface. The dominant bond formation mechanism was therefore believed to be in transition from thermal to sintering-creep processes during this time period.
- In phase 4, freeze bond strength however started to increase again after 24 hours and reached the highest strength of 300 kPa after 14 days, which is within the range of the strength of solid ice samples. Bond development in this phase was governed by sintering-creep processes, where bond strength increased as a result of sintering

of ice asperities in contact at the freeze bond. With continued application of confinement in prolonged submersion times, creep-induced deformation of asperities, in conjunction with crushing and particle rearrangement contributed to further strength development in this phase.

- In phase 5, Freeze bond strength is believed to asymptote to the strength of solid ice as a result of the sintering-creep processes in prolonged submersion times.

The bell-shaped curve observed in phase 1-3 of strength-submersion time relationship was also observed in previous freeze bond experiments [1, 2]. An empirical equation was derived from the data that estimated bond strength in terms of submersion time for each of the initial ice temperatures tested. Microstructural analysis of the contact interface is suggested for more detailed analysis of sintering processes.

6.1.2. Confinement effects

The effects of confinement pressure were investigated for confinements ranging from 10 to 100 kPa, which were chosen based on the range of confinements expected to occur during the formation of ice ridges/rubble, as well as interactions. To investigate the simultaneous effect of submersion time and confinement on freeze bond strength, four submersion times (30 minutes, 3 hours, 3 days, and 7 days) representative of the stages of bond development observed in submersion time tests were used. The shear strength of freeze bonds was found to linearly increase by a factor of 2-3 with increasing confinement for all submersion times tested. The rate of increase in strength with increase in confinement was observed to follow

the same trends observed in the submersion time tests, with the highest rate of increase occurring after 7 days of submersion, where strength increased from 188 to 387 kPa as confinement increased. Sintering-creep and crushing of asperities at the contact interface were proposed as the physical processes involved in the strength development in these tests. Ice rubble studies show similar confinement pressure dependency of strength, where shear strength linearly increases with increase in confinement pressure, signifying the important role that confinement plays on the overall strength of ice rubble/ridges. While submersion time was observed to highly affect the rate of increase in strength with increasing confinement for these constant area freeze bond tests, especially for prolonged submersion times where sintering effects were more intensified, the ice rubble tests of Shayanfar [3, 4] conducted for consolidation times ranging from 0 to 70 hours suggest that consolidation time did not have as significant effect for those conditions. This may be due to differences in thermal processes, as well as differences in the development of contact area and pressures in ice rubble as compared to the freeze bond test specimens used in this study. During the ice rubble tests, it was observed that the ice took a considerably longer time to reach equilibrium temperature with water in comparison to block-block scale (two hours compared to 30 minutes). This suggests that longer time scales may be required for the ice in keels to “warm up” to the point where sintering-creep processes observed in the freeze bond tests become more prevalent in ice rubble freeze bonds. To examine this further, ice rubble tests under prolonged submersion times are recommended in the future to allow for further investigation of links between these two scales. In addition, to allow for a more direct comparison of these constant area freeze bond tests with ice rubble freeze bonds,

more work is needed to understand the nature of contact area between ice rubble blocks under different conditions. This is a highly important area for future work, since conditions that produce smaller contact areas in ice rubble could result in higher local contact pressures, which would be expected to promote sintering-creep processes that may produce stronger bonds over smaller areas. Alternatively, conditions that produce larger contact areas between ice rubble blocks may result in lower average contact pressures, which may yield weaker bonds over larger areas. Since the strength of the ice rubble will depend on both the size and strength of the individual freeze bonds, the interplay between contact area and pressure for ice rubble masses needs further investigation. These important aspects are beyond the scope of the present work, and are being considered by Afzali et al. [5] and others.

6.1.3. Deformation rate effects

Freeze bond failure and shear strength were found to be highly dependent on the rate of shear deformation. Tests were conducted for deformation rate ranging from 0.01 to 100 mm/s. The amount of sample strain before failure was higher at lower deformation rates as a result of creep processes taking place before failure. While the time to failure increased with decrease in deformation rate, as expected, the rate of this increase was not a linear function of deformation rate, which highlights the higher capacity of ice for energy dissipation at slower deformation rates. Two submersion times of 30 minutes and 24 hours were considered in these tests, which are representative of thermal and sintering-creep

stages of bond development observed in submersion time tests. From these results, shear strength was found to decrease with increase in deformation rate for both submersion times, with average strength decreasing from around 290 to 50 kPa, i.e. deformation rate was observed to result in a decrease in strength by a factor of around 6. Strength values of the 30 minutes tests were slightly higher than the 24-hour tests, as was the case for the submersion time tests. The results of these tests have specific importance in ice rubble/ridge failure models, as freeze bond failure has been identified as one of the controlling mechanisms in the failure of these features, and such ice features in nature would have drift speeds covering a range of values, leading to rate effects in full scale interactions. Strength-deformation rate data available for ice rubble/ridges as well as rate dependency of compressive strength of solid ice show similar trendline as in freeze bond results, suggesting that rate effects in ice ridges/rubble are highly dependent on properties of ice as a material rather than inertial and pore pressure effects as have been suggested by other researchers as causal mechanisms during failure of these features.

6.1.4. Comparison of the effects of parameters tested

Of the parameters tested, submersion time and deformation rate appear to have the most significant influence on strength development, each causing the strength to vary by a factor of 6.

Short and prolonged submersion times exhibited substantial strength development in these tests, accompanied by periods of low strength in between. This has significant importance in brash ice channels where freeze bonds are continuously formed and broken as marine vessels pass through the channel, as well as ice rubble/ridge interactions, where prolonged contact times are expected. While increasing confinement proved to increase freeze bond strength, the rate of this increase was directly linked to the submersion period, following trends observed in submersion time tests. Perhaps the most important observation in these tests was the significant influence of sintering-creep processes on the strength development of the bonds. Sintering-creep processes, which take place over longer time scales, were observed to dominate the development of strength for prolonged submersion times. Further investigation is needed to better understand the combined effect of multiple factors, such as the simultaneous influence of both submersion time and deformation rate, since it was not possible within the scope of this program to conduct sufficient numbers of tests to adequately assess interactions between different effects.

As stated earlier, the significant influence of deformation rate on the failure strength of freeze bonds further highlights the role of freeze bond strength rate-dependency on the overall failure behavior of ice rubble/ridges. This is important during ice rubble pile-up events, shipping, as well as ice ridge gouging events, where freeze bonds can be deformed under a wide range of rates, which can considerably influence the loads applied by these features. Based on the results of these experiments, under slow deformation rates, ice can undergo larger deformations before failure of freeze bonds, which results in significantly higher freeze bond strengths. While the increasing strength at lower rates can be a hazard

in many ice rubble/ridge load conditions, interestingly, studies have shown that this can be beneficial in ice rubble pile-up events, where the increased strength of the rubble pile can act as an ice barrier protecting the structure [6].

6.1.5. Implications of freeze bond strength on strength of ice rubble/ridges

Sintering-creep processes involved in strength development of freeze bonds specifically over prolonged submersion times are of particular importance in ice ridge keel and rubble load models as these features can be formed days, weeks, or months before an interaction occurs. Sintered blocks of ice have been observed during previous field experiments, where ridge keels were observed to be smoothed out at the bottom with substantial neck formation between the ice blocks [7]. Current ice ridge/rubble models assume the ice rubble to be a cohesionless granular material with Mohr-Coulomb criteria used to describe strength properties. The results of our freeze bond experiments suggest that strength properties of ice rubble/ridges cannot be described by a single relationship and that several parameters simultaneously influence strength properties, which should be accounted for in models. It was also observed that it is possible for the freeze bond strength in longer submersion times and higher confinement pressures to reach the strength of solid ice. Ice rubble thus can be modeled as a solid porous material with solid ice properties as the freeze bond interface properties [8].

Comparison of the results observed in confinement and deformation rate tests for individual freeze bonds with previous ice rubble and ridge experiments showed similar trends of strength development and failure at both scales. The magnitude of the changes in strength of freeze bonds with regards to confinement were higher over prolonged submersion times, due to creep and sintering processes as well as crushing of asperities in contact between the ice blocks. While confining pressure has been studied as the main mechanism controlling ice rubble strength development to date, the results of freeze bond tests signify the importance of understanding the role of consolidation time, specially prolonged consolidation times on the overall strength of rubble structure, and its influence on the impact of other parameters such as confinement pressure. Comparison of the thermal equilibrium processes in large masses of ice rubble [3] and block-block freeze bond tests suggests that the time scales are much longer in ice rubble scale, and that longer times are required for effects observed in block-block scale to take place. Furthermore, more information is needed regarding how local contact pressures between individual blocks change as a function of the average ice rubble confinement pressure. Contact pressures between ice blocks in ice rubble structure are influenced by the degree of compaction within the rubble structure, and thus do not increase in direct proportion to the increase in average ice rubble confining pressure. Direct measurements between ice blocks within the ice rubble structure, using pressure sensors, can be used for direct comparison of results with block-block scale.

Loading rate-dependency of freeze bond failure proved to be one of the controlling mechanisms in ice rubble/ridge failure, where a similar decreasing trend of shear strength

was observed as deformation rate increased. While ice rubble failure strength is also influenced by inertial and high pore pressure effects [9], rate-dependency of freeze bond strength observed in these tests suggests the failure properties of ice rubble/ridges to be closely tied to failure behavior of ice as a material rather than inertial and high pore pressure effects. More tests on the ice rubble scale can help further understand the influence of freeze bond strength and failure on the overall rate dependency of ice rubble/ridges.

6.2. Recommendations for Future Work

The following points are recommended as improvements to the experimental procedure and methods to be used in future freeze bond experiments:

- Measurements of the length and diameter of samples before and after each test can help better quantify how creep processes evolve as a function of submersion period.
- Measurement of surface roughness of the samples would be beneficial for estimation of freeze bond thickness. This can also help better understand sintering and creep processes between contacting asperities and can be used in sintering models for estimation of the real contact surface between the ice blocks.
- Sample strains during shear was recorded from the MTS machine and string potentiometers attached to the AFPB rig. To distinguish between the deformation of freeze bonds and ice under the loading pins, it is suggested for the strains to be measured directly from the samples.

Experiments conducted in this study have served to advance understanding of freeze bond strength development and failure. Further tests are suggested to advance this work as suggested below:

- Freeze bond strength development needs to be further studied in prolonged submersion times. Limited availability of coldroom facilities allowed for a limited number of long submersion time tests to be conducted in this test program.
- Interaction between parameters tested, such as the simultaneous effect of confinement pressure and submersion time is an important topic for future work. Results presented in this thesis provide valuable information regarding the simultaneous effect of submersion time and confinement pressure on strength development. Further work is needed to characterize the processes involved and provide models that can characterize freeze bond strength in terms of submersion time and confinement pressure, which can be an alternative to the Mohr-Coulomb model assumption that is currently used in many numerical models.
- While the results provided in this thesis signify the role of sintering processes in freeze bond strength development, sintering mechanisms under submerged conditions especially at larger scales are yet to be fully understood. A series of tests are suggested to be conducted using the side by side configuration of cylindrical ice blocks used by Ghobadi et al. [10], to measure the neck growth between thermally equilibrated submerged ice blocks, specifically when under an external normal pressure. This can help better characterize sintering mechanisms under submerged conditions especially at larger scales, which can be added to the thermal model of

Ghobadi et al. [10]. Preliminary tests were conducted using this configuration for contacting samples with no external pressure, which showed substantial ice growth between the blocks after 1 week of submersion. An extensive test program is however required to fully investigate this process.

- Freeze bond experiments should be conducted in the field to better understand in-situ sea ice properties, which can be directly linked to ice rubble field experiments under saline conditions. The AFPB shear method used in these experiments was used in a set of preliminary field freeze bond and solid saline ice shear experiments in St. Anthony, NL, to examine the suitability of using this approach in field conditions. The results of these experiments, which were presented at the 2018 Arctic Technology Conference [11], have been presented in Appendix B. While the method and apparatus used in these tests show promising results, further data are needed to better characterize solid and freeze-bonded sea ice strength.
- A more detailed investigation of the development of contact areas and associated local pressures between ice rubble blocks for different conditions is highly important in linking the strength of rubble with the research presented here. All freeze bonds considered the present study corresponded to specimens with constant contact area, which provides valuable insight into freeze bonds and the underpinning physics. To link these findings with full-scale ice rubble and ridges, additional research on the effects of compaction and localized ice failure processes, as well as block size, shape and orientation on the process of contact area and

pressure development between individual blocks within an ice rubble mass is needed.

6.3. References

- [1] A. H. V. Repetto-Llamazares, “Experimental studies of shear failure on freeze-bonds in saline ice part I: set-up, failure mode and freeze-bond strength.” *Cold Regions Science and Technology*, vol. 65, no. 3, pp. 286–297, 2011.
- [2] I. M. Bueide and K. V. Høyland, “Confined Compression Tests on Saline and Fresh Freeze-Bonds,” in *Proceedings of the 23rd International Conference on Port and Ocean Engineering Under Arctic Conditions*, Trondheim, Norway, 2015.
- [3] H. Shayanfar, “An experimental investigation on the strength and failure behavior of freshwater ice rubble,” MSc Thesis, Memorial University of Newfoundland, 2018.
- [4] H. Shayanfar, E. Bailey, and R. Taylor, “Medium-scale laboratory investigation of the effects of confining pressure on ice rubble strength and failure behavior.” *Cold Regions Science and Technology*, Under Review.
- [5] S. Afzali, R. Taylor, R. Sarracino, E. Bailey, and M. T. Boroojerdi, “Investigation of the Effect of Block Size, Shape and Freeze-Bond Strength on Flexural Failure of Freshwater Ice Rubble using the Discrete Element Method,” in *Proceedings of the 38th International Conference on Ocean, Offshore and Arctic Engineering*, Glasgow, Scotland, 2019.
- [6] A. Barker and G. W. Timco, “Overview of ice rubble generators and ice protection structures in temperate regions,” in *Proceedings 18th International Conference on Port and Ocean Engineering under Arctic Conditions*, Potsdam, US, 2005.

- [7] A. Marchenko and C. Chenot, “Regelation of ice blocks in the water and the air,” in *Proceedings of the 20th International Conference on Port and Ocean Engineering Under Arctic Conditions*, Luleå, Sweden, 2009.
- [8] E. Bailey, R. Taylor, and K. R. Croasdale, “Mechanics of Ice Rubble over Multiple Scales,” in *Proceedings of the 34th International Conference on Ocean, Offshore and Arctic Engineering*, St. John’s, Canada, 2015.
- [9] P. Liferov and B. Bonnemaire, “Ice rubble behaviour and strength: Part I. Review of testing and interpretation of results,” *Cold Regions Science and Technology*, vol. 41, no. 2, pp. 135–151, Feb. 2005.
- [10] M. Ghobadi, E. Bailey, and R. Taylor, “Thermal behaviour and growth of submerged ice blocks: Experimental and Numerical Results,” in *Proceedings of the 34th International Conference on Ocean, Offshore and Arctic Engineering*, St. John’s, Canada, 2015.
- [11] M. T. Boroojerdi, R. Taylor, S. Mohammadafzali, E. Bailey-Dudley, I. Turnbull, and R. Hossain, “Field Experiments on Shear Strength of Solid and Freeze-Bonded Sea Ice,” in *Proceedings of the Arctic Technology Conference*, Houston, USA, 2018.

Appendix A: Preliminary freeze bond experiments, presented at the 2016

Arctic Technology conference, St. John's, NL.

OTC-27424-MS

Experimental Study on Shear Strength of Freeze Bonds in Freshwater Ice

M. T. Boroojerdi, Memorial University of Newfoundland; E. Bailey, Centre for Arctic Resource Development (CARD); M. Ghobadi, and R. Taylor, Memorial University of Newfoundland (MUN)

Copyright 2016, Offshore Technology Conference

This paper was prepared for presentation at the Arctic Technology Conference held in St. John's, Newfoundland and Labrador, Canada, 24–26 October 2016.

This paper was selected for presentation by an ATC program committee following review of information contained in an abstract submitted by the author(s). Contents of the paper have not been reviewed by the Offshore Technology Conference and are subject to correction by the author(s). The material does not necessarily reflect any position of the Offshore Technology Conference, its officers, or members. Electronic reproduction, distribution, or storage of any part of this paper without the written consent of the Offshore Technology Conference is prohibited. Permission to reproduce in print is restricted to an abstract of not more than 300 words; illustrations may not be copied. The abstract must contain conspicuous acknowledgment of OTC copyright.

Abstract

The strength of rubble mass depends on the degree of consolidation between the ice blocks as well as the strength of the ice blocks themselves. The origin of the contact forces between the ice blocks is uncertain, but has been attributed to thermal freezing and sintering. A series of freeze-bond tests were conducted on freshwater ice blocks to gain a greater understanding of the fundamental physical properties affecting ice bonding. The parameters investigated in this test program were the contact period/submersion time and the initial temperature of the ice blocks. Freeze bonds were made by putting two ice blocks in contact in a confinement frame and applying a normal load. The frame was then submerged in water at freezing point for a specific period of time before testing. The bond was sheared using Asymmetric Four-Point Bending (AFPB) method, which produces a nearly pure shear stress state in center of the specimen. Results showed that varying the submersion time from 1 minute to 26 hours for ice samples with initial ice temperature of -18°C , the strength of the bond initially increased and reached the maximum at 5 minutes and then started to gradually decrease, reaching a constant value after 3 hours of submersion. The effect of initial ice temperature on the bonding process was also studied by varying the temperature from 0°C to -18°C , whilst the submersion time was kept constant at 30 minutes. As the temperature was decreased an increase in strength was observed.

Introduction

Ice rubble plays an important role in many different engineering problems, ranging from ice-structure interactions with oil and gas infrastructure, to river and lake engineering, to ship-ice interactions in northern shipping routes, as well as coastal engineering applications in icy ports. In cold water environments (lakes, seas and oceans) ice ridges are common features which form due to compression or shear in the ice cover. Due to the size and strength of these features (once consolidated) they can cause damage to offshore structures and vessels operating in these environments. An understanding of their strength and failure processes is therefore needed to improve confidence in loads estimates associated with ice rubble.

As soon as an ice ridge comes to rest after its formation, ice blocks will start to bond at their contact points to form what are commonly referred to as freeze bonds. Figure 1 shows a schematic illustration of an ice ridge. In the sail above, freeze bonding is largely controlled by atmospheric and sintering processes. In the keel below, consolidation processes are more complex, where not only are freeze bonds forming between ice blocks, but a consolidated layer is also growing due to atmospheric cooling. Freeze bonding processes in the keel are initially controlled by the cold reserves in the ice blocks. Once the ice blocks have warmed to the surrounding water temperature, bonding processes will be controlled by oceanic conditions. Sintering may also act to ‘smooth out’ the keel and increase freeze bond area, which will be discussed in more detail in the discussion section of this paper.

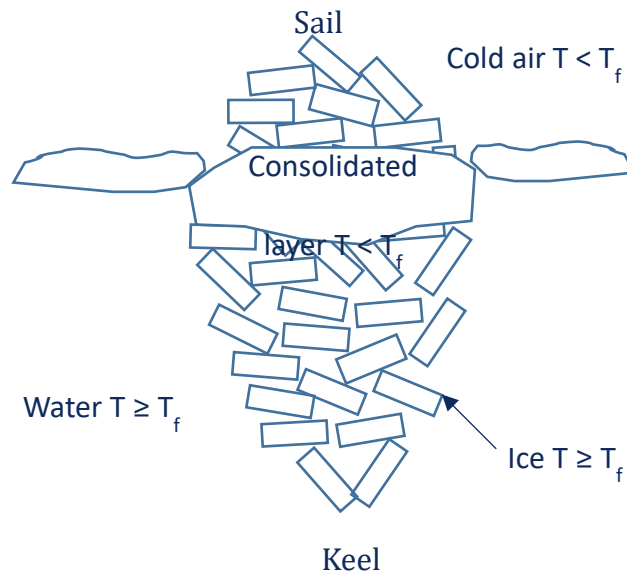


Figure 1. Schematic illustration of ice ridge in winter.

Freeze bonds have been shown to influence the mechanical properties of ice rubble and have been linked to the observed peak load before failure (Ettema & Urroz, 1989; Liferov and Bonnemaire, 2005). As a result several experiments have been performed to investigate the strength of freeze bonds (Ettema and Schafeer, 1986, Shafrova and Høyland, 2008, Marchenko and Chenot, 2009, Repetto-Llamazares et al., 2011 and Høyland and Møllegaard, 2014). All these experiments consisted of forming freeze bonds by placing two pieces of ice in contact, leaving them for a specified period and subsequently shearing the bond. There is considerable spread in the measured freeze bond strengths, which is in part due to the different testing conditions but also due to the number of different parameters that are affecting strength of the freeze bond (submersion time, ice temperature, ice salinity, normal pressure, contact period, and contact area). In most of these tests, unwanted normal stresses are also generated during shear as a result of the test set-ups used.

Overall, the processes affecting freeze bonds strength and therefore ice rubble failure mechanism are complicated. While research on this subject has increased in the past decade there are still areas that require further investigation. In particular, very few freeze bond tests have been carried out on freshwater ice blocks, which are important for low salinity (e.g. Caspian Sea) and freshwater environments. The role of pressure on the freeze bonding process also requires further investigation, as well as understanding the development of the bond strength over extended submersion times. This paper presents results from a series of freeze bond experiments carried out on freshwater ice blocks, where the effects of submersion time and initial ice temperature are investigated to gain more insight into the freeze-bonding process.

Experimental method

Freshwater ice cylinders 10 cm in length and 9 cm in diameter were used to prepare the freeze bonded samples. Two ice cylinders were loaded in the confinement frame shown in Figure 2. A load was applied to the samples using a hand driven gear that moves one end forward while the other remains fixed to a load cell. The load was transferred to the sample via three springs which ensured the load was spread uniformly across the sample. In order to make sure that the samples were perfectly aligned three wedges were used to support the samples during setup; two supports were placed near the platens and the third directly underneath the freeze bond. Once in the correct position, a normal load was applied by turning the gear until the load cell registered the correct load. The frame was then submerged in a freshwater bath held at its freezing temperature (0°C). During submergence, the normal load was monitored continuously using Durham Instruments Quantum X Amplifier and Catman software.

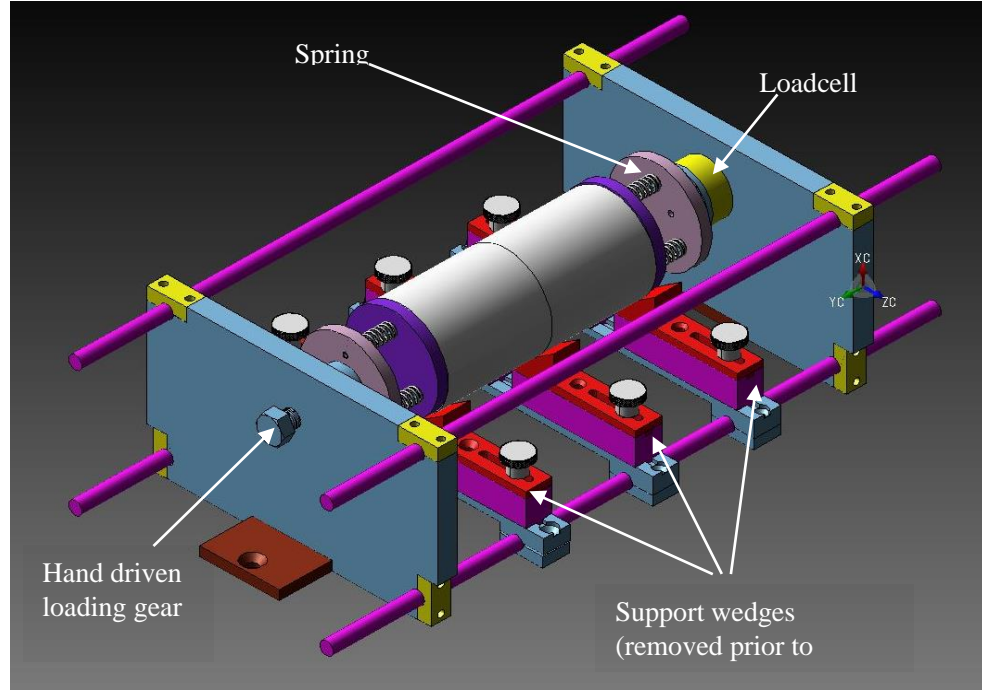


Figure 2. Two freeze-bonded samples loaded in the confinement frame.

The frame was removed from water after a pre-specified period of time, and the bond was sheared using Asymmetric Four-Point Bending (AFPB) method (Figure 3). AFPB method has been previously used as an improved method to measure the shear strength of sea ice (Frederking and Timco, 1984) and to measure the bond strength between two rafted ice blocks (Bailey et al., 2012). The AFPB apparatus consists of two plates with a bar and ball mounted on each plate. The bottom plate is fixed to the Material Testing System (MTS) machine, while the upper plate is free to rotate about the load application point. Samples were positioned such that the freeze bond was at the centre of the loading axis and equidistant from the middle indenters. The plates are aligned so that the bars and balls are positioned asymmetrically about the loading axis and the centre of the specimen. Under these conditions, the outer pins generate a counter-clockwise rotation, while the inner pins create a counteracting force in the clockwise direction, producing a nearly pure shear stress state in the centre of the specimen. Figure 4 shows the geometry of the load application and the shear forces and bending moment diagrams. In this figure, P is the applied load, L and αL are the distance between the outer and inner loading pins, respectively, and the central loading axis. Assuming a parabolic stress distribution at the bond, the maximum shear stress τ_{max} at the centre of a circular beam is given by:

$$\tau_{max} = \frac{4}{3} \frac{(1-\alpha)}{(1+\alpha)} \frac{P_{max}}{\pi r^2} \quad (1)$$

where P_{max} is the peak load at failure, r is the radius of the sample, and α relates to the loading geometry. In these tests the values of L and α were set to 9.5 mm and 0.033, respectively.

During all tests, the cold room temperature was held at a nominal temperature of 0°C to keep the water near freezing temperature and to maintain similar temperatures for both testing and submersion. Testing was also carried out directly after submersion to determine the strength in a state as close to in situ as possible. The displacement, time and load of the MTS machine were monitored in real time and logged continuously. A high speed video camera was used to monitor the failure behaviour

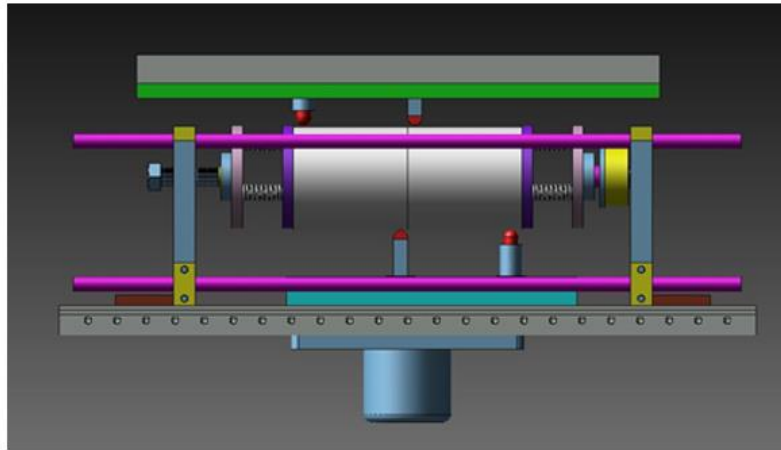


Figure 3. Confinement frame loaded in the AFPB rig

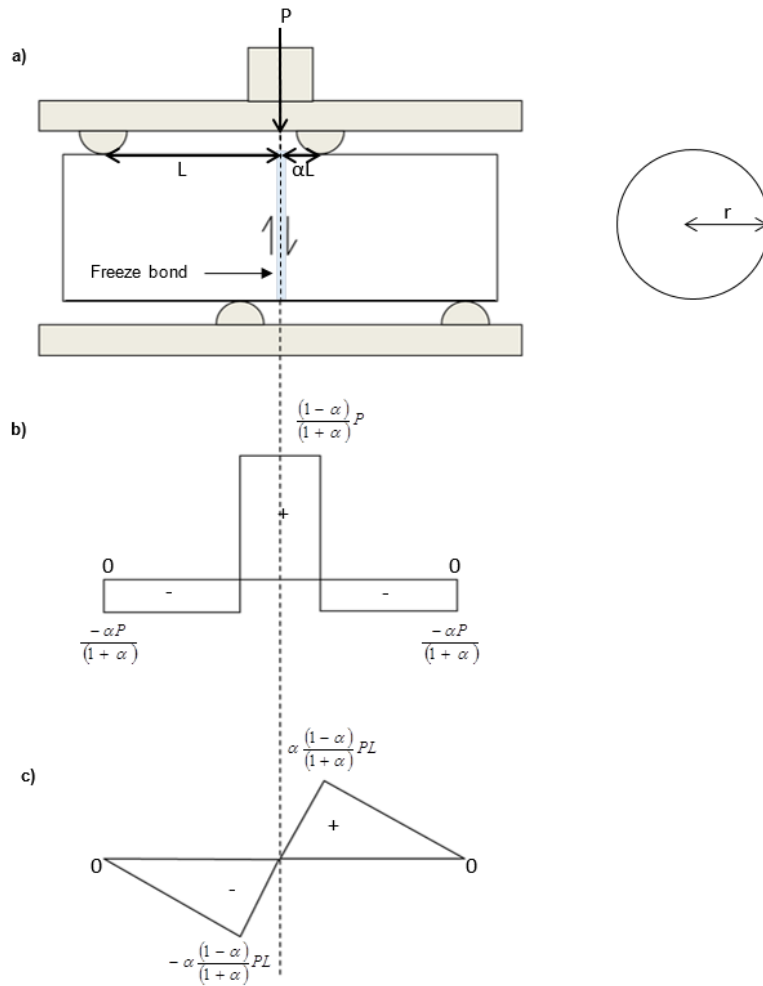


Figure 4. AFPB rig, showing diagrams of a) the load geometry b) the shear forces c) the bending moments (after Bailey, 2012)

Results

A total of 25 freeze bond tests have been conducted in order to investigate the influence of initial ice temperature and submersion time on the strength of the bond between two cylindrical ice samples. A summary of the test parameters used in each test is given in Table 1. Effects of submersion time on the strength of freeze bonds was studied for initial temperature of -18°C where the submersion time was varied from 1 minute to 26 hours. In addition to the above, in order to investigate the effect of temperature on the freeze bond strength, whilst the submersion time was kept constant at 30 minutes, a number of tests were conducted varying the initial ice temperature from -18°C to 0°C . The submersion time of 30 minutes was chosen as this was the time it took for a sample of these dimensions with an initial temperature of -18°C to equilibrate to the surrounding water temperature. All samples in the test program were deformed at a rate of 5 mm/s.

During all tests, a normal pressure was applied to the samples to simulate the contact pressures arising between ice blocks due to buoyancy forces. Figure 5 shows the typical behaviour measured during submersion for a test where the initial normal pressure applied to the sample was 26.2 kPa. It can be seen that a small drop in load occurred over the submersion time (1.87 kPa in 300 seconds), which is likely to have been caused by creep in the ice specimen. To ensure reported values reflect this relaxation effect, confinement values reported in Table 1 are the time-averaged values taken over the duration of the experiment.

Table 1. Test matrix for the freeze bond tests

Test series	Initial ice temperature (°C)	Actuator rate (mm/sec)	Submersion time (minutes)	Average normal pressure (kPa)
Effects of submersion time	-18	5	1, 2, 5, 10, 20, 30, 60, 180, 300, 420, 1020, 1440, 1560	23
Effects of temperature	0, -5, -7, -10, -15, -18	5	30	23

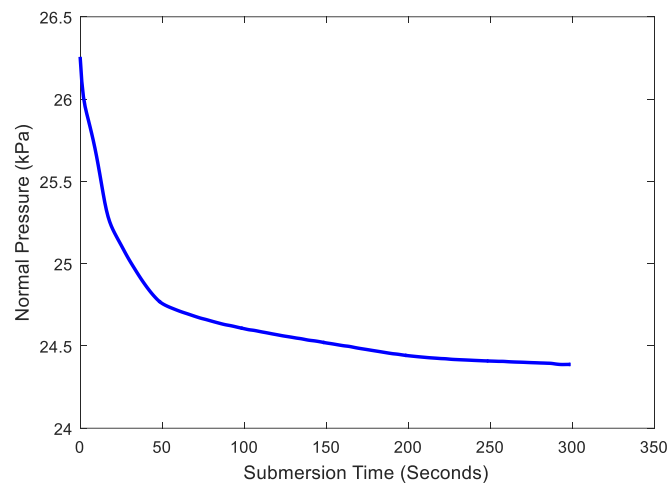


Figure 5. Change in normal pressure with submergence time for samples that had an initial applied pressure of 26.2 kPa and an initial ice temperature of -18°C.

Examination of the shear force versus time figures showed that all tests (with the exception of one) exhibited brittle failure, which was characterized by an abrupt and instantaneous drop off load (see Figure 6a). The only test that exhibited a more ductile failure was the test where the submersion time was 30 minutes and the initial ice temperature was -10°C (see Figure 6b). In this plot a period of strain hardening can be observed before failure. After bond failure, a residual frictional force was observed in all tests as the samples were sheared

further past each other. The shear strength for each test was calculated using equation 1 and finding the peak load at failure.

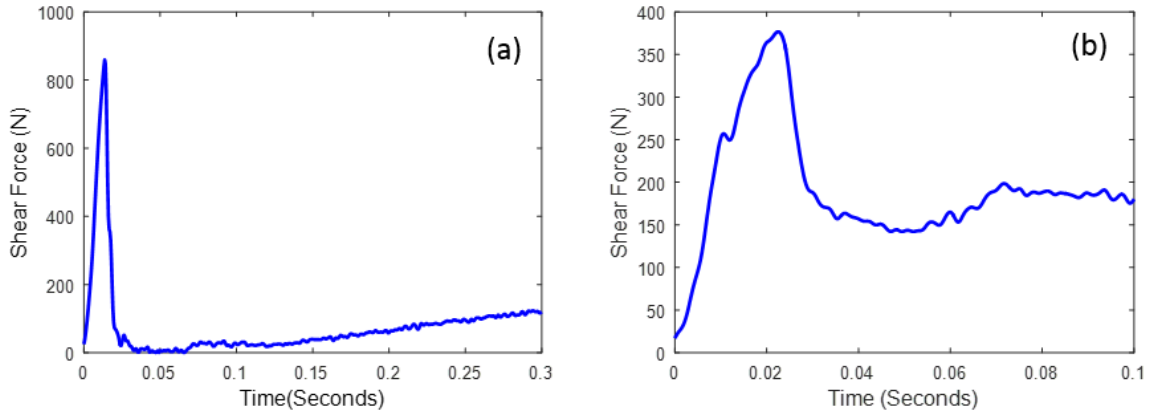


Figure 6. Typical load curves showing brittle behaviour (a) and ductile behavior (b) observed during the freeze bond tests. In test (a) and (b) the submersion times and initial ice temperatures were 5 minutes and 30 minutes and -18°C and -10°C , respectively.

Effects of Submersion Time

Figure 7 shows how the bond strength between two ice pieces varied as submersion time was increased from 1 minute to 26 hours for the case of an initial temperature of -18°C and a confining pressure of 23 kPa. The figure shows an initial increase in strength, which corresponds to the bond formation phase, followed by a gradual decrease in strength, as the bond temperature increased and started to weaken. For these experiments, peak strength of 250 kPa was observed at 5 minutes of submersion and strength values began to level out to a value of about 58 kPa after 3 hours of submersion. The first data point measured for the 7 hours test was unusually high (220 kPa) and therefore was repeated. The second value was lower (120 kPa) but still slightly higher than the expected trend. These deviations from the trend we believe are due to the natural variability of the ice. Further testing is currently underway to attain additional data which will help to investigate this anomaly.

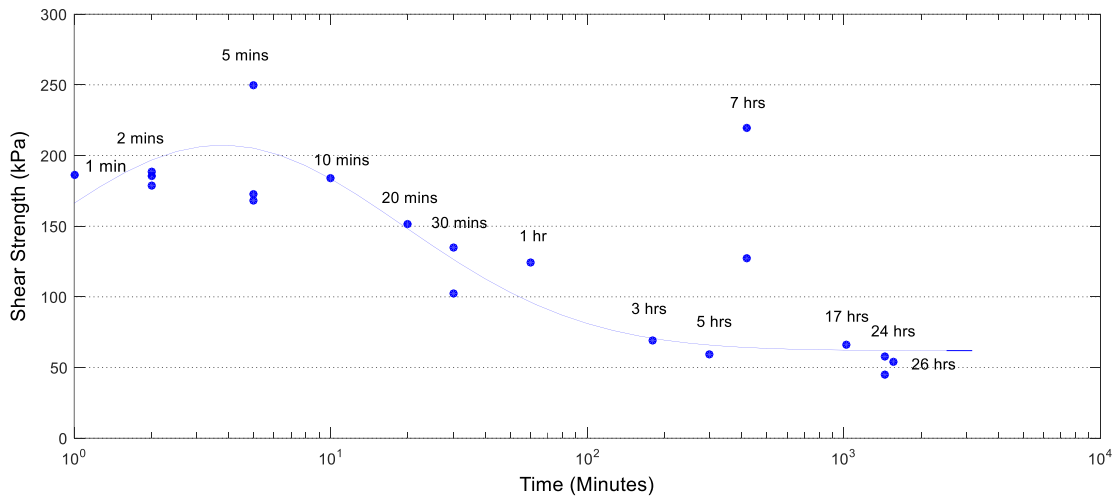


Figure 7. Shear strength vs. submersion time for ice with an initial temperature of -18°C that was confined under a load of 23 kPa and deformed at a constant rate of 5 mm/s showing bond formation-softening phases of strength development

Effects of Initial Ice Temperature

The effect of initial ice temperature on freeze bond strength was investigated by varying the initial ice temperature from 0 to -18°C . In all these tests, samples were tested after 30 minutes of submersion, confined under a normal load of 23 kPa and deformed at a constant rate of 5 mm/s. Figure 8 shows that the freeze bond strength increased with decreasing temperature. This is firstly because the colder the ice, the greater the rate of heat transfer and the more ice growth that will take place. Secondly, the colder the freeze bond the greater its strength due to the well-known increase in the plastic flow stress that occurs with decreasing temperature.

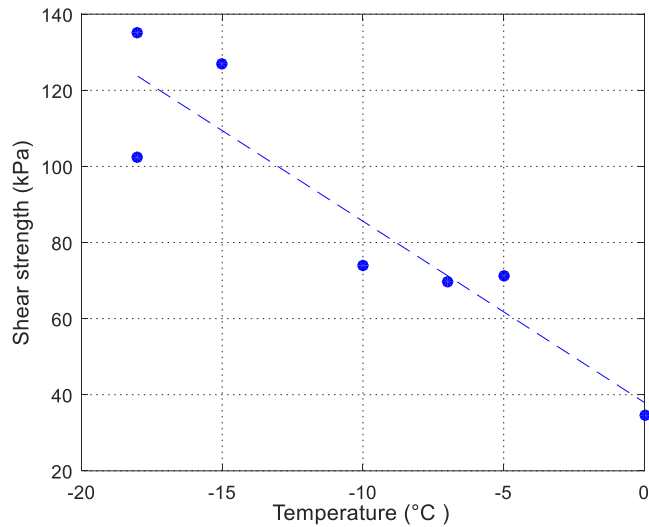


Figure 8. Shear strength as a function of temperature for ice with initial temperature ranging from -18°C to 0°C that was confined under a load of 23 kPa and deformed at a constant rate of 5 mm/s.

Discussion and Conclusions

This paper presents the results from a series of freeze bond tests that have been conducted to investigate the influence of submersion time and initial ice temperature on the strength of the bond between two cylindrical ice blocks. The strength of the bonds was tested in shear using the Asymmetric Four-Point Bending (AFPB) method, which produces a region of near pure shear in the centre of the specimen. Understanding freeze bonding processes is important for the development of ice rubble models, where bond strength between ice pieces is a key parameter in defining the failure behaviour of ice rubble.

The freeze bond strength was found to be highly dependent on submersion time, whereby the strength initially increased with submersion time, reaching peak strength around 5 minutes, and then gradually decreased and levelled out to a constant value. The initial strengthening stage is likely to be dominated by freezing as heat is transferred from the water to the ice blocks causing a freeze bond to form. Once the cold reserves in the ice blocks are used up, the bond strength will start to deteriorate as the freeze bond temperature equilibrates to that of the surrounding water. This type of behaviour was also observed by Repetto-Llamazares et al. (2011), who suggested that the width and height of the strength-submersion time curve will be governed by the initial temperature of the ice. Our results showed that it took approximately 3 hours for the freeze bond strength to stabilize to a constant value for ice with initial temperature of -18°C . The effects of localized crushing at the loading pins and the effects of random fractures may have contributed to variability in the data at short submersion times. It is recommended that additional tests be carried out using a compliant material between the ice and loading pins to alleviate any local stresses.

A clear trend of increasing strength was observed as the temperature was decreased from 0 to -18°C, when the submersion time was held constant at 30 minutes. Figure 9 shows the comparison of the results of the current study with the results of Shafrova and Høyland (2008) where they measured the strength of freshwater freeze-bonded samples that were submerged for 24, 48 and 60 hours. All data shows an increase in shear strength as the temperature decreases. The results of Shafrova and Høyland (2008) are higher than those measured in this program, which we believe is due to differences in test set up and the methodology. In the Shafrova and Høyland (2008) work, samples were deformed under uniaxial compression with the freeze-bond at a 45° angle to the loading direction. In addition, it appears that samples were machined after freeze-bond formation, which would likely have altered the strength of the sample. In current study, samples were sheared right after they were removed from the water in an attempt to better represent in-situ conditions.

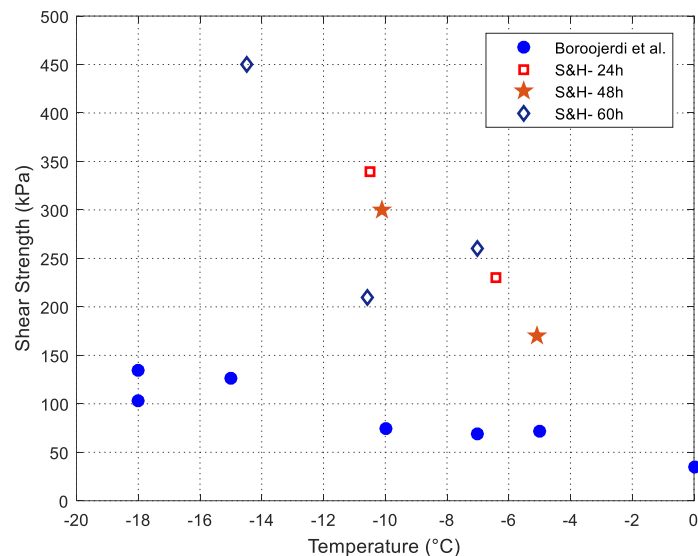


Figure 9. Comparison of the effects of temperature.

A key question that requires further investigation is what will happen to the inter-block bond strength after extended periods of submersion (as is the case in nature)? Will strength values stabilize at some limiting value? Or will bonds continue to soften until they have no residual strength? It is also possible that the keel will become more consolidated over time as sintering processes extend the surface area of the freeze bond? Images taken of the underside of ridges show that surfaces are ‘smoothed out’ suggesting sintering or melting of the ice blocks in the keel. Sintering is defined as the extension of the contact area between particles near their melting point, where the reduction in surface energy provides the main driving force. This means that more angular and irregular surfaces, such as the junctions between ice blocks, are more unstable and hence there is a driving force to move mass to the concave neck area of the bond (Blackford, 2007). Additional tests are currently

underway by the authors to investigate these processes, in particular the role of sintering over longer submersion periods.

Acknowledgements

The authors gratefully acknowledge core funding for the CARD program at C-CORE by Hibernia Management and Development Company, Ltd. (HMDC) and Terra Nova Development (Suncor Energy Inc. – Operator). Financial support from the Research and Development Corporation (RDC) of Newfoundland and Labrador for aspects of this work is gratefully acknowledged.

References

- [1] Bailey, E., Sammonds, P., and Feltham, D.L. 2012. The consolidation and bond strength of rafted sea ice. *Cold Regions Science and Technology*. Vol. 83, pp. 37-48.
- [2] Blackford, J.R. 2007. Sintering and microstructure of ice: a review. *Journal of Physics D: Applied Physics*. Vol. 40, No. 21, pp. 355-385.
- [3] Ettema, R., and Urroz, G.E. 1989. On internal friction and cohesion in unconsolidated ice rubble. *Cold Regions Science and Technology*. Vol. 16, No. 3, pp.237-247.
- [4] Ettema, R., and Schaefer, J. A. 1986. Experiments on freeze-bonding between ice blocks in floating ice rubble. *Journal of Glaciology*. Vol. 32, No. 112, pp. 397-403.
- [5] Frederking, R.M.W., and Timco, G.W. 1984. Measurement of shear strength of granular/discontinuous-columnar sea ice. *Cold Regions Science and Technology*. Vol. 9, No. 9, pp. 215-220.
- [6] Høyland, K.V., and Møllegaard, A. 2014. Mechanical behavior of laboratory made freeze-bonds as a function of submersion time, initial ice temperature and sample size. *Proceedings of the 22nd IAHR International Symposium on Ice*, Singapore, August 11-15, 2014.
- [7] Liferov, P., and Bonnemaire, B. 2005. Ice rubble behaviour and strength: Part I. Review of testing and interpretation of results. *Cold Regions Science and Technology*. Vol. 41, No. 2, pp.135-151.
- [8] Marchenko, A., and Chenot, C. 2009. Regelation of ice blocks in the water and the air. *Proceedings of 20th International Conference on Port and Ocean Engineering under Arctic Conditions*. Luleå, Sweden, June 9-12, 2009.
- [9] Repetto-Llamazares A. H. V., Høyland K. V., and Evers, K. U. 2011. Experimental studies of shear failure on freeze-bonds in saline ice part I: set-up, failure mode and freeze-bond strength. *Cold Regions Science and Technology*. Vol. 65, No. 3, pp. 286-297.
- [10] Sanderson, T.J. 1988. *Ice mechanics and risks to offshore structures*. Graham & Trotman, London, England.
- [11] Shafrova, S., and Høyland, K. V. 2008. The freeze-bond strength in first-year ice ridges. Small-scale field and laboratory experiments. *Cold Regions Science and Technology*. Vol. 54, No. 1, pp. 54-71.

Appendix B: Freeze bond field experiments, presented at the 2018 Arctic Technology Conference, Huston, Texas

OTC-27424-MS

Field Experiments on Shear Strength of Solid and Freeze-bonded Sea ice

Marjan Taghi Boroojerdi, Memorial University
Rocky Taylor, Memorial University
Soroosh Mohammadafzali, Memorial University
Eleanor Bailey-Dudley, C-CORE
Ian Turnbull, C-CORE
Ridwan Hossain, Memorial University

Copyright 2018, Offshore Technology Conference

This paper was prepared for presentation at the Arctic Technology Conference held in Houston, Texas, USA, 5–7 November 2018.

This paper was selected for presentation by an Arctic Technology Conference program committee following review of information contained in an abstract submitted by the author(s). Contents of the paper have not been reviewed by the Offshore Technology Conference and are subject to correction by the author(s). The material does not necessarily reflect any position of the Offshore Technology Conference, its officers, or members. Electronic reproduction, distribution, or storage of any part of this paper without the written consent of the Offshore Technology Conference is prohibited. Permission to reproduce in print is restricted to an abstract of not more than 300 words; illustrations may not be copied. The abstract must contain conspicuous acknowledgment of OTC copyright.

Abstract

Sea ice rubble/ridge strength and interaction mechanics are highly important in the design of structures and subsea infrastructure for ice prone offshore environments. To better characterize sea ice conditions in northern Newfoundland, a series of field tests were conducted on landfast ice in Pistolet Bay, NL in February 2018. This paper presents a summary of recent shear strength tests on solid and freeze-bonded ice specimens, to help improve understanding of ice rubble properties and behaviour under field conditions. Both horizontal and vertical sea ice samples were tested under dry and submerged conditions, as well as freeze-bonded ice samples under submerged conditions. Sea ice samples were sheared using the Asymmetric Four-Point Bending (AFPB) method, which has been shown to produce a near pure shear region at the center of the specimen. For the dry tests, cores were sheared directly after collection so as to test them in conditions as close to in-situ as possible. For submerged tests, cores were submerged for a specific period of time before shearing. Freeze-bonded samples were prepared using a confinement frame which applied a pressure of 25 kPa to the specimens during submergence. These data for AFPB field tests

are an important consideration in modelling the strength of ice rubble/ridges and are the first of their kind. From this work it may be concluded that the AFPB method is a promising approach for studying shear strength of both solid and freeze-bonded specimens in the field and additional testing is recommended. New field testing approaches, such as the one presented here, will help improve understanding of in-situ sea ice properties and behavior, which ultimately supports the development of new ice-structure interaction models, which directly benefits oil and gas, shipping, renewable energy, and public works projects in ice prone Arctic and Sub-Arctic regions.

Overview

Understanding local ice conditions and associated material properties are essential for offshore hydrocarbon exploration and production, marine operations and coastal engineering applications in ice environments. Field measurements and in-situ experiments play a vital role in helping fill gaps in data and knowledge needed to characterize such ice environments and to guide the development of new and improved methods for the design and operation of ice-class structures.

In 2015, a five-year field program was initiated at C-CORE and Memorial University to collect data on ice dynamics, metocean conditions, and ice and snow physical properties offshore Newfoundland and Labrador. The collection and compilation of high-quality data to improve understanding of regional ice conditions and to aid in the development of new models to enhance the safety and efficiency of marine and offshore operations in ice is a major goal of this work.

As part of this program, three field expeditions on the land-fast ice of Pistolet Bay at the northern tip of Newfoundland were carried out in 2016, 2017 and 2018. The purpose of this fieldwork was to: (1) collect data to empirically assess snow and ice temperatures as a function of air temperature, humidity, wind speed, incoming shortwave and longwave radiation, and; (2) conduct mechanical tests to help characterize sea ice strength. While ice strength characterization activities have been focused primarily on improving understanding of scale effects associated with flexural failure, supporting the development of new approaches for collecting in-situ strength data is an important complementary goal of this work.

To this end, a test apparatus was designed and fabricated for the winter 2018 expedition to allow an investigation of the suitability of the Asymmetric Four-Point Bending (AFPB) method for measuring shear strength of solid and freeze-bonded sea ice specimens in the field. This is a new type of field test and data obtained from this program are the first of their kind. This approach provides an opportunity to fill an important gap, since the shear strength of ice and bonds between blocks is an important input in modelling the overall strength and behaviour of ice rubble and ridges for a variety of ice engineering applications. In this paper, a summary of the fieldwork, experimental set-up and initial results of these

shear strength tests on solid and freeze-bonded sea ice specimens, along with details of the ice conditions during those experiments, is presented.

Field Location and Ice Conditions

The field expedition took place on the land-fast ice on the eastern edge of Pistolet Bay at about $51^{\circ}30'N/55^{\circ}45'W$ located at the northern tip of Newfoundland near the communities of St. Anthony and Raleigh, NL; see Figure 1 (a). Based on a historical Freezing Degree Days (FDD) analysis of regional ice thickness, it was determined that the land-fast ice is unlikely to be significantly greater than 80 cm and a site with water depths around 1.5-2 m was selected using a nautical chart of Pistolet Bay.

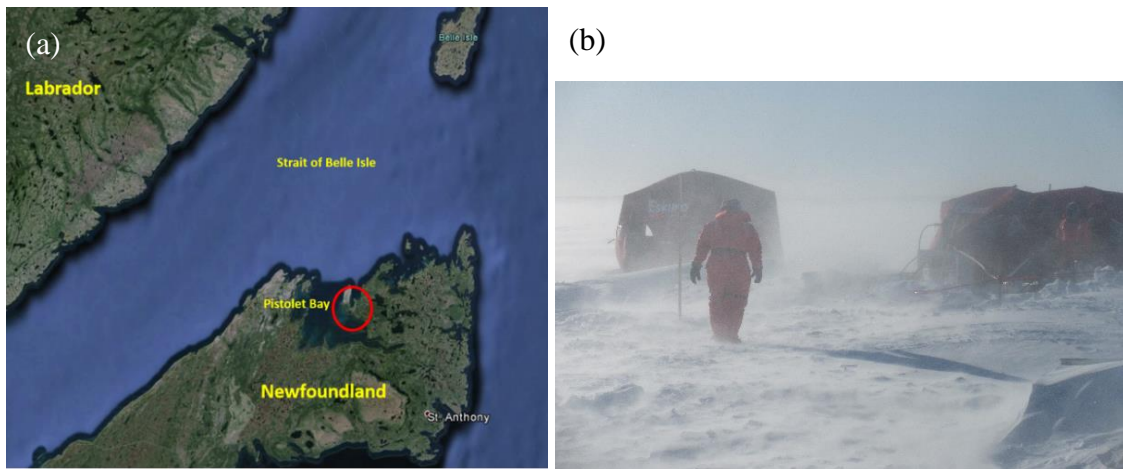


Figure 1- (a) Map of Pistolet Bay and surrounding region; (b) field location with shelters, equipment and testing site.

Upon arrival at the site, the safety team ventured onto the ice on foot, travelling progressively further offshore from our originating onshore location near a shallow beach area and continuing onward until a large area of flat, level ice in sufficient water depth was reached. To ensure safety, a series of holes was drilled in the ice along this route to verify safe operating thicknesses and to demarcate a safe transit route that was subsequently used for the duration of the program. In 2018, as in previous years, the work site was less than 500 m from shore, and the water depth was approximately 1.8 m. All field equipment and personnel were then transported to the site by snowmobile and the shelters and equipment were set up onsite (Figure 1b) and the team began to survey and characterize the local ice and meteorological conditions.

To assess the distribution of ice thickness in the region surrounding the worksite, a series of measurements were taken using manual drill-hole measurements, as well as an electromagnetic (EM) profiler. While the traditional drill-hole method is still the most accurate method to measure the ice thickness, drill-hole measurements are more time-

consuming and provide point measurements, whereas EM is more suitable for collecting larger volumes of data over bigger areas (Haas et al., 2014). To allow for calibration of the EM sensor, a total of 20 datapoints of coincident drill-hole and EM ice thickness measurements were taken at the same date/time and GPS location. EM measurements were collected using a GSSI Profiler EMP-400 with coil spacing of 1.2 m, with the frequencies set to 5 kHz, 9 kHz and 15 kHz and the height set to 20 cm, along with a TDS Recon-400 Personal Digital Assistant (PDA). Figure 2 shows the procedure used to obtain the electromagnetic and physical thickness measurements. First, a conductivity measurement at a selected GPS location was taken using the EM profiler, then a 4 inch hole was drilled at the same location using a manual ice auger. Next, the snow depth was measured using a meter stick in an adjacent undisturbed area. Finally, the total ice thickness was measured by lowering a Kovacs ice thickness gage into the hole, pulling upward until the opened T-bar bridged across the hole at the bottom of the ice, allowing a reading of ice thickness to be taken using the integrated measuring tape.

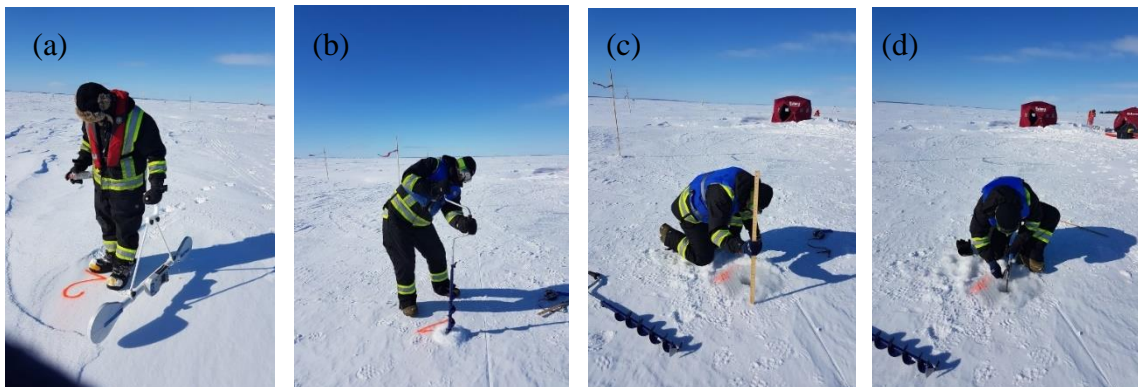


Figure 2 - Thickness measurement procedure: (a) auguring; (b) snow thickness measurement; (c) ice thickness measurement, and; (d) EM profiler conductivity measurement.

As shown in the histogram in Figure 3(a), a range of ice thickness measurements were obtained, and the average ice thickness was found to be 50.25 ± 2.75 cm. These data were subsequently used to calibrate the profiler for the ice thickness measurements using the same approach as Jingxue et al. (2007). It was found that the best calibration curve for this device, shown in Figure 3 (b), could be obtained using a frequency of 15 kHz. This exponential curve was found to be consistent with the curve obtained by Jingxue et al. (2007) and Eicken (2009) for ice thickness in the range of 40-70 cm, although the calibration of the EM profiler is site-, device- and frequency-specific and should be performed for any new setup. From this data it is also observed that while this EM profiler produces errors on point estimates of ice thickness of up to 20%, it does serve as a fast alternative to manual drilling and is a useful tool for field assessment and general site evaluation over large areas where areal averages of ice thickness are of interest.

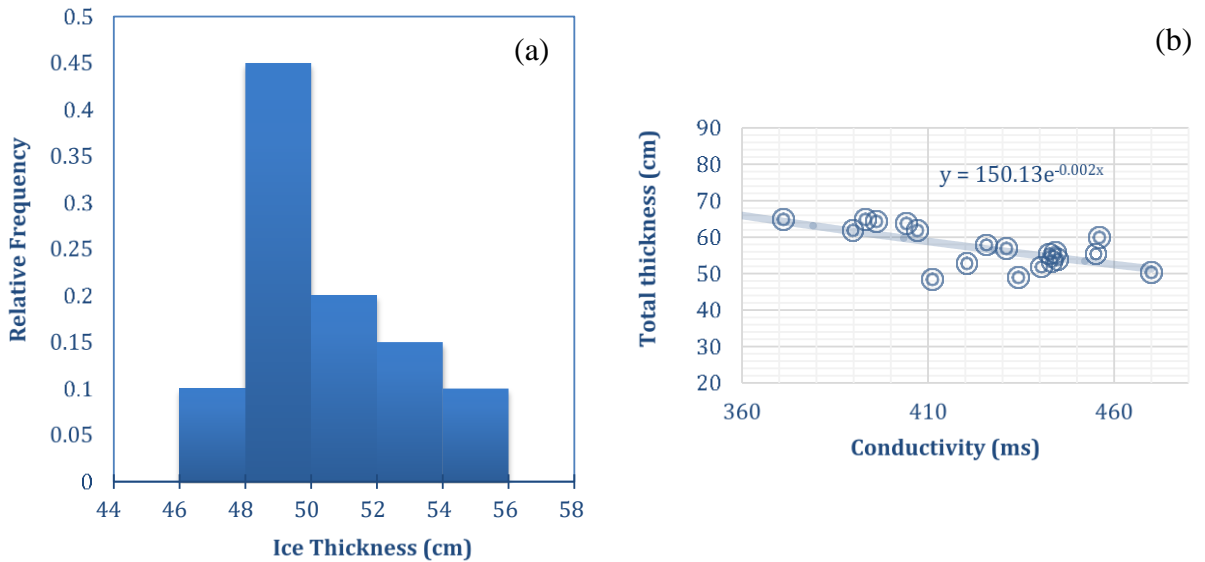


Figure 3- Plots showing: (a) histogram of ice thickness measurements; (b) calibration curve developed for EM sensor using ice thickness and conductivity measurements

To allow for measurement of sea ice properties and also to extract ice samples for shear tests, ice cores were extracted using a Kovacs Mark II corer, which can be used to retrieve samples of 9 cm in diameter and up to 1 m long. Standard coring procedures were followed to extract vertically oriented cores (parallel to ice growth direction) as shown in Figure 4 (a, b). For the shear tests on solid ice, a number of horizontally oriented samples (perpendicular to ice growth direction) were also required. Horizontal samples were obtained by coring through the side of large ice blocks that were cut out using a chainsaw and lifted onto a sled with the aid of a gantry and chain hoist, as shown in Figure 4 (c).

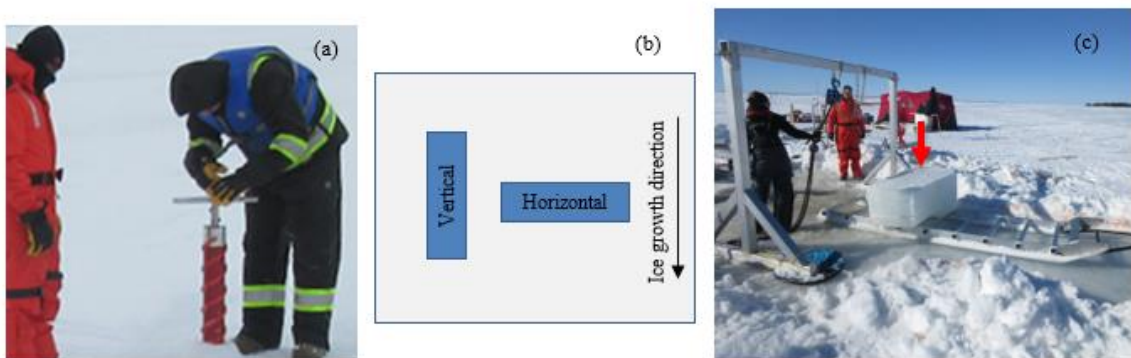


Figure 4 – Ice core collection: (a) vertical core drilling; (b) schematic of orientation of cores relative to ice growth direction; (c) sea ice blocks extracted using gantry and sled for horizontal coring.

To obtain temperature data through the thickness of a full core, measurements were taken at specific depths (typically 10 cm increments) in the core. This was accomplished by drilling a small hole into the center of the sample at the location and the stainless steel probe of a handheld Fisher Scientific digital thermometer was used to obtain a temperature measurement. The overall average temperature of all of the cored test specimens collected during this program was -4.84 ± 1.97 °C. To show the temperature profiles as a function of depth, temperature data collected from full-length cores have also be plotted, such as the ones shown in Figure 5 (a).

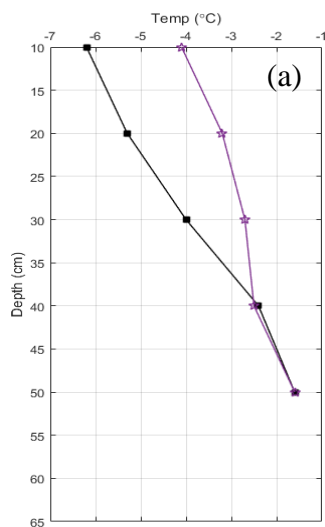


Figure 5 – (a) sample ice temperature profiles; (b) preparing core sections for salinity and density measurements.

To allow for measurement of sea ice salinity and density, each ice core was then cut into approximately 5 cm sections as shown in Figure 5 (b). Each section of the core was stored in an airtight plastic bag and assigned a unique reference number to identify the date/time, GPS location and depth of the core. To calculate the ice density, the mass of each sample was measured on an OHAUS high resolution scale and the volume was calculated using dimension measured with a pair of digital calipers or measuring tape (depending on the size of the sample). The average density of the cores collected during this program was found to be 864.6 ± 82.2 kg/m³. The salinity was measured by melting the core sections overnight and then taking the salinity measurement the following morning using a temperature-compensated Model #S98200 Fisher Scientific conductivity/salinity meter. The cores collected during this field program were found to have an average salinity of 4.106 ± 1.408 ppt.

Test Description

Freeze bond experiments conducted to date have measured the strength of bonds between ice blocks under different conditions, such as different submersion times, confinement, initial ice temperatures and deformation rates (e.g. Ettema and Schaefer, 1986; Shafrova and Høyland, 2008; Marchenko and Chenot, 2009; Repetto-Llamazares, 2011; Helgøy et al., 2013; Høyland and Møllegaard, 2014; Bueide and Høyland, 2015; Boroojerdi et al., 2016). While most experiments have been conducted in the laboratory, Shafrova and Høyland (2008) and Marchenko and Chenot (2009) have conducted a series of freeze bond experiments in the field. Using uniaxial compression tests on freeze bonded sea ice samples bonded at a 45° angle, Shafrova and Høyland (2008) found that the strength of the bond varied from 14 to 73 kPa for samples that were submerged for 48 hours, and observed that the ratio of the strength of the freeze bond to the compressive strength of the solid ice was between 0.008 to 0.082. Marchenko and Chenot (2009) conducted direct shear tests on vertically oriented freeze bonds formed in air, and found the strength to vary from 2 to 70 kPa. Their submerged tests however showed no bond formation after 2 days of submersion, presumably due to high oceanic heat fluxes measured.

The primary goal of this series of experiments was to evaluate the suitability of a new type of field test that has been adapted from the laboratory, namely the AFPB shear tests. In light of this objective, the test matrix for this series was chosen to cover a range of scenarios. Conditions considered included the shear strength of dry and submerged solid sea ice samples, as well as the shear strength of freeze bonds that form between two submerged samples of ice under confining pressure. For the solid ice tests, horizontally-oriented and vertically-oriented ice core samples were tested under dry conditions, as well as after a specified period of submergence. The strength development of the bond between submerged ice blocks after a defined period of time for a constant confinement of 25kPa was also of interest. A summary of conditions for this test series is provided in Table 1.

Table 1 – Test Matrix for Shear Strength Field Experiments

Type of test	Dry/submerged	Confinement	Ice growth direction – location	Submersion time	repeats
Solid shear	Dry	Unconfined	Horizontal- Middle	-	4
			Vertical- Middle	-	6
	Submerged	Unconfined	Vertical- Middle	5 min	2
				3 hrs	2
24 hrs				2	
Freeze bond	Submerged	Confined (25 kPa)	Vertical- Middle	5 min	1
				1 hr	1
				24 hrs	1

The AFPB apparatus used consists of four loading pins positioned asymmetrically from the center of the loading axis, as shown in Figure 6 (a). The inner pins generate a force in the

counterclockwise direction while the outer pins generate a clockwise load, resulting in a pure shear region in between the inner pins. Using this method, shear strength τ_{max} can be determined using the following equation:

$$\tau_{max} = \frac{4}{3} \frac{(1 - \alpha)}{(1 + \alpha)} \frac{P_{max}}{\pi r^2},$$

where P_{max} is the peak measured load at failure, r is the radius of the sample. The parameter α is a constant defined by the fraction of the distance between the center point of the inner pin and the loading axis divided by the distance of the center of the outer pin from the loading axis, which was set to 0.106 in these experiments.

In addition to the AFPB, as shown in Figure 6 (a), a confinement frame was used for the freeze bond tests to apply specified pressure of 25 kPa to the sample. Additional details about the AFPB and confinement frame can be found in Boroojerdi et al. (2016). This AFPB apparatus was installed in the mobile hydraulic compressive testing frame shown in Figure 6 (b).

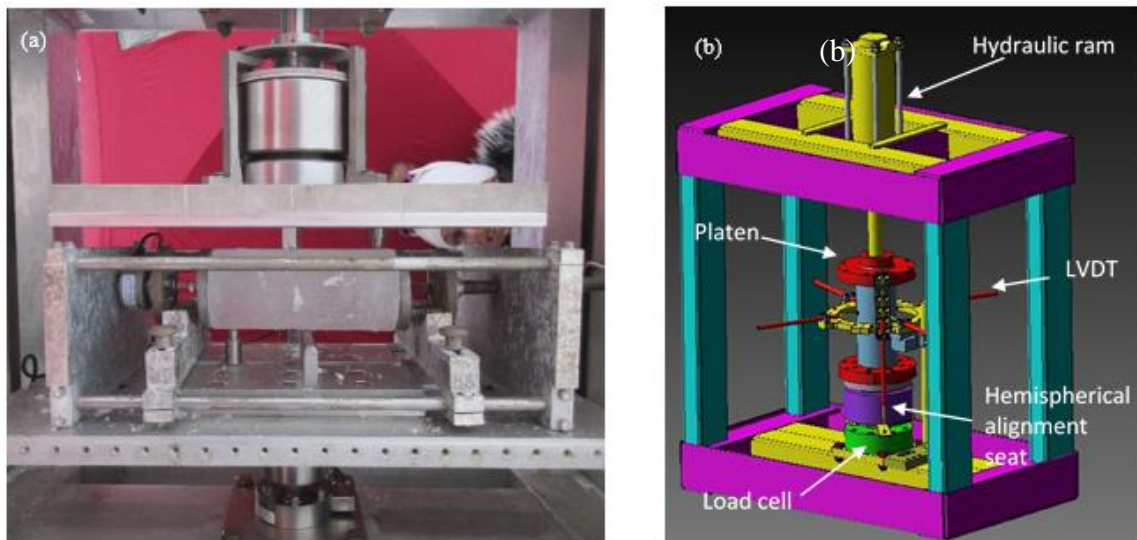


Figure 6 – (a) Installed AFPB apparatus and ice sample in confinement frame; (b) mobile hydraulic compressive testing frame.

To prepare the specimens for testing, solid ice cores were first cut to 20 cm lengths. Dry tests were conducted on the samples immediately after cutting. Other conditions required some additional preparation. For submerged solid ice tests, a channel was cut in ice cover and samples were submerged in sea water for a specific period of time before installing in the AFPB for testing. For the freeze bond tests, a 20 cm ice sample was cut in half and the pair of samples (9 cm in diameter and 10 cm in length) were put in the confinement frame and loaded to the appropriate level. The confinement frame and mounted specimen was

then submerged in the pre-cut channel using snow fences that were screwed on level ice with ice screws for the specified amount of time. Once the prescribed time had elapsed, the samples were removed from the water, installed in the Asymmetric Four-Point Bending apparatus and tested.

During testing, the shear load was applied using a hydraulic ram that was set to move at constant rate of 5 mm/sec. Shear load was measured using a 5 kN loadcell positioned as illustrated in Figure 6 (b). To ensure that the loading pins were perfectly aligned on the samples, an alignment seat was attached to the top plate of the AFPB apparatus. The vertical displacement of the ram was measured using a Linear Variable Differential Transformer (LVDT). Load, time, and displacement were monitored continuously using the Catman software, which was installed on a Panasonic Tough Book located inside the adjacent shelter as shown in Figure 7. Instrumentation was connected to the laptop using a HBM Durham Instruments data acquisition box. Dimensions of each sample were taken before and after each test (for submerged samples) and the temperature of each sample was again measured after being sheared.



Figure 7 – Field experiment set-up showing ice sample in confinement frame, with AFPB apparatus installed in test frame and connected to hydraulics and power pack.

Results and Discussion

Sample shear load curves obtained during testing have been presented below for the case of a solid ice specimen submerged for 24 hours (Figure 8a) and a freeze bonded sample submerged for 24 hours (Figure 8b). While some initial peaks and load drops exist in the freeze bond test, this is likely due to localized crushing under the pins and quickly settles out. In both samples, while the main part of the load build-up phase is approximately linear and ultimately results in a brittle failure, the magnitude of peak shear load for solid ice is

about 5 times higher than the freeze bonded ice. It should be also be noted that for both samples, failure occurs at about the same time (~3.5 sec after the onset of loading), which corresponds to a displacement of about 17.5 mm. Given that both samples were submerged for similar submersion times, further data collection and analysis are recommended to investigate if similar observations result for different conditions. Such insights would provide valuable guidance for the selection of simplified failure criteria, such as a critical strain limit, which could help in the development of numerical modelling approaches, such as Discrete Element Models (e.g. Mohammadafzali et al., 2016), which are used for modelling macroscale ice rubble and ridge processes.

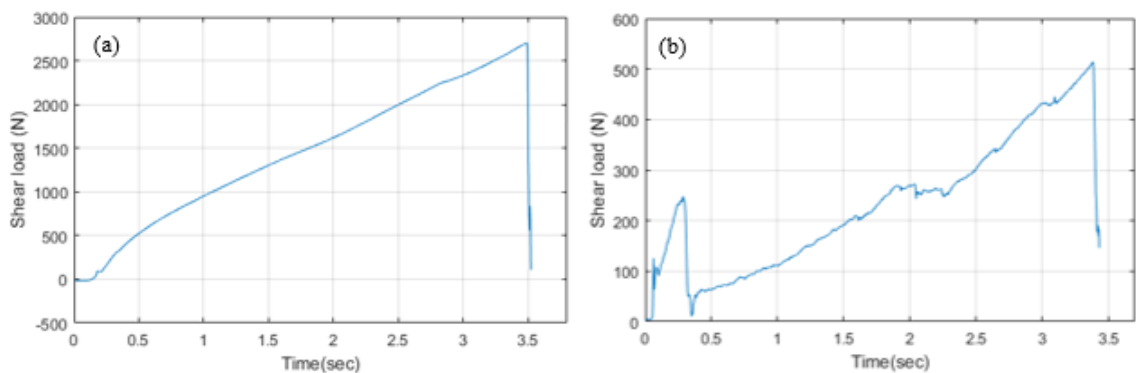


Figure 8 – Sample shear load vs time curves for: (a) solid ice submerged for 24 hours; (b) freeze-bonded ice test submerged for 24 hours.

While detailed analysis of individual test results is beyond the scope of the present paper, a summary of the shear strengths values measured in this program are presented in Figure 9. As can be seen from this plot, for dry test conditions, horizontal samples are observed to have a lower strength, ranging from 289 to 546 kPa, compared to the strength of dry, vertical samples for the same test conditions (423-641 kPa). It is also observed that the group of shear tests conducted on vertical samples under wet conditions have a somewhat lower range of strengths (292 to 586 kPa) than their dry counterparts. Freeze bond strength values are significantly lower than solid ice strength values, ranging from 68 to 120 kPa, which is approximately 15%-25% of the strength of the solid ice shear strength, depending on conditions. While it is evident that the duration of the submersion time does affect the measured strength values, there are too few data points in the present series to draw conclusions and rather further testing is recommended to explore these effects in greater detail.

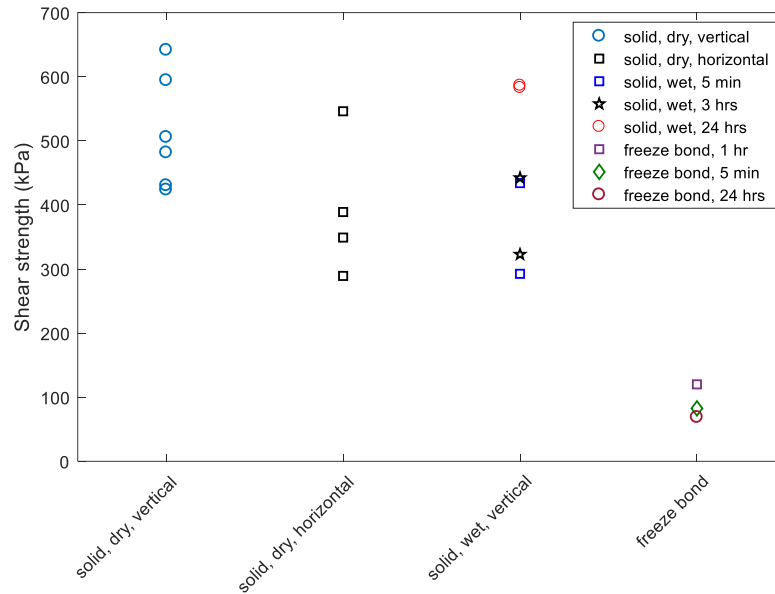


Figure 9 – Shear strength values measured in solid, and freeze bond tests.

Concluding Remarks

This paper presents an overview of recent field tests carried out by our research group to explore the suitability of the AFPB testing approach for adaptation and use for field collection of shear strength data for solid and freeze-bonded ice. Initial results have been presented along with a discussion of how this work may be extended. In general, it was observed that the shear strength of horizontal dry solid ice block samples collected showed lower strength values compared to vertical samples. The strengths of the submerged solid ice blocks were observed to be slightly lower than test results for dry specimens. While it appears that submersion time does have an effect on the strength, no conclusions can be made at this point since there are too few data and these values may be affected by a variety of factors such as the initial temperature of the samples, which could cause affect the extent of bond formation. While lower freeze-bond strength values were observed relative to solid ice tests, it is important to consider how these processes may change over longer times, since other factors such as the interplay between thermal and creep-sintering mechanisms may play an important role has been shown to play an important role in freshwater ice (Boroojerdi et al., In Preparation) and similar processes may be present for sea ice freeze bonds.

These AFPB field data are the first of their kind, and serve to provide insight into processes of interest for modelling the strength of ice rubble/ridges. Through continued advancement of our understanding of in-situ sea ice properties and behavior, new such field will support the development of enhanced methodology for modelling ice loads to improve the design of of structures for oil and gas, shipping, renewable energy and public works projects in Arctic and Sub-Arctic regions. While methods and apparatus used in this test program show promising results, further tests are recommended to better understand and characterize the shear strength of solid and freeze-bonded sea ice.

Acknowledgements

The authors gratefully acknowledge funding for this work by Hibernia Management and Development Company, Ltd. (HMDC), and InnovateNL. We additionally thank C-CORE for in-kind support of this work, as well as all participants and contributors to this field program. Specifically, the authors would like to thank Robert Pritchett, Mohamed Aly, and Reza Zeinali Torbati, without whom these tests would not have been done.

References

- [1] Boroojerdi, M.T., Bailey, E., Ghobadi, M., Taylor, R.S., (2016). Experimental Study on Shear Strength of Freeze Bonds in Freshwater Ice. Proceedings of Arctic Technology Conference 2016, St. John's, NL.
- [2] Bueide, I.M., Høyland, K.V., 2015. Confined Compression Tests on Saline and Fresh Freeze-Bonds. Presented at the Proceedings of the International Conference on Port and Ocean Engineering Under Arctic Conditions.
- [3] Eicken, H. (2009). Field techniques for sea ice research. Fairbanks: University of Alaska Press.
- [4] Ettema, R., Schaefer, J.A., 1986. Experiments on freeze-bonding between ice blocks in floating ice rubble. *Journal of Glaciology* 32, 397–403.
- [5] Haas, C., Ingham, M., & Mahoney, A. (2014). Field techniques in sea-ice research. In *Cold Regions Science and Marine Technology* (pp. 1–47). Prais, France,: Eolss Publishers, 20 p.
- [6] Helgøy, H., Astrup, O.S., Høyland, K.V., 2013. Laboratory work on freeze-bonds in ice rubble, Part II: Results from individual freeze-bond experiments, in: Proceedings of the 22nd International Conference on Port and Ocean Engineering under Arctic Conditions. Presented at the Port and Ocean Engineering under Arctic Conditions, Espoo, Finland.
- [7] Høyland, K.V., Møllegaard, A., 2014. Mechanical behavior of laboratory made freeze-bonds as a function of submersion time, initial ice temperature and sample size, in: Proceedings of the 22nd IAHR International Symposium on Ice. Singapore.
- [8] Jingxue, G., Bo, S., & Gang, T. (2007). The application of electromagnetic-induction on the measurement of sea ice thickness in the Antarctic, 4(3), 214–220.
- [9] Marchenko, A., Chenot, C., 2009. Regelation of ice blocks in the water and the air, in: Fransson, L. (Ed.), . Presented at the 20th International Conference on Port and Ocean Engineering under Arctic Conditions.

- [10] Mohammadafzali, S., Sarracino, R., Taylor, R.S., Stanbridge, C.W., Marchenko, A., (2016). Investigation and 3D Discrete Element Modeling of Fracture of Sea Ice Beams. Proceedings of Arctic Technology Conference 2016, St. John's, NL.
- [11] Repetto-Llamazares, A.H.V., 2011. Experimental studies of shear failure on freeze-bonds in saline ice part I: set-up, failure mode and freeze-bond strength. *Cold Regions Science and Technology*. 65, 286–297.
- [12] Shafrova, S., Høyland, K.V., 2008. The freeze-bond strength in first-year ice ridges. Small-scale field and laboratory experiments. *Cold Regions Science and Technology*. 54, 54–71.